Investigations into Poxvirus-Host Interactions

by

Wondimagegnehu Mulatu Teferi

A thesis submitted in partial fulfillment of the requirements for the degree of

Doctor of Philosophy

in

Virology

Department of Medical Microbiology and Immunology

University of Alberta

ABSTRACT

Poxviruses, such as vaccinia virus (VACV) and myxoma virus (MYXV), actively modulate various cellular structures and functions to ensure effective replication and transmission. In the contrary, cells use several restriction mechanisms to mitigate these viruses. This evolutionary relationship is the basis for poxvirus-host interactions. Although some of these interactions have been described, given the large number of proteins encoded by poxviruses, a significant number of them are yet to be discovered.

To further our understanding of poxvirus-host interactions, we performed large-scale small interfering RNA (siRNA) screens in MDA-MB-231 cells and identified human host factors that modulate MYXV replication. Using human whole-genome (21585 genes) and sub-genomic (kinases and phosphatases, 986 genes) siRNA libraries, we identified 711 antiviral (siRNA pools that enhanced MYXV replication) and 333 proviral genes (siRNA pools that inhibited MYXV replication). Cluster analysis of these genes identified a number of enriched pathways and processes including inflammatory and mitogen-activated protein kinase pathways, the cell cycle and glycolysis. We further studied some of these pathways.

Decreasing the glycolytic activity of cells through siRNA silencing of key glycolytic enzymes, such as phosphofructokinase (PFK)-1, or treatment with 2-deoxy-D-glucose reduced the replication of MYXV. In contrast, enhancing glycolytic activity through over-expression of glycolytic enzymes, such as 6-phosphofructo-2-kinase/fructose-2,6-bisphosphatase 3 (PFKFB3), increased virus replication confirming that infection is favoured by aerobic glycolytic metabolism. Similarly, according to our siRNA screen results, siRNAs that trap cells in G1-phase of the cell cycle by inhibiting

the G1/S-checkpoint stimulated MYXV growth. This observation was reproduced by arresting cells at G1 with a chemical inhibitor of cyclin-dependent kinases 4/6. Moreover, the inhibitor also enhanced the oncolytic potentials of the virus.

We also investigated the interaction between poxviruses and the repressive chromatin. VACV infection enhanced markers of the repressive chromatin through SUV39H1/2 dependent manner while MYXV did not change them. Our preliminary studies suggested that VACV might use the repressive chromatin to produce a widespread reduction in cellular gene expression.

Overall these studies demonstrate that poxviruses interact with various cellular processes. A detailed understanding of these processes could help to identify anti-poxvirus drug targets and enhance the oncolytic potentials of these viruses.

DEDICATION

I dedicate this thesis to my father, Mr. Mulatu Teferi Damtew, and my mother, Mrs.

Aselefech Kebede Woldemikael.

ACKNOWLEDGMENT

TABLE OF CONTENTS

LIST OF FIGURES

LIST OF TABLES

LIST OF ABBREVIATIONS

2DG	2-Deoxy-$_D$-glucose
5-FU	5-Fluorouridine
AMPK	Adenosine monophosphate-activated protein kinase
ANOVA	Analysis of variance
APC	Anaphase promoting complex
AraC	Cytosine arabinoside
ATCC	American type culture collection
bp	base pair
BrdU	5-Bromo-2-Deoxyuridine
CAK	Cyclin-dependent kinase-activating kinase
Cdc20	Cell division cycle 20
CdC25	Cell division cycle 25
CDGS	Chromatin dependent gene silencing
Cdh1	Cell division cycle 20 (Cdc20)-homolog 1
CDK/Cdk	Cyclin-dependent kinase
cDNA	complementary deoxyribonucleic acid
Cip/Kip	Cdk interacting protein/ kinase inhibitor protein
CKI	Cyclin-dependent kinase inhibitor
CPXV	Cowpox virus
DAPI	4',6-Diamidino-2-phenylindole dihydrochloride
DAVID	Database for Annotation, Visualization and Integrated Discovery
DMSO	Dimethyl sulfoxide
DNA	Deoxyribonucleic acid
dNTP	Deoxynucleoside triphosphate
dsRNA	double-stranded RNA
DTT	Dithiothreitol
EBV	Epstein Barr virus
ECF	Entry fusion complex
EGFP	Enhanced green fluorescent protein

EV	Extracellular virion
F1,6,BP	Fructose 1, 6-bisphosphate
F2,6BP	Fructose 2,6-bisphosphate
F6P	Fructose 6-phosphate
FACS	Fluorescence-activated cell sorting
FUCCI	Fluorescent ubiquitination-based cell cycle indicator
G6P	Glucose 6-phosphate
GLUT	Glucose transporter
GM-CSF	Granulocyte macrophage-colony stimulating factor
GPT	guanine phosphoribosyl transferase
h	hour
HAART	Highly active antiretroviral therapy
HBV	Hepatitis B virus
HBx	Hepatitis B virus protein X
HCMV	Human cytomegalovirus
HCV	Hepatitis C virus
HDAC	Histone deacetylase
HIF-1	Hypoxia inducible factor-1
HIV	Human immunodeficiency virus
HK	Hexokinase
HKMT	Histone lysine (K) methyltransferase
hpi	hours post-infection
HPV	Human papilloma virus
HSF-1	Heat shock transcription factor 1
HSV	Herpes simplex virus
HTLV-1	Human T-cell lymphotropic virus-1
ICP0	Infected cell protein 0
ICP27	Infected cell protein 27
IFN	Interferon
INK4	Inhibitor of cyclin dependent kinase 4
ITR	Inverted terminal repetitions

IV	Immature virion
KAT	Lysine (K) acetyltransferase
kbp	kilo base pair
KDM	Lysine demethylase
KEEG	Kyoto Encyclopedia of Genes and Genomes
KSHV	Kaposi's Sarcoma-associated herpesvirus
LB	Lysogeny broth
MAPK	Mitogen activated protein kinase
MEF	Mouse embryonic fibroblast
min	minute
miRISC	microRNA-induced silencing complex
miRNA	micro RNA
MOCV	Molluscum contagiosum virus
MOI	Multiplicity of infection
MPA	Mycophenolic acid
MPXV	Monkeypox virus
mRNA	messenger RNA
MV	Mature virion
MYXV	Myxoma virus
NIH	National Institute of Health
NTP	Nucleoside triphosphate
ORF	Open reading frame
PACR	Poxvirus Anaphase promoting complex (APC)/cyclosome regulator
PANTHER	Protein Analysis Through Evolutionary Relationships
PBS	Phosphate buffered saline
PCR	Polymerase chain reaction
PDC	Pyruvate dehydrogenase complex
PDH	Pyruvate dehydrogenase
PDK	Pyruvate dehydrogenase kinase
PET	Positron emission tomography

PFK-1	6-phosphofructokinase-1-kinase (phosphofructokinase-1)
PFK-2	the kinase activity of PFKFB
PFKFB	6-phosphofructo-2-kinase/ fructose-2,6-bisphosphatase
PFKL	Phosphofructokinase, liver
PFKM	Phosphofructokinase, muscle
PFKP	Phosphofructokinase, platelet
PHD2	prolyl-hydroxylase domain containing 2
PI	Propidium iodide
PI3K	Phosphatidylinositol 3-kinase
piRISC	PIWI-interacting RNA-induced silencing complex
piRNA	PIWI interacting RNA
PK	Pyruvate kinase
Plk1	Polo-like kinase 1
PPP	Pentose phosphate pathway
PTGS	Post-transcriptional gene silencing
qPCR	quantitative polymerase chain reaction
R1	Ribonucleotide reductase, large subunit
R2	Ribonucleotide redcutase, small subunit
RISC	RNA-induced silencing complex
RNA	Ribonucleic acid
RNAi	RNA interference
RNR	Ribonucleotide reductase
RRM1	Ribonucleotide reductase, large subunit
RRM2	Ribonucleotide reductase, small subunit
RT-PCR	Reverse transcriptase polymerase chain reaction
siRISC	small interfering RNA-induced silencing complex
siRNA	small interfering RNA
SOD1	Superoxide dismutase 1
SSMD	Strictly standardized mean difference
ssRNA	single-stranded RNA
TCA	Tricarobxylic acid cycle

TK	Thymidine kinase
TLR	Toll-like receptor
TNF	Tumor necrosis factor
UA	University of Alberta
UV	Ultraviolet (light)
VACV	Vaccinia virus
VACV-Cop	Vaccinia virus, Copenhagen strain
VACV-WR	Vaccinia virus, Western Reserve strain
VARV	Variola virus
VHL	von Hippel Lindau
Vpr	Virus protein R
WHO	World Health Organization
WV	Wrapped virion
YFP	Yellow fluorescent protein

CHAPTER 1: INTRODUCTION

1.1   Poxviruses

The family *Poxviridae* consists of large DNA viruses including variola virus (VARV), which is the causative agent of smallpox, one of the deadliest diseases in human history, and vaccinia virus (VACV), a virus responsible for the successful eradication of smallpox. Smallpox killed, blinded and disfigured countless numbers of people since at least the time of the Ancient Egyptians until it was stopped in the last quarter of the 20th century (1). The World Health Organization (WHO) implemented a successful worldwide vaccination campaign against smallpox using live VACV and declared the world free of smallpox in 1980 (2). In addition to that, VACV and other members of the *Poxviridae* family, such as myxoma virus (MYXV), have been used as models for advancing our knowledge in the fields of virology, immunology, molecular biology and cell biology. Furthermore, these viruses are currently being investigated as potential vectors for gene therapy and oncolytic agents for virotherapy of cancer (3, 4).

As obligate intracellular pathogens, poxviruses encode a large number of proteins that enable them to modulate various cellular processes to facilitate their replication. On the other hand, cells are also equipped with multiple antiviral mechanisms to prevent and control infection. This evolutionary struggle for dominance has resulted in a very extensive interaction between poxviruses and their cellular hosts at the molecular level (5). The primary aim of this PhD project has been to further our understanding of the interactions between poxviruses and their hosts. The studies carried out in this project identified a number of cellular factors that affect the replication of poxviruses using RNA interference (RNAi) technologies. Moreover, some of these factors, including glycolysis, the cell cycle control system and chromatin dynamics were studied in detail.

The first chapter of this thesis reviews our current understanding of the structure and replication of poxviruses as well as their public health importance and biomedical applications. Moreover, the mechanisms of RNAi and challenges associated with high throughput RNAi screens are explained in the chapter. Furthermore, various cellular processes and pathways that are relevant to the project are discussed in last sections of the first chapter.

1.1.1 Structure and replication of poxviruses

The family of poxviruses is divided into two major subfamilies based on their natural hosts (6, 7). *Chordopoxvirinae* encompasses viruses that infect vertebrates whereas *entomopoxvirinae* contains viruses that infect insects. The family also has a few unclassified members. Ten genera are included in the *chordopoxvirinae* subfamily. They include *avipoxvirus, capripoxvirus, cervidpoxvirus, crocodylidpoxvirus, leporipoxvirus, molluscipoxvirus, orthopoxvirus, parapoxvirus, suipoxvirus, and yatapoxvirus*. VARV and VACV belong to the genera of *orthopoxviruses* whereas MYXV is a member of *leporipoxviruses*. Since VACV is the most studied member of the *Poxviridae* family, the structure and replication of poxviruses discussed below is primarily based on studies conducted on VACV.

1.1.1.1 *Ultrastructural components of poxvirus virions*

Poxviruses are large enveloped viruses with a barrel or brick shaped non-symmetrical morphology **(Figure 1.1A and B)**. In the case of VACV, the virion has an approximate dimension of 360 × 270 × 250 nm, which makes it discernable via light microscopy (8). Poxviruses contain an internal core, a core wall, lateral bodies and surface envelope(s) **(Figure 1.1C)** (8). They are classified into two structural forms based

on their envelopes (7). The mature virion (MV) has a single lipid bilayer membrane (9). On the other hand, extracellular enveloped (EV) virion is essentially a MV surrounded by an additional lipid membrane resulting in two lipid bilayer membranes (10, 11). In addition to the difference in the number of envelopes, MV and EV also differ in the composition of the glycoproteins studded on the outer-most envelope (12). Moreover, certain proteins, such as A25 and A26, are present in the envelope of MV while they are absent in the inner envelope of EV (13, 14). Even though both MV and EV are infectious forms, MV is more abundant than EV.
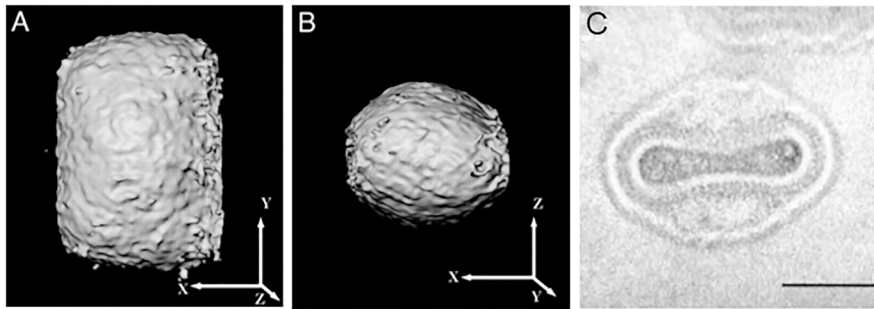
Figure 1.1.The structure of poxviruses. Poxviruses are brick (A) or barrel (B) shaped complex viruses. The ultrastructure (C) of the mature virion (MV) consists of a virion core surrounded by a core wall. The dumbbell shaped core contains the nucleoprotein complex and the transcription apparatus for early gene expression. Lateral bodies, whose composition and function is not clearly understood, occupy the concavities of the core on both sides. The MV is surrounded by a single lipid bilayer membrane. The images in (A) and (B) were taken from reference (8) with permission and they demonstrate volumetric representation of reconstructed virions from cryo-electron tomography images. Image (C) was taken from reference (9) with permission and it represents a transmission electron microscopy image of MV.

Poxviruses have a dumbbell-shaped core that is composed of a viral nucleoprotein complex, which includes the viral DNA, enzymes, transcription factors and nucleocapsid proteins (7, 15, 16). The core appears to be surrounded by a double-layered core wall

containing pore-like structures of unknown function (8, 17). Lateral bodies, whose composition and function are yet to be described, are situated at the concavities of the dumbbell-shaped core (16). Studies have identified at least 70 proteins associated with MV of VACV (17). Three of these proteins (A3, A4 and A12) are found in the core wall, 22 proteins are part of the nucleoprotein complex of the core and 20 proteins are envelope proteins (17-20). The function and localization of the remaining virion proteins are not known.

1.1.1.2 *Poxvirus genome organization*

Poxviruses have a linear double-stranded DNA genome ranging in length from 140 – 300 kilo base-pair (bp) (7). The two strands of the genome are connected by a hairpin loop structure at both ends **(Figure 1.2)** (21). Both the right and left terminal regions of the genome have homologous sequences that are oriented in opposite directions. These regions are termed inverted terminal repetitions (ITRs) and they contain a number of open reading frames (ORFs), the concatemer resolution sequence and multiple short repeated sequences in tandem **(Figure 1.2)** (22, 23). Most poxviruses contain more than 150 ORFs (24). VACV, for example, has around 200 ORFs (25) and MYXV has 171 ORFs (26). The ORFs are non-overlapping and intron-less (24). Around 50 genes are conserved in all poxviruses and close to 50 additional genes are conserved among members of the *chordopoxvirinae* subfamily (24, 27). Most of the conserved genes are located in the central regions of the genome and they are involved in crucial functions such as transcription, replication and assembly (24, 27, 28). In contrast, species-specific genes are located at the peripheries of the genome and they are involved in modulating host-functions.
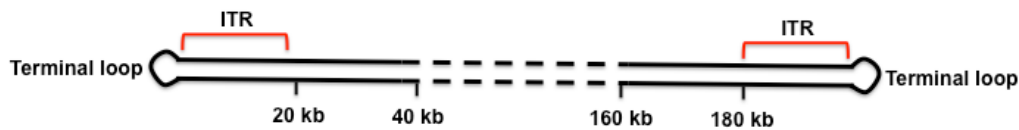
Figure 1.2. Poxvirus genome organization. Poxviruses have a linear double stranded DNA genome ranging in size from 140 – 300 kilo base pair (kbp). Their genomes have terminal loops connecting the two strands. Adjacent to the terminal loops, there are inverted terminal repetitions (ITRs), which have a few open reading frames and multiple short repeats in tandem. Figure is adapted with modification from reference (29).

1.1.1.3 The replication cycle of poxviruses

Poxviruses replicate exclusively in the cytoplasm of infected cells (7). And similar to any other virus, they utilize cellular systems and infrastructures, such as endocytosis, cytoskeleton and translation machinery, for their replication. However, what sets poxviruses apart from a number of other viruses is their dependence on their own proteins for genome replication and transcription. The basic components of the poxvirus replication cycle include entry, early gene expression, uncoating, DNA replication, late gene expression, assembly and egress **(Figure 1.3)** (29). Our understanding of the poxvirus replication cycle is primarily based on studies of VACV. In this section, the replication cycle of VACV is discussed and any known discrepancies observed in other poxviruses will be explained.

Entry: As mentioned above, MV and EV are two infectious forms of VACV that differ in the number of lipid bilayer membranes and the protein composition of their outer membranes. Although both MV and EV use plasma membrane fusion and endocytosis for entry, their entry mechanisms are not identical due to the differences described above

(30-33). In the case of MV, attachment to the plasma membrane is achieved using four VACV envelope proteins that bind to glyosaminoglycans and laminins (34-37). Following attachment, MV is internalized through endocytosis or membrane fusion **(Figure 1.3)**. During endocytosis, the virus is engulfed by an acidic endosome, and then the MV membrane fuses with that of the endosomal membrane (32, 38, 39). Both plasma and endosomal membrane fusion events lead to the release of virion components into the cytoplasm **(Figure 1.3)**. The mechanism of membrane fusion is not clearly understood, however, it is dependent on a 12-protein entry fusion complex (EFC) (30). Since the proteins that make the EFC are conserved in all species of poxviruses, it is possible that other members of the family also utilize similar mechanisms of entry (30). In the case of EV, both plasma membrane fusion and endocytosis are also used for entry. However, the outer membrane of EV is dissolved in the extracellular environment following attachment or in the endosome following endocytosis (40, 41). The inner membrane, which is similar to that of the MV membrane, fuses with the plasma membrane or endosomal membrane completing entry into the cytoplasm **(Figure 1.3)**. At this point, EV attachment proteins and the mechanism of EV outer membrane dissolution are not clearly known.

MYXV appears to prefer membrane fusion to endocytosis for entry into cells since low pH and chemical inhibition of macropinocytosis do not affect MYXV infection of cells (42).
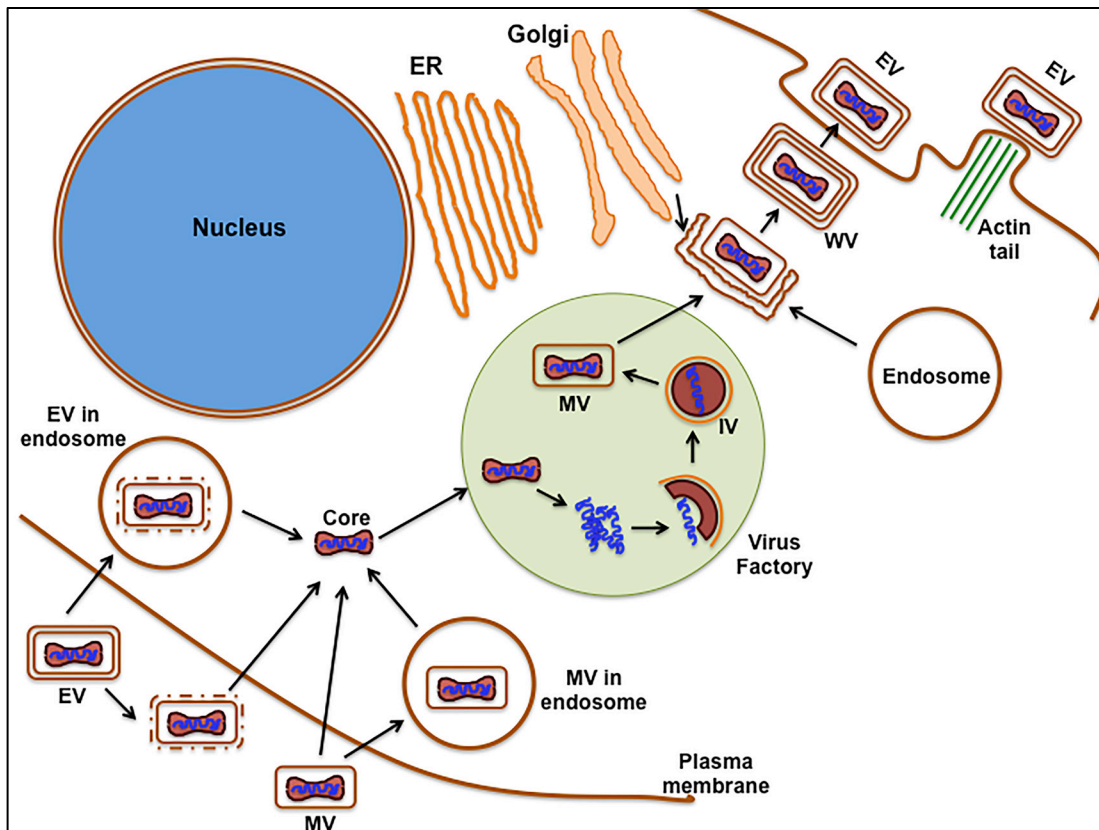
Figure 1.3. The replication cycle of VACV. The two infectious forms of VACV, mature virion (MV) and extracellular virion (EV) can enter cells either through membrane fusion or endocytosis. The outer membrane of EV is dissociated in the extracellular environment or inside endosomes. The inner membrane of EV or the membrane of MV fuse either with the plasma membrane or the endosomal membrane resulting in the release of the core into the cytoplasm. The core is then transported to the perinuclear region using microtubules and the viral genome uncoats after early gene expression. Next, DNA replication and intermediate and late gene expression occur in the virus factory. Virion assembly occurs in virus factory with the formation of crescents, which change into spherical immature virions (IVs) after incorporation of core proteins, viral DNA and the early transcription apparatus. Proteolytic processing of the core proteins leads to maturation of the IVs resulting in the formation of MVs. Most MVs are released through cell lysis. Some of the MVs obtain two additional membranes either from endosomes or the *trans*-Golgi and make wrapped virions (WVs). WVs are released through exocytosis losing their outer-most membranes. These released virions, now named EVs, are projected to and infect adjacent cells using actin tails. Figure is not drawn to scale and it is based on the descriptions and illustrations in (43).

Gene expression and uncoating: The gene expression system of poxviruses is temporally programmed (29, 44). There are three groups of viral genes based on the timing of their expression (44). Early genes are expressed prior to DNA replication and intermediate and late genes are expressed after DNA replication (7, 45). VACV has 118 early, 53 intermediate and 38 late genes (46). Consensus promoter sequences have been identified for each temporal class of genes.

Once the viral core is released into the cytoplasm, it is transported using the microtubule cytoskeletal system to the perinuclear region where a virus factory is established **(Figure 1.3)** (47, 48). The nucleoprotein complex at the core of VACV has all the enzymes and transcription factors required for the transcription of early genes including DNA-dependent RNA polymerase, poly(A) polymerase, topoisomerase, capping enzymes, and early transcription factors (49, 50). Early mRNAs are detected within 20 min of infection and they reach to peak levels around 100 min after infection (51). Early genes primarily encode for enzymes needed for DNA replication, intermediate transcription factors, growth factors and a number of proteins involved in immunomodulation.

The next event in the replication cycle is uncoating, which is the fragmentation of the virion core. Uncoating also signals the transition from early gene expression towards DNA replication. DNA replication is a necessary event for the expression of intermediate and late genes as inhibition of DNA replication leads to continuation of early gene expression but no intermediate and late gene expression (45). Intermediate genes, which are expressed after DNA replication, encode for transactivators of late gene transcription (51). Finally, late genes are transcribed and their mRNAs are usually detected after 140

min of infection with VACV and continue to increase for several hours after infection (51). Late genes encode for viral structural proteins and factors that are needed for early gene transcription. Most of the late gene products are assembled with the genome to make a progeny virion.

DNA replication: Poxviruses encode and express enzymes such as DNA polymerase, ligase, and topoisomerase, which are needed for replicating their DNA inside virus factories (25, 26). Moreover, various members of the *orthopoxvirus* genus express proteins and enzymes that are involved in the synthesis of deoxyribonucleoside triphosphates (dNTPs), such as ribonucleotide reductase (RNR) and thymidine kinase (TK), since cellular dNTP production is increased only during S-phase of the cell cycle in normal cells (52-54).

Despite our extensive understanding of the biology of poxviruses, we still do not exactly know how poxviruses replicate their DNA. Two models of DNA replication have been proposed based on currently available evidence **(Figure 1.4)**. The first one is semidiscontinuous DNA replication from a lagging strand using RNA primers and the second is a self-priming model of DNA replication (29). The first model is based on RNA oligomers that are used as primers by the viral DNA polymerase to generate discontinuous complementary DNA oligomers, which are joined together by ligase **(Figure 1.4)**. Evidence for the first model includes the presence of virus-encoded helicase-primase and ligase (55, 56). The second model is similar to the rolling hairpin model of parvovirus DNA replication (57, 58). In this model, a nick is inserted close to the hairpin sequences of the viral genome. Next, using self-priming, the viral polymerase replicates the hairpin structure, which then folds back to act as a primer. This process

results in a large multi-genomic concatemer DNA **(Figure 1.4)**. Following the expression of late genes, the concatemer is resolved into individual genomic DNAs by a Holliday junction endonuclease (resolvase), A22 in the case of VACV (59-61). However, the presence of nicks and the enzyme responsible for nicking the DNA are not identified. Despite the incompleteness of the evidences, it is possible that both models can be used for poxvirus DNA replication.
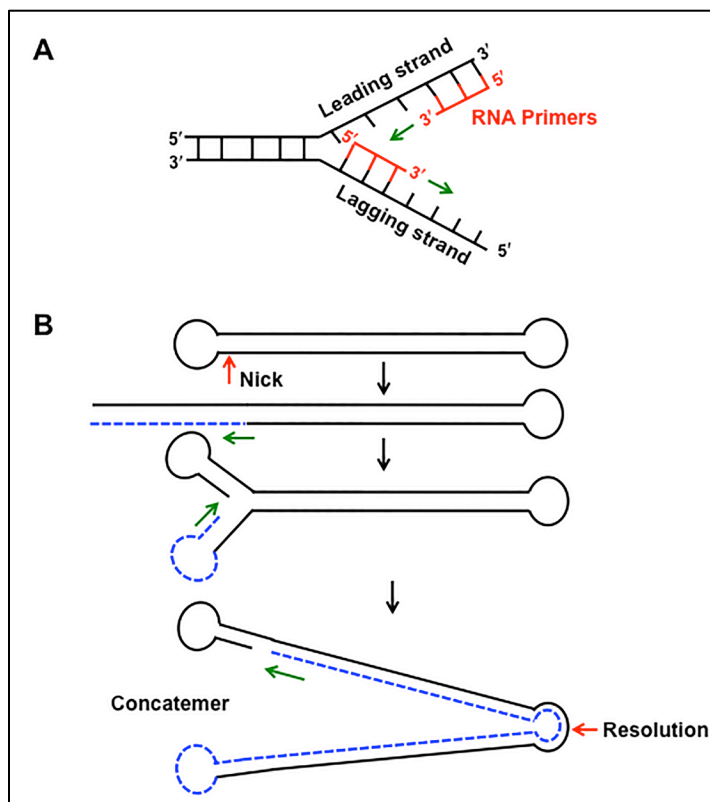
Figure 1.4. Poxvirus DNA replication models. (A) RNA primer-based semidiscontinuous replication model. In this model, RNA primers are synthesized by the viral primase alone or by making a heterodimer with cellular subunits. The primers are extended by the viral DNA polymerase in a semidiscouninous fashion. Then the discontinues strands will be joined by a viral ligase. (B) In the rolling hairpin model, a nick is inserted close to the viral inverted terminal repetition (ITR) region. Then using self-priming, the viral DNA polymerase synthesizes multi-genomic concatemers, which will be resolved later in the life cycle of the virus. Figure is adapted with modification from (29).

DNA replication typically starts 1 – 2 h after infection in the case of VACV, although variations exist based on the cell type and multiplicity of infection (MOI) (62). However, in other species of *Poxviridae* such as MYXV, it could take longer to start DNA replication since these viruses have longer replication cycles (63).

Assembly and release: Assembly of poxviruses begins with the formation of crescents in the virus factories **(Figure 1.3)** (29, 64-66). Each crescent has a single lipid bilayer membrane that is supported by a honeycomb lattice around the membrane formed by scaffolding proteins (9, 67, 68). In the case of VACV, the scaffold is derived from trimers of D13 (69). Although the origin of the membrane of the crescents has been debated for a long time, current evidence points to the endoplasmic reticulum (ER) as the source of the membrane (70). As the crescents grow and start to become spherical, they incorporate a granular material containing immature core proteins. Subsequently a nucleoprotein complex named nucleoid, which contains the viral DNA and the transcription apparatus, is inserted into the sphere before the spheres are sealed (29). At this point the sphere is named immature virion (IV) **(Figure 1.3).**

The transition from IV to MV is marked with the disassembly of the protein scaffold surrounding the lipid membrane (envelope) (71). Moreover, maturation also involves the proteolytic cleavage of certain core as well as membrane proteins (72). In most instances, the MVs are released when the infected cells are lysed. However, some of the MVs are wrapped with a double membrane derived from *trans*-Golgi or endosomes resulting in the formation of wrapped virion (WV), which has a total of three membranes **(Figure 1.3)** (73-75). WV is transported to the periphery of the cell using the cellular microtubule cytoskeleton and it is released by exocytosis (76, 77). During exocytosis the

outermost membrane of WV fuses with the plasma membrane leading to the formation of a virion with two membranes, the EV. The EV usually remains attached to the cell surface until it is directed to and infects an adjacent cell using actin projectiles that are formed by reorganization of the cortical actin beneath the plasma membrane **(Figure 1.3)** (78, 79). Similar actin projectiles are also formed in MYXV infected cells although their number is smaller than that of VACV infected cells (80). These actin projectiles facilitate cell-to-cell spread of EV. In some strains of VACV and certain species of poxviruses, such as fowlpox virus, EV is generated when the MV buds through the plasma membrane acquiring an addition membrane rather than through a WV intermediate (81, 82).

1.1.2   Use of poxviruses in health care and biomedical research

Our understanding of poxvirus biology and immunology has allowed us to exploit these viruses for clinical and biomedical applications. Poxviruses are being used as vectors for developing prophylactic and therapeutic vaccines as well as for gene therapy. They are also under investigation for oncolytic treatment of cancer. Moreover, poxviruses and their proteins play a crucial role as research tools in various biomedical disciplines.

1.1.2.1   Poxvirus-based vectors for vaccine development and cancer treatment

Several studies have been conducted to utilize VACV and other poxviruses for recombinant vaccine development and cancer treatment (83-85). Poxviruses are ideal vaccine vectors for a number of reasons including excellent coding potential and induction of potent humoral and cell mediated immunity (86-89). Clinical trials have been conducted using attenuated VACV strains and avipoxviruses (90) as vaccine vectors against human immunodeficiency virus (HIV) (91-93) and influenza virus (94). Poxvirus based therapeutic vaccines have also been tested for cancer treatment (95-97).

1.1.2.2 Oncolytic poxviruses

Advances in cancer care have improved survival rates for a number of cancers, however the rates have not increased to desired levels (98). As a result, various novel therapeutic approaches are being investigated. One of these new approaches is the use of live oncolytic viruses to selectively kill cancer cells (99). A number of viruses from different families have demonstrated oncolytic potential and there are several clinical trials being conducted. Notably, adenovirus has been approved in China for the treatment of head and neck tumors (100).

VACV and MYXV are candidate oncolytic viruses with antitumor potentials against brain (101, 102), pancreatic (103, 104) and breast cancer (105, 106) as well as leukemia (107, 108). Since VACV has a wide tropism and host range, most studies have been focused on increasing its specificity and selectivity. One of such approaches has been the generation of recombinant VACV strains that lack enzymes involved in dNTP synthesis, such as TK and RNR, to limit virus replication to cancer cells that have high dNTP pools (54, 109, 110). Studies have also focused on increasing the oncolytic efficiency of VACV by inserting foreign genes (111). JX-594, which is a recombinant VACV with deletions of its TK gene, encodes for a human granulocyte-macrophage colony stimulating factor (GM-CSF) and it is currently in clinical trials for the treatment of refractory cancers of various origins (112-114).

MYXV causes a fatal disease called myxomatosis in European rabbits and as a result it was used as a biological pest control method to reduce the large population of European rabbits in Australia and New Zealand in the late 1950s (115-117). MYXV is nonpathogenic to species other than lagomorphs including immunodeficient animals,

however it is able to selectively replicate in cancer cells both in culture and animal models (4, 117, 118). This selectivity is attributed to the prevalence of abnormalities in Akt and interferon (IFN) induction pathways in many cancer cells (119-121). This feature makes MYXV a very desirable oncolytic agent. However, there are a few hurdles in developing MYXV for clinical use. One of them is its reduced ability to disseminate to multiple tumor areas in animal models, which could potentially be improved by inserting a VACV actin remodeling F11 gene into its genome (80, 101, 122, 123). The other major hurdle in approving MYXV for clinical applications is the lack of prior large-scale human use like VACV. Investigators will be expected to demonstrate the safety of the virus with properly controlled clinical trials.

Some enzymes and proteins of poxviruses have been used as tools in biomedical research. The VACV DNA polymerase and its 3′-to-5′ proofreading exonuclease activity have been used to develop a simple and efficient method for cloning PCR products to vectors in a technology commercialized as In-Fusion® Cloning (124). Moreover, Topo cloning is a widely used cloning technology that utilizes VACV topoisomerase I (125).

1.1.3   Diseases caused by poxviruses and their threats on public health

Four genera of the *chordopoxvirinae* subfamily of poxviruses can infect humans (126). These include *orthopoxvirus, parapoxvirus, yatapoxvirus* and *molluscipoxvirus (126)*. Four species of the *orthopoxvirus* genus, including VARV, cowpox virus (CPXV), monkeypox virus (MPXV), and VACV, are human pathogens (127). VARV and molluscum contagiosum virus (MOCV) are the only poxvirus species that can solely infect humans, while the rest are zoonotic in nature with animal-to-human transmission. VACV is transmitted to humans in iatrogenic or laboratory-incident settings (128).

1.1.3.1 Human diseases of poxvirus origin

Smallpox, which is caused by VARV infection, is characterized by high-grade fever and widespread, painful mucocutaneous rash (129, 130). A severe form of the disease has a mortality rate in the range of 10% to 75% (126). Survivors of smallpox infection are usually severely scarred, blinded or both. In the second half of the 19th century, WHO used VACV, a virus with elusive origins (131), for a successful smallpox eradication campaign.

MPXV, a zoonotic infection prevalent in Central and West Africa, is the cause of a severe smallpox-like illness named human monkeypox with a mortality rate of ~16% (127, 132). Although the risk of human-to-human transmission is low, there is a concern that MPXV might mutate enhancing its transmission potential and resulting in epidemics.

Human CPXV and VACV infections result in benign lesions at the sites of inoculation, however they can cause severe systemic diseases in immunocompromised patients (126, 133-135). An outbreak of severe human and cattle disease caused by VACV-like virus was observed in South America in the last few years (136). MOCV causes a self-limited skin disease characterized by a benign solitary nodule (137).

1.1.3.2 Public health threats caused by poxviruses

Despite the successful eradiation of smallpox, VARV and other zoonotic poxviruses still pose a significant public health threat. Since the cessation of smallpox vaccination, susceptibility to orthopoxviruses, such as MPXV, has increased (138). There is a concern that adaptation of these orthopoxviruses in human populations, which currently have the lowest levels of immunity, could increase their virulence and might result in epidemics and pandemics similar to that of smallpox.

The other threat is the reemergence of smallpox. Even though there are only two officially known stocks of VARV in the USA and Russia, there is some doubt that all the stocks in other laboratories around the world were totally destroyed. An example for this is the discovery of forgotten vials containing live VARV at the National Institute of Health (NIH) laboratory in Bethesda, USA in 2014 (139). As a result there is a great concern that epidemics or even pandemics of smallpox can occur if such stocks are released accidently or fall in the wrong hands. A mathematical model predicted that infection of 1000 people with VARV could lead to a global pandemics in 180 days (140).

Because of these concerns scientists are urged to continue developing safe, effective, inexpensive and stable vaccines. Moreover, anti-poxvirus drug development efforts should be strengthened because only two drugs, cidofovir and ST-246, are currently undergoing clinical studies for treating poxvirus infections (29, 141-143).

1.2 RNA interference

For the first time in 1998, Fire *et al.* described the role of double-stranded RNA (dsRNA) in the regulation of gene expression (144). Prior to that, researchers demonstrated that experimental introduction of anti-sense RNA into cells was able to achieve modest suppression of gene expression (145-147). However, Fire *et al.* (1998) observed that delivery of dsRNA into cells achieved much more potent down regulation of gene expression than that of either sense or anti-sense single-stranded RNA (ssRNA) (144). Since then RNAi has been studied extensively and its various functions and molecular components have been described. Moreover, its potential has been exploited for biomedical research and therapeutics.

One of the greatest contributions of our knowledge of RNAi is the development of technologies to conduct loss-of-function studies at the genetic level and large-scale RNAi screens at the whole-genome level. These technologies have enabled us to decipher the functions of a number of unknown genes as well as to describe the genetic basis of various cellular phenotypes including diseases. Moreover, these technologies have also helped to describe virus-host interactions by identifying cellular proteins, processes and pathways that are important for the replication of various families of viruses.

In this section I will outline the mechanisms of RNAi as well as the benefits and challenges of large-scale RNAi screens. I will also briefly describe various RNAi screens performed to identify cellular factors that affect VACV replication.

1.2.1 Mechanisms of RNA interference

RNAi is an evolutionarily conserved process, which is involved in the regulation of gene expression (148, 149), chromatin modification (150, 151) and genome stability (152, 153) as well as inactivation of foreign nucleic acids (154, 155). The molecular mechanisms of RNAi described below are based on an excellent review by Ipsaro *et al.* (2015) (156). RNAi involves the silencing of gene expression using small dsRNA molecules that are generated from precursor RNA molecules. Following their generation, these small RNAs are loaded into effector complexes that achieve suppression of gene expression using various mechanisms. There are three small RNA species that are involved in RNAi: microRNA (miRNA), small interfering RNA (siRNA) and PIWI-interacting RNA (piRNA). These small RNA species can silence gene expression using one or both effector mechanisms of RNAi, which include post-transcriptional gene silencing (PTGS) and chromatin-dependent gene silencing (CDGS) (151). PTGS involves
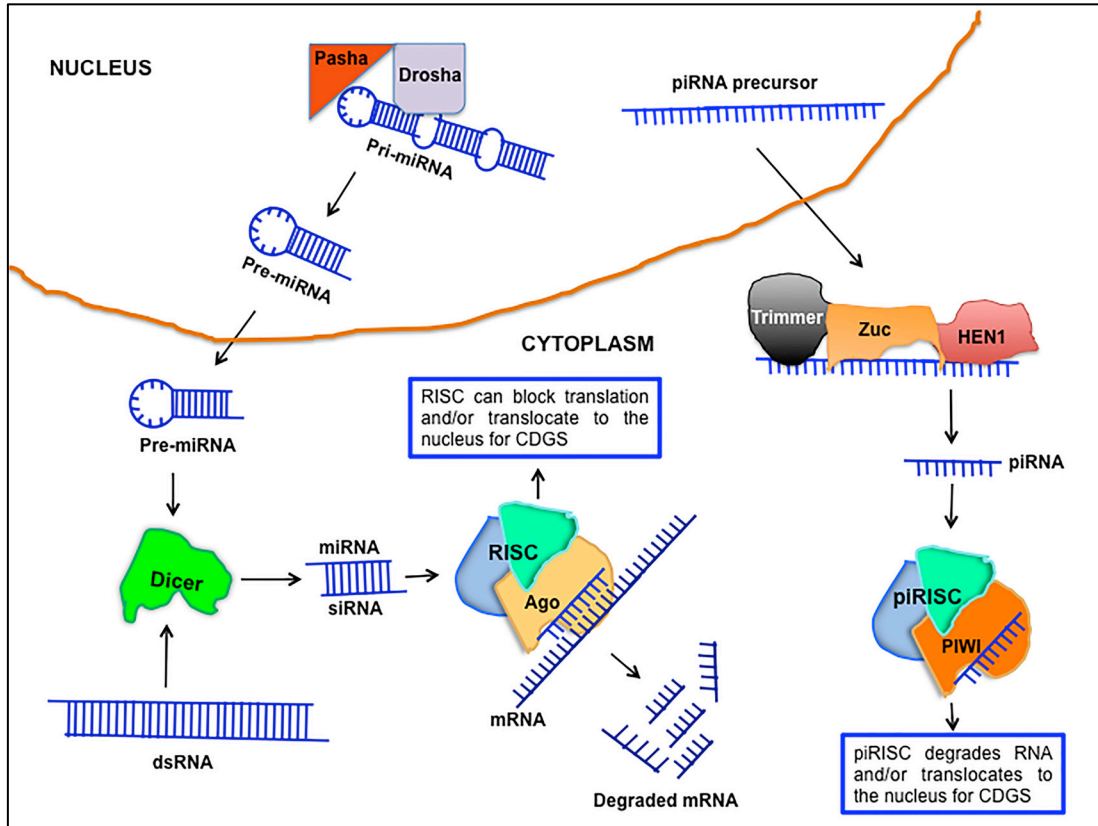
Figure 1.5. RNA interference pathways. Primary microRNAs (pri-miRNAs) are transcribed in the nucleus and they are processed by a microprocessor with RNAse III activity into pre-miRNAs. The microprocessor is a heterodimer of Drosha and Pasha. The pre-miRNAs are then exported to the nucleus and further processed by Dicer to make mature miRNAs. Similarly, long double-stranded RNAs (dsRNAs) of various origins are exported to the cytoplasm and get processed by Dicer to make endogenous short interfering RNAs (siRNAs). The guide strands of siRNA and miRNA duplexes are then loaded to the RNA-induced silencing complex (RISC) to make siRISC and miRISC, respectively. siRISC leads to slicing of complementary messenger RNA (mRNA) while miRISC causes mRNA degradation or translational block. Precursors of piRNAs are transcribed from piRNA cluster loci and exported to the cytoplasm where they are further processed by Zucchini, "Trimmer" and HEN1. The mature piRNAs are loaded to piRISC. piRISC can degrade mRNA, however, it primarily functions in the nucleus where it leads to silencing of transposons and repetitive sequences in the pericentromeric region using chromatin-dependent gene silencing (CDGS). siRISC and miRISC can also use CDGS. Figure is based on illustrations and description in reference (156).

degradation of messenger RNAs (mRNAs) and translational inhibition. In contrast, CDGS is a process of transcriptional or co-transcription silencing that uses epigenetic mechanisms, such as DNA and histone methylation. Both effector mechanisms utilized proteins that belong to the Argonaute family. The Argonaute family proteins are divided into three clades: Ago, PIWI and warm-specific ago (Wago) (reviewed in reference (157)). Argonaute family proteins have four domains: N-terminal, ZAP, MID and PIWI. ZAP and MID domains are involved in binding small RNAs and PIWI domain contains RNAse H-like activity that is needed for slicing of RNA molecules (158, 159).

miRNA: miRNAs are encoded by miRNA genes and they are transcribed in the nucleus to form 5′-capped and polyadenylated ssRNA precursors that fold and base-pair to generate dsRNA molecules with a hairpin structure **(Figure 1.5)** (160, 161). These dsRNA molecules are called primary miRNAs (pri-miRNAs). Pri-miRNAs are processed into smaller pre-miRNAs by a nuclear RNAse III-containing microprocessor (162). The microprocessor is a heterodimer complex of DGCR8 (Pasha) and Drosha, which is an RNAase III protein (163, 164). The pre-miRNAs are then exported to the cytoplasm using exportin 5 where they are further processed by Dicer, which is also an RNAse III, to make mature miRNAs that are 21-25-nt in length **(Figure 1.5)** (165-167).

The miRNA duplex then divides into passenger and guide strands and the guide strand is loaded into Ago protein-containing RNA interference silencing complex (RISC) to form miRISC **(Figure 1.5)** (168). miRISC binds complementary mRNA molecules and slices them using the RNAase H-like activity of Ago (169, 170). Moreover, the complex also recruits GW182 proteins that are involved in non-slicing mechanisms of gene silencing, which include mRNA decapping and degradation as well as translational

inhibition (171-173). Since miRNAs are not perfectly complementary to their target mRNAs, non-slicing mechanisms of silencing are more potent than slicing of mRNAs (156, 174, 175).

siRNA: the precursors of endogenous siRNAs are generated by various mechanisms including transcription of inverted repeats and transposons as well as bidirectional transcription (176-179). Once these dsRNA precursors are generated they are exported to the cytoplasm to be processed by dicer in the same way as miRNAs **(Figure 1.5)** (180, 181). Then their guide strands are loaded to Ago dependent RISC complexes to make siRISC (181). Mature siRNAs, which are ~21-nt in length, make a perfect base pair with their complementary mRNAs, which makes them efficient in silencing gene expression through slicing of target mRNAs (156, 182).

piRNA: the pericentromeric heterochromatin region of the genome contains repetitive DNA sequences and transposon elements. This region is also enriched with clusters of piRNA loci, which are transcribed to make ssRNA precursors of piRNAs (183, 184). These ssRNA precursors are exported to the cytoplasm and they are processed by an endonuclease called Zucchini (Zuc) and a mysterious exonuclease named "Trimmer" (156, 185-187). 2′-O-methylation of the 3′-end of the RNA is carried out by HEN1 (188). The mature piRNA, which is 26-31-nt in length, is then loaded to a PIWI containing effector complex named piRISC **(Figure 1.5)** (156). piRISC is able to slice complementary RNA targets, however, its effector mechanisms primarily involve translocation to the nucleus where it binds nascent complementary RNA transcripts at the site of transcription leading to recruitment of chromatin-modifying complexes and the formation of repressive heterochromatin (189-192).

1.2.2 High-throughput RNAi screens: methods and challenges

RNAi based silencing mechanisms have been used to conduct loss-of-function studies through sequence-specific knockdown of genes both in culture and whole organisms. Most importantly, the development of high-throughput genome-scale RNAi screening technologies has transformed biomedical research and led to the identification of a number of new intracellular pathways, gene functions, host-pathogen interactions and drug targets (193).

RNAi mediated loss-of-function studies begin with the generation of RNAi reagents, such as mature siRNAs or siRNA precursors that can be introduced into cells. In most cases, generation of these RNAi reagents involves identification of target sequences inside mRNA of interest, which can be performed by using bioinformatics tools (194). Once target sequences are identified, mature or precursor siRNA duplexes are synthesized. Mature siRNAs are generally synthesized as 21-mer duplexes and they are able to induce RNAi in mammalian cells without provoking IFN response (195).

siRNA precursors can be generated in various forms. Dicer substrate siRNAs (D-siRNAs) are siRNA precursors that are longer and more potent than the conventional 21-mer siRNAs (196, 197). Unlike siRNAs, which are directly loaded into the RISC complex, D-siRNAs are processed by Dicer before they are loaded in to the silencing complex.

Short hairpin RNAs (shRNAs) are plasmid encoded siRNA precursors that are expressed and processed into mature siRNAs in transfected cells. shRNAs can be passed to daughter cells during mitosis and they can be used to achieve more stable and prolonged suppression of target genes (198). Moreover, controlled expression of shRNAs

could be achieved using inducible gene expression systems such as tetracycline-controlled transcription (199). shRNAs can also be inserted in lentiviral vectors for efficient delivery and expression (200).

Endonuclease-prepared siRNAs (esiRNAs) are small RNA fragments generated by RNAse III digestion of dsRNA *in vitro* (201, 202). The dsRNA is generated by polymerase chain reaction (PCR) from a complementary DNA (cDNA), which is reverse transcribed from mRNA of interest. esiRNAs reduce off-target effect, which is a common challenge in RNAi experiments (203).

There are a number of ways to deliver these RNAi reagents into cells. The most common method is using cationic lipid-based transfection reagents for siRNA, esiRNA and shRNA delivery (204, 205). As mentioned above, shRNAs could also be inserted into viral vectors and can be transduced into cells (200). In smaller animals such as *Caenorhabditis elegans,* long dsRNAs could be introduced into cells by microinjection; moreover, they can also be delivered to live organisms by feeding them on dsRNA expressing *Escherichia coli* (144, 206).

Using the aforementioned RNAi reagents, a number of genome-scale and sub-genomic (e.g. kinases, phosphatases and druggable genome) RNAi libraries have been developed for various species including *Homo sapiens* and *Mus musculus* and they were used to perform hundreds of high-throughput RNAi screens (193). Due to differences in the efficiency of individual siRNAs/shRNAs in silencing a particular gene as well as having off-target effects, these libraries include multiple siRNAs/shRNAs in arrayed or pooled formats to target a single gene. In the arrayed format, multiple siRNAs/shRNAs are used independently to silence a single gene whereas in the pooled format, the

siRNAs/shRNAs are pooled together. Pooled formats have been shown to have a better silencing efficiency than arrayed formats (207). Most RNAi library reagents are available in 96- or 384-well plates.

Most high-throughput RNAi screens involve common steps, including selection of the RNAi library and appropriate cell lines, generation of a measurable phenotype or reporter system, selection and optimization of transfection settings including transfection reagents, siRNA concentrations and appropriate positive and negative controls (208, 209). Next, small-scale pilot screens are usually performed to optimize all the necessary settings for a high quality RNAi screen before embarking on large-scale screens (208). That is then followed by a primary screen, which is usually performed in duplicates or triplicates to reduce false positive and false negative rates (209). Some researchers prefer to replicate the screen in a different cell line or using a different reporter system. After applying robust quality control, data normalization and data analysis methods on the results of the primary screens, hits are selected. It is also a common practice to perform a small-scale secondary screen including the hits and other genes of interest (209). Finally, the hits need to be validated.

Validation of the results of high-throughput screens is important because of the abundance of both false-positive and false-negative results associated with RNAi screens. RNAi screens particularly show high false positive rates due to off-target effects of siRNAs/shRNAs used in the screens (210). Off-target effects usually occur when siRNA/shRNA targets mRNAs other than the one it is designed to target. This happens when exogenous siRNAs/shRNAs act like miRNAs and target mRNAs through conservative complementarity seeding rather than through perfect base paring (211).

False positives can also include hits that have critical functions in a number of cellular processes, such as the proteasome, and are detected through their indirect effect on the phenotype being studied (212). High false discovery rate is suggested to be one of the factors responsible for the modest level of hit-overlap observed in related RNAi screens.

A number of techniques could be used to validate hits and minimize false discovery rates including "redundancy", "rescue", the C911 method and the newer genetic-engineering methods (193, 213). The "redundancy" method involves increasing the number of independent siRNAs/shRNAs to minimize the rate of off-target silencing (213). This method is most appropriate for large-scale screens and it can be achieved by using a library containing siRANs/shRNAs that are independently designed and different in sequence compared to those used in the primary screen. The second method involves rescuing a phenotype by inducing RNAi-resistant mRNA, which has silent mutations in the target region to prevent perfect base pairing or a homologous mRNA from a closely related species with a different sequence (193, 214). The RNAi-resistant mRNA fails to rescue a phenotype if it is due to an off-target effect. The third method is the C911 test where a new set of siRNA/shRNA, which is similar to the original siRNA/shRNA except mutations in nucleotides 9-11, is generated and tested (215). The new siRNA/shRNA continues to target off-target mRNAs through seed complementarity of nucleotides 2-8, however, it is not able to degrade an on-target mRNA. Novel methods of genome-editing and -engineering, such as CRISPR-cas9 systems, can also be used for validation of positive results and follow up studies (193).

Following validation of hits, the last step in RNAi screens is analysis of hits by categorizing them into various functional groups based on intracellular localization,

biological function, intracellular pathways and clinical disorders. There are a number of bioinformatics tools that can be utilized for this purpose including NIH's DAVID (database for annotation, visualization and integrated discovery) (216, 217), PANTHER (protein analysis through evolutionary relationships) (218, 219) and COMPLEAT (protein complex enrichment analysis tool) (220). Pathway and protein complex enrichment is crucial not only to characterize important pathways and protein complexes, but also to identify potential false negatives (193). When a specific pathway is enriched with validated hits, further examination of the remaining members of the pathway may enable to identify false negatives.

1.2.3 RNAi screens for identification of host factors that modulate virus replication: a focus on RNAi screens involving VACV

High throughput RNAi screens have been used to identify a number of cellular factors, pathways and functional groups that positively or negatively affect the replication of various classes of viruses. Researchers have conducted these screens to further our understanding of host-pathogen interactions as well as to identify possible antiviral drug targets. Some of the most studied viruses using RNAi screens include HIV (221-223), influenza virus (224-227), hepatitis C virus (HCV) (228-230) and VACV (231-236).

Even though each of these studies identified validated novel genes that are dependency factors for the various tested viruses, the overall overlap of the hits at gene level was only modest. This was exemplified by a meta-analysis of nine genome-wide RNAi screens for HIV replication where the overlap rate between any two screens was <7% (237). Similarly, ~10% overlap was observed among any two of the seven screens performed by various groups to identify host factors required for the replication of

influenza virus (238). The reasons for the low overlap rates include high false discovery rates as well as differences in cell types, reagents and reporter methods used in the screens. Despite the low levels of hit overlap between related screens at the gene level, high level of overlap was observed for pathways and protein complexes as shown by meta-analysis of both HIV and Influenza virus screens (223, 239).

Three large-scale siRNA screens were performed in HeLa cells to identify host factors that influence VACV virus replication **(Table 1.1)**. The first screen was performed by Mercer, J. *et al.* (2012) and used a human druggable genome library targeting 7000 genes (234). In the screen, HeLa cells were infected with VACV-EGFP, a recombinant VACV that expresses enhanced green fluorescent protein (EGFP) under the synthetic early/late promoter. Fluorescence imaging was performed after 8 h of infection. Analysis of the results of the screen identified 188 genes that reduced virus replication when silenced. Further examination revealed the role of the ubiquitin-proteasome system in uncoating and initiation of DNA replication.

Sivan, G. *et al.* (2013) performed a whole human genome siRNA screen (~21500 genes) and identified 576 and 530 pro- and antiviral genes, respectively **(Table 1.1)** (231). The screen was performed in HeLa cells using an IHD-J/GFP strain of VACV. GFP fluorescence was determined 18 h after infection to measure virus replication and spread. Pathway enrichment analysis of the results found that translation, ubiquitin-proteasome and ER-to-Golgi transport systems were enriched with proviral genes. In addition to that, several nuclear pore proteins including Nup62 were observed to play a role in virus morphogenesis.

Table 1.1. RNAi screens performed to identify host factors that affect VACV replication.

Host	VACV Strain	Phenotype	Library	Pro-viral	Anti-viral	Notable Finding	Ref.
Drosophila (DL1)	VACV-*lacZ*	Immunofluorescence microscopy at 48 hpi	Kinome dsRNA (~440)	8	-	AMPK plays a role in virus entry	(236)
Human (HeLa)	VACV-EGFP	Fluorescence microscopy at 8 hpi	Druggable siRNA (7000)	188	-	Cullin3 –based ubiquitin ligase and proteasome needed for uncoating and DNA replication	(234)
Human (HeLa)	IHD-J/GFP	Fluorescence microscopy at 18 hpi	Whole-Genome siRNA (~21,500)	576	530	Nup62 is required for vrial morphogenesis	(231)
Human (HeLa)	VACV-WR (A5-GFP)	Fluorescence microscopy at 48 hpi	Druggable siRNA (6719)	153	149	DNA damage and repair pathways have antiviral effect	(233)
Human (A549)	VACV-A4-Venus YFP	1° screen-FACS followed by Deep seq at 12 hpi 2° screen-Fluorescence at 20 hpi	Whole-genome pooled-cell lentiviral shRNA (>17,000)	34	-	Heat shock factor 1 plays proviral role	(235)

FACS=Flow cytomery assisted cell sorting, GFP=Green fluorescent protein, EGFP=Enhanced GFP, YFP=Yellow fluorescent protein, AMPK=Adenosine monophosphate activated kinase, hpi=hours post infection

The third screen performed by Beard, PM. *et al.* (2014) used siRNA libraries of the human druggable genome (6719) and identified 153 proviral and 149 antiviral genes by infecting HeLa cells with the Western Reserve (WR) strain of VACV that expresses a GFP tagged A5 protein (233). Fluorescence microscopy was performed 48 h post infection. The screen identified previously known proviral proteins, such as adenosine

monophosphate – activated kinase (AMPK) and proteins of the translation machinery as well as novel antiviral processes, such as the cellular DNA damage response pathways.

Comparison of the above screens was also performed by Beard, PM. *et al.* (2014) and indicated no overlap between the three screens at the gene level. However, pairwise comparisons showed 1.3% to 8.7% overlap. These findings are similar to that of the HIV and influenza screens mentioned above. Despite these low levels of gene overlaps, pathway overlaps between the screens were common.

A stringently validated RNAi screen was performed by Filone, CM. *et al.* (2014), where pooled-cell lentiviral shRNA library targeting more than 17,000 human genes was used **(Table 1.1)** (235). Using a recombinant VACV that expresses Venus yellow fluorescent protein tagged A4, the researchers identified 34 validated proviral hits. Their subsequent studies demonstrated the proviral role of heat shock factor 1 (HSF1) during VACV infection. They demonstrated that during VACV infection HSF1 is phosphorylated and translocated to the nucleus leading to up regulation of its target genes (235). In addition to the above RNAi screens in human cells, a kinome screen in Drosophila cells identified the role of AMPK in VACV entry through modulation of actin dynamics **(Table 1.1)** (236).

In contrast to the screens described above where siRNAs/shRNAs were used to target host genes, an RNAi screen was performed using siRNAs that target VACV genes. In this screen, 80 VACV early genes were targeted with 3 independent siRNAs in a high throughput format (240). The screen was performed using a recombinant VACV that expresses EGFP under early or intermediate VACV promoter (240). The screen identified

that a previously described VACV protein, D5 (a viral helicase/primase), plays a crucial role in virus uncoating.

Even though the current methods used in RNAi screens need further optimization to reduce false discovery rates and to increase concordance between similar screens, high throughput RNAi screens have helped to advance our knowledge of virus-host interactions through the discovery of novel proteins and pathways that modulate virus replication as described above. Based on this fact, my colleagues and I performed a genome-scale RNAi screen and identified a number of cellular factors that affect the replication of MYXV in human cells. To my knowledge this is the only published RNAi screen for MYXV to date. The experimental methods and the results of our screen will be discussed in the next chapters.

1.3   Virus-host interactions

As obligate intracellular pathogens, the replication of viruses is dependent on various cellular infrastructures. These infrastructures include the translation machinery, the proteasome, the cytoskeleton and its molecular motors as well as the cargo-transport systems. In addition to these, a number of viruses use lipid bilayer membranes originating from several intracellular organelles including the ER, Golgi apparatus, endo-lysosomes and the plasma membrane to demarcate their intracellular replication sites as well as to generate their envelopes. Eukaryotes, on the other hand, have evolutionarily acquired multiple antiviral mechanisms to mitigate infection with viruses. As a result, the successful replication of a virus requires not only the ability to manipulate and utilize cellular infrastructures but also the capacity to circumvent these antiviral mechanisms.

Consequently, the process of co-evolution has resulted in an elaborate network of interactions between viruses and their hosts.

Poxviruses replicate in the cytoplasm and they encode most of the enzymes they need for genome replication and gene expression. However, their successful replication and spread depends on their ability to modulate a wide variety of cellular processes and systems including those mentioned above. Poxviruses are also master modulators of both the innate and adaptive immunity. For example, some species of the *chordopoxvirinae* subfamily of poxviruses utilize decoy cytokine and chemokine receptors (viroceptors), such as IFN-α/β/γ viroceptors, to block activation of the immune system (reviewed in (241)).

Various families of poxviruses also produce a number of anti-apoptotic proteins to inhibit infected cells from undergoing apoptosis (242). Moreover, poxviruses also interact with and activate pro-survival pathways, such as mitogen activated protein kinase (MAPK) and phosphatidylinositol 3-kinase (PI3K)/Akt pathways (243, 244).

These interactions are better understood for some species of the poxvirus family, such as VACV, while they are not well understood in the other species. Moreover, given the large number of proteins that poxviruses encode, it is very likely that several novel interactions remain to be discovered.

To further our understanding of poxvirus-host interactions, we performed sub-genomic and genome-wide RNAi screens and identified more than one thousand candidate genes and a number of previously known and unknown pathways that affect the replication of MYXV. Among the top pathway-hits of the screen are glycolysis and the cell cycle control system. Further analysis and study of these pathways demonstrated

that MYXV replication is enhanced by increasing glycolytic activity as well as by arresting cells at G1-phase of the cell cycle. Moreover, I also studied the interaction between the cellular chromatin system and poxviruses with a focus on VACV. In the next sections I will briefly describe glycolysis, the cell cycle control system and the cellular chromatin system and give examples on how viruses including poxviruses interact with these processes. The results of my studies will be presented in chapters 3, 4 and 5.

1.3.1 Interaction between viruses and cellular energy metabolism

Mammalian cells have a complex network of interdependent metabolic pathways, such as glycolysis, tricarboxylic acid (TCA) cycle (Kreb's cycle), pentose phosphate pathway, nucleotide synthesis pathways, β-oxidation of fatty acids and the urea cycle. These pathways function to produce energy in the form of ATP and to generate substrates for various cellular processes. Hereditary or acquired abnormalities of enzymes or regulatory processes of metabolism are involved in the pathogenesis of various disorders. For example, abnormalities in glycolysis and fatty acid synthesis pathways have been implicated in the pathogenesis of cancer (245-248).

The interaction between viruses and cellular energy metabolic pathways has been a strong area of research for a number of decades. Researchers have been interested in determining how various cellular metabolic states affect virus replication as well as how viruses modulate cellular energy metabolism. The pace of such studies has been accelerated in the last decade due to advances in metabolomics and carbon flux studies (249).

Using metabolomics, it is currently possible to determine the metabolic signature of cells during virus infection by simultaneously measuring the levels of diverse

metabolites. Moreover, the contribution of substrates, such as glucose and glutamine, to pathways and metabolites can be determined using carbon flux studies, which utilize radioactive carbon-tagged substrates. Furthermore, the role of different metabolic states on virus infection have been studied using routine chemical inhibitor, gene knockdown and over-expression studies. Metabolic reprograming events associated with infection with viruses, such as VACV, herpes simplex virus (HSV), human cytomegalovirus (HCMV), Kaposi's sarcoma-associated herpes virus (KSHV), HIV, Hepatitis C virus (HCV), adenovirus and influenza have been determined using these methods. In general, the studies have discovered the three most commonly reprogramed metabolic pathways during virus infection: aerobic glycolysis, glutaminolysis and fatty acid synthesis (250). These studies have been recently reviewed in reference (250).

In the next section, glycolysis and its inputs to several metabolic processes will be discussed. Moreover, a brief review of the interaction between glycolysis and various virus families will be presented.

1.3.1.1   *Glycolysis*

Glycolysis and its rate limiting steps: Glycolysis is a metabolic pathway, which converts glucose to pyruvate with a net production of two ATP molecules from a single molecule of glucose (251). After entry into cells through glucose transporters (GLUTs), glucose is phosphorylated by hexokinases (HKs) and then it is converted to pyruvate by a series of chemical reactions **(Figure 1.6)** (251). Glycolysis has three irreversible reactions, which are targets of major regulatory processes (251). The enzymes that catalyze these reactions include HK, 6-phosphofructo-1-kinase (PFK-1) and pyruvate kinase (PK) **(Figure 1.6)**.
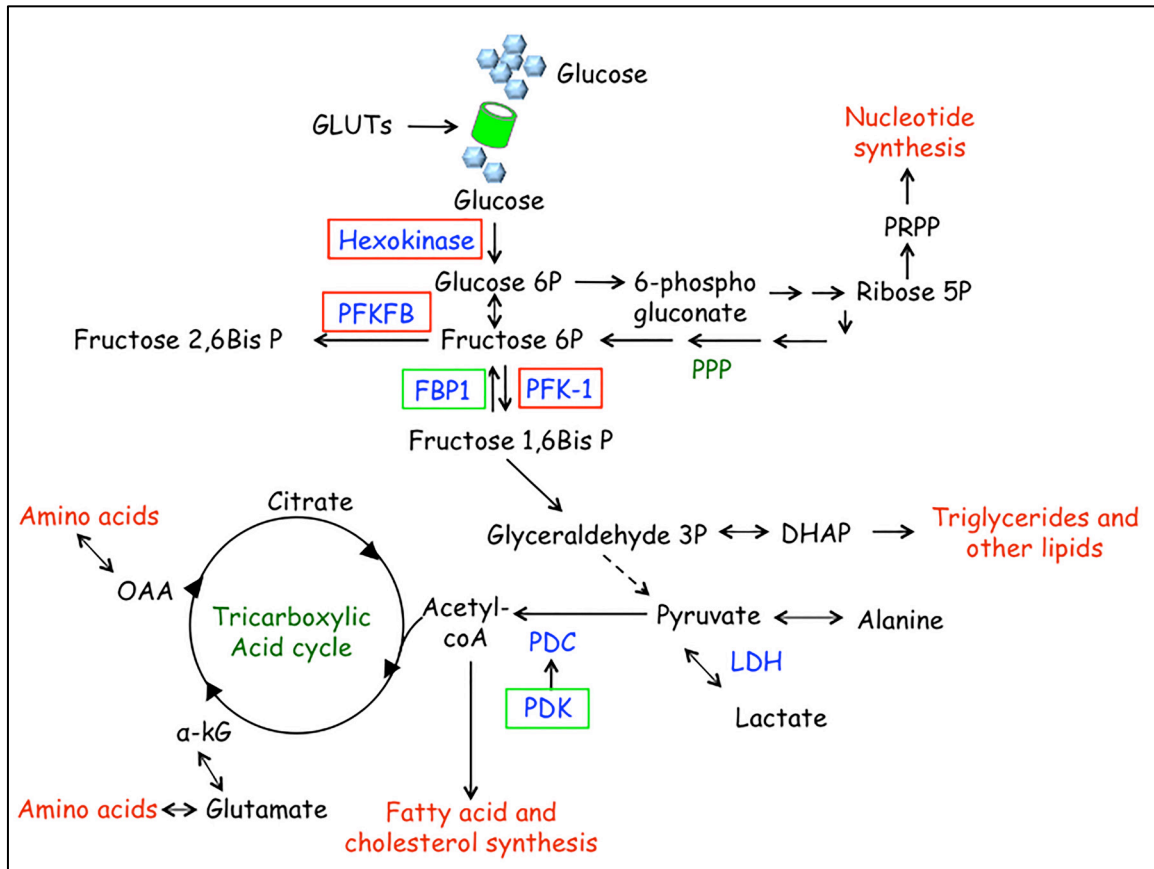
Figure 1.6. Glycolysis and other cellular energy metabolic pathways. Glucose enters cells through glucose transporters (GLUTs) and it is phosphorylated by hexokinases to produce glucose-6-phosphate (Glucose 6P), which isomerizes to fructose-6-phosphate (Fructose 6P). Fructose 6P can be further phosphorylated by either 6-phosphofructo-1-kinase (PFK-1) to give rise to fructose-1,6-bisphosphate (F1,6BP) or by 6-phosphofructose-2-kinase/fructose-2,6-bisphosphatase (PFKFB) to give rise to fructose-2,6-bisphosphate (F2,6BP). The rate-limiting step of glycolysis is catalyzed by PFK-1. F2,6BP is a potent allosteric activator of PFK-1. F1,6BP is converted to pyruvate through a series of chemical reactions. Pyruvate, in the presence of abundant oxygen, is decarboxylated by pyruvate dehydrogenase complex (PDC) to acetyl-CoA, which is a substrate for the tricarboxylic acid (TCA) cycle or fatty acid and cholesterol synthesis. In anaerobic settings, pyruvate is converted to lactate through lactate dehydrogenase (LDH) and PDC is inhibited by pyruvate dehydrogenase kinase (PDK). Glycolytic intermediates can be used for nucleotide and amino acid synthesis. Red and green boxes indicate subunits, isoforms or single proteins encoded by proviral and antiviral genes, respectively, identified by our RNAi screens (Chapters 3 and 4). PPP, pentose phosphate pathway. OAA, oxaloacetic acid. α-KG, α-ketoglutarate. PRPP, 5-P-α-D-ribosyl 1-pyrophosphate. Figure is based on descriptions in (252).

33

The rate limiting step of glycolysis is the conversion of fructose-6-phosphate (F6P) to fructose-1,6-bisphosphate (F1,6BP), which is catalyzed by PFK-1 (253, 254). There are three isoforms of PFK-1: liver (PFKL), muscle (PFKM) and platelet (PFKP). PFKL is the most catalytically active isoform (255). Fructose-2,6-bisphosphate (F2,6BP), which is a phosphorylation product of F6P through the kinase activity of 6-phosphofructo-2-kinase/fructose-2,6-bisphosphatase (PFKFB), is a potent allosteric activator of PFK-1 (256-258). PFKFB is a bifunctional enzyme with four isoforms (PFKFB 1-4) encoded by different genes. The kinase activity of PFKFB is termed PFK-2.

Aerobic glycolysis: In the presence of abundant oxygen in normal mammalian cells, glycolysis-derived pyruvate is converted to acetyl-CoA and joins the TCA cycle and oxidative phosphorylation to produce large amounts of ATP. As the production of ATP increases, oxygen acts as a negative regulator and decreases the activity of glycolysis (259, 260). However, in oxygen deprived anaerobic states, pyruvate is fermented to lactate, which then is recycled to make more glucose in a process called gluconeogenesis (261). Most cancer cells, on the other hand, have a high rate of glycolysis and they convert the resulting pyruvate into lactate even in the presence of abundant oxygen (260, 262, 263). This phenomenon, which was first described by Otto Warburg, is termed aerobic glycolysis or ''the Warburg effect'' (264). Cancer cells express markedly elevated levels of glycolytic enzymes such as PFKFB and have high concentration of F2,6BP, which results in increased activity of PFK-1 (265-267). Studies have also showed that other rapidly proliferating cells, such as lymphocytes, demonstrate aerobic glycolysis (268, 269).

Glycolytic intermediates: The intermediate metabolites of glycolysis are utilized in various metabolic pathways that generate nucleotides, lipids and amino acids. The glycolytic intermediate glucose-6-phosphate (G6P) is used as a substrate for the pentose phosphate pathway, which produces metabolites such as ribose-5-phosphate for nucleotide synthesis as well as reduced nicotinamide adenine dinucleotide phosphate (NADPH) for lipid synthesis **(Figure 1.6)** (270, 271). Moreover, intermediates of glycolysis, such as dihydroacetone phosphate and 3-phosphoglycerate, as well as acetyl-CoA are utilized for lipid synthesis **(Figure 1.6)**. Furthermore, 3-phosphoglycerate can be used to synthesize amino acids such as serine, cysteine and glycine while pyruvate can be utilized to produce alanine. It is suggested that the reason why rapidly proliferating cells up-regulate their glycolytic activity, despite the presence of abundant oxygen, is to produce precursors that are needed for the production of macromolecules (252).

Regulation of glycolysis: Hypoxia inducible factor-1 (HIF-1), a heterodimer of HIF-1α and HIF-1β, is a major regulator of glycolysis (272, 273). In normoxic conditions, the oxygen sensing enzyme prolyl-hydroxylase domain containing 2 (PHD2) is active and it hydroxylates two proline residues of HIF-1α (274, 275). This leads to von Hippel-Lindau (VHL)-mediated ubiquitination and degradation of HIF-1α (274, 275). However, in hypoxic conditions, PHD2 is inactive and HIF-1α remains stable, binds HIF-1β and translocates to the nucleus (276, 277). HIF-1 leads to transcriptional up-regulation of glucose transporters and glycolytic enzymes (278, 279). HIF-1 also increases the conversion of pyruvate to lactate by up-regulating the expression of pyruvate dehydrogenase kinase (PDK), which inactivates pyruvate dehydrogenase

complex (PDC) through phosphorylation (280). PDC catalyzes the conversion of pyruvate to acetyl-CoA **(Figure 1.6)**.

The PI3K/Akt pathway is another major regulator of glycolysis. PI3K/Akt promotes glycolytic activity through phosphorylation and activation of PFKFB (PFK-2) (281), increased expression and membrane translocation of GLUTs (282), phosphorylation and inactivation of FoxO (283), a major suppressant of glycolytic gene expression, and also through increased activity of HIF-1 (284, 285).

Myc also plays a role in the activation of glycolysis by up-regulating the expression of GLUTs and glycolytic enzymes including PFK-1 (286, 287). On the other hand, p53 activation down regulates the glycolytic activity of cells through the expression of p53 inducible gene, TP53-induced glycolysis and apoptosis regulator (TIGAR), which leads to reduced production of F2,6BP, a major allosteric activator of PFK-1 (288, 289).

1.3.1.2 *Viral modulation of glycolysis and other energy metabolic pathways*

Scientists have made important observations and discoveries by studying the interaction between viruses and cellular energy metabolic pathways for more than half a century. These discoveries have been accelerating in the last decade because of advances in metabolomics, as mentioned above. Some of these studies have identified important antiviral drug targets. Most of the progress in this regard has been recently reviewed in reference (250).

Herpesviruses are among the most studied viruses for their interaction with cellular energy metabolism. In fact, the first comprehensive metabolomic study for virus infection was conducted for human cytomegalovirus (HCMV) by Munger *et al*. (2006) (290). HCMV infection increases glycolytic flux as evidenced by increased glucose

uptake, up-regulated expression of GLUTs and key glycolytic enzymes, such as PFK-1, as well as increased glycolytic metabolites, such as F2,6BP, phosphoenol pyruvate and lactate (290-293). HCMV infection also increases the metabolites of the TCA cycle and pyrimidine synthesis pathways (290). Moreover, fatty acid synthesis is up-regulated in HCMV infected cells through the contribution of glycolysis to the carbon flux towards fatty acids (294). Chemical inhibition of fatty acid synthesis reduces the replication of HCMV (294). In contrast to HCMV, HSV-1 infection results in a modest reduction in glucose uptake, lactate production and glycolytic flux suggesting viruses that belong to the same family may have differing effects on cellular energy metabolism (293).

Latent infections with KSHV or Epstein-Barr virus (EBV) also increase glycolysis as shown by enhanced glucose uptake and increased expression of GLUTs and glycolytic enzymes (295-297).

Adenovirus (298), HCV (299-301) and influenza virus (302, 303) also increase the glycolytic activity of infected cells. Carbon flux studies demonstrated that during adenovirus infection, increased carbon uptake through glycolysis results in the production of viral DNA (298). On the other hand, it is suggested that increased glycolysis in HCV infected cells contributes to fatty acid synthesis by supplying intermediates (250).

Some viruses, such as HIV, modulate glycolytic activity in a cell type-specific manner as demonstrated by enhanced glycolytic activity in CD_4^+ T-lymphocytes but reduced activity in macrophages (304, 305).

Studies have demonstrated that VACV does not depend on glycolysis for its replication, nor does it increase lactate production; however, it is dependent on fatty acid synthesis and glutaminolysis (306-308). VACV growth is suppressed in a glutamine-free

medium, but it is not affected by glucose deprivation (307). During VACV infection, the carbon flux to the TCA cycle originates from glutamine, rather than glucose (307). The fatty acid synthesis pathway is also crucial for VACV as it has been shown that inhibitors of fatty acid synthase suppress VACV replication (306). Moreover, energy production is up-regulated in VACV infected cells through β-oxidation of fatty acids (306).

Paradoxically, VACV infection increases the stability and transcriptional activity of HIF-1, the main up-regulator of glycolysis, under normoxic conditions (309). This is achieved by VACV C16 protein, which binds and inactivates PHD2 (309). In the absence of active PHD2, HIF-1α will be stabilized since PHD2 is needed for the hydroxylation and subsequent degradation of HIF-1α by the ubiquitin-proteasome system. In VACV infected cells, HIF-1 leads to increased expression of GLUT1 and PDK-1 (309). C16 also plays a role in the induction of glutamine-dependent metabolic state during VACV infection (308). The reason why VACV infection increases the activity of HIF-1 and the expression of pro-glycolytic genes despite its lack of dependence on glycolysis is not currently known. On the other hand, MYXV inoculation was shown to increase the production of lactate in chorioallantoic membrane cells of chick embryo suggesting enhanced activity of glycolysis during MYXV infection (310).

As described above, certain viruses such as HCMV induce glycolysis in all studied cell types, while others, such as HIV, induce glycolysis in a cell type-dependent manner. In contrast, viruses, such as HSV-1, do not induce glycolysis. The glycolytic status of cells infected with VACV is controversial. On the other hand, regardless of their ability to induce glycolysis, viruses such as HCMV, HSV-1, and Dengue virus all require functioning glycolysis. For example, treating cells with 2-deoxy-D-glucose

(2DG), which is an inhibitor of glycolysis, blocks the replication of HCMV and HSV-1 (311, 312). Similarly, inhibition of glycolysis with oxamate (a pyruvate analog that inhibits glycolysis) or 2DG significantly reduces Dengue virus replication (313).

Experiments also demonstrated the importance of functioning glycolysis on the survival of latently infected cells. Inhibition of glycolysis with 2DG or oxamate in cells with latent KSHV infection results in apoptosis (296). Likewise, suppression of glycolysis through siRNA silencing of HK2 in cells with latent EVB infection leads to cell death (297). For certain viruses, inhibition of glycolysis has no effect on their replication. For example, even if HIV increases glycolysis in T-lymphocytes, inhibition of glycolysis with 2DG or oxamate does not reduce virus replication (314). Similarly, VACV is able to replicate in the absence of extracellular glucose (307).

In summary, viruses interact with cellular energy metabolic pathways and modulate them for their own replicative advantages. As a result, these interactions can be exploited and targeted for the development of antiviral drugs.

1.3.2 Interaction between viruses and the cell cycle control system

Cell cycle is a highly controlled process, which is responsible for generating daughter cells. When a cell passes through the cell cycle, a number of structural and functional processes undergo temporally regulated changes. These changes are mediated by a large number of proteins and pathways that collectively constitute the cell cycle control system. Several virus families interact with and manipulate the cell cycle control system in order to benefit their own replication.

In the next sections, the cell cycle control system will be discussed briefly. Additionally, the different mechanisms that are used by various virus families will be outlined and a few examples will be used to demonstrate these mechanisms.

1.3.2.1 *The cell cycle control system*

The cell cycle has four phases: Gap 1 (G1), Synthesis (S), Gap 2 (G2) and Mitosis (M). Terminally differentiated permanent cells and resting stable cells are in a quiescent state called G0, while labile cells continue to divide, passing through the cell cycle repeatedly. The commitment to enter into the cell cycle from G0 or to continue the next cycle in labile cells during early G1 is decided by a number of intracellular and extracellular factors, such as mitogens, availability of nutrients and cell-cell adhesion signals (315). Once a cell commits to enter the cell cycle, replication of DNA and duplication of centrosomes is performed during the S-phase of the cell cycle. In G2-phase the cell examines the replicated DNA for any lesions including mismatches and single-strand or double-strand breaks. After any DNA lesion is repaired, the cell then enters mitosis.

Mitosis itself is divided into 5 phases: prophase, prometaphase, metaphase, anaphase and telophase (described in detail in (316)). During prophase, the replicated DNA condenses to form sister chromatids, which are attached to each other at the centromere by kinetochores. During prometaphase, the nuclear membrane disintegrates and mitotic spindles attach the polar centrosomes with the kinetochores. Then the chromatids align to the equatorial axis of the cell during metaphase. In anaphase, the mitotic spindles start to pull the sister chromatids apart leading to their transportation towards the poles. Then during telophase, the mitotic spindles disassemble and nuclear

membranes reassemble around the chromatids at both ends. Finally the cell itself divides into two daughter cells through a process called cytokinesis.

The cell cycle has checkpoints where a dividing cell ascertains that all the events in a specific phase of the cell cycle are completed with integrity and all the necessary steps to commit to the next phase are finalized (317). These checkpoints include the Start/restriction checkpoint (in yeast and mammals respectively) in late G1 controlling entry to S-phase; the G2/M checkpoint at the end of G2, which is responsible for regulating entry to mitosis; and the spindle checkpoint, which controls metaphase-to-anaphase transition (318-320). Each of these checkpoints is regulated by elaborate molecular mechanisms, which constitute the cell cycle control system.

The major mediators of the mammalian cell cycle control system are serine/threonine cyclin-dependent protein kinases (Cdks), and their regulators, cyclins **(Figure 1.7)**. Cdks and cyclins that are involved in cell cycle regulation include G1-Cdks (Cdk4, Cdk6) that are activated by G1 cyclins [D-type cyclins (D1, D2 and D3)], G1/S- and S-Cdk (Cdk2), which is activated by G1/S cyclins [E-type cyclins (E1 and E2)] or S cyclins [A-type cyclins (A1, A2)] based on the phase of the cell cycle as well as M-Cdk (Cdk1) that is regulated by M-cyclins [B-type cyclins (B1, B2, B3)] (recently reviewed in reference (321, 322)). Cdks are ubiquitously expressed throughout the cell cycle, whereas the level of cyclins is transcriptionally and proteolytically regulated depending on the specific phases of the cell cycle (323).

The cell cycle control system also has additional mediators, such as Cdk-inhibitors (CKIs), Cdk-activating kinases (CAKs) and Cdk-activating phosphatases **(Figure 1.7)**. There are two families of CKIs: INK4 (inhibitor of Cdk4) family and
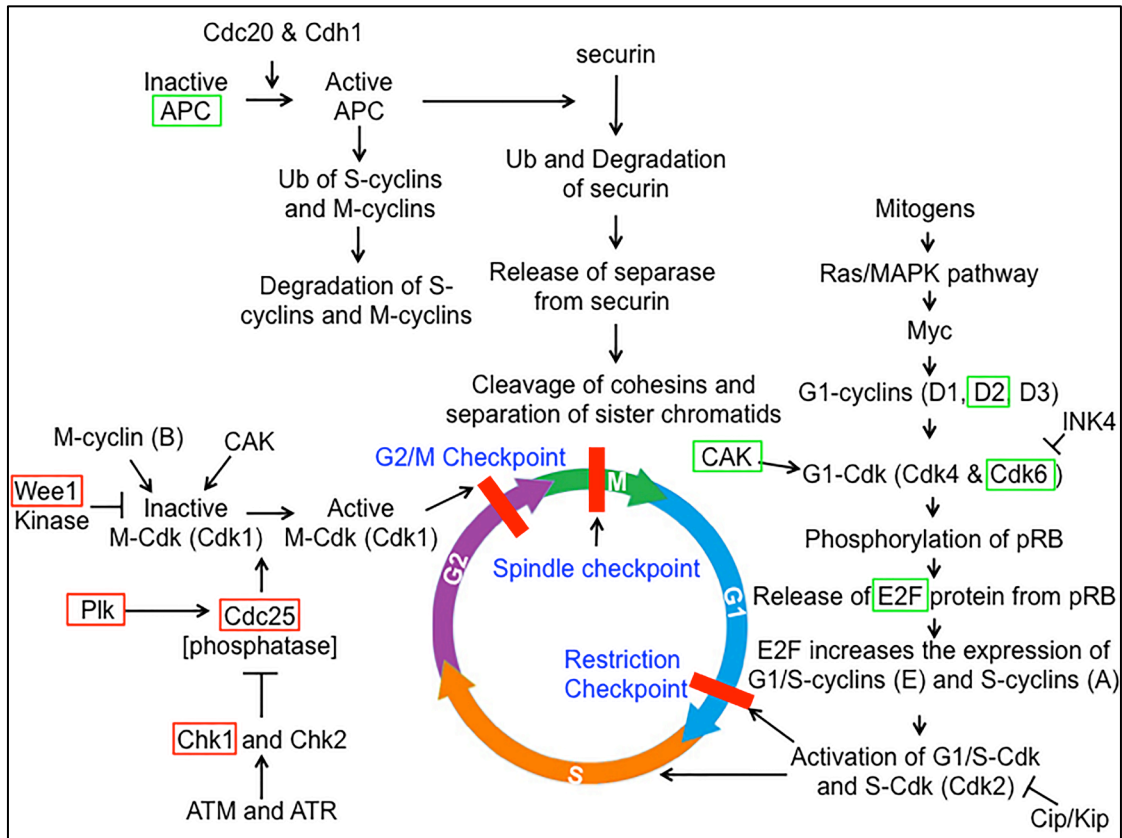
Figure 1.7. The cell cycle control system. The cell cycle is regulated at three checkpoints: the restriction checkpoint, the G2/M checkpoint and the spindle assembly checkpoint. At the restriction checkpoint, mitogens activate the Ras/Mitogen activated protein kinase (MAPK) pathway leading to the expression of Myc. Myc in turn enhances the expression of G1 cyclins, which activate G1-cyclin dependent kinases (Cdks) 4 and 6 with the help of Cdk-activating kinase (CAK). Activated G1-Cdks hyperphosphorylate retinoblastoma (pRB) leading to the release of E2F, which is normally bound to pRB and kept inactive. E2F increases the expression of G1/S and S cyclins, which activate the corresponding Cdks leading to entry to S-phase. Late at G2, the G2/M checkpoint ascertains that DNA is properly replicated and damage-free. Passage through the checkpoint requires active Cdk1-cyclinB complex, which is activated by CAK and Cdc25. The spindle assembly checkpoint ascertains proper chromatin alignment and mitotic spindle attachment during metaphase. At metaphase-to-anaphase transition, securin, a protein that binds and inactivates separase, is degraded following its polyubiquitylation by activated anaphase promoting complex (APC). The active separase then degreases cohesin, the protein that attaches the sister chromatids, leading to chromosome segregation. Red and green boxes indicate subunits, isoforms or single proteins encoded by proviral and antiviral genes, respectively, identified by our RNAi screens (Chapters 3 and 4). Figure is based on the description in (316).

Cip/Kip (Cdk interacting protein/ kinase inhibitor protein) family (reviewed in (324, 325)). INK4 family members include p15 ^{INK4B}, p16^{INK4A}, p18 ^{INK4C} and p19^{INK4D}. They bind Cdk4 and Cdk6, competitively blocking the activation of the Cdks by cyclin D (326, 327). Cip/Kip family proteins are p21 (Waf1, Cip1), p27 (Kip1) and p57 (Kip2). These proteins can inhibit a broad spectrum of cyclin-Cdk complexes almost at every phase of the cell cycle (328). In addition to inhibiting multiple phases of the cell cycle, Cip/Kip proteins can stabilize cyclin D-Cdk4/6 complex, promoting entry to G1-phase (329, 330). p21 is transcriptionally regulated by p53 tumor suppressor protein (331).

In early G1-phase of the cell cycle, several types of signaling pathways and processes including MAPK/Ras pathway, NFκB pathway, cytokine-induced pathways, and cell-cell adhesion molecule-induced pathways as well as Notch and Wnt signaling pathways induce the expression G1 cyclins (332). MAPK/Ras pathway is one of the most understood pathways through which mitogens increase the level and activity of the transcription factor Myc (323, 333-335). Myc leads to transcriptional up-regulation of a number of cell cycle related genes including G1- cyclins (D-type cyclins), G1/S-cyclins (E-type cyclins), S-cyclins (A-type cyclins), M-cyclins (B-type cyclins), Cdk4/6, Cdk2 and Cdk1 (323). As the level of D-type cyclins increases, they displace the inhibitory INK4 proteins from Cdk4/6 leading to partial activation of the kinases **(Figure 1.7)**. Full activation of Cdk4/6 requires additional phosphorylation of Cdk4/6 with CAK (336, 337). Once Cdk4 and Cdk6 are fully activated, they phosphorylate retinoblastoma protein (pRB) (338). Normally the transcription factor E2F is bound and sequestered by pRB, however, phosphorylation of pRB with cyclin D-Cdk4/6 and cyclin E-Cdk2 leads to the release of E2F **(Figure 1.7)** (338-341). E2F then activates the transcription of E-type

cyclins, A-type cyclins, genes involved in nucleotide synthesis (TK, RNR2, dihydrofolate reductase, thymidylate synthetase) and cell division cycle 25 (Cdc25) (322, 342). Activated cyclin E-Cdk2 plays a role in S-phase entry through various mechanisms including phosphorylation and destabilization of Cip/Kip proteins (343-347). Cyclin A-Cdk2 promotes DNA replication in S-phase through phosphorylation and activation of various proteins including DNA polymerase alpha-primase (348-351). Following the completion of DNA replication, cyclin A binds Cdk1 during late G2-phase. Transition from G2 to M-phase requires an active cylin B-cdk1 complex (mitosis-promoting complex), which is tightly regulated at the G2/M checkpoint where the replicated DNA is examined for lesions (**Figure 1.7)** (the regulation mechanism is reviewed in (319, 352)).

In late G2, the level of cyclin B starts to increase and it forms a complex with Cdk1. However, the cyclin B-Cdk1 complex is exported from the nucleus where its targets are (353). When the cell decides to enter mitosis, the nuclear export of the complex is inhibited through phosphorylation of cyclin B by Cdk1 and polo-like kinase 1 (Plk1) (354). Once in the nucleus, the cyclin B-Cdk1 complex is subjected to activating phosphorylation of Cdk1 at a threonine residue by CAK and inhibitory phosphorylation on a tyrosine residue by Wee1 (355, 356). Full activation of the complex requires dephosphorylation of the tyrosine residues of Cdk1 by Cdc25 (357, 358). The phosphatase activity of Cdc25 itself is regulated by Chk1 and Chk2 kinases, which are down-stream effectors of the ATR and ATM dependent pathways of the DNA damage response **(Figure 1.7)** (359).

Once a cell enters mitosis, the mitosis spindle checkpoint regulates the transition from metaphase to anaphase. This checkpoint is primarily regulated by a multisubunit E3

ubiquitin ligase called anaphase-promoting complex (APC) **(Figure 1.7)** (360). APC has two co-activators: cell division cycle 20 (Cdc20) and Cdc20 homolog 1 (Cdh1) (361). APC^{Cdc20} plays a role in metaphase-to-anaphase transition, whereas APC^{Cdh1} is activated late in mitosis and remains active throughout G1. Cdk1 phosphorylates APC in early mitosis, increasing its affinity for Cdc20 (362). APC^{Cdc20} is kept inactive by spindle checkpoint proteins until spindle assembly is successfully completed in metaphase (363). When the cell decides to transition to anaphase, active APC^{Cdc20} catalyzes ubiquitination of securin, a protein that binds and inactivates separase, leading to proteasomal degradation of securin (364). Following the degradation of securin, separase degrades cohesin, which is a complex that keeps the two sister chromatids attached together (365). At this point the two sister chromatids can segregate and complete the cell cycle. APC also leads to the degradation of cyclin A, cyclin B and a number of S-phase-induced proteins that are involved in nucleotide synthesis and DNA replication.

1.3.2.2 *Virus induced disruption of the cell cycle control system*

Various families of both RNA and DNA viruses deregulate the cell cycle control system to benefit their replication. Some viruses arrest cells at a particular phase of the cell cycle while others induce G0 cells to enter the cell cycle (366). Viruses disrupt the cell cycle regulation pathways for multiple reasons. Small DNA viruses, which do not encode their own nucleotide synthesis and DNA replication enzymes, promote cells to enter the S-phase of the cell cycle to utilize cellular DNA replication tools. On the other hand, larger DNA viruses that encode these enzymes prevent cells from entering the S-phase to avoid competition for these substrates. Other viruses prevent entry into mitosis possibly to avoid disruption of certain organelles and the cellular cytoskeleton, which

they utilize for replication, assembly or egress (366). Viruses can also manipulate the cell cycle to prevent apoptosis and evade immune detection.

Viral deregulation of the cell cycle has been identified as one of the major mechanisms through which certain viruses induce cancer. As a result, understanding of these mechanisms will be of paramount importance to devise methods for prevention and treatment of virus-induced cancer. Moreover, the proteins and mechanisms that are used by viruses to deregulate the cell cycle can be targets for antiviral drug development. Furthermore, understanding how oncolytic viruses interact with the cell cycle control system will enable us to identify synergistic, potentiating or antagonistic effects of cancer chemotherapeutic agents that are currently in clinical use, if these oncolytic viruses and the drugs are used in combination.

In the next paragraphs, I will describe a few of the mechanisms used by selected viruses to modulate the cell cycle control system. A more comprehensive review has been recently presented in reference (367).

Virus induced entry into the cell cycle: Certain viruses, such as hepatitis B virus (HBV) and MYXV promote quiescent G0 cells to enter into G1 while others, such as human papilloma virus (HPV) and adenovirus, induce entry of cells into the S-phase of the cell cycle.

HBV nonstructural protein HBx promotes entry of infected primary hepatocytes into G1 phase from their quiescent state by decreasing the levels of p15 and p16 and increasing the levels of cyclins D1 and E as well as p21 and p27 (368, 369). Moreover, HBx also promotes arrest of cells at G1 phase of the cell cycle (368, 370).

MYXV infection of cells synchronized at G0/G1-phase of the cell cycle by serum deprivation results in entry of the cells into the cell cycle and accumulation in S- and G2/M-phases (371). The proposed mechanism involves an ankyrin repeat-containing MYXV protein, M-T5, which interacts with the E3-ubiquitin ligase, cullin-1, leading to the ubiquitination and degradation of Cip/Kip proteins such as p27 (371). Similarly, an artificial MYXV-SFV hybrid known as malignant rabbit fibroma virus (MRV) has also been shown to induce accumulation of rabbit fibroblasts in G2/M-phase of the cell cycle (372). In contrast, SFV did not alter cell cycle events in infected cells (372). Similarly, VACV infection of rabbit fibroblasts has also been shown to lead to rapid transition of cells into the cell cycle and their accumulation in S-phase with associated reduction in the levels of cyclins A and B and Cdk2 and Cdk1 (373). Mechanisms for these alterations have not been identified.

Different strains of HPV are the causative agents for a number of benign and malignant tumors including wart (verruca vulgaris), oropharyngeal cancers and cervical cancer (374). Induction of malignancy by these tumors has been well studied with the identification of viral oncoproteins E6 and E7, which deregulate the cell cycle control system by inhibiting the functions of p53 and pRB, respectively. E6 leads to ubiquitination and proteasomal degradation of p53 (375-378). In contrast, E7 binds to the pocket region of pRB protein family, preventing the sequestration of E2F as well as leading to the proteosomal degradation of pRB (379-383). Other small DNA viruses, such as adenoviruses and polyomaviruses, also promote entry of cells into the S-phase of the cell cycle using similar mechanisms to benefit from the activation of the cellular DNA replication machinery during S-phase (367).

Virus-induced G0/G1 and G1/S arrest: RNA viruses such as influenza A virus H1N1 strain and severe acute respiratory syndrome (SARS)-corona virus as well as DNA viruses such as EBV induce G0/G1 arrest (384-389). Moreover, influenza A virus has been shown to preferentially infect cells at G1-phase of the cell cycle (390). Likewise, DNA viruses such as HSV-1 have been shown to induce G1/S arrest of infected cells. However, HSV-1 and other herpesviruses have also been shown to induce G2/M arrest or entry to the cell cycle depending on the experimental setting or whether the infection is lytic or latent (367).

Influenza A infected cells demonstrated reduced levels of D and E cyclins and hyperphosphorylated pRB as well as increased levels of p21 leading to cell cycle arrest at G0/G1 (384). One of the mechanisms suggested for this arrest is related to the ability of influenza A virus NS1 protein in inhibiting the activity of Ras homologue family member A (RhoA) protein, which is a GTPase involved in G1/S progression (385).

Herpesviruses, such as HSV-1, are large DNA viruses that replicate in the nucleus of infected cells. Most members of the family induce both lytic and latent infections and the type of infection determines the way these viruses manipulate the cell cycle (366, 367). The mechanism used by HSV-1 for G1/S arrest involves infected cell protein 27 (ICP27) and ICP0 (391, 392). ICP27 has been shown to cause G1/S-block by inducing the hypophosphorylation of pRB while the mechanism used by ICP0 is not clearly known (392, 393). It is speculated that, since herpesviruses encode their own DNA polymerase and a number of enzymes involved in dNTP synthesis, they prevent cells form entering S-phase to avoid competition (367).

Virus-induced G2/M arrest: Viruses use diverse methods to arrest cells at the G2/M checkpoint including inhibition of the mitosis-promoting complex, down-regulation of the expression of cyclin B, induction of inhibitory phosphorylation to Cdk1 or up-regulation of the expression of p21. Moreover, viruses can also block up-stream activators of Cdk1-cylin B complex, such as Cdc25, and inhibit the nuclear translocation of Cdk1-cyclin B complex (367, 394). Moreover, some viruses allow entry to mitosis but block exit of cells from mitosis.

As discussed above, ICP0 can induce both G1/S and G2/M arrest. A study showed that ICP0 induces G2/M arrest by using an ATM and Chk2 dependent phosphorylation and inactivation of Cdc25C (395). In the absence of active Cdc25, the inhibitory phosphate groups of Cdk1 induced by Wee1 kinase continue to inactivate Cdk1. Another herpesvirus, human herpesvirus 6 (HHV-6) also induces G2/M arrest using various mechanisms including activation of Chk1 and Chk2, inactivation of Cdc25 and up-regulation of the expression of Wee1 kinase and p21 (396-398).

HIV-1 virus protein R (Vpr) has been shown to play a major role in regulating various processes important for the replication cycle of HIV including the induction of G2/M arrest through multiple mechanisms (367, 399). The mechanisms include S-phase activation of ATR leading to phosphorylation and activation of Chk1 and cell cycle arrest at G2/M phase (400). Moreover, Vpr has also been shown to increase the kinase activity of Wee1 and suppress the activity of Cdc25 resulting in Cdk1 inhibition (401-405).

The reason why viruses induce G2/M arrest is not clearly known for the majority of viruses. However, a few reasons have been proposed including creating a favorable environment for enhanced transcription and translation of viral genes as exemplified by

increased transcription of HIV-1 genes in G2 phase (394, 406). It has also been suggested that some viruses prevent entry into mitosis to keep the cell intact for replication and assembly (394). In the case of HIV, G2/M arrest of infected cells might play a role in inhibiting antiviral immunity by blocking clonal expansion of immune cells (407, 408).

There are also a few viruses including EBV and human T-cell lymphotropic virus (HTLV1) that are able to counteract G2/M arrest by inactivating upstream signaling proteins, such as Chk1 and Chk2 (367).

Viral modulation of the APC: Several viral proteins are involved in modulation of the activities of APC (reviewed in reference (409)). HTLV-1 Tax and HBV HBx proteins have been shown to activate APC. On the other hand, HCMV's pUL21a and pUL97, Orf virus PACR (poxvirus APC/cyclosome regulator), HPV E2 and Adenovirus E1A and E4orf4 have been shown to inhibit APC using different mechanisms (409). For example, HCMV pUL21a binds APC and leads to its dissociation by inducing proteosomal degradation of APC subunits, APC4 and APC5, through unknown mechanism (410). The importance of this process is highlighted by the observation that the replication of the virus is significantly inhibited in the absence of pUL27a (410, 411). The parapoxvirus Orf virus, which infects sheep and goats, encodes PACR protein, which is an APC11 mimic with a dead catalytic domain (412). The protein incorporates itself into APC and inhibits the function of the complex (413). PACR is encoded by MCOV, crocodile poxvirus and squirrel poxvirus, in addition to parapoxviruses. However, *orthopoxviruses* and *leporipoxviruses* do not have homologues (412).

Why viruses modulate APC is not well understood. One of the reasons could be the creation of pseudo-S phase scenarios where cellular dNTP synthesis machinery

remains active (409). This might be particularly important for HCMV and Orf virus, which do not encode their own TK and RNR2 enzymes (409). On the other hand, APC might also target certain viral proteins for degradation and viruses might attempt to prevent this by inhibiting the complex (409).

Overall the above discussion has demonstrated how various families of mammalian viruses interact with different proteins and pathways that are involved in cell cycle regulation. Moreover, known or proposed mechanisms through which viruses benefit their own replication by modulating the cell cycle control system have also been presented. In certain situations, experiments have also shown the impact of arresting cells at a particular phase of the cell cycle on virus replication.

1.3.3   Interaction between viruses and cellular epigenetic mechanisms

In the intricate eukaryotic nucleus, epigenetic mechanisms modulate the activity of genes and determine phenotypic traits without altering DNA sequences. In the last few decades a significant progress has been made in understanding these mechanisms, which include alterations of DNA methylation patterns, chromatin-modifications, long noncoding RNAs and RNAi. This section focuses on reviewing our current understanding of epigenetics with a focus on chromatin structure and function. Moreover, the interaction between viruses and cellular chromatin regulation is discussed.

1.3.3.1   Chromatin structure

Chromatin is a highly organized DNA-protein complex, which condenses and fits the eukaryotic DNA into the nucleus. The basic structural elements of chromatin are nucleosomes, which, in association with various proteins, fold in an orderly fashion to make the chromatin (414, 415). Each nucleosome is composed of ~147 bp of DNA

wrapped around an octamer of histones that tightly bind DNA because of their net positive charge (416, 417). The core histones are H2A, H2B, H3 and H4 and they exist as dimers in the nucleosome **(Figure 1.8)**. A 20-70 bp of DNA that is associated with linker histone H1 attaches each nucleosome to its neighbor (418, 419).   An array of nucleosomes compacts to form a 30-nm chromatin fiber, which then undergoes further compaction to form higher order chromatin structures (419-421).

Histones are small, 11-21 kDa, proteins that are enriched with positively charged amino acid residues such as arginine and lysine. Each histone molecule has two domains: a central globular domain (histone-fold) and N- and C-terminal tails (422, 423). The globular domain binds DNA and other histones to form the nucleosomal core particle whereas the tails protrude outside the nucleosome and they are involved in protein-DNA and protein-protein interactions (424). The tails, particularly the N-terminal tail, undergo high degree of post-translational modifications, which play a significant role in chromatin regulation of various cellular processes.
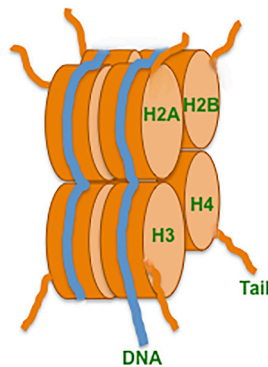
Figure 1.8. Nucleosome. A nucleosome is the basic structural element of chromatin. It consists of dimers of four different types of histones (H2A, H2B, H3 and H4). The tails of the core histones protrude out of the nucleosome core particle. DNA wraps around the nucleosome.

Cytoimaging studies demonstrate heterogeneity in the density of staining of different regions of the nucleus **(Figure 1.9)**. These differences were later shown to correspond to the degree of compaction of chromatin. In the late 1920s, Emil Heitz was able to discern these areas of differential staining into euchromatin and heterochromatin (425). Further studies through the decades were able to characterize the nature of euchromatin and heterochromatin.
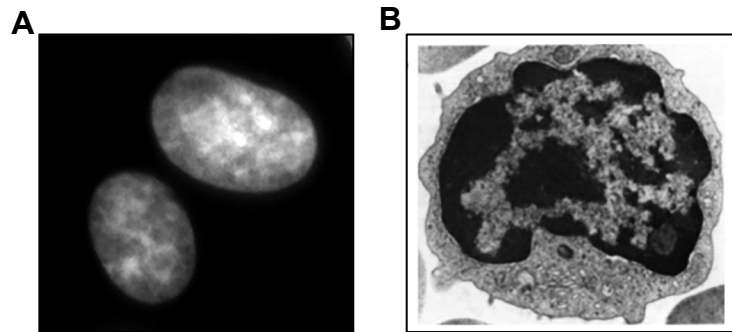
Figure 1.9. Heterogeneous density of staining of the nucleus. (A) DAPI staining of the nucleus of BSC40 cells shows heterochromatin (bright) and euchromatin (dark) domains. (B) An electron micrograph of mouse T-lymphocyte shows euchromatin and heterochromatin regions corresponding to lighter and darker stained areas, respectively. Image in panel (B) is taken with permission from (426).

Euchromatin corresponds to nuclear regions that have lighter intensity of staining. It is less condensed and enriched with transcriptionally active genes. Heterochromatin, on the other hand, is densely stained, highly condensed and it is generally gene-poor and transcriptionally less active. The euchromatin occupies internal areas in the nucleus while the heterochromatin is found at the periphery. Studies have shown that euchromatin areas replicate first, followed by replication of heterochromatin areas later during the S-phase of the cell cycle (427, 428).

Densely staining nuclear regions, which are designated as heterochromatin, can be further subdivided into constitutive and facultative heterochromatin (reviewed in (429)). Constitutive heterochromatin corresponds to regions of the nucleus that are stably condensed and dense. Facultative heterochromatin, however, designates heterochromatin areas found inside euchromatin regions and shows spatial and temporal variations in density of staining based on intracellular or extracellular environmental conditions.

1.3.3.2   *Chromatin dynamics at the molecular level*

Given the structural importance of the chromatin in organizing and compacting genomic DNA into the nucleus, any cellular process that requires access to DNA should first interact with the chromatin and alter its composition and/or compactness. This makes the chromatin a dynamic structure, which is modulated to allow regulation of cellular processes such as transcription, DNA replication and repair, cell division and differentiation as well as genome stability and nuclear architecture. Regulation of chromatin dynamics at the nucleosome level involves changing canonical core and linker histones with variants, post-translational modification of histones and remodeling of the chromatin using ATP-dependent chromatin remodeling complexes (reviewed in Refs (430-432)). There exists a strong interaction between these various processes (433). For example, certain histone variants have a predilection to a specific type of histone modification, and also specific histone modifications interact with particular chromatin remodeling systems.

Histone variants: Each of the histones, except H4, has multiple nonallelic variants. In humans there are 94 genes distributed in four clusters encoding for 57 histone variants (434). These variants are different from their canonical counterparts by a few

residues, longer sequences or even extra domains (435, 436). These differences result in alterations in the structure and/or property of variant histones compared to canonical ones. Consequently, incorporation of a variant histone into a nucleosome affects the structure and/or function of the nucleosome.

Histone variants tend to be incorporated into specific areas of the genome as well as in association with specific cellular processes. For example, the H3.3 variant of H3 is primarily localized to areas of active transcription (437, 438), while centromere protein A (CENP-A), another variant of H3, is localized to centromeres and is involved in the formation of kinetochores during mitosis (439).

Histone post-translational modifications: The N-terminal tails of core histones protrude out of the nucleosome core particle and they are subjected to various post-translational modifications that significantly alter chromatin state dynamics and regulate various biological processes. These modifications, among others, include acetylation, methylation, phosphorylation, ubiquitination, ADP-ribosylation, sumoylation, and acylation (440). In the following sections, a detailed account of histone methylation is given, whereas histone acetylation and phosphorylation are discussed briefly.

A standardized nomenclature for histone post-translational modifications, the Brno nomenclature, was devised following the first meeting of the Epigenome Network of Excellence (NoE) (441). The nomenclature includes, starting from the left, the histone name followed by the modified residue and the type of modification. In the nomenclature, me, ac, ph and ub are used for methylation, acetylation, phosphorylation and ubiquitination, respectively. The number given to a particular residue corresponds to its position from the N-terminal end of the protein. In the case of methylation, numbers

after 'me' indicate the degree of methylation of a particular lysine or arginine residue. For example, H3K36me2 stands for di-methylation of the 36th lysine residue on histone H3.

Histone acetylation: Histone acetylation-deacetylation is a dynamic process with a short half-life that takes place in sites of active transcription, DNA damage repair and replication (442). Histone acetylation is catalyzed by lysine acetyltransferases (KATs), which covalently attach an acetyl group on lysine residues. Compared to other histone modifying enzymes, KATs demonstrate less substrate specificity (443). A different set of enzymes, histone deacetylases (HDACs), removes acetyl groups from lysine residues of histones.

Histone lysine acetylation results in a relaxed chromatin structure by neutralizing the net positive charge of histones (444-446). This reduces the forces that bind histones to the negatively charged DNA and to each other in the nucleosome. The resulting relaxed chromatin structure allows access to various enzymes and proteins that are involved in transcription, DNA replication and repair (447-450). In addition to the effect on chromatin structure, histone acetylation is involved in the recruitment of bromodomain-containing chromatin-modifying proteins and transcription regulators (451, 452).

Histone Phosphorylation: Phosphorylation is a common post-translational modification of histones. It is involved in a number of cellular processes including DNA repair, transcription, chromosome condensation and regulation of other histone post-translational modifications (453).

One of the most studied histone modification events is phosphorylation of H2A.x, an H2A variant, at serine 139 in areas of double-strand DNA breaks (454).

Phosphorylated H2A.x (γ-H2A.x) is involved in recruitment of regulatory and effector proteins of the DNA damage response (455). Moreover, the events triggered by γ-H2A.x lead to an ATM-dependent relaxation of the chromatin in the vicinity of the damaged DNA in order to allow access to proteins involved in repair (456).

Histone methylation: Histone methylation plays a very critical role in the regulation of transcription, DNA replication, DNA repair, cell cycle, nuclear architecture, embryogenesis and development (An excellent review of establishment, regulation and impact of histone methylation is presented in (457)).

Histone methylation takes place on lysine or arginine residues. Lysine residues can be mono-, di- or tri-methylated, whereas arginine residues can only be mono- or di-methylated. Lysine residue methylation is more studied and its biological consequences are better understood than arginine methylation.

Histone lysine methyltransferases (HKMTs) catalyze the transfer of methyl groups from S-adenosyl-L-methionine to various lysine residues of histones. Methylation can be enzymatically reversed by lysine demethylases (KDMs). Following the discovery of the first HKMT, Su(Var) 3-9 Homolog 1 (SUV39H1), 15 years ago, a number of HKMTs and KDMs have been identified and characterized (457, 458). HKMTs are classified into eight groups (HKMT1-HKMT8) with several of subtypes in each group designated by numbers, e.g. HKMT1A, HKMT1B (457). Almost all of the HKMTs belong to the class of SET domain-containing proteins. The only exception is HKMT4, which does not have a SET domain. The SET domain is a 130 amino acid catalytic domain (459). KDMs are also classified into eight groups (KDM1 – KDM8) with subclasses designated by letters in the same way as HKMTs (457). HKMTs have a very

unique substrate profile both in terms of the specific lysine residue that they methylate within a histone and the degree of methylation on a particular lysine residue (460).

1.3.3.3 Chromatin domains

Genome-wide analyses of histone post-translational modifications, specifically methylations, have led to the description of chromatin domains and states (461). These analyses have discovered the presence of two major chromatin domains/compartments: active chromatin and repressed chromatin (462). Repressed chromatin is further subdivided into three environments: constitutive heterochromatin, polycomb repressed chromatin and null chromatin. Active chromatin corresponds to the euchromatin region of the nucleus and it is extremely heterogeneous, containing molecular signatures of various chromatin states. It is enriched with acetylation of H3 and H4 and various types of methylations associated with transcriptional activity including H3K4me3, H3K36me3, and H3K79me3 (457, 462). Repressed domains in the euchromatin region are termed facultative heterochromatin and they share molecular signatures with other repressed chromatin domains including H3K9me3 and/or H3K27me3 enrichment (463, 464). Constitutive heterochromatin is characterized by the abundance of H3K9me2, H3K9me3, H4K20me3 and heterochromatin protein 1 (HP1) (457, 462). It is predominantly found at repetitive sequences including centromeres, telomeres, satellite sequences and transposons (429). On the other hand, polycomb repressed chromatin is enriched with H3K27me3 and polycomb repressive complex 2 (PRC2) proteins (465). Even though null chromatin does not have a particular type of molecular signature, both H3K9me3 and H3K27me3 are abundant (462).

1.3.3.4 *H3K9 methylation: genesis and biological role*

As described in the previous sections, H3K9me2 and H3K9me3 are predominantly associated with repetitive sequences of the constitutive heterochromatin. In addition to that, they are also found in euchromatin regions as H3K9me2 and H3K9me3 broad domains. Moreover, H3K9me2 and H3K9me3 are found in the euchromatin, in the form of facultative heterochromatin, at promoters and gene bodies resulting in transcriptional suppression. Furthermore, H3K9me3 marks are deposited in areas of double-strand DNA breaks to effect transient suppression of gene expression until repair is completed (466).

There are six SUV39H family of methyltransferases that di- or tri-methylate H3K9 (467). They include SUV39H1 (HKMT1A), SUV39H2 (HKMT1B), EHMT2 (euchromatin histone-lysine N-methyltransferase 2, HKMT1C, G9a), EHMT1 (GLP, HKMT1D), SETDB1 (SET domain, bifurcated 1, HKMT1E) and SETDB2 (HKMT1F) (467). All of these HKMTs have the catalytic SET domain.

SUV39H1 and SUV39H2 are predominantly involved in establishing H3K9me2 and H3K9me3 using H3K9me1 as a substrate in constitutive heterochromatin domains **(Figure 1.10)** (468, 469). However, they also play a role in H3K9 tri-methylation of euchromatin regions including promoters and double-strand DNA break sites to generate facultative heterochromatin (466).

G9a and GLP make a complex with other proteins and predominantly mono- or di-methylate H3K9 in euchromatin regions resulting in suppression of gene transcription (470). SETDB1 tri-methylates H3K9, predominantly in euchromatin regions, leading to

the formation of facultative heterochromatin (471). SETDB2 is also involved in tri-methylation of H3K9 primarily in repetitive regions of the genome (472).
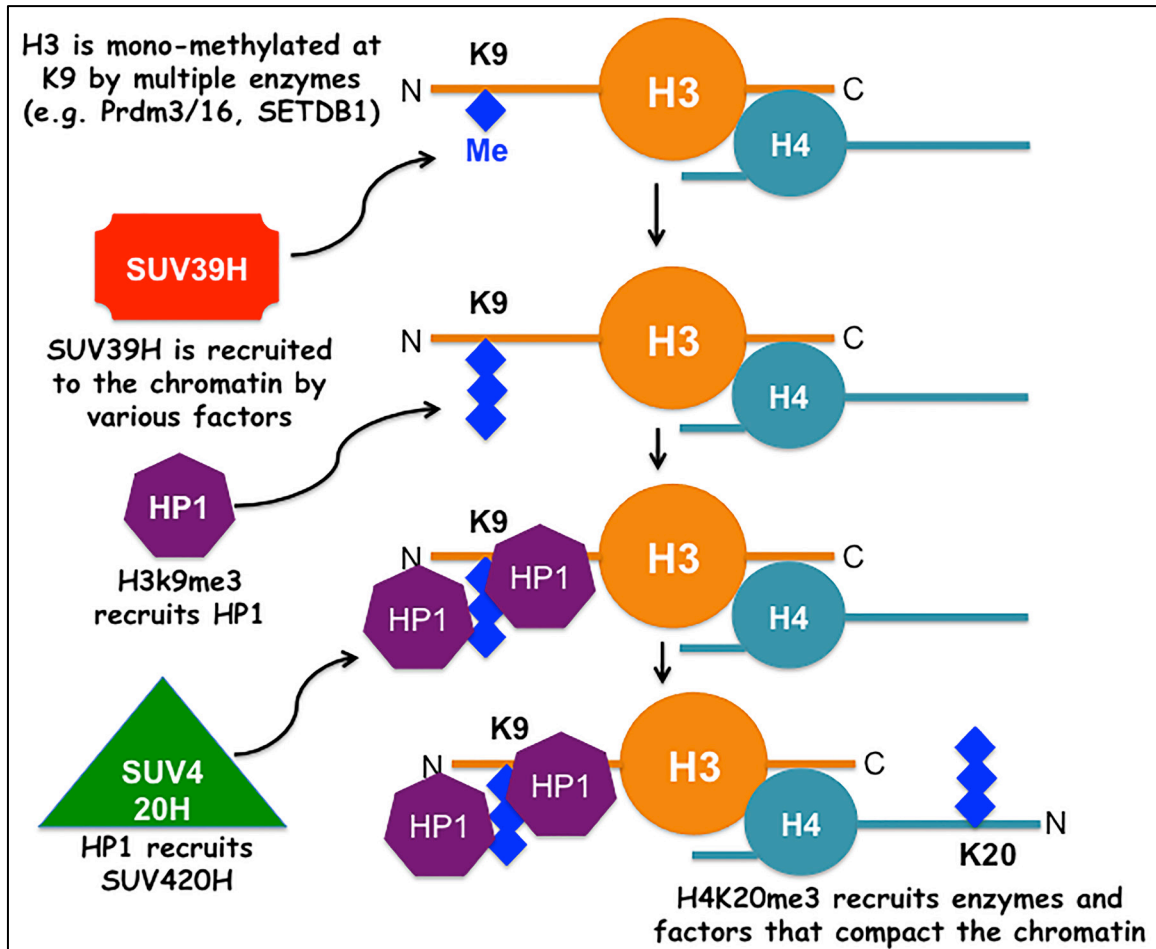
Figure 1.10. H3K9 and H4K20 methylation pathways. Depending on the chromatin domain and state as well as the stimuli responsible for heterochromatin formation, multiple factors recruit SUV39H to the chromatin. SUV39H di- or tri-methylates H3K9me, which is formed by several different enzymes. H3K9me3 then recruits heterochromatin protein 1 (HP1) through its chromodomain. HP1 further recruits SUV420H, which methylates H4 at K20. Finally H4K20me3, in association with a number of other chromatin proteins, recruits chromatin modifying enzymes and factors, leading to the formation of the repressive chromatin (heterochromatin). Figure is based on descriptions and illustrations in (468, 469).

H3K9me3 has strong affinity to chromodomain-containing proteins such as HP1 (473). HP1 proteins have an N-terminal chromodomain, and C-terminal chromoshadow domain (474). Recruitment of HP1 proteins to H3K9me3-enriched regions leads to the formation of a high-order compacted chromatin **(Figure 1.10)**. This is achieved by dimerization of HP1 proteins through their chromoshadow domains and recruitment of enzymes such as SUV420H1, which tri-methylates H4 at K20 (468, 469). Finally, HP1 proteins and H4K20me3 recruit a number of chromatin-modifying factors.

1.3.3.5   *Interactions between viruses and chromatin*

In the co-evolution of viruses and their cellular hosts, cells have been devising tools to prevent and control infection with viruses, whereas viruses have mastered tools to evade the cellular hosts' immune responses and create favorable intracellular environment for successful replication. The chromatin and its regulation are among the processes that are at the center stage of this co-evolution. Two recent review papers have detailed the interaction between viruses and their host's chromatin regulatory systems (475, 476).

Cells utilize chromatin modification systems and pathways in various ways to suppress virus replication **(Figure 1.11)**. One of these ways is modification of the chromatin composition of promoters of genes responsible for antiviral immunity in order to activate them during virus replication. One of the most studied innate antiviral immune mechanisms is the production of IFN by infected cells to mount a strong antiviral environment both in the infected cells as well as neighboring cells. A study conducted by Josse T. *et al.* (2012) (477) demonstrated that the locus of IFN-β is situated in close proximity to the pericentromeric heterochromatin in non-infected fibroblasts and
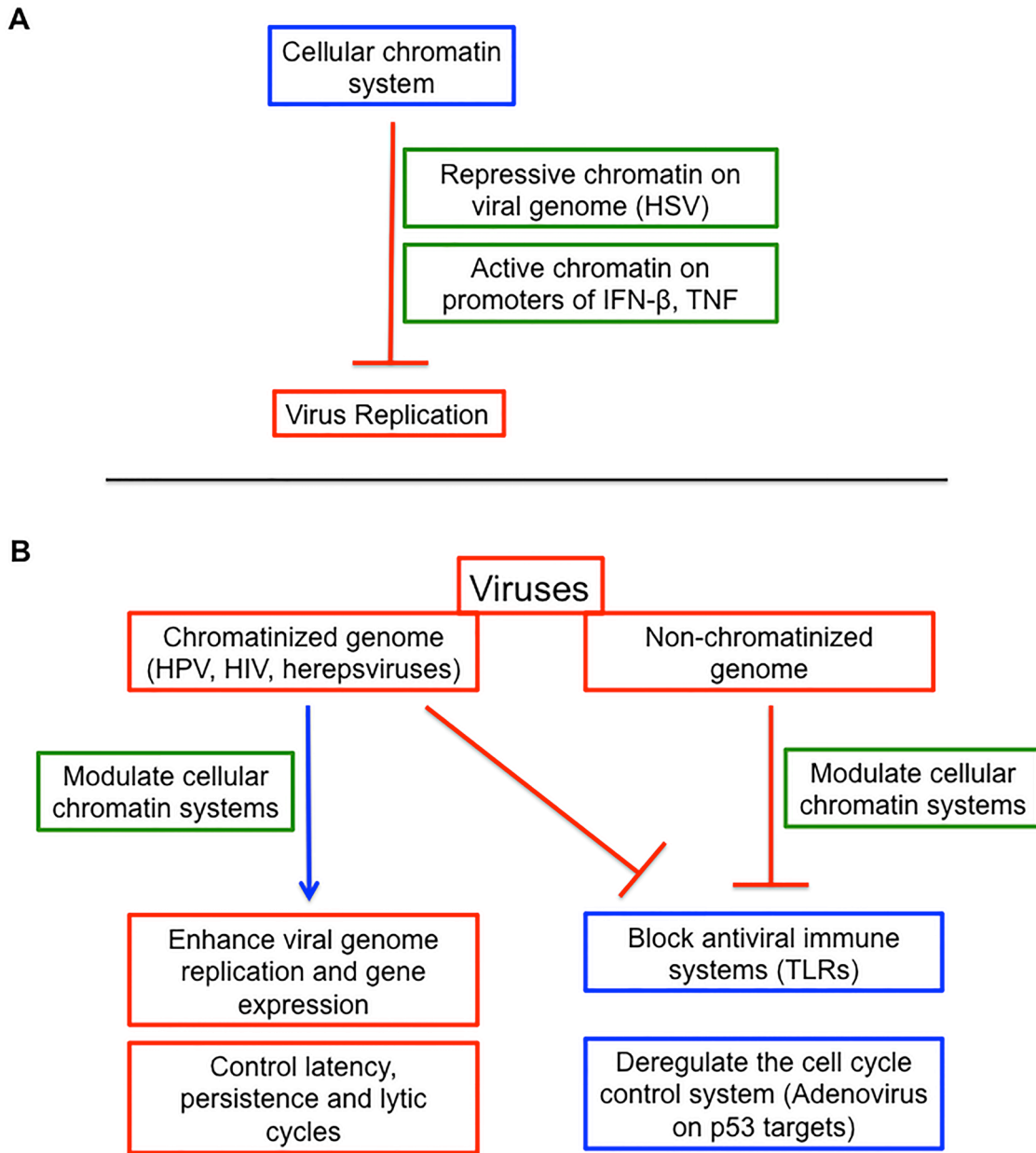
Figure 1.11. Interaction between viruses and the cellular chromatin system. Cells inhibit virus replication through the chromatin system by depositing repressive chromatin on viral genomes as well as by modifying the promoter regions of antiviral genes and inducing their expression (Panel A). Viruses also utilize the cellular chromatin modification system to enhance the expression of their genes, to transition from lytic stage to latency or persistence (Panel B). Moreover, viruses also use the chromatin system to inhibit the expression of pattern recognition receptors and antiviral genes as well as to deregulate the cell cycle control system.

macrophages. The promoter region of the gene is also enriched with the repressive H3K9me3 marker. However, during infection of the cells with Newcastle Disease Virus or Rift Valley fever virus, the locus drifts away from the pericentromeric heterochromatin and its promoter becomes enriched with chromatin markers associated with enhanced gene expression. This leads to increased levels of IFN-β during infection. Similarly, a study conducted in 2012 by Han X. *et al.* showed that Toll-like receptor 8 (TLR8)-mediated recognition of HIV ssRNA by macrophages leads to the production of tumor necrosis factor (TNF)-α through chromatin remodeling of the promoter region of TNF-α towards a transcriptionally favorable form (478).

The other strategy through which cells attempt to control virus infection is by putting repressive chromatin on the genome of viruses to prevent their replication. This is particularly true for viruses that replicate in the nucleus, including herpesviruses. Herpesviruses, such as HSV-1 and HSV-2, are large DNA viruses. Their replication cycle involves lytic (productive) infection in epithelial cells and a period of prolonged latency in neuronal cells. HSV-1 genome is not associated with cellular histones and there is no evidence of formation of nucleosomes in the virion (479). However, the DNA becomes chromatinized while in the nucleus of infected cells and exists as an episomal structure named minichromosome (480, 481). Moreover, cells also suppress the expression of lytic-associated virus genes through H3K9 and H3K27 methylation of viral genome-associated histones (482, 483). On the other hand, lytic infection is associated with histone modifications that characterize active chromatin such as H3K4me3 (484, 485). A similar repressive process is used in other herpesviruses, such as HCMV, EBV and KSHV (486) and HPV (487, 488).

On the other hand, viruses have also devised mechanisms to make the intracellular environment favorable for their replication **(Figure 1.11)**. For the purpose of understanding these processes, viruses can be classified as those that have a chromatinized genome (e.g. HBV, Herpesviruses, HPV and HIV), and those with a non-chromatinized genome. Viruses with chromatinized genomes exploit chromatin systems to modulate their gene expression, to facilitate replication of their genome as well as to switch between lytic and latent/persistent states. Papillomaviruses are small DNA viruses whose genomes are organized into nucleosomes by associating with cell-derived histones (489). They infect cells at the basal layers of stratified epithelial cells. Following infection, papillomaviruses remain in the nucleus of infected cells as extrachromosomal units in association with cellular histones. Their replication and persistence strategy involves tethering their genome to cellular chromatin and going through mitosis with the cellular chromatin and partitioning their genome to daughter cells (490, 491). Papillomaviruses tether their genome to sites of active chromatin (492, 493). The viral protein E2, which binds specific viral DNA sequences, recruits a double bromodomain containing protein, Bromodomain protein 4 (Brd4) (492, 493). Brd4 then binds the DNA-attached E2 with hyperacetylated regions of the cellular genome, which corresponds to the transcriptionally active euchromatic region (494). Utilizing this process, the virus both takes advantage of the euchromatic region for viral gene expression as well as the mitotic systems of the cell for its replication. Similarly, members of the *herpesviridae* and *retroviridae* (become chromatinized upon integration to the host genome) utilize chromatin regulatory mechanisms for establishing latent infections as well as to control their gene expression (495-497).

In addition to exploiting the cellular epigenetic mechanisms for replication, gene expression and latency, viruses, both chromatinized and non-chromatinized, alter the chromatin composition of cells to suppress the expression of immune-associated genes **(Figure 1.11)**. For example, HPV type 16 evades detection of its dsDNA genome in the cytoplasm of infected cells by the dsDNA sensor, TLR9, through down regulating the expression of TLR9 (498). This is achieved by the E7 oncoprotein, which recruits H3K4 demethylases and deacetylases to regions of the TLR9 promoter, leading to transcriptional repression of the gene (498).

Certain oncogenic viruses exploit the cellular epigenetic system to increase the rate of cell replication by inhibiting cell cycle checkpoints **(Figure 1.11)**. For example, the role of HBV protein HBx in hepatocarcinogenesis has been linked to modulation of cellular epigenetic mechanisms (reviewed in (499)). One of the mechanisms involves HBx-mediated up-regulation of H3K4 methyltransferase (SMYD3), which was suggested to enrich the promoter regions of C-MYC with H3K4me3 leading to increased transcription of C-MYC (500). C-Myc is a prominent upstream regulator of the late G1-checkpoint of the cell cycle as described in section 1.3.2.

The elaborate interaction between viruses and cellular epigenetic systems can be exploited to generate antiviral therapeutics. One of the areas of active research is focused on exposing latent/persistent viruses such as HIV and KSHV to the immune system or anti-viral drugs by reactivating their replication through induction of chromatin modifications that favor genome replication and gene expression. The current highly active antiretrovirus therapy (HAART) for the treatment of HIV is very effective in inhibiting the replication of HIV. However, HAART is not successful in eradicating the

virus from various dormant cells where it hides as a provirus, integrating in the genome of host cells. Research has been focused on reactivating HIV replication in these latent sites by inducing chromatin modifications, such as histone hyperacetylation by using HDAC inhibitors, so that the immune system and anti-HIV drugs can detect virus-infected cells (501, 502).

Although poxviruses have been used as models to study various aspects of virology, there is paucity of information and understanding of the interaction between poxviruses and the cellular chromatin. In this study the effect of poxvirus infection of cells on the repressive chromatin is described.

1.4   Objectives and overview of the research project and outcomes

Poxviruses manipulate and exploit various cellular structural components and processes to successfully complete their replication cycles. On the other hand, cells utilize multiple restriction mechanisms to prevent and control infection and transmission of these viruses. This evolutionary relationship between poxviruses and their hosts is what constitutes poxvirus-host interactions.

Several researchers have contributed in deciphering some of theses interactions using single-gene and single-process based studies. Since cellular processes and pathways undergo extensive networks of interactions with each other, genome-scale and system-wide studies would play critical roles in broadening our understanding of these interactions. The recent advances in RNAi technologies, which include the availability of genome-wide RNAi libraries and automated high throughput screening systems, have created the platform to carry out such studies.

In this research project, high throughput sub-genomic and genome-wide siRNA screens were performed with the general objective of identifying and characterizing novel poxvirus-host interactions. MYXV was used as a model in the project and the screens were performed in a human breast cancer cell line. The specific objectives were as follows:

1. To identify human cellular genes (host factors) that modulate the replication of MYXV

2. To describe cellular processes and pathways that are enriched with these MYXV host factors

3. To explain, in greater detail, some of the novel and interesting cellular processes and pathways that we discover

Prior to performing our genome-wide siRNA screens, screening methods were designed and optimized and kinome test screens were conducted. Next a two-step genome-wide screen, which involved primary and validation screens, was carried out and more than 1000 candidate genes (hits), which influenced the replication of MYXV in a human breast cancer cell line, were identified. A custom siRNA library derived from randomly selected hits and non-hits was screened to predict reproducibility rates and a 25% rate of true positivity was determined for the candidate genes.

Subsequently, functional class and pathway enrichment analyses of the hits were conducted using DAVID and PANTHER algorithms and identified a number of pathway-hits. These pathways included both previously known and novel poxvirus host factors. I selected two of these pathways and processes, glycolysis and the cell cycle, for further study.

The results showed a positive correlation between the activity of glycolysis and MYXV growth. I also demonstrated that arresting cells at G1-phase of the cell cycle enhanced the replication of MYXV. Furthermore, the oncolytic potential of MYXV was enhanced by treating cells with a drug that causes G1-arrest.

In this research project, I also studied the interaction between poxviruses and the cellular repressive chromatin and found that some members of the *orthopoxvirus* genus, such as VACV and CPXV, enhanced the repressive chromatin, while leporipoxviruses, such as MYXV, did not. My studies also showed that early gene expression, but not late gene expression, is important for the induction of the repressive chromatin in VACV infected cells. A preliminary result in the project also suggested a role for VACV-induced repressive chromatin in down-regulating cellular gene expression.

Through detailed understanding of poxvirus-host interactions, it would possible to exploit the mechanisms involved in the interactions to identify anti-poxvirus drug targets as well as to enhance the oncolytic potential of poxviruses. Moreover, deciphering these interactions would enable us to uncover novel cellular processes and networks.

CHAPTER 2: MATERIALS AND METHODS

2.1 Cell Culture and Related Methods

The cell lines used in this research project are listed in **Table 2.1**. The table also includes the tissue of origin of the cell lines, their sources and the media used to propagate them. The cell lines were tested for mycoplasma contamination by PCR (Invitrogen) when they were first obtained from their sources and also periodically while they were propagated in the laboratory. **Table 2.2** shows the types and components of the culture media used in this study.

2.1.1 Propagation of cells in culture

Cells were propagated in 150mm tissue culture treated dishes (Corning). When the cells were confluent, medium was aspirated and the cells were washed once with phosphate buffered saline (PBS) [140mM NaCl; 3mM KCl; 10mM Na_2HPO_4-$7H_2O$; 2mM KH_2PO_4]. Afterwards 5mL trypsin-versene solution [0.72% NaCl, 0.02% KCl, 0.01% Na_2HPO_4, 5mM EDTA pH 8.0, complemented with 0.25% trypsin (Gibco)] was added and the cells were incubated at 37°C until they were fully detached. Next, 5mL of medium containing fetal bovine serum (FBS) (Sigma) was added and the cells were counted by mixing 40μL of cell sample with an equal volume of trypan blue dye (Invitrogen) and utilizing the Countess™ automated cell counter (Invitrogen). An appropriate number of cells was seeded on culture dishes (Corning) or multi-well plates (Corning) for propagation or subsequent experiments.

For long-term storage, cryovials (Thermo Scientific) of cells were kept in liquid nitrogen by resuspending them in culture medium-containing 20% FBS and 10% dimethyl sulfoxide (DMSO) (Sigma) at a concentration of ~1 million cells per 1mL.

Table 2.1. List of cell lines used in the project

Name of cell line	Tissue of origin	Source	Culture Media	Remark
BGMK	African green monkey kidney epithelium	Diagnostic Hybrids	MEM + 10% FBS	Buffalo Green Monkey Kidney cells
BSC40	African green monkey kidney epithelium	ATCC	MEM + 5% FBS	
MDA-MB-231	Human metastatic adenocarcinoma of the breast; obtained from pleural effusion	Marry Hitt (UA)	DMEM/F12 Ham + 10% FBS + 1% L-glutamine	
MCF7	Human metastatic adenocarcinoma of the breast; obtained from pleural effusion	Marry Hitt (UA)	DMEM + 10% FBS + 1% L-glutamine	More differentiated than MDA-MB-231 cells
T47D	Human metastatic ductal carcinoma of the breast; obtained from pleural effusion	ATCC	RPMI-1640 + 10% FBS + 1% L-glutamine	
PANC-1	Human pancreatic epithelioid carcinoma	ATCC	DMEM + 10% FBS + 1% L-glutamine	
Capan-2	Human pancreatic adenocarcinoma	ATCC	RPMI-1640 + 10% FBS + 1% L-glutamine	
U87-MG	Human brain grade IV astrocytoma (glioblastoma)	ATCC	MEM + 10% FBS + 1% MEM NEAA	
U118-MG	Human brain grade IV astrocytoma (glioblastoma)	ATCC	DMEM/F12 + 10% FBS + 1% L-glutamine	
W8	Mouse embryonic fibroblasts	Michael Hendzel (UA)	DMEM/F12 + 10% FBS	Wild-type forms of D5 cells
D5	Mouse embryonic fibroblasts	Michael Hendzel (UA	DMEM + 10% FBS	These cells are SUV39H1/2 double null (503)
HeLa S3	Human cervical adenocarcinoma	ATCC	DMEM + 10% FBS	

ATCC – American Type Culture Collection; UA – University of Alberta

Table 2.2. List of reagents used for cell culture

Name of medium	Full name	Source
MEM	Modified Eagle's Medium	Invitrogen
DMEM	Dulbecco's modified Eagle's medium	Sigma
DMEM/F12 Ham	DMEM: nutrient F-12 Ham	Sigma
RPMI-1640	Roswell Park Memorial Institute, media	Sigma
Opti-MEM I		Gibco
FBS	Fetal bovine serum	Sigma
MEM NEAA	MEM non-essential amino acids	Invitrogen
L-glutamine		Invitrogen

2.1.2 Cell viability assays

An Alamar blue dye assay was performed to measure cell viability (504). In experiments where cell viability was determined, medium was aspirated and cells were incubated with 50μM resazurin (Alamar blue dye) (Sigma) in phenol red-free medium for 2-3h at 37°C. Fluorescence was measured using an EnVision® plate reader with 560nm excitation and 590nm emission filter settings.

2.2 Virus Culture and Titration Methods

In this section the viruses used in the project are described. A list of the viruses used in this study and their sources are presented in **Table 2.3**. This section also explains general infection protocols, virus bulking and purification methods as well as assays used to determine endpoint virus growth or virus yield, such as plaque assay and β-galactosidase assay.

Table 2.3. List of viruses used in the project

Virus	Genus and strain	Wild-type vs recombinant	Source	Remark
vMYX-LacZ	Myxoma virus, Lausanne	Recombinant	G. McFadden	Expresses *lacZ* gene under late poxvirus promoter (505)
VACV-WR	Vaccinia virus, Western Reserve	Wild-type	ATCC	
VACV-Cop	Vaccinia virus, Copenhagen	Wild-type	ATCC	
CPXV	Cowpoxvirus, Brighton	Wild-type	ATCC	
SFV	Shope Fibroma virus,	Wild-type	ATCC	
ΔF1L-VACV	Vaccinia virus, Copenhagen	Recombinant; F1L replaced with E/L-EGFP	M. Barry	Described in detail in (506)
ΔF4L-VACV	Vaccinia virus, Western Reserve	Recombinant; F4L replaced with p7.5-neoR-gusA	D. Gammon; D. Evans	Described in detail in (109)
ΔN2L-VACV	Vaccinia virus, Western Reserve	Recombinant; clean kockout of N2L	M. Desaulniers; D. Evans	Described in detail in (507)
ΔE5R-VACV	Vaccinia virus, Western Reserve	Recombinant; E5R replaced with GPT/YFP	W. Teferi; D. Evans	
rE5R-VACV	Vaccinia virus, Western Reserve	Revertant; E5R inserted back to ΔE5R-VACV	W. Teferi; D. Evans	

E/L-EGFP – EGFP under early-late poxvirus promoter, p7.5-neoR-GusA – neomycin resistance and bacterial gusA genes under p7.5 promoter, GPT/YFP – a fusion protein of yellow fluorescent protein and guanine phosphoribosyl transferase

2.2.1 Viruses used in the project and general infection protocols

A recombinant MYXV (strain Lausanne), vMYX-LacZ, which encodes the *lacZ* gene inserted into an intergenic locus and driven by a late poxvirus promoter (505), was a

gift from Dr. G. McFadden (University of Florida). This virus was predominantly used in the experiments described in Chapters 3 and 4. The Western Reserve (WR) strain of VACV was primarily used for the experiments in Chapter 5. All the viruses used in this study are listed in **Table 2.3**.

To infect cells with viruses, cells were seeded into tissue culture-treated dishes or multi-well plates so that cells were approximately 90% confluent at the time of infection. Viruses were diluted in PBS to the indicated multiplicity of infection (MOI). After aspirating medium and washing with PBS, the cells were incubated with the infectious inoculum for 45 – 60 min for VACV strains and 1 – 2h for MYXV strains. Subsequently, the infectious inoculum was aspirated, medium was added and the incubation continued for various time points as required by the experimental design.

2.2.2 Method for generating purified high-titer virus stocks

High titer purified virus stocks were generated for all the viruses listed in **Table 2.3** based on previously described methods (508). BGMK cells were used to bulk MYXV strains and BSC40 cells were used for VACV strains. The cells were grown in roller bottles (Corning) until they reached confluency ($\sim 10^8$ cells/roller bottle). Infectious inoculum was prepared at an MOI of 0.05 by dissolving viruses in PBS. Media from the roller bottles was removed and the infectious inoculum was added. The roller bottles were incubated at 37°C for 45 – 60 min for VACV strains or 1 – 2h for MYXV strains. Afterwards, the infectious inoculum was replaced with medium and incubated for 72h (VACV) or 96h (MYXV). Following incubation, medium was collected into polypropylene centrifuge tubes (Beckman Coulter) and the cells were washed with PBS once, collecting the washouts in the same tubes. The cells were detached using versene-

trypsin solution, collected into the same centrifuge tubes and pelleted by centrifugation at 2000 ×g for 10 min using a Beckman Coulter centrifuge. The pellets were resuspended in 10mM Tris-HCl pH 9, and intracellular virus was released by three cycles of freezing (−80°C)-thawing (37°C) followed by dounce-homogenization. After removing cellular debris by centrifugation (2000 ×g for 10 min), the supernatant was slowly poured over 36% sucrose-10mM Tris-HCl pH 9 solution in a centrifuge tube and centrifuged at 26500 ×g for 80 min using a Beckman Coulter centrifuge and the JS-13.1 rotor (Beckman Coulter). The supernatant was subsequently decanted and the pellet was resuspended in PBS, titrated (see section 2.2.3), aliquoted and stored at −80°C for future use.

2.2.3 Virus titration assays

For experiments where virus yield was determined by performing endpoint titrations, cells were scrapped off the culture dishes and collected in 15mL CELLSTAR$^®$ centrifuge tubes (Greiner bio-one). Viruses were released by three rounds of freeze-thaw followed by homogenization, as described above. Confluent BGMK cells (for MYXV strains) or BSC40 cells (for VACV strains) grown in 60mm dishes (Corning) were infected with serial dilutions of the lysates and incubated for 96h and 48h, respectively. Titers of VACV strains were determined by counting plaques [plaque forming units (PFU)] after enhancement by fixing and staining with crystal violet solution [15% ethanol, 2% glacial acetic acid, 2% formaldehyde and 0.5 % crystal violet] for 30 min at room temperature. MYXV titers were determined by counting foci [foci forming units (FFU)]. To enhance MYXV foci in the case of vMYX-LacZ infected cells, the cells were fixed with 2% paraformaldehyde (Sigma) in PBS, stained with X-gal solution containing

0.5M $K_3Fe(CN)_6$, 0.5M $K_4Fe(CN)_6$, 1M $MgCl_2$ and 100mg/mL of X-gal (Invitrogen), and counted to determine the number of $LacZ^+$ foci.

2.2.4 β-galactosidase assay

β-galactosidase assays were performed using a commercial kit (Promega). Following infection, medium was aspirated and cells were lyzed with Reporter Lysis Buffer (Promega) for 15 min at room temperature. The lysed cells were mixed with one volume of 2× assay buffer [200mM sodium phosphate buffer (pH 7.3), 2mM $MgCl_2$, 100mM β-mercaptoethanol and 1.33mg/mL ONPG], incubated for 1h at 37°C, and the reaction stopped with three volumes of 1M Na_2CO_3 (ACROS). The absorbance was measured at 420nm using a PerkinElmer EnVision® plate reader.

2.2.5 Ultraviolet (UV) inactivation of viruses

Aliquots from virus stocks were diluted to appropriate working titers, and then transferred to 60mm tissue culture treated dishes (Corning) and placed ~5cm away from a UV lamp source in a biosafety cabinet (Beckman) for 30 minutes. Complete UV-inactivation was confirmed by infecting monolayers of cells with UV-inactivated virus samples, where no plaques were formed.

2.3 siRNA Libraries and RNA Interference Methods

In this section, siRNA libraries and the methods used to perform siRNA screens and other independent RNAi experiments are explained.

2.3.1 siRNA libraries

The Silencer® phosphatase and kinase ("kinome") library was purchased from Ambion (Austin, TX). The library comprised three different siRNAs targeting each of

267 human phosphatases and 719 human kinases, resuspended in 96-well plates at a concentration of 5μM. We pooled the three siRNAs that target each gene prior to performing the screens (207). The Silencer Select® whole-genome siRNA library was also purchased from Ambion. The library comprised 21,585 pooled siRNAs, targeting all the known genes in the human genome, and resuspended at a concentration of 2μM in 96-well plates. Each pool contained three different siRNAs directed against a given gene. Dharmacon siGENOME™ Human SMARTpool® custom siRNA library was purchased from Dharmacon/ Thermo Scientific (Waltham, MA). The library comprised 88 siRNAs, which were selected from the hits and non-hits of our whole-genome siRNA screens (described in Chapter 3). The library contained four siRNAs targeting a specific gene, pooled and resuspended at a concentration of 2μM in 96-well plates. The separate and individual siRNAs that were used to validate the hits identified in the screens and to perform further experiments were purchased from Qiagen or Ambion **(Table 2.4)**.

2.3.2 siRNA transfection and vMYX-LacZ infection protocol used in the siRNA screens

A reverse transfection protocol was used to perform all of the siRNA screens using a final siRNA concentration of 10nM for the kinome screens, 5nM for the whole-genome screens and 20nM for the Dharmacon custom library screens after effective siRNA concentrations were determined for each library. The required volumes of the pooled-siRNAs were aliquoted into 96-well plates and resuspended to a volume of 20μL/well in a solution containing 0.1μL/well of DharmaFECT 4 transfection reagent (Thermo Scientific) and Opti-MEM I medium. The mixture was incubated for 30-to-45 min at room temperature and then overlaid with 5000 cells per well with freshly

trypsinized MDA-MB-231 cells in DMEM/F12 medium supplemented with 10% FBS and 1% L-glutamine. The cells were incubated at 37°C in a 5% CO_2 atmosphere for 3 days and then the media was replaced with 20μL of PBS containing vMYX-LacZ. After incubation of the cells in the infectious inoculum for 1h, 80μL of fresh medium was added. The virus was applied at an MOI of 0.1 for the kinome, Dharmacon custom library and whole-genome primary screens. An MOI of 1 was used for the whole-genome validation screen to spread out inhibitory siRNAs by increasing the mean (see Chapter 3). The cells were cultured for 48h, lysed using a single freeze-thaw in reporter lysis buffer (Promega), and then assayed for β-galactosidase activity as described above.

Table 2.4. List of siRNAs used in the project

siRNA	Source	Catalogue number
AllStars Negative Control	Qiagen	1027280
DNA primase, large subunit (PRIM2)	Qiagen	S101388163
Glyceraldehyde 3-phosphate dehydrogenase (GAPDH)	Ambion	4390849
Phosphofructokinase, liver (PFKL)	Ambion	4390824
Phosphofructokinase, liver (PFKL)	Qiagen	S100040614
Phosphofructokinase, muscle (PFKM)	Qiagen	S100604828
Pyruvate dehydrogenase kinase 3 (PDK3)	Qiagen	S100287560
Ribonucleotide reductase, large subunit (R1)	Qiagen	S100020741
Vaccinia-related kinase 1 (VRK-1)	Ambion	4390624
Vaccinia-related kinase 2 (VRK-2)	Qiagen	S102758784

2.3.3 siRNA transfection methods used for independent RNAi experiments

Other siRNA transfection assays used a forward method of transfection in which 5000, 200000, or 500000 cells were seeded per well in 96-, 24-, or 6-well plates (Corning) overnight, respectively. The cells were treated for 3h with a mix of siRNA and DharmaFECT 4 transfection reagent, appropriate medium was added, and the cells cultured for another 2 – 3 days before virus infection and/or other analyses were conducted.

2.4 Polymerase Chain Reactions and Other Molecular Biology Techniques

A number of molecular biology techniques were utilized in this project including semi-quantitative reverse transcription polymerase chain reaction (RT-PCR) and real-time RT-PCR. These methods are discussed as follows.

2.4.1 RNA isolation and quantitation

Total RNA isolation was conducted by using Trizol® reagent (Ambion) according to the manufacturer's protocol. Following medium aspiration and washing with PBS, cells were lysed with Trizol by adding 1mL of the reagent per $10cm^2$ surface area of culture. For example, 1mL of Trizol was used for each well of a 6-well plate. After ensuring complete lysis of the cells by up and down pipetting, the lysate was transferred into microcentrifuge tubes (Fisher Scientific), incubated for 5 min at room temperature and chloroform (Fisher Scientific) (200µL per 1mL Trizol) was added. The tubes were shaken vigorously for 15 seconds, incubated for 3 min at room temperature, centrifuged at 12000 ×g for 15 min at 4°C and the aqueous phase was collected into new tubes. RNA isolation was performed by adding 100% isopropanol (Sigma) (0.5mL per 1mL of Trizol), followed by incubation at room temperature for 10 min and centrifugation at 12000 ×g

Table 2.5. Primers used in this study

Gene	NCBI ID		Primer Sequences	Tm (°C)
PFKL	NM_002626.4	FWD	GAAGATGAAGACAGACATTC	48.1
		REV	CCTCTGATGAGTACAGGTTG	52.2
PFKM	NM_000289.1	FWD	CAGATCAGTGCCAATATAAC	48.3
		REV	TAGTATTGAGTGCTGTGTCA	50.7
PFKFB3(rat)	NM_057135.1	FWD	GTGTGTGAGGAACTAACCTA	51.2
		REV	CACTCTTGTCAAGGAAGTAG	50.0
CDK6	NM_001145306.1	FWD	TATAGGTTTAGGGAGTGTACC	50.3
		REV	GGAGATAGACAAGATGGATAC	49.3
PRIM2	NM_000947.2	FWD	AAACTCCTCAACCCAAAC	49.9
		REV	CCCCCACCTCTACAAAAA	51.7
VRK2	AB000450.1	FWD	AGGCCATAATGGGACAATAGAGT	55.7
		REV	TTCTGTCTTCTCCTTGTGCTTTC	55.1
GAPDH		FWD	ACCACAGTCCATGCCATCAC	57.7
		REV	TCCACCACCCTGTTGCTG	57.9
VACV-I3L	Gene ID: 3707605	FWD	CAACAAATTAAACGGAGCCA	51.4
		REV	AGCCACCACTTCTCTATCA	52.7
VACV-A3L	Gene ID: 3707520	FWD	GATGGCAATAGTGGAAGA	48.9
		REV	CGATAACAGGGGAATGAA	48.9
VACV-E5R	Gene ID: 3707594	FWD	GGAATTGGTGGAAAAGTG	49.3
		REV	CCTACGAACAGGCATACA	51.4
WASF1	NM_001024936.1	FWD	AGTGCCAAGAGCACCTCATG	57.6
		REV	AACACAGGTGTTCTGCCTG	55.4
FAM169A	NM_015566.2	FWD	ACAGCTGTGGCACTTTACC	55.5
		REV	TACATGAGAGAAGACAGTGG	51.0
EEF2	NM_001961.3	FWD	GTGATGAAGTTCAGCGTCAGC	56.4
		REV	TCATGTACAGCCGGTTGTGC	58.0
CASP3	NM_032991.2	FWD	CTCAGTGGATTCAAAATCC	48.3
		REV	CCACTGTCTGTCTCAATGC	53.3
XPO1	NM_003400.3	FWD	GTACATAGTAGGTCAATACC	46.6
		REV	TCCCACACTTGATTAGGGAG	53.7
SRSF2	NM_001195427.1	FWD	GATTGGTAACCTAATTTGTGG	49.1
		REV	ACAAGGCATCTTTACACAGG	52.7
PIH1D1	NM_017916.2	FWD	TCATCAACATCTGCCACT C	52.2
		REV	TTGTCCTCAAGGCCCTCC	57.1
APEX2	NM_001271748.1	FWD	GACCTGAATACAGCCCACC	55.4
		REV	CAGTGGTCAGAGCCCATC	55.3
E4Lf-XhoI	Gene ID: 3707593	FWD	CGTACTCTCGAGATACCGAATAA GAGATAGCGAAG	60.9
E4Lf-SalI	Gene ID: 3707593	REV	GTACACGTCGACGTAGCCGTATA ACCACAATAC	62.2

E6Rf-PacI	Gene ID: 3707595	FWD	CGTACTTTAATTAAGAGTGCATT GACTTTGTTAGTG	57.9
E6Rf-NotI	Gene ID: 3707595	REV	GTACACGCGGCCGCCGCCTATAA GTTCTCCTAATTCG	56.8
FWD-K1L-Ct-myc	Gene ID: 3707647	FWD	ATTACTAAAAATTGAAATTTTAT TTTTTTTTTTTGGAATATAAATGG ATCTGTCACGAATTAATAC	61.6
REV-K1L-Ct-myc	Gene ID: 3707647	REV	AGATCTTTACAGATCCTCTTCTGA GATGAGTTTTTGTTCGTTTTTCTT TACACAATTG	64.3
FWD-K1L-Nt-myc	Gene ID: 3707647	FWD	ATAAAAATTGAAATTTTATTTTTT TTTTTGGAATATAAATGGAACA AAAACTCATCTCAGAAGAGGATC TGATGGATCTGTCACGAATT	67.2
REV-K1L-Nt-myc	Gene ID: 3707647	REV	AGATCTTTAGTTTTTCTTTACACA ATTG	51.1

FWD-forward primer, REV-reverse primer

for 10 min at 4°C. The pellet was then washed with 70% ethanol (Commercial Alcohols), centrifuged at 7500 ×g for 5 min, air-dried and dissolved in nuclease free water and stored at −20°C for future use. RNA was quantified using NanoDrop 1000 spectrophotometer (Thermo Scientific).

2.4.2 Complementary DNA synthesis

Complementary DNA (cDNA) was synthesized by using iScript cDNA synthesis kit (BioRad) or SuperScript® III reverse transcriptase kit (Invitrogen), according to the manufacturers' protocol. Total RNA (0.25 − 1μg) was mixed with 4μL of 5× iScript reaction mix, 1μL of iScript reverse transcriptase and nuclease free water to a total reaction volume of 20μL. The reaction mix was then incubated at 25°C for 5 min, 42°C for 30 min and 85°C for 5 min using a T100™ Thermal Cycler (BioRad). In the case of SuperScript® III reverse transcriptase kit, RNA (0.25 − 1μg) was mixed with 1μL of 50μM Oligo(dT), 1μL of 10mM dNTP mix and nuclease free water to a final volume of

13μL. The mixture was incubated for 5 min at 65°C and 1 min on ice. Next 4μL of 5×
First Strand buffer, 1μL of 0.1M dithiothreitol (DTT), 1μL of 40 units/μL RNaseOUT
and 1μL of 200 units/μL Superscript III reverse transcriptase were added into the above
mixture, incubated at 50°C for 1h and then 70°C for 15 min. The cDNA was diluted 2 – 5
fold for use in polymerase chain reactions (PCR). For all the experiments where semi-
quantitative or real-time RT-PCR was performed, equal amounts of RNA were used for
each sample.

2.4.3   Semi-quantitative PCR

Semi-quantitative PCR was used to determine the silencing efficiency of siRNAs
as well as the expression levels of plasmid-encoded tagged genes. The reactions were
performed by using the primers described in Table 2.5 and *Taq* DNA polymerase as
directed by the supplier (Thermo Scientific). A reaction mix was prepared in 0.2mL PCR
tubes (BioRad) by combining 1× *Taq* buffer, 0.2mM of each dNTP, 2mM $MgCl_2$, 0.5μM
of each primer, 1.25U of *Taq* polymerase, cDNA and water to a final volume of 50μL.
The reaction mix was incubated in T100™ Thermal Cycler (BioRad) as follows: initial
denaturation at 95°C for 10 min, followed by 25 – 30 cycles of denaturation at 94°C for 3
min, annealing for 1 min at a temperature 5°C below the lowest melting temperature of
the primer sets, extension at 72°C for 1 min followed by final extension for 10 min at
72°C. Agarose gel electrophoresis was carried out to quantify the PCR amplicons as
described in Section 2.4.5.

2.4.4   Real time reverse transcription polymerase chain reaction (RT-PCR)

Real time RT-PCR was performed by using SsoAdvanced™ SYBR® Green
Supermix (BioRad) according to the manufacturer's protocol, to determine relative levels

of mRNAs between various samples. The gene-specific primers used in these experiments are described in Table 2.5. A 20μL reaction mix was prepared in a well of Microseal® 96-well Skirted PCR Plate, Low-Profile (BioRad), by adding 1× SsoAdvanced Universal SYBR® Green Supermix, 0.5μM of each primer, cDNA and nuclease-free water. The PCR reactions were performed in CFX Connect™ Real-Time PCR Detection System (BioRad) by using the following cycling conditions. Initial denaturation was conducted at 95°C for 30 seconds followed by 40 cycles of denaturation at 95°C for 15 seconds, annealing for 30 seconds and extension at 72°C for 30 seconds. Annealing temperatures were set at 5°C below the lowest temperature of the primer sets. Finally, melting curves were made by a serial 0.5°C increment in temperature from 65°C to 95°C. The reactions were performed in triplicates. GAPDH was used as a housekeeping gene and non-infected cells were used as control samples unless specified otherwise. Relative changes in transcript levels were computed by using comparative C_T (the $2^{-\Delta\Delta CT}$) method (509).

2.4.5 Agarose gel electrophoresis and gel purification

Semi-quantitative analysis of RT-PCR products and isolation and purification of PCR products and restriction enzyme digests were performed by using agarose gel electrophoresis. Agarose gels were prepared by dissolving 1 – 1.5 % ultrapure agarose (Invitrogen) in Tris-Acetate-EDTA (TAE) buffer containing 1× SYBR® Safe DNA Gel Stain (Invitrogen). DNA was then mixed with 6× DNA Gel Loading Dye (Thermo Scientific) and loaded into the gel. Electrophoresis was conducted in a TAE buffer using a voltage setting of 50V to 100V, depending on the desired rate of separation. DNA

ladders (100 bp, 1kb or 1kb plus) (Fermentas-Invitrogen) were used to estimate the sizes of DNA bands on the gel.

For cloning experiments, gel purification was conducted after a band was precisely cut out of the gel using a clean scalpel under UV light and using a GeneJET Gel Extraction Kit (Thermo Scientific), according to the manufacturer's instructions.

2.4.6 DNA extraction and quantitation

Total cellular and viral DNA was extracted from infected cells using a method involving phenol extraction and ethanol precipitation of DNA (510). The extracted viral DNA was used as a template for generating K1L expression plasmids (Section 2.5.2) or E5R deletion mutants and their revertants (section 2.6). BSC40 cells were infected with VACV-WR at MOI of 5 for 48h, then medium was aspirated, washed with PBS and lysed with DNA extraction lysis buffer [1.2% SDS, 50mM Tris-HCl pH 8.5, 4mM EDTA, 4mM $CaCl_2$ and 0.4mg/ml Proteinase K] for 3h at 56°C. The lysates were transferred to microcentrifuge tubes (Fisher Scientific) and equal volume of phenol-chloroform-isoamyl alcohol (Sigma) was added. Following a brief vigorous shaking, the tubes were centrifuged at 18000 ×g for 15 min at 4°C and the aqueous phase was collected in new microcentrifuge tubes and the extraction step was repeated once more. The DNA was subsequently precipitated in 95% ethanol (at a 3:1 ratio to the aqueous phase) supplemented with 10% 3M sodium acetate pH 5. The mix was incubated at −80°C for 3h and centrifuged at 18000 ×g for 30 min at 4°C. The pellet was washed once with 75% ethanol, centrifuged at 18000 ×g for 15 min at 4°C, air-dried and resuspended in nuclease free water. The concentration of DNA was measured by using NanoDrop 10000 (Thermo Scientific).

2.5 Plasmids and Plasmid Transfection Assays

Plasmids were used to express enzymes such as PFKM and PFKFB3 or tagged proteins such as Myc-DDK-PRIM2 and K1-myc for microscopic imaging studies. In the next sections the plasmids used in the project and their sources are described. Moreover, methods used for bacterial transformation, plasmid isolation and transfection are explained.

2.5.1 Plasmids used in the project

pIRES-EGFP plasmids (Invitrogen) encoding human PFKM (NCBI accession number NM_000289.1) or rat PFKFB3 (RB2K6 splice variant) genes as well as the empty forms were a gift from Dr. J. Bolaños (Universidad de Salamanca, Spain) (511). A plasmid encoding Myc-DDK-tagged PRIM2 (NCBI accession number NM_000947.4) was purchased from Origene. C-terminal myc-tagged VACV K1L (NCBI reference number: AY621082.1) expression plasmid was generated as described in Section 2.5.2.

2.5.2 Generation of K1L expression plasmids

To generate C-terminal myc-tagged K1L constructs, PCR was performed using FWD-K1L-Ct-myc and REV-K1L-Ct-myc primers listed in **Table 2.5**. FWD-K1L-Ct-myc contained the synthetic early-late poxvirus promoter (ELp) to allow the expression of the gene during VACV infection. The PCR product was resolved using agarose gel electrophoresis and the appropriate-sized band was purified as described in section 2.4.5. The DNA fragment was cloned into PCR2.1®-TOPO vector (Invitrogen) by mixing 1μL of the vector with 4μL of the purified PCR product and 1μL of salt solution, and incubated at room temperature for 20 min, according to the manufacturer's instructions. The TOPO reaction was electroporated into electrocompetent E. coli cells following the

supplier's instructions (Invitrogen). Colonies were isolated after 24h of incubation at 37°C, plasmid mini-preps (Invitrogen) were made and tested for accuracy of the insert using restriction enzyme digestion.

2.5.3 Plasmid isolation and generation of glycerol stokes

Electrocompetent E. coli cells were transformed with each of the plasmids described above according to the manufacturer's instructions, plated on agar media overnight and colonies were picked and grown in 100 – 500mL lysogeny broth (LB) media. The plasmids were extracted from bacterial cells using Midi- or Maxi-Prep kits (Thermo Scientific) and quantified using NanoDrop 1000 (Invitrogen). Restriction enzyme digestion, PCR and/or Western blotting were used to ascertain the accuracy of the inserts. Glycerol stokes were made for long-term storage of transformed bacteria at −80°C by mixing bacterial culture with equal volume of 60% sterile glycerol.

2.5.4 Plasmid transfection protocols

Cells were seeded overnight in 24-well plates, at a density of ~200,000 cells per well. A transfection mix was prepared by mixing Opti-MEM, 0.5 – 2μg of plasmid DNA and Lipofectamine 2000 transfection reagent (Invitrogen) at a 3:1 ratio to a total volume of 100μL per well. The transfection mix was incubated at room temperature for 30 min. Medium was aspirated from the cells and the transfection mix was applied as directed by the manufacturer. After 24 – 72h post-transfection, virus infection or various assays were performed depending on the design of the experiment.

2.6 Generation of E5R knockout and revertant VACV mutants

A mutant VACV-WR with a deletion in the E5R gene (ΔE5R-VACV) was

generated as follows. PCR was used to amplify 484 bp region of E4L (E4Lf) [NC_006998.1: 48814 – 49298] and 565 bp region of E6R (E6Rf) [NC_006998.1: 50235 – 50800] genes that flank E5R from a VACV-WR genomic DNA. E4Lf-XhoI and E4Lf-SalI primer pair was used to amplify E4Rf while E6Rf-PacI and E6Rf-NotI were used to amplify E6Rf **(Table 2.5)**. Following gel purification, appropriate restriction enzymes (XhoI and SalI for E4Lf and PacI and NotI for E6Rf) were used to digest the ends of the PCR products. Next, E4Lf and E6Rf were sequentially cloned into the pDGloxPKO^{DEL} vector flanking the EcoGPT/YFP cassette, using the same restriction enzymes as above (512). During the generation of the pDGloxPKO^{DEL}[E4Lf-E6Lf] plasmid containing both the left and right flanking regions, accuracy of the inserts was ascertained by restriction digestion. Sequencing was also used to check the accuracy of the final plasmid.

To generate ΔE5R-VACV, BSC40 cells were infected with VACV-WR at an MOI of 2 for 2h, then the cells were transfected with 2g of linearized pDGloxPKO^{DEL}[E4Lf-E6Lf] using the plasmid transfection protocols described in section 2.5.4. After 72h of incubation, virions were extracted with three rounds of freeze-thaw. Three cycles of mycophenolic acid (MPA) drug selection, using medium supplemented with MPA (25mg/mL), hypoxanthine (15mg/mL), and xanthine (250mg/mL), and three rounds plaque purification under agar were used to isolate and purify ΔE5R-VACV (513). Semi-quantitative PCR was performed to confirm purity of the ΔE5R-VACV stock.

To generate an E5R revertant virus (rE5R-VACV), PCR was used to amplify the E5R gene and the ~500 bp E4L and E6R flanking regions (E4Lf-E5R-E6Rf) using E4Lf-Xho and E6Rf-NotI primers and VACV-WR genomic DNA. The PCR product was gel

purified and cloned into pCR2.1-TOPO vector (Invitrogen) to generate TOPO-E4Lf-E5R-E6Rf. The accuracy of the insert was confirmed using restriction digestion and sequencing. Next, BSC40 cells were infected with ΔE5R-VACV at MOI of 2 for 2h and then transfected with a linearized TOPO-E4Lf-E5R-E6Rf plasmid using Lipofectamine 2000. After 72h of incubation, the progeny virions were extracted by three cycles of freeze-thaw. Five rounds of agar selection and purification was performed to isolate virions that do not express yellow fluorescent protein (YFP). PCR was also used to confirm the purity of the rE5R-VACV stock.

2.7 Western Blotting

Culture medium was aspirated from cells in multi-well plates or dishes and washed with PBS once. The cells were then lysed in NP-40 lysis buffer [150mM NaCl, 20mM Tris·HCl pH 8.0, 1mM EDTA, 0.5% NP-40] or RIPA buffer [50mM Tris pH 8.0, 150 mM NaCl, 1% NP-40, 0.5% sodium deoxycholate, 0.1% SDS] containing a protease inhibitor tablet (Roche) for 30 – 60 min on ice. The lysates were centrifuged at 10000 ×g for 10 min and the supernatants were transferred to new microcentrifuge tubes and stored at −20°C for future use.

Protein concentration was determined using Bradford assay (Bio-Rad protein assay) where 1× Bradford dye reagent was mixed with a sample of lysate and incubated for ~10 min at room temperature. Similarly, serial dilutions of a known protein concentration of bovine serum albumin (BSA) (Sigma) were also mixed with the dye and incubated. The absorbance of the mixtures was measured at 595nm using a PerkinElmer EnVision® plate reader and the protein concentration of the lysates was extrapolated from a standard curve generated by plotting the absorbance of the known BSA standards.

Before protein samples were loaded and separated using SDS-PAGE, they were mixed with SDS- PAGE loading buffer [0.4% SDS, 0.4% β-mercaptoethanol, 40% glycerol, 50mM Tris pH 6.8, 1mg/mL bromophenol] at a 4:1 ratio. The samples were boiled for 10 min in a water bath and loaded into gels. When electrophoresis was complete, the proteins were transferred from the gel to a nitrocellulose membrane (Thermo Fisher Scientific) using a wet transfer method. Next, blocking was performed by incubating the membrane for 1h at room temperature in Odyssey blocking buffer–PBS solution. The membrane was incubated in primary antibody **(Table 2.6)** dissolved in Odyssey blocking buffer and PBS (1:1) solution for 3h at room temperature or over-night at −4°C. Next, the membrane was washed with PBS three times and incubated for 3h at room temperature in secondary antibody **(Table 2.6)** dissolved in the same buffer. Finally the membrane was washed two times in PBS-T [150mM NaCl; 10mM KPO4; 0.1% Tween-20] and once in PBS and scanned using an Odyssey® infrared imaging system (LI-COR Biosciences).

2.8   Microscopy and Image Analysis

Immunofluorescence microscopy was used to determine the localization of proteins such as PRIM2 and for quantitative analysis of chromatin markers in Chapters 4 and 5, respectively. Cells were seeded on coverslips in 24-well plates, washed twice with PBS, fixed with 4% paraformaldehyde (Sigma) for 30 min, quenched with 0.1M glycine (Fisher Bioreagents) for 10 min and then incubated in a blocking buffer containing 3% BSA (Sigma) in 1%Triton X-100 (MP Biochemicals) in PBS for 1h at room temperature. Then the cells were incubated overnight at 4°C in primary antibody **(Table 2.6)**, washed three times with PBS, and incubated in an appropriate secondary antibody **(Table 2.6)** for

Table 2.6. List of antibodies used in the project

Primary antibodies

Antibody	Source Species	Commercial Source	Catalog number	Dilution for WB	Dilution for IF
Ribonucleotide reductase, large subunit (R1)	Goat polyclonal	Santa Cruz Biotechnology	sc-11733	1:500	
Vaccinia-related kinase-1 (VRK-1)	Goat polyclonal	SantaCruz Biotechnology	sc-15239	1:500	
Vaccinia-related kinase-2 (VRK-2)	Rabbit polyclonal	Sigma	V2140	1:500	
Enhanced green fluorescent protein (EGFP)	Rabbit polyclonal	BD BioSciences	83672	1:500	
DNA primase, large subunit (PRIM2)	Rat monoclonal	Cell Signaling Technology	4726	1:500	1:100
Myc tag	Mouse monoclonal	Cell Signaling Technology	2276	1:1000	
β-actin	Mouse monoclonal	Sigma	A5441	1:10000	
H3K9me3	Rabbit polyclonal	Active Motif	39765		1:1000
H4K20me3	Rabbit polyclonal	Abcam	AB9053		1:1000
BrdU	Mouse monoclonal	Sigma	B8434		1:100
VACV I3	Mouse monoclonal	ProSci	10D11	1:1000	1:1000
Secondary antibodies for WB					
Anti rabbit IRDye 680CW	Goat	LI-COR Biosciences	926-32221	1:10000	
Anti rat IRDye 680CW		LI-COR Biosciences		1:10000	
Anti mouse IRDye 800CW	Goat	LI-COR Biosciences	926-32210	1:10000	
Anti mouse IRDye 800CW	Donkey	LI-COR Biosciences	926-32212	1:10000	
Secondary antibodies for IF					
Anit mouse AF488	Goat	Molecular Probes (Invitrogen)			1:2000
Anti rabbit Cy5	Goat	Molecular Probes (Invitrogen)			1:2000

WB – Western blot, IF – immunofluorescence

3h at room temperature. Next, the cells were washed three times and incubated for 30 min at room temperature in a solution containing 4',6-diamidino-2-phenylindole dihydrochloride (DAPI) [Invitrogen] and rhodamine phalloidin (Invitrogen) to counterstain DNA and actin, respectively. Finally the coverslips were mounted on slides. An Applied Precision DeltaVision microscope was used to image the specimens using 60× objective lens in all the imaging studies described in this thesis.

All immunofluorescence microscopy experiments were conducted at least three times. Images were exported from the softWorx software of the DeltaVision microscope as 16-bit TIFF files and rescaled to 8-bit range using Photoshop CS for Macintosh (Adobe) with a similar scale of background reduction applied to all images. Image analysis was performed using ImageJ1, a Java based image-processing software program. Random samples of 5-8 medium-power (60×) image fields were selected from both control and experimental groups and total nuclear intensities of a protein-of-interest and DAPI were determined. The nuclear intensities of the protein-of-interest (e.g. H3K9me3) were normalized by dividing the values to that of DAPI. The relative fold change of the intensities was calculated by dividing the normalized intensities of the protein-of-interest of the experimental group to that of the control group. The fold changes of three independent experiments were averaged, standard deviations were calculated and the results were plotted in bar graphs. Image J was also used to determine the variations in the intensities of H3K9me3 and DAPI along the longest diameters of the nuclei by measuring pixel-to-pixel intensities, which demonstrate plot profiles.

2.9   Flow Cytometry

Flow cytometry studies were conducted to determine the proportion of cells in each phase of the cell cycle (Chapter 4) and to measure histone methylation levels using immunofluorescence staining (Chapter 5).

For cell cycle analysis, cells were treated with drugs for 24 – 72h, or transfected with siRNAs for 48 – 72h, and then detached with trypsin-versene solution as described in section 2.1.1. The cells were recovered by centrifugation for 5 min at 2000 ×g, washed twice with PBS, centrifuged, resuspended in 70% ethanol, and incubated on ice for 1h. The cells were then treated with 1μg/mL of ribonuclease (Thermo Scientific) for 30 min, stained for 1h in 1μg/mL propidium iodide (ACROS), and counted using an LSR Fortessa cell analyzer (BD Biosciences). FlowJo software was used for cell cycle analysis.

Abcam's flow cytometry intracellular staining protocol was used for antibody staining. Cells were detached, centrifuged and washed with PBS as above. The cells were then fixed with 0.01% formaldehyde (Sigma) for 15 min on ice, centrifuged, and permeablized with 0.1% triton X-100 (MP Biochemicals) in PBS for 15 min on ice. After centrifugation, the cells were incubated in blocking buffer [3% BSA in 0.1% triton X-100 and PBS] for 1h. Next, the cells were incubated with H3K9me3 primary antibody **(Table 2.6)** at a dilution of 1:1000 over night at 4°C, washed and then incubated in VACV I3 antibody at a dilution of 1:1000 for 3h at room temperature. Following washes with PBS, the cells were incubated with Cy5 (dilution 1:2000) and AF488 (dilution 1:2000) **(Table 2.6)** secondary antibodies for 3h at room temperature. Finally, the cells were washed with PBS twice and cell counting and analysis were performed as described above.

2.10 GAPDH, Lactate and ATP Assays

Spectrophotometric assays were used to measure glyceraldehyde-3-phosphate dehydrogenase (GAPDH) activity [using a KDalert™ GAPDH kit (Ambion)], lactate [using method described by (514)] and ATP [using an ATP determination kit (Invitrogen)] levels as per the manufacturers' instructions.

2.10.1 GAPDH assay

GAPDH activity assay was performed to determine the efficiency of our siRNA transfection protocol in knocking down GAPDH. MDA-MB-231 cells were transfected with siRNAs targeting GAPDH **(Table 2.4)** for 72h in 96-well plates. Medium was aspirated and 200µL KDalert™ lysis buffer was added into each well, incubated at 4°C for 20 min and complete lysis was ensured by pipetting the each sample up and down. Next, 10µL of lysate was transferred in triplicate into wells of a new 96-well plate and mixed with 90µL of KDalert™ master mix and fluorescence was measured using a PerkinElmer EnVision® plate reader at excitation and emission of 560nm and 590nm, respectively. The linearity of the dynamic range was ascertained by measuring enzyme activity of a serial dilution of GAPDH enzyme included in the kit.

2.10.2 Lactate assay

To measure lactate levels, medium was collected from cells treated with 2DG, or transfected with PFKFB3 or PFKM plasmids or PDK3 siRNAs and 10µL medium was mixed with glycine (320mM), hydralazine (Sigma) (320mM), NAD^+ (Sigma) (2.4mM), L-lactate dehydrogenase (from rabbit muscle, Sigma) (2U/L) and water to a final volume of 100µL (final concentrations are indicated in the parenthesis). Following a 10 min incubation at room temperature, the absorbance was measured at 340nm using a

PerkinElmer EnVision® plate reader. Linearity of the dynamic range of the experiment was confirmed using a serial dilution of lactic acid (BioVision).

2.10.3 ATP assay

ATP levels were determined in cells treated with 2DG or transfected with PFKFB3 or PFKM plasmids or PDK3 siRNAs. Following aspiration of culture medium, cells were lysed with Reporter Lysis Buffer (Promega) for 15 min at room temperature. Then 10μL of lysate was mixed with standard reaction solution for ATP determination containing 1× reaction buffer, 1mM DTT, 0.5mM D-luciferin and 2.5μL of 5mg/mL firefly luciferase. Luminescence was measured using a PerkinElmer EnVision® plate reader. Similar to the above experiments, the linear range of the experimental outcomes was confirmed using serial dilutions of ATP solution.

2.11 5-Fluorouridine Uptake Assay

Transcriptional activity was examined using immunofluorescence-based 5-fluorouridine (5-FU)-uptake into nascent transcripts as previously described (515, 516). Briefly, medium was aspirated from VACV infected or non-infected cells and replaced with medium containing 1mM 5-FU. Following incubation at 37°C for 20 min, medium was aspirated, the cells were fixed and immunofluorescence staining and imaging were carried out using methods described in section 2.8. Anti-BrdU primary antibody (Sigma), which cross reacts with 5-FU, was used at 1:100 dilution over night at 4°C, anti-VACV I3 antibody was used at 1:1000 dilution at room temperature for 3h **(Table 2.6)**.

2.12 Chemicals Inhibitors Used in these Studies

Etoposide was purchased from the University of Alberta hospital pharmacy, 2DG and PD-0332991 were obtained from Sigma and Selleckchem, respectively. L-Sulforaphane and proTAME were purchased from Sigma and Boston Biochem, respectively. Cytosine arabinoside (araC) and cycloheximide were purchased from Sigma. For cell treatments, aliquots were taken from stock solutions of the drugs and dissolved to appropriate concentrations in culture media. DMSO-treated cells were included as controls for drugs dissolved in DMSO.

2.13 Statistical and Bioinformatics Analysis

Inter-plate variability for all the screens was normalized by subtracting the median of each plate from the raw results of each well on a specific plate. Following this normalization, the mean of the replicates was calculated. Data quality analysis was conducted using frequency distribution and correlation plots. We used a strictly standardized mean difference (SSMD) method to analyze the kinome and whole-genome validation screens and the Z-score method to analyze the primary whole-genome and the siRNA toxicity screens (517-519). The online tools PANTHER (218), DAVID (216, 217), and PINdb (520) were used to search for gene associations and relationships. In other studies, bar graphs represent means and standard deviations. Student's t-test or two-way ANOVA were used to compare the data and the results were considered to be significant if $p \leq 0.05$.

CHAPTER 3: RNA INTERFERENCE SCREENS FOR CELL FACTORS AFFECTING MYXOMA VIURS REPLICATION

A version of the data presented in this chapter were published in:

Teferi, W. M., Dodd, K., Maranchuk, R., Favis, N., and Evans, D. (2013). A whole-genome RNA interference screen for human cell factors affecting myxoma virus replication. Journal of Virology. **87**(8): 4623-41**.**

I performed the siRNA screens described in this chapter with invaluable technical support from Mr. Rob Maranchuk, manager of the RNAi core at the Li Ka Shing Institute of Virology, University of Alberta. Nicole Favis collaborated in performing the GAPDH assay experiments in Figure 3.3. VRK-1 and VRK-2 experiments described in Figure S1 (appendix) were performed in collaboration with Kristopher Dodd. All of the rest of the experiments presented in this chapter were performed by myself. I wrote the original manuscript with editorial contributions from my supervisor, Dr. David Evans.

3.1   INTRODUCTION

New evidence continues to emerge showing that poxviruses interact with several cellular structures and functions to complete the core events of their replication cycle, to promote pro-growth and anti-apoptotic states as well as to counter both innate and adaptive antiviral immunity. Since poxviruses encode a large number of proteins, it is expected that they undergo extensive interaction with poxvirus-infected cells encoding >20,000 genes.

RNAi screens create a suitable platform to explore these interactions at larger and even genome scale and to get insights into the many possible cellular functions that affect the growth of poxviruses. These methods were pioneered in *Drosophila* cells, and were subsequently used to survey what mammalian cell functions modulate the growth of viruses, such as HIV (221, 223) and influenza virus (226). Poxviruses were less studied using these methods by the time we conducted our screens. The only completed study was a kinome screen performed in *Drosophila* cells, which identified important cellular factors that play a role in VACV endocytosis (236).

MYXV, the prototypic member of the *Leporipoxvirus* genus of poxviruses, is known to encode many proteins that interfere in processes related to cell growth, apoptosis and innate and adaptive immune defenses (241, 521, 522). Many of these virus proteins exhibit narrow species specificity and thus MYXV naturally infects only rabbits and hares. However, it can replicate in some human and mouse cells if key defenses, such as those regulated by Akt/PKB (523) or type I IFNs (120), are disrupted. This has led to the suggestion that MYXV may have value as a safe and selective oncolytic agent since these systems are often impacted by cell transformation (524, 525). The ability of MYXV

to replicate in certain cancer cells of mouse or human origin makes it an interesting model to study cellular factors that affect virus replication in general and virus tropism in particular as well as to identify mechanisms to optimize the oncolytic potential of the virus.

Recognizing the substantial gap in our understanding of poxvirus-host interactions, we decided to conduct a series of high throughput RNAi screens in MYXV infected human cancer cells using human kinome and whole genome siRNA libraries. These screens identified >1000 genes that appear to modulate the growth of MYXV in MDA-MB-231 cells, a human breast cancer cell line. Screening of a custom siRNA library targeting the "hits" and "non-hits" of the whole-genome screens showed that about 25% of the "hits" were highly likely to be true positives. These genes modulate a variety of pathways, some of which have been previously shown to play a role in poxvirus replication (e.g. the cytokine/chemokine-mediated inflammatory pathways and MAPK pathways) whereas others (e.g. the cell cycle and glycolysis) are more novel discoveries. The validity of a subset of these "hits" was confirmed using independent methods. The results provide insights into both basic poxvirus biology, as well as the host factors affecting MYXV growth in transformed human cells.

3.2 RESULTS

3.2.1 Optimization of siRNA screening methods

Before embarking upon a large-scale siRNA screen, we performed experiments to optimize the choice of cells and the transfection, infection, and assay methods. We also tested these technologies using a screen of the kinome (~1000 genes encoding siRNA

pools targeting human phosphatases and kinases) prior to screening the whole human genome.

For the optimization experiments, as well as the final screens, we used an MDA-MB-231 human breast cancer cell line (526) and a recombinant MYXV encoding an *E. coli lacZ* gene inserted between the M10L and M11L genes and regulated by a late virus promoter (505). The *lacZ* gene permits more accurate titration of the virus and, because poxvirus late genes are not expressed in the absence of replication, the β-galactosidase produced by vMYX-LacZ provides a measure of the levels of virus replication.

We used MDA-MB-231 cells because they showed an intermediate level of permissiveness to MYXV infection compared to other common human cell lines **(Figure 3.1A)**, and thus they should facilitate detection of both stimulatory and inhibitory siRNAs. These cells have also been studied intensively over many years, providing a wealth of literature on specific signaling pathways. We also examined how well the β-galactosidase assay correlated with virus yield (i.e. focus forming units or FFU). Although there is not a linear relationship between the two assays, the same relative relationship is seen between the levels of β-galactosidase and the number of FFU, when different cell types are infected with vMYX-LacZ at MOI=0.1 **(Figure 3.1B)**. This showed that the LacZ assay provides a good surrogate assay that should be predictive of MYXV yields.

We also tested what effect the cell density and multiplicity of infection have on MYXV growth kinetics, when assayed using the β-galactosidase reporter **(Figure 3.1C and D)**. Based upon these experiments, we identified MOI=0.1-to-1 and a 48h infection

period as providing infection conditions that are least likely to suffer from signal saturation while still generating a good signal-to-noise ratio.
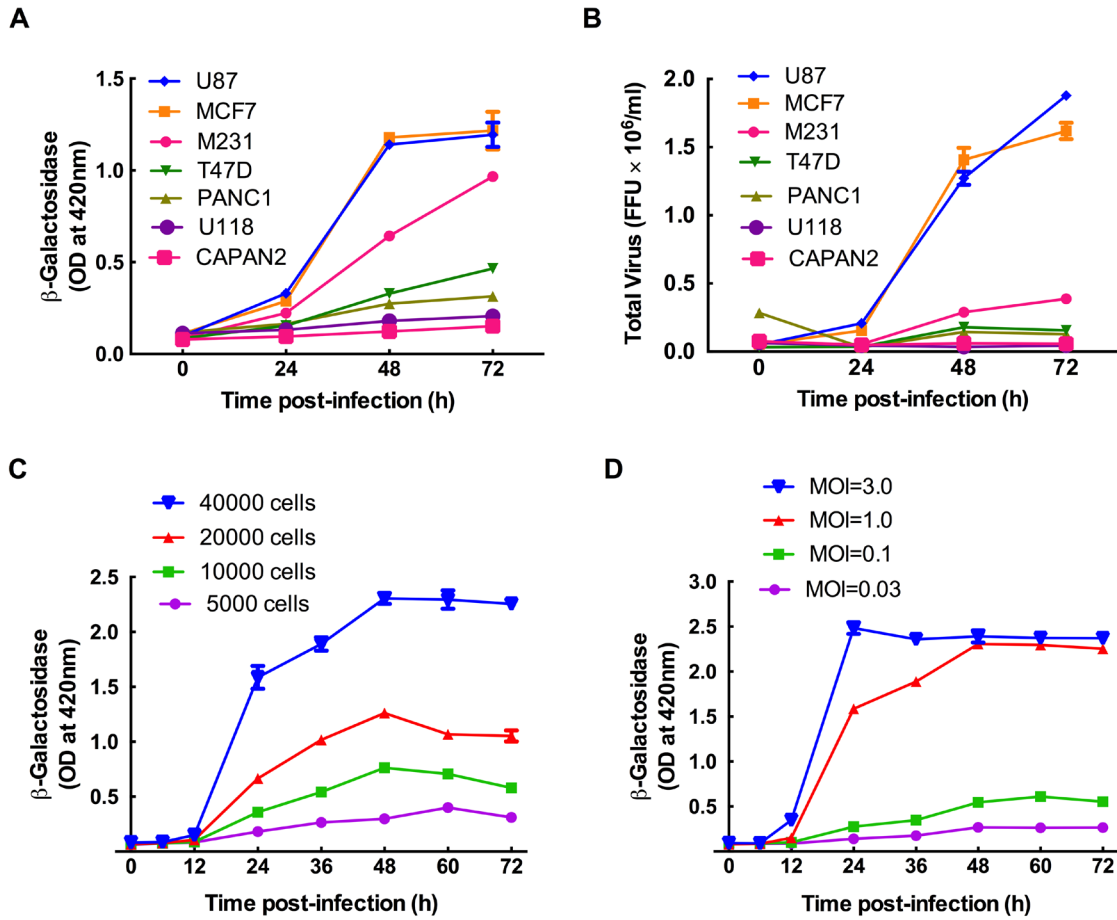
Figure 3.1. MYXV growth in MDA-MB-231 cells. MDA-MB-231 cells support intermediate level of virus growth compared to the other human cell lines (Panels A and B). U87, MCF7, MDA-MB-231 (M231), T47D, PANC1, U118 and CAPAN2 cells were seeded into 96-well plates, cultured for 24h, and then infected with MYXV at MOI=0.1. The cells were lysed at the indicated time points and assayed for β-galactosidase activity (A) and focus forming units (FFU) (B). MYXV growth kinetics in MDA-MB-231 cells (Panels C and D). MDA-MB-231 cells were cultured for 24h in 96-well plates at densities ranging from 5000 – 40 000 cells per well, and then infected with MYXV at MOI=1 (Panel C). Alternatively, 40 000 cells were plated per well and infected with MYXV at the indicated multiplicities of infection. β-galactosidase activity was measured at the indicated time points and is reported as optical density (OD) The data are representative of two independent experiments.

We tested the effect of our transfection system, which is based on AllStars negative control siRNA and DharmaFECT 4 transfection reagent, on cell viability and MYXV replication by using Alamar blue cell viability assay and β-galactosidase assay, respectively. There was no statistically significant difference in cell viability and virus replication between AllStars siRNA transfected and non-transfected MDA-MB-231 cells **(Figure 3.2)**. Based on this, AllStars siRNA was used as a negative control in our screens and subsequent independent experiments.
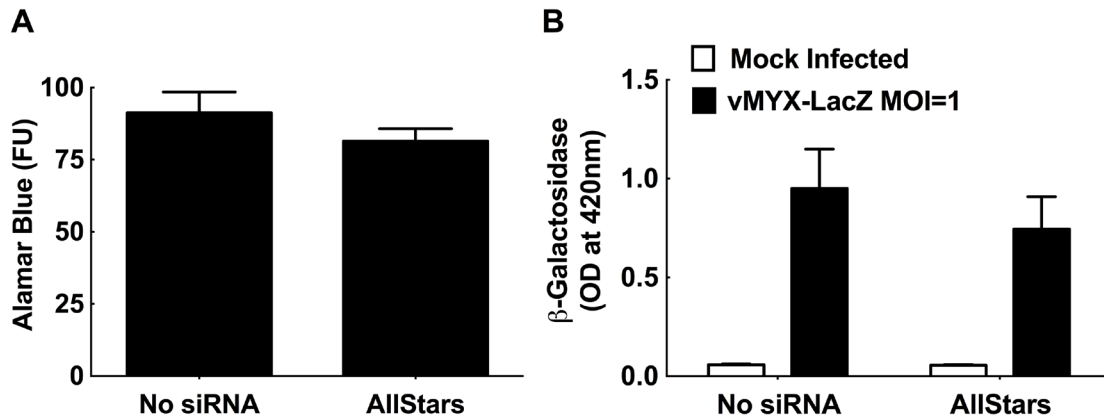
Figure 3.2. The effect of siRNA transfection reagents on cell viability and MYXV replication. MDA-MB-231 cells were transfected with AllStars negative control siRNA (10nM) for 72h followed by Alamar blue viability assay, which is presented with arbitrary fluorescence units (FU) (Panel A). The cells were infected with v-MYX-LacZ at MOI of 1 for 48h following 72h transfection with AllStars siRNA. Then β-galactosidase assay was determined by measuring optical density (OD) (Panel B). The data are representative sample of three independent experiments.

We also optimized the efficiency of siRNA delivery and silencing by transfecting MDA-MB-231 cells with different amounts of GAPDH siRNAs and measuring silencing using a GAPDH activity assay. We observed that siRNA concentrations ≥1nM can

reduce the GAPDH activity by ~70% **(Figure 3.3)**. We subsequently used siRNAs targeting the mRNAs for the large subunit of cellular ribonucleotide reductase (R1) and the phosphofructokinase liver isoform (PFKL), as positive controls in the larger screens. MYXV encodes an R2 subunit of ribonucleotide diphosphate reductase, but during infection the virus R2 protein must complex with the cellular R1 subunit to form an enzyme that catalyzes the rate-limiting step in dNTP biogenesis (109, 527). As predicted, siRNA knockdown of cellular R1 produced a 50-70% reduction in virus replication **(Figure 3.4.)**. PFKL was initially identified as a strong and reproducible hit in the kinome screen, which is described in detail in Chapter 4.
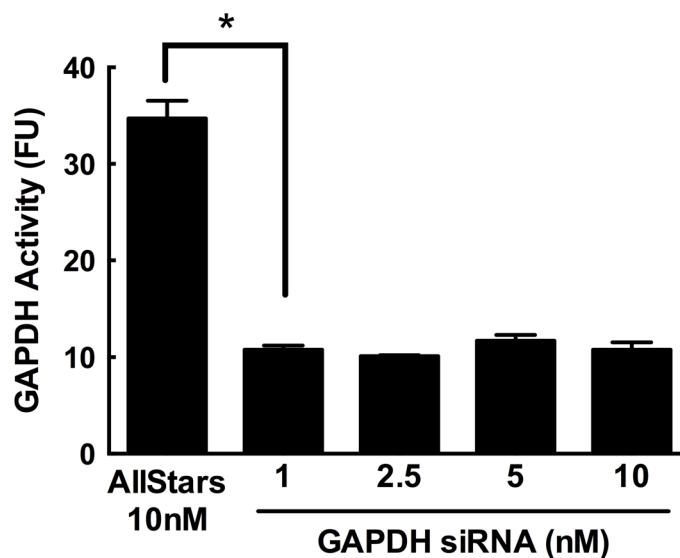
Figure 3.3. Optimization of reverse-transfection protocols using GAPDH siRNAs. MDA-MB-231 cells were seeded in 96-well plates at a density of 5000 cells per well, and reverse transfected with the indicated concentrations of siRNAs. The cells were lysed three days later, and assayed for GAPDH activity using a fluorescence-based assay. Even the lowest concentrations of siRNAs (1 nM) produced a ~70% reduction in GAPDH activity, compared to cells transfected with 10nM negative control siRNA ("AllStars"). The data are representative of three independent experiments and "*" indicate p≤0.05.

Based on the experiments, we designed a screening method in which we seeded MDA-MB-231 cells into 96-well plates at a density of 5000 cells per well, reverse-transfected the cells with 5-10nM siRNA for 3 days, and then infected the cells with vMYX-LacZ at an MOI=0.1-1. Two days later, the cells were lysed and assayed for β-galactosidase.
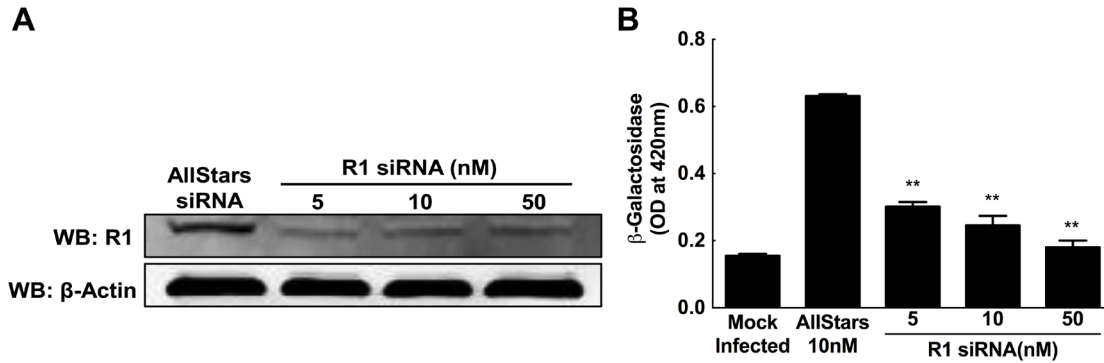
Figure 3.4. Validation of an internal positive control using siRNAs targeting cellular ribonucleotide reductase. MDA-MB-231 cells were seeded in 96-well plates at a density of 5000 cells per well, and reverse transfected with the indicated concentrations of siRNAs targeting the cellular ribonucleotide reductase large subunit (R1). The cells were cultured for three days, infected with MYXV for 48h, and assayed for R1 protein by western blotting (A) and for virus-encoded β-galactosidase activity (B). The siRNAs reduced the level of β-galactosidase activity by 50-70% and this was correlated with a reduction in the levels of R1 protein. The data are representative of three independent experiments. Significance is indicated relative to the AllStars controls: (**, *p≤0.001*).

3.2.2 Kinome test screen

We next tested these methods by performing two duplicate RNAi screens with siRNA library targeting ~1000 human kinases and phosphatases. Each gene in the screen was targeted with a pool of three different siRNAs, based upon a previous study which

had shown that pooled siRNAs produced better penetrance than single siRNAs, without

causing an unmanageable increase in false-positives (207). Analysis of the degree of
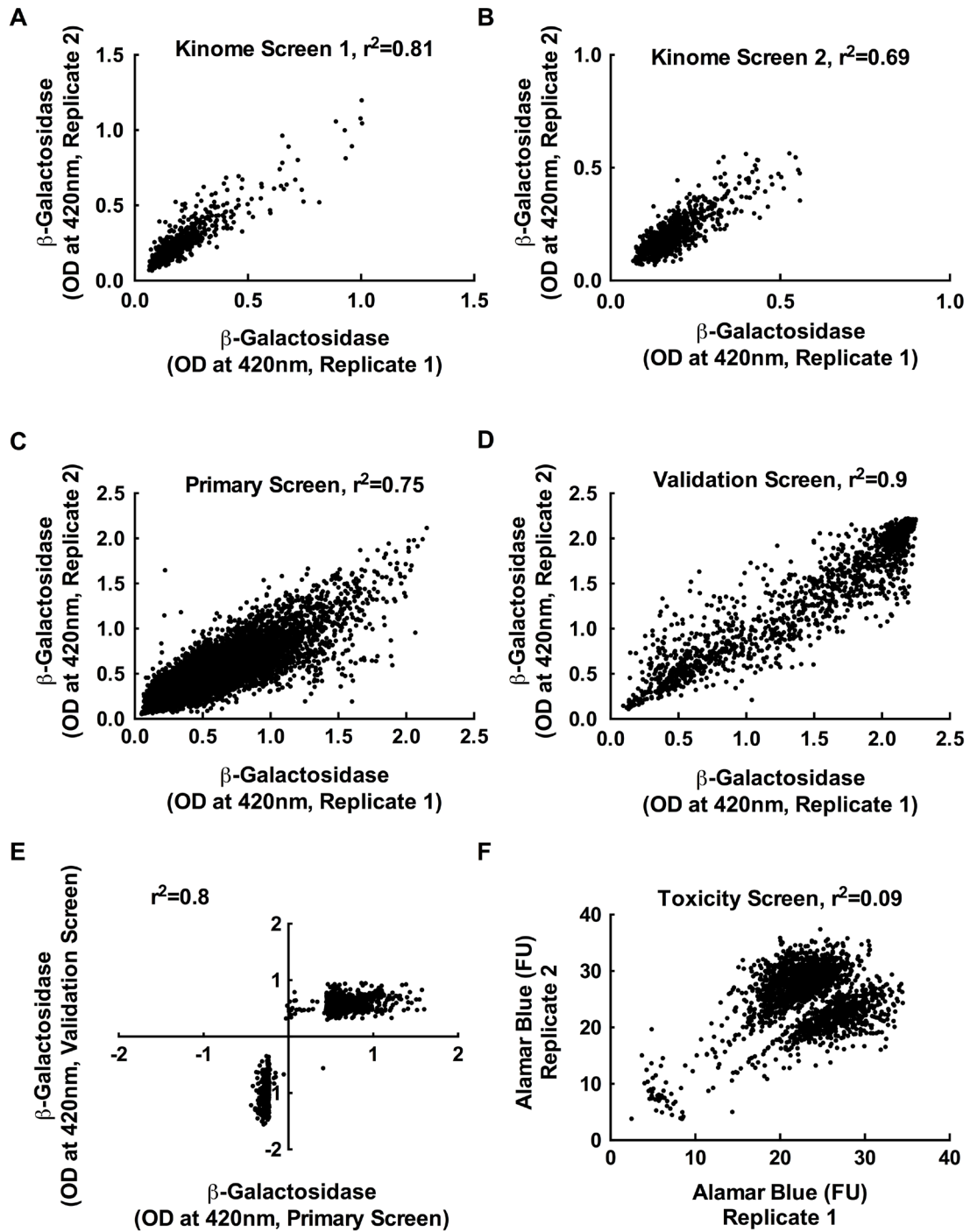
Figure 3.5. Experimental reproducibility. Each experiment was performed in duplicate and using β-galactosidase assays to measure virus growth. The figure shows the reproducibility of paired replicates from the first (A) and the second (B) kinome screens, from the primary whole genome screen (C), and from the validation screen (D). Panel (E) shows a comparison of data obtained in the validation screen (a rescreen of the proviral and antiviral hits identified by the whole genome screen, along with a small number of neutral control hits) *versus* the signals detected in the original whole-genome primary screen. Panel (F) illustrates how a cluster of toxic siRNAs were identified, using Alamar blue assays. Shown are the correlation coefficients (r^2) for the different experiments.

correlation between the duplicates within each screen showed that the methods were generally robust with the coefficient of determination varying from $R^2=0.7$ to $R^2=0.8$ in the second and first screens, respectively **(Figure 3.5A and B)**. The siRNAs that affected virus replication were identified using the strictly standardized mean difference (SSMD) method, which minimizes the rates of false discovery and false non-discovery in siRNA screens (517-519). Out of the 986 genes targeted by this library, we identified 70 siRNA pools that inhibited (SSMD ≤ -3) and 26 that increased (SSMD ≥ 3) virus growth **(Table S1)**. These hits could be assigned to many different pathways with genes relating to apoptosis, inflammation, and cell growth regulation comprising the most prominent targets **(Figure 3.6A and B)**. Perhaps most notable are the several strongly inhibitory hits within the ERB-B signalling pathway. Although the ErbB-2 receptor is not highly expressed in MDA-MB-231 cells (528), MYXV growth factor could still potentially signal through this route (529) and would affect the Akt/PKB pathway that is important for MYXV growth (119). PIK3CA (phosphoinositide-3-kinase alpha) regulates this pathway and siRNAs targeting PIK3CA were highly inhibitory. Many inhibitory siRNA pools also targeted enzymes linked to glycolysis **(Figure 3.6A)** and in a logically

consistent manner. For example, silencing PFKL (phosphofructokinase-1, liver) reduced MYXV replication whereas silencing a phosphatase that opposes PFK-1 activity, FBP1 (fructose-1,6-bisphosphatase 1), increased virus replication **(Table S1)**.
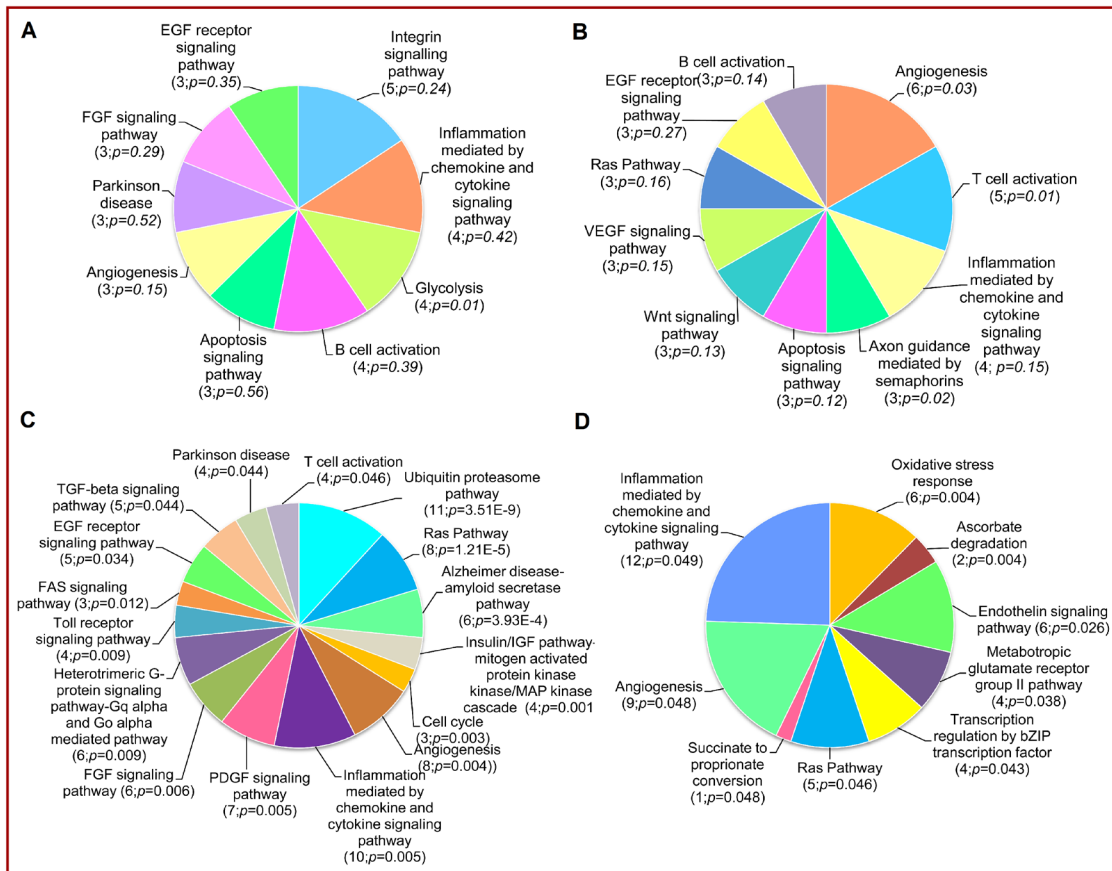
Figure 3.6. Pathway analysis of gene hits. PANTHER (Protein ANalysis THrough Evolutionary Relationships) was used to look for relationships between the genes identified by the kinome (charts A and B) or the whole-genome (C and D) screens, and which either decreased (charts A and C) or increased (B and D) virus replication. The values in parenthesis indicate the number of gene hits in each pathway and the estimated p-values.
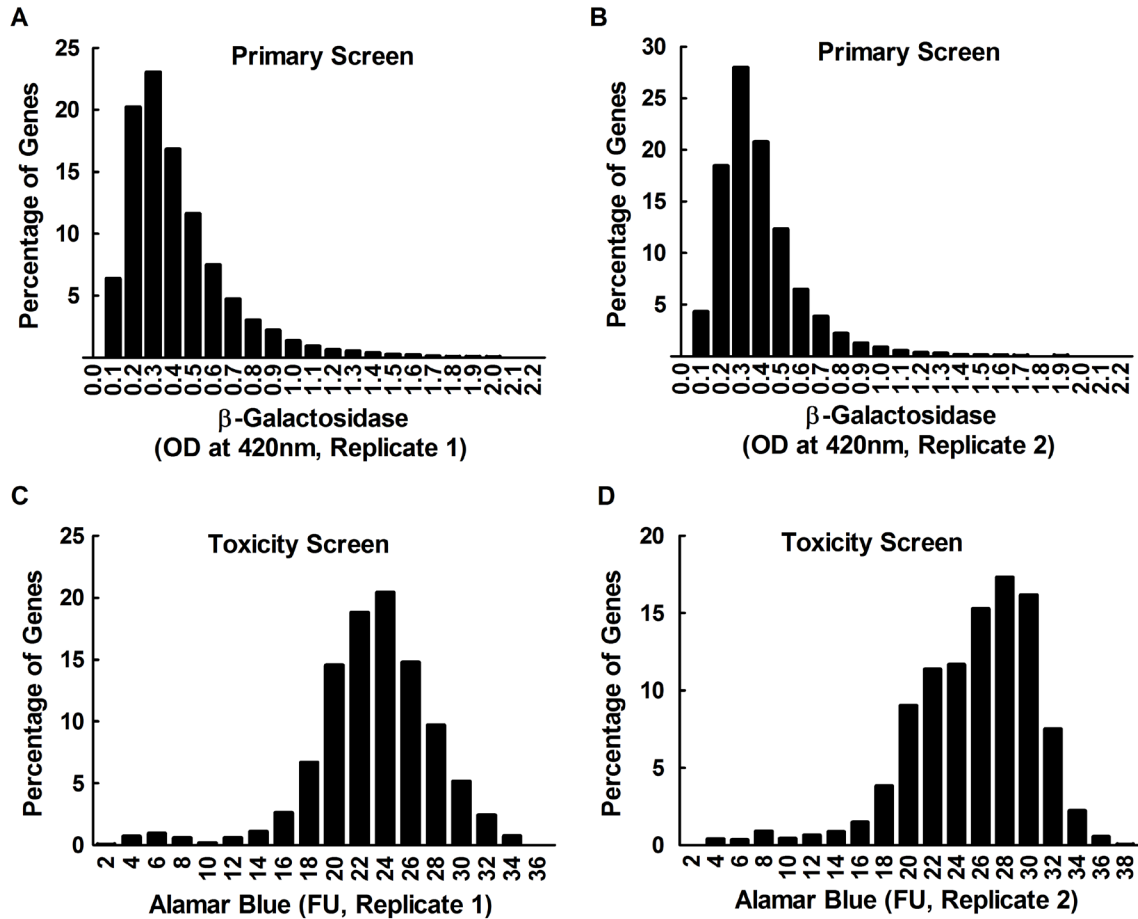
Figure 3.7. Data frequency distribution plots. The virus-encoded β-galactosidase optical density/absorbance measurements, acquired as replicates in the whole genome primary screen, were binned into 0.1 intervals and the centers of the intervals were plotted against the percentage of genes falling into each bin (panels A and B). Both replicates produced positively skewed distribution curves with the medians being ~15% less that the means. In contrast, the Alamar blue toxicity screen showed no strong evidence of a data skew. In this case the data were binned into 2 fluorescent unit intervals and the centers of the intervals were again plotted against the percentage of genes that fall in each bin (panels C and D). The mean and median values were essentially identical in both replicates.

We also retested four of the hits using different siRNA silencing reagents and virus yield experiments to gain some insights into the reliability of the screen. Three of the four hits [PFKL; pyruvate dehydrogenase kinase isozyme 3 (PDK3); vaccinia related kinase 2 (VRK2)] could be independently verified whereas the fourth [vaccinia related kinase 1 (VRK1)] could not (please see Chapter 4 and Appendix for the results). We did not detect hits involving the AMPK gene, as was reported in Drosophila (236), but humans encode multiple isoforms of AMPK and its subunits (236) and this redundancy may have obscured any hits. This small-scale survey indicated that the methods we were using were sufficiently robust to identify practical numbers of true positive hits.

3.2.3   Whole-genome primary siRNA screen

We next screened 21,585 pooled siRNAs, which target all known genes in the human genome. The screens were conducted in duplicate using the same methods described above. The data quality analysis showed that both replicates produced positively skewed frequency distribution curves **(Figure 3.7A and B)** suggesting that more siRNAs increased virus replication than decreased it. The duplicates showed a good degree of correlation with $R^2=0.75$ **(Figure 3.5C)**. These data were analyzed by applying Z-score statistics (519, 530) to the normalized results of the screen. Z-score was used in preference to SSMD because the number of siRNAs was large enough to produce a frequency distribution approximating a Gaussian curve, albeit with a slight positive skew **(Figure 3.7A and B)**. Like the frequency distribution curves **(Figure 3.7A and B)**, the Z-score method also detected more siRNAs that increased virus replication than decreased it **(Figure 3.8)** and this asymmetry complicated how one should select the genes identified in this screen. We thus applied two approaches to initially define these hits.

First, we included all the siRNAs that produced Z-scores ≥ 1.96 or ≤ -1.96, and which comprised 5% of the genes in the screen. However, this included relatively few siRNAs that inhibited MYXV growth and we wanted to retest if this effect was real. Therefore we also included a further subset of siRNAs, which comprised 5% of the most-inhibitory siRNAs in the Z-score curve. This led to further inclusion of siRNAs with Z-scores between -1.96 and -1.33 **(Figure 3.8)**. In the end, we identified 1588 siRNAs that fit these criteria, 1048 with Z-score ≥ 1.96 and 540 with Z-score ≤ -1.33. These siRNAs were picked and re-plated and used in another round of screening.
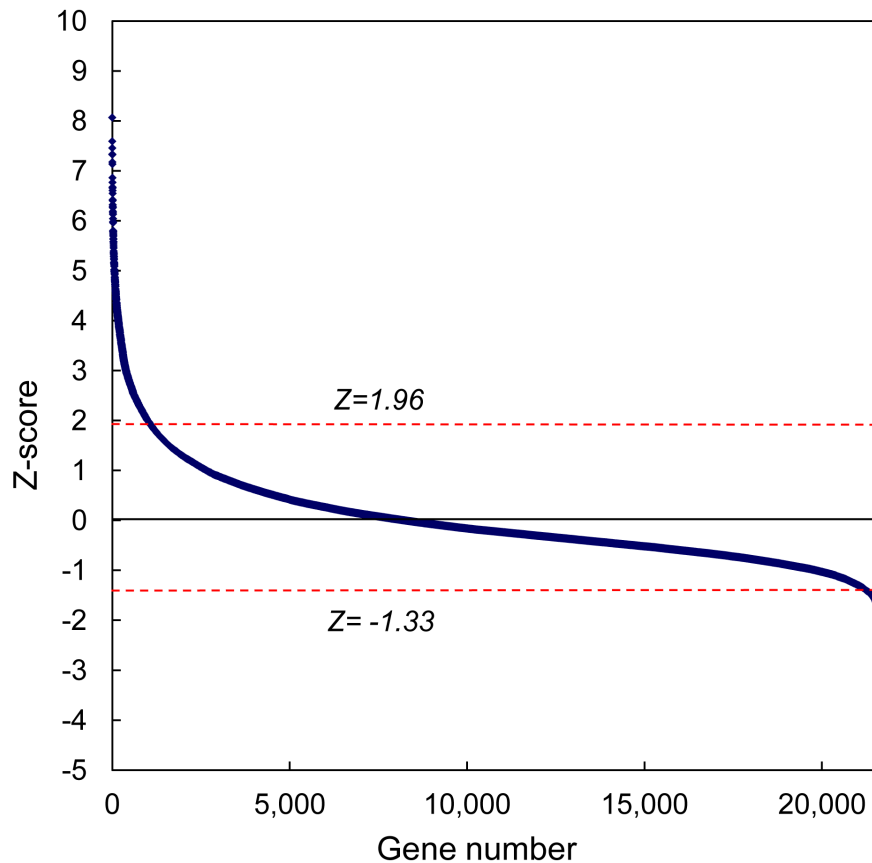
Figure 3.8. Z-score analysis of data from the whole-genome screen. A Z-score was calculated for each gene, using the means of the replicates after prior normalization using the plate means. Genes with Z-score ≥1.96 and ≤-1.33 were identified as potential hits and were included in the validation screen. See text for further discussion of the selection criteria.

3.2.4 Validating the whole-genome primary siRNA screen

We rescreened 1721 siRNAs in duplicate in a validation screen. These comprised 1588 siRNA hits from the whole-genome primary screen, 69 additional high-scoring hits from the kinome screens (hits not detected by the whole-genome screen), and 64 randomly selected "non-hit" controls (i.e. Z-score ≈ 0) from the whole-genome screen. We also incorporated the positive control siRNAs targeting PFKL as well as the R1 subunit of the cellular ribonucleotide reductase into all the plates.
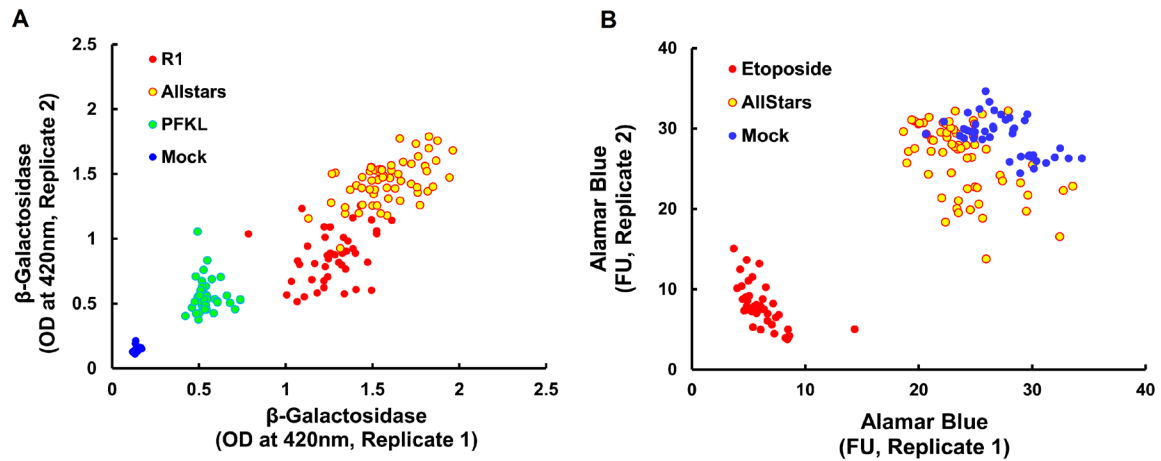
Figure 3.9. Assay reproducibility and discriminatory capacity. Panel A. Each of the plates used in the validation screen included extra wells containing siRNAs targeting the cellular ribonucleotide reductase (R1) and PFKL genes, as well as the AllStars control siRNA. The virus was also omitted from some wells to provide a blank for the β-galactosidase assays. The scatterplot illustrates the manner in which these replicate datapoints cluster across the multiple assay plates and shows that the screening method can readily discriminate between siRNAs that have no (AllStars), moderate (R1), or strongly (PFKL) inhibitory effects. Panel B. Each of the plates in the toxicity screen included extra wells where the cells were either mock treated, treated with a poisonous topoisomerase inhibitor (20 µM etoposide), or transfected with AllStars siRNA. The Alamar blue fluorescence assay readily discriminates between wells containing cells killed by etoposide *versus* wells containing AllStars transfected or mock-treated cells.

The validation screen was conducted in duplicate and showed a high degree of correlation between the duplicates with R^2=0.9 **(Figure 3.5D)**. We also determined the degree of correlation between the normalized means of the whole genome and of the validation screens and again noted a high degree of agreement between the screens with R^2=0.8 **(Figure 3.5E)**. As one would expect, these data also re-clustered into the three pre-selected groups representing inhibitory, stimulatory, and neutral siRNA pools **(Figure 3.5E)**. The controls also clustered into predicted groups with the mock-infected wells producing the lowest reading for β-galactosidase activity while the level of activity detected in infected cells treated with the two inhibitory positive controls (R1 and PFKL siRNAs) clustered between the levels detected in mock-infected cells and in the MYXV-infected cells treated with the "Allstars" control siRNA **(Figure 3.9A)**. The validation screen thus provided some confidence that these methods can reproducibly detect siRNA pools that modulate the growth of MYXV in MDA-MB-231 cells.

Table 3.1. Comparison of the results of the whole-genome validation and custom siRNA library screens

		Dharmacon custom siRNA library			
		Hits: increased MYXV replication	Hits: decreased MYXV replication	Non-hits	**Total**
Validation screen	Hits: increased MYXV replication	8 (27.6%)	3 (10.3%)	18 (62.1%)	29
	Hits: decreased MYXV replication	4 (13.3%)	7 (23.3%)	19 (63.3%)	30
	Non-hits	5 (17.2%)	2 (6.9%)	22 (75.9%)	29
	Total	22	21	45	**88**

3.2.5 Determining reproducibility using Dharmacon custom siRNA library screens

Some insights into the reproducibility and reliability of the methods are obtained by comparing the results of the kinome and whole genome screens. By definition, the kinome siRNAs comprise a subset of the whole genome set, but the two libraries were designed separately and employ different chemical modifications. Of the 96 genes detected in the two initial kinome screens, 28% were subsequently detected again in the whole genome primary screen. We included all 96 hits in the whole genome validation screen, and again detected 37.5% as hits.

To further analyze the degree of reproducibility of the results of our screens, we purchased a custom siRNA library from a different company. The library contains a pool of four siRNAs targeting each of 88 genes (59 hits and 29 non-hits of the whole genome screens) in 96-well plates. The hits were selected randomly from statistically significant pathway-hits. After the screens were performed in triplicates and normalized, we used SSMD ≥ 3 and SSMD ≤ -3 cut-offs for hit selection. The custom library screen found 25.4% of the hits of the whole-genome screens as high probability true positives and 75.9% of the non-hits as high probability true negatives **(Table 3.1 and Table S2)**. Thus taking the two comparisons together approximately one fourth to one third of the genes identified by our methods can be verified using independent libraries and screens. This is higher than the aforementioned meta-analysis of genes affecting HIV replication, but we have the advantage of using similar transfection, infection, and assay protocols.

3.2.6 Screen for siRNA toxicity

We were concerned that these methods do not exclude cytotoxic siRNAs. To identify which of the 1721 siRNAs might be toxic, we measured cell viability at the end

of the 3-day transfection period, using the same transfection protocol and an Alamar blue

cell viability assay (504). The data clustered into three groups **(Figure 3.5F)**. Most of the

siRNAs in the replicate assays clustered into two groupings in the upper right hand

quadrant, which exhibited no signs of toxicity as judged by the strong fluorescence

signals. [Why we saw two clusters of signals is unclear, although it is unrelated to the

siRNAs or to transfection because untreated cells, and cells transfected with "Allstars"

control, produced the same two data clusters **(Figure 3.9B)**]. In contrast, a small group of

siRNAs produced very low viability scores in both replicates. These scores are typically

produced by toxic agents, such as etoposide, which was added as an internal control to

wells in each plate in the screen **(Figure 3.9B and 3.10)**. These findings showed that the

Alamar blue screen readily detects toxic siRNAs.
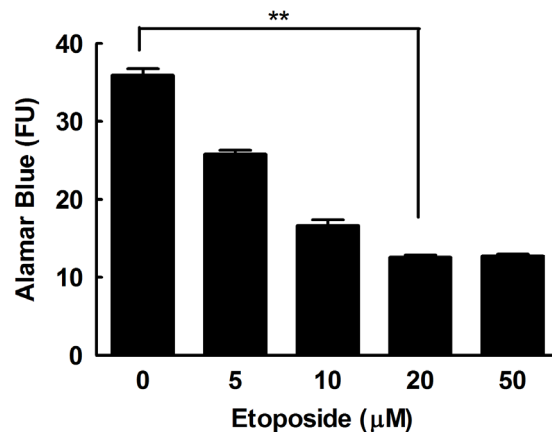
Figure 3.10. Titration of etoposide in MDA-MB-231 cells. MDA-MB-231 cells were plated overnight in 96-well dishes (5000 cells/well) and then cultured in media containing 0-50µM etoposide for three more days. An Alamar blue cell viability assay showed that a 70% reduction in fluorescence (maximal killing) could be achieved using 20µM drug. The data are representative of three independent experiments (**, $p \leq 0.001$).

The data obtained from the siRNA toxicity screen were normalized and the frequency distributions **(Figure 3.7C and 3.7D)** permitted analysis using Z-score statistics. Toxic siRNAs were defined as those with Z-score $\leq$ -1.96. The screen identified 32 toxic siRNAs of which many belong to the ubiquitin-proteasome pathway including the UBC gene encoding ubiquitin C **(Table 3.2)**. Many of these proteasomal genes play some role in regulating or supporting the cell cycle, as do other toxic gene targets like the human WEE1 homolog, PLK1, and RAN. In hindsight this may not have been too surprising. Bortezomib (Velcade®) is a recognized chemotherapeutic agent, that inhibits the 26S proteasome and induces apoptosis in transformed cells (531). Our screen has clearly identified MDA-MB-231 cell sensitivity to siRNAs targeting different components of the 26S proteasome, and further validates the method used to discover siRNAs that "inhibit" MYXV replication. Recent papers have suggested that proteasome inhibitors might find some utility as anti-poxviral agents (532, 533). However, our data do highlight the critical importance of examining the effects of these drugs on cell viability, especially over longer times of exposure and considering cell type.

3.2.7 Analysis of "hits"

We used the SSMD method to analyze the results of the validation screen. Those siRNAs that exhibited SSMD scores $\leq$ -3 or $\geq$ 3 were defined as the final hits in the screen although these conservative criteria likely overlook weaker, but still biologically real hits (see below). Overall, we identified 711 siRNAs that promoted MYXV growth in MDA-MB-231 cells and 333 siRNAs that inhibited its replication **(Table S2)**. This is 4.8% of all the siRNAs/genes we screened. Genes that increased and decreased

Table 3.2. Toxic siRNAs

Gene symbol	Gene name	Z score
LOC729093	hypothetical protein LOC729093	-1.97
PSMD11	proteasome (prosome, macropain) 26S subunit, non-ATPase, 11	-2.01
CYP51A1	cytochrome P450, family 51, subfamily A, polypeptide 1	-2.01
PSMC4	proteasome (prosome, macropain) 26S subunit, ATPase, 4	-2.02
RAN	RAN, member RAS oncogene family	-2.02
LOC728242	X antigen family, member 2-like	-2.02
IFITM1	interferon induced transmembrane protein 1 (9-27)	-2.04
PSMD3	proteasome (prosome, macropain) 26S subunit, non-ATPase, 3	-2.07
TFAP4	transcription factor AP-4 (activating enhancer binding protein 4)	-2.10
SNRPEL1	small nuclear ribonucleoprotein polypeptide E-like 1	-2.14
RGS3	regulator of G-protein signaling 3	-2.15
LOC119358	similar to hCG2040270	-2.18
ZFP3	zinc finger protein 3 homolog (mouse)	-2.21
LOC728991	hypothetical LOC728991	-2.23
FAM55B	family with sequence similarity 55, member B	-2.43
SLC38A10	solute carrier family 38, member 10	-2.45
KIAA1604	KIAA1604 protein	-2.52
PLK1	polo-like kinase 1 (Drosophila)	-2.53
FLJ22675	hypothetical gene supported by AK026328	-2.63
PSMD1	proteasome (prosome, macropain) 26S subunit, non-ATPase, 1	-2.84
C9orf135	chromosome 9 open reading frame 135	-2.85
PSMD8	proteasome (prosome, macropain) 26S subunit, non-ATPase, 8	-2.93
WEE1	WEE1 homolog (S. pombe)	-2.98
TTLL8	tubulin tyrosine ligase-like family, member 8	-3.06
ALB	Albumin	-3.08
LOC644828	hypothetical LOC644828	-3.30
LOC728689	similar to eukaryotic translation initiation factor 3, subunit 8, 110kDa	-3.35
RPL21	ribosomal protein L21	-3.47
LOC728962	similar to 60S ribosomal protein L7	-3.47
UBA52	ubiquitin A-52 residue ribosomal protein fusion product 1	-3.49
SF3B1	splicing factor 3b, subunit 1, 155kDa	-3.52
UBC	ubiquitin C	-5.45

MYXV replication when silenced were defined as antiviral and proviral hits, respectively. In the contrary, siRNAs that target proviral genes and reduce virus replication are termed antiviral siRNAs and *vice versa*. In this thesis, the term 'hits' refers to genes, not the siRNAs that target them.

These hits were categorized using the PANTHER classification system (218). The method compares the list of hits affecting MYXV growth with a reference list containing all the genes in the human genome, categorized as to putative or known function. Those pathways that were statistically over-represented, with a p-value ≤ 0.05, were considered to be biologically significant. Among the pathways involving genes that decreased the replication of MYXV, when silenced, were the previously noted ubiquitin-proteasome system, the Ras and mitogen activated protein kinase (MAPK) pathways, chemokine and cytokine inflammatory pathways, and the cell cycle **(Figure 3.6C)**. Among the pathways that significantly increased virus growth, when genes in these pathways were silenced, were the oxidative stress response, ascorbate degradation, and endothelin signalling pathways **(Figure 3.6D)**. A few pathways are represented in both categories of hits (the Ras and chemokine/cytokine signalling pathways) although the statistics are more solid in the MYXV growth inhibiting siRNA category.

We also examined the relationship between the hits using the PIN database (520) of interacting nuclear proteins. We noted that several genes encoding proteins that are part of transcription complexes appear to have an anti-viral activity, that is, knocking down these genes enhanced MYXV growth. For example, we detected hits in proteins that are components of the TFIID transcription initiation factor (TAF4 and TAF9) and a TFIID-related complex (TRRAP, TAF4, and TAF9). Several (3 of 10) proteins

comprising the TFIIH initiation/elongation complex (ERCC2, GTF2H1, and CCNH) were also detected in our screen.

Although 1044 gene hits are still too many to investigate in detail, we elected to explore a subset of these hits and pathways to gain some insights into whether the screen had reliably identified new cell factors affecting MYXV replication. Based upon the data summarized in **Table S2** and **Figure 3.6**, we chose to study a subset of genes that play important roles in glycolysis and the cell cycle.

3.3   SUMMARY AND BRIEF DISCUSSION

We performed several siRNA screens and identified a total of 1044 genes (hits) that affect the replication of MYXV in MDA-MB-231 cells, a breast cancer cell line. These genes represent 4.8% of the known genes in the human genome. We also identified 32 siRNAs that are toxic to cells. Of the hits, twice as many genes appeared to serve an antiviral than a proviral role. That is, virus growth was stimulated by siRNAs targeting 711 genes and inhibited by 333 siRNA pools. This is not the outcome that one would expect if many siRNAs simply decrease cell fitness, and thus renders cells less supportive of virus growth, and suggests that organisms might encode a great many minor systems that collectively create innate antiviral defenses.

We conducted a cluster enrichment analysis for pathways and identified a number of pathways enriched with our hits including MAPK/Ras pathway, glycolysis, apoptosis signalling pathway and cell cycle control system.

The degree of overlap of the hits in pairwise comparison of our screens ranges from 25.4% to 37.5%. Compared to the degree of hit overlap in pairwise comparisons for hits of screens for other viruses such as HIV, influenza virus and VACV, our screens

showed a much higher rate of overlap. This high rate of hit-overlap is due to the fact that our screens utilized the same cell lines and transfection protocols, unlike the comparisons made for other viruses, discussed in Chapter 1.

Overall, our screens have identified important gene- and pathway-hits that can be used as a basis for future studies, which will be conducted to fully document the cellular factors that affect the replication of poxviruses.

CHAPTER 4: THE ROLE OF GLYCOLYSIS AND THE CELL CYCLE CONTROL SYSTEM IN MYXV REPLICATION

A version of the data presented in this chapter, except the data on sulforaphane and proTAME treatments, were published in:

Teferi, W. M., Dodd, K., Maranchuk, R., Favis, N., and Evans, D. (2013). A whole-genome RNA interference screen for human cell factors affecting myxoma virus replication. Journal of Virology. **87**(8): 4623-41**.**

I performed all of the experiments presented in the chapter. I also wrote the original manuscript with editorial contributions from my supervisor, Dr. David Evans.

4.1   INTRODUCTION

A number of viruses, which belong to diverse families, modulate cellular energy metabolism and the cell cycle control system to create favorable conditions for their replication. Viruses usually modulate three important metabolic pathways, including glycolysis, fatty acid synthesis and glutaminolysis, to generate energy and to increase the production of precursors and intermediates for the synthesis of macromolecules such as proteins, membrane lipids and nucleotides (250). Glycolytic enzymes and metabolites also regulate cell proliferation and apoptosis downstream of PI3K and Akt pathways (260, 534-536).

VACV has been shown to reprogram cellular energy metabolic pathways towards enhanced fatty acid synthesis and glutaminolysis. Inhibition of these pathways negatively affects the replication of the virus (306-308). MYXV, on the other hand, enhances the production of glycolytic end products such as lactate in primary chorioallantoic cells suggesting enhanced glycolysis in infected cells (310).

Our siRNA screens identified glycolysis as one of the top pathway-hits, which affected the replication of MYXV in MDA-MB-231 cells. Here we performed independent siRNA silencing, small chemical inhibition and glycolytic gene over-expression experiments and demonstrated that MYXV replication is enhanced in cells with increased aerobic glycolytic activity, while inhibiting glycolysis reduced virus replication.

Similarly, both RNA and DNA viruses modulate the cell cycle control system in various manners. Some viruses, such as small DNA viruses, promote entry into the cell cycle, while others interfere with cell cycle checkpoint proteins and pathways resulting in

cell cycle arrest at their preferred phases of the cell cycle (367). VACV infected cells rapidly enter to the cell cycle and accumulate in S-phase (373). Similarly, MYXV has been shown to induce entry to the cell cycle and accumulation of cells in S- and G2/M-phases of the cell cycle through M-T5 protein mediated degradation of CKIs (371). Our screens also identified the cell cycle control system as one of the top pathway-hits. Our analysis and independent experiments showed that cells arrested at late G1-phase of the cell cycle enhance MYXV replication. Moreover, a small chemical that leads to G1 arrest increases the oncolytic potential of MYXV. In addition to glycolysis and the cell cycle control system, we also described the effect of silencing of the accessary subunit of human DNA primase (PRIM-2) on the replication of MYXV virus.

4.2   RESULTS

4.2.1   Glycolytic enzymes were identified as major hits in our siRNA screens

After uptake, glucose is phosphorylated to glucose 6-phosphate by hexokinases (HK) and then converted into pyruvate in eight additional steps. The rate limiting step in glycolysis is catalyzed by PFK-1 (253) and three PFK-1 isoforms have been identified in liver (PFKL), muscle (PFKM), and platelets (PFKP). PFK-1 is allosterically regulated by fructose-2,6-bisphosphate, which is produced from fructose 6-phosphate by 6-phosphofructose-2-kinase/fructose-2,6-bisphosphatase (PFKFB) (256-258). PFKFB is a homodimeric enzyme and there are four different isoforms each encoded by different genes (PFKFB1-to-4). Many of these enzymes in (or regulating) the glycolytic pathway were major hits in the kinome screens **(Figure 3.6)**, with siRNAs targeting PFKL, PFKM, HKIII, and PFKFB1 all inhibiting MYXV replication and siRNAs targeting glucose-6-phosphate isomerase (GPI) and fructose-1,6-bisphosphatase 1 (FBP1)

stimulating virus growth **(Table S1)**. Most of these hits (except for HKIII and GPI) were also detected in the whole-genome screens, although the effects on *LacZ* expression were obscured by other higher scoring siRNAs and thus the glycolytic pathway does not
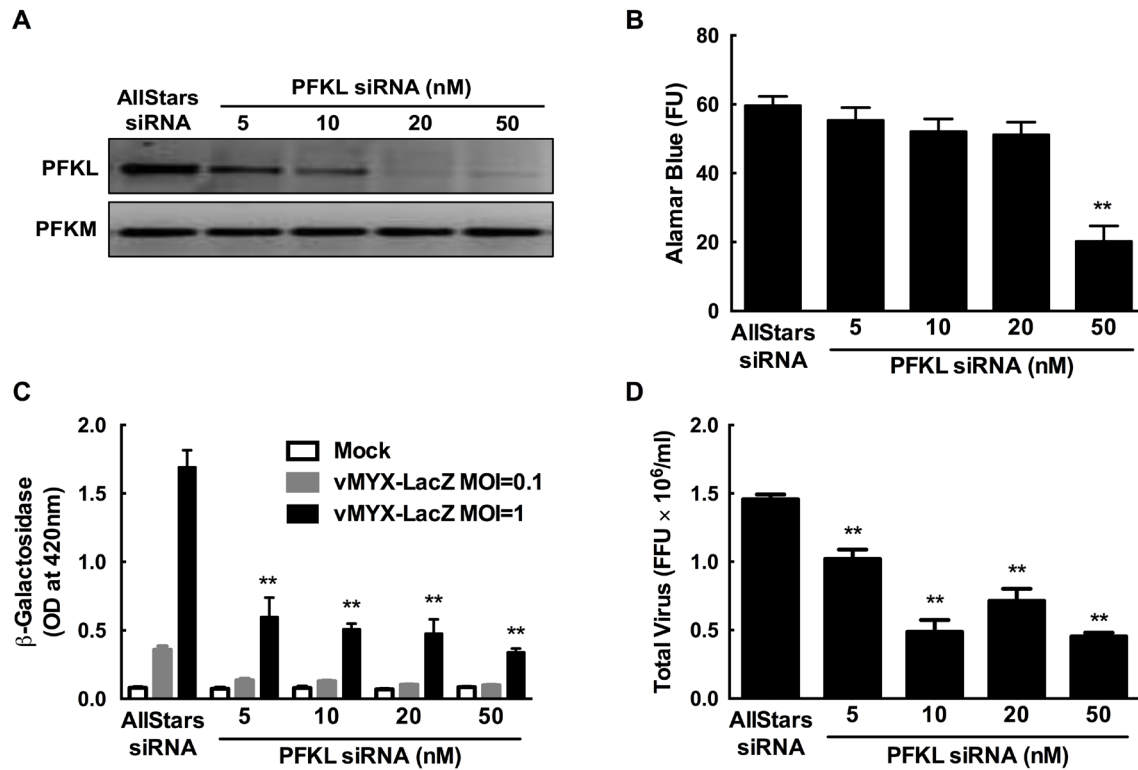
Figure 4.1. siRNA silencing of liver phosphofructokinase (PFKL) inhibits MYXV replication. MDA-MB-231 cells were transfected with siRNA against PFKL for 3 days and then lysed and RT-PCR used to measure specific knockdown of the liver (PFKL) rather than the muscle (PFKM) isozyme transcript (Panel A). The transfected cells were also screened for viability using an Alamar blue assay (fluorescence units, FU) (B) or infected with MYXV for 48h at multiplicities of infection (MOI) of 0.1 and 1 for β-galactosidase assay (C) and MOI of 1 for virus yield (D). The RT-PCR reactions showed that 10-50nM siRNA was needed to knock down the PFKL transcript with toxicity only being observed ≥50nM PFKL siRNA (B). Virus growth was significantly (**, *p≤0.001*) reduced using even the lowest doses of siRNAs, relative to cells treated with the negative control siRNA. The data are representative of three independent experiments.

appear amongst the final pathway-hits from the whole-genome screen **(Figure 3.6)**. The fact that the enzymes that promote glycolysis (e.g. PFKL) also promote MYXV replication, and enzymes that negatively regulate glycolysis (e.g. FBP1) reduce MYXV growth, led us to hypothesize that MYXV infection is highly favored in cells utilizing glycolytic metabolism. The experiments described in the following sections were performed to confirm if this was correct.
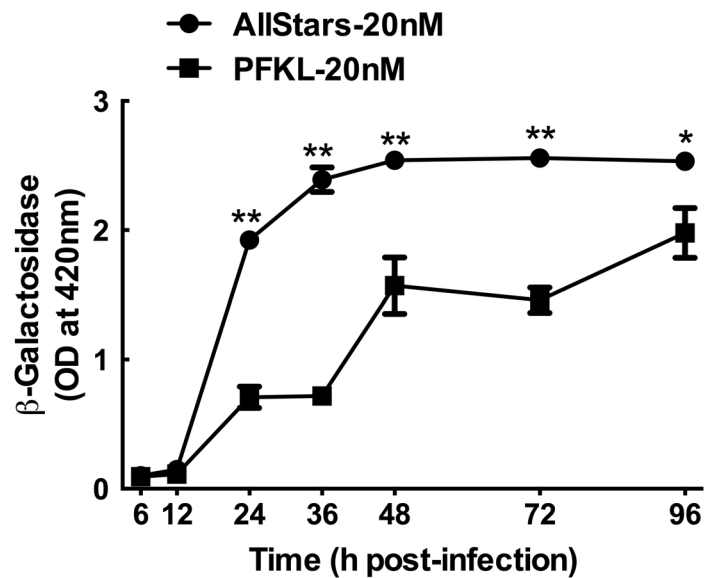
Figure 4.2. The growth kinetics of vMYX-LacZ in PFKL siRNA transfected cells. MDA-MB-231 cells were transfected with the indicated concentrations of AllStars or PFKL siRNA for 72h. Then the cells were infected with vMYX-LacZ at MOI of 1. At the indicated time points after infection, the cells were lysed and β-galactosidase activity was determined. Cells transfected with PFKL siRNA showed a significant reduction in virus replication starting from 24h post infection. The data are representative of three independent experiments and the significance is indicated relative to AllStars negative control siRNA transfected cells: (*, $p \leq 0.01$; **, $p \leq 0.001$).

4.2.2   Inhibition of glycolysis reduces the replication of MYXV

Among our hits in the glycolytic pathway, we elected to focus on PFK-1 (PFKL and PFKM) and PFKFB, enzymes that regulate the rate limiting steps of glycolysis. We first used RT-PCR to verify the knockdown of PFKL mRNA in MDA-MB-231 cells. Cells were transfected with different concentrations of PFKL siRNA for 3-days and then RT-PCR, and PFKL-specific primers, were used to measure the residual levels of PFKL transcripts. As little as 5nM siRNA was needed to achieve some knockdown of PFKL over a 3-day period, although better silencing was seen using 20-50nM siRNA and without off-target effects on PFKM **(Figure 4.1A)**. However, the highest concentrations
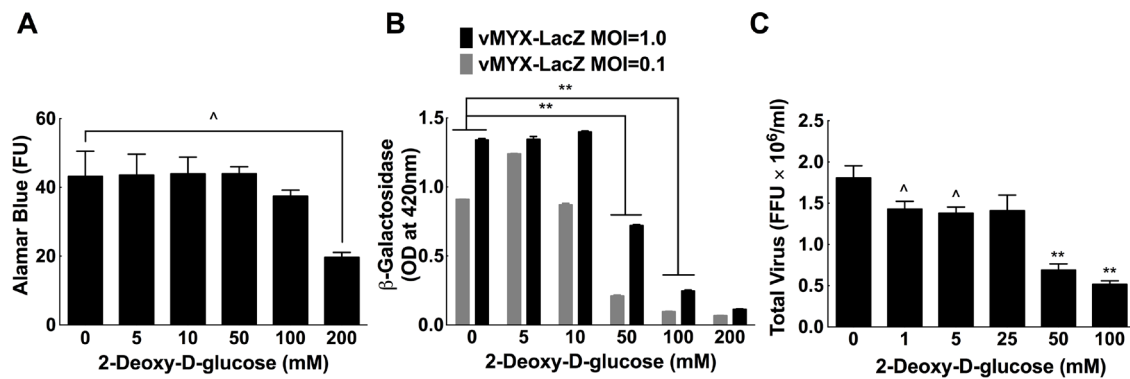
Figure 4.3. A glycolytic inhibitor, 2-deoxy-D-glucose (2DG), also inhibits MYXV growth. MDA-MB-231 cells were pre-treated with 2DG for a day and then infected with MYXV for 48h in the continued presence of 2DG. An Alamar blue assay was then used to measure cell viability (A) and virus growth was measured using β-galactosidase (B) and plaque (C) assays. The plaque assay experiments were conducted using multiplicity of infection of 1. A significant (^, $p \leq 0.05$; **, $p \leq 0.001$) reduction in virus growth was seen in cells treated with ≥50mM 2DG using the β-galactosidase assay or with doses as low as 1mM by plaque assay. No significant toxicity was detected at 2DG concentrations <100mM. The data are representative of three independent experiments.

of PFKL siRNA (50nM) produced significant toxicity **(Figures 4.1B)**. These concentrations of PFKL siRNA were also retested to see what effects they had on β-galactosidase expression and virus yields over a 48h infection cycle. Both assays detected a 2-3-fold reduction in virus gene expression and yields (FFU) using 10-20nM siRNA. These are conditions where one detects little or no toxicity **(Figure 4.1C and D)**. We also examined the growth kinetics of MYXV in PFKL siRNA transfected cells and determined that silencing of PFKL results in a reduction in virus replication at all time points starting from 24h post infection **(Figure 4.2)**. Similar results were obtained using 2-deoxy-D-glucose (2DG), a chemical inhibitor of glycolysis. In these experiments, 2-3-fold reductions in gene expression **(Figure 4.3B)** and virus yields **(Figure 4.3C)** were
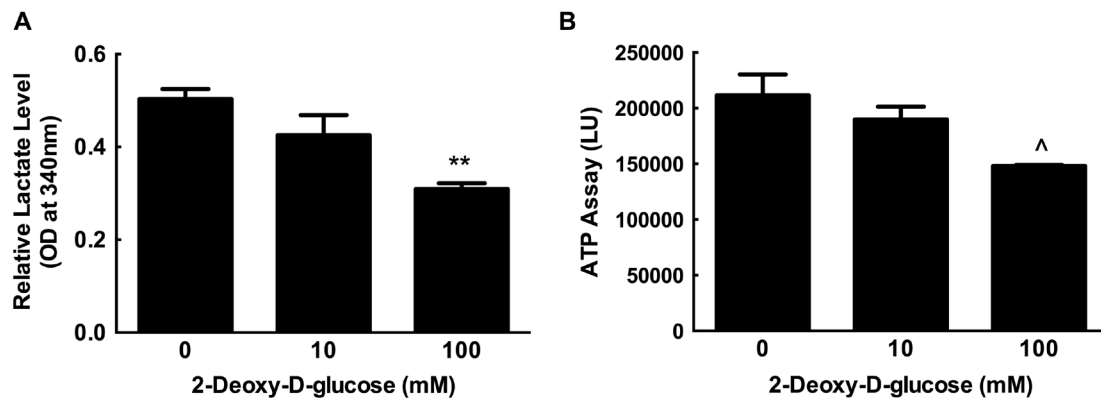
Figure 4.4. Treating cells with 2-deoxy-D-glucose (2DG) reduces the levels of lactate and ATP. MDA-MB-231 cells were treated for 24h with 0, 10, or 100mM 2DG and the effects on the concentrations of lactate in the media (A) and ATP in the cell lysates (B) were determined using colorimetric (OD, optical density) and luminescence (LU, luminescence unit) assays, respectively. Although 10mM 2DG causes some reduction, 100mM 2DG is required to significantly reduce the levels of lactate and ATP. The data are representative of three independent experiments and the significance is indicated relative to untreated control cells: (^, $p \leq 0.05$; **, $p \leq 0.001$).

again detected in the presence of 50-100mM 2DG, concentrations causing little or no toxicity **(Figure 4.3A)**. To prove that 2DG was working, we also measured the levels of lactate and ATP. Both compounds were significantly reduced in cells treated with higher (100mM) concentrations of 2DG showing that glycolysis is inhibited under these conditions **(Figure 4.4)**.

4.2.3   MYXV replication is enhanced by increasing glycolytic activity

We also tested whether a reciprocal increase in virus yield could be obtained by increasing the amount of glycolysis in MYXV-infected cells. For this purpose, we used pIRES-EGFP plasmids encoding PFKM or PFKFB3, plasmids which have been shown to increase glycolytic activity in transfected COS-7 cells (537). RT-PCR showed one can also obtain higher levels of expression of these genes in MDA-MB-231 cells **(Figure 4.5A)**, although this did not have any effect on MYXV growth under standard cell culture conditions **(Figure 4.5B and C)**. However, we noted that the culture medium used in all of these studies contains high levels of glucose (17.5 mM) and were concerned that this might have been saturating the glucose flux through the glycolytic pathways. Therefore we repeated the experiments in media containing 10 or 2.5mM concentrations of glucose. Although this somewhat reduced the cell viability, relative to cells grown in DMEM/F-12 **(Figure 4.5B)**, we now saw increased virus growth in PFKM-transfected cells whether measured using β-galactosidase (~1.5-fold, **Figure 4.5C**) or using plaque assays (~2.5 fold, **Figure 4.5D**). We also detected a ~2-fold increase in virus yield in cells transfected with PFKFB3 **(Figure 4.5D)**, although this was not correlated with an increase of β-galactosidase expression **(Figure 4.5C)**. Increased glycolytic activity was confirmed by a ~40% and ~60% increase in lactate level in MDA-MB-231 cells transfected with
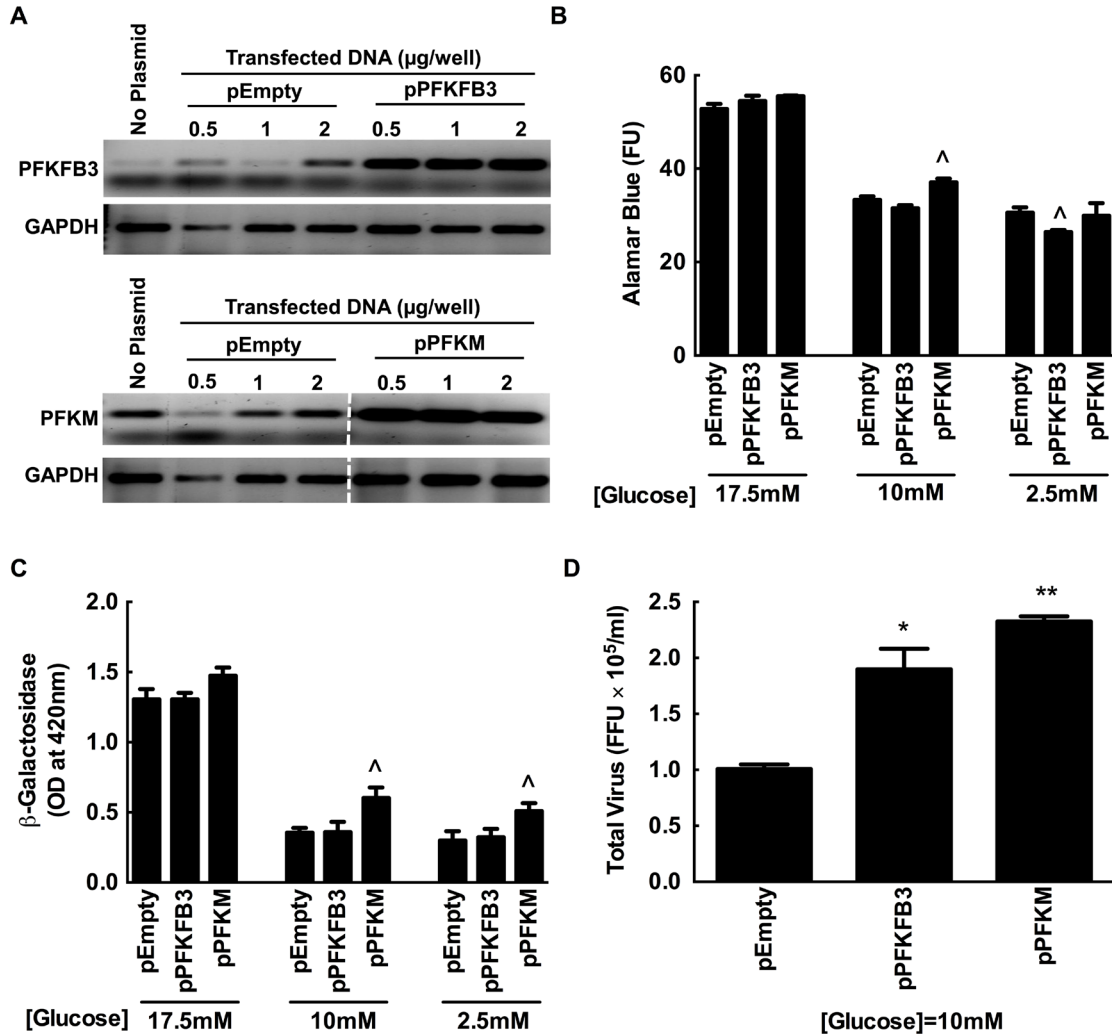
Figure 4.5. MYXV growth is enhanced by phosphofructokinase in low glucose media. MDA-MB-231 cells were transfected with either an empty plasmid (pEmpty), or with plasmids encoding PFKM or PFKFB3, and cultured for 3 days in standard DMEM/F12 media. RT-PCR was used to detect the expression of the transfected genes (A). In a parallel study, cell survival was measured after transfecting MDA-MB-231 cells using 1 µM plasmids, and then culturing the cells for three days in DMEM/F-12 medium containing 17.5 (normal), 10, and 2.5mM glucose (B). Other cells were also infected with MYXV at MOI=0.1 for two days and virus replication measured using β-galactosidase (C) or plaque (D) assays. Although dropping the glucose concentration reduces cell viability and thus virus yields, the effect on virus yields can be partly reversed by enhancing the expression of PFKM and to a lesser extent PFKFB3. The data are representative of three independent experiments. Significance is indicated relative to the pEmpty vector controls: (^, $p{\le}0.05$; *, $p{\le}0.01$; **, $p{\le}0.001$)
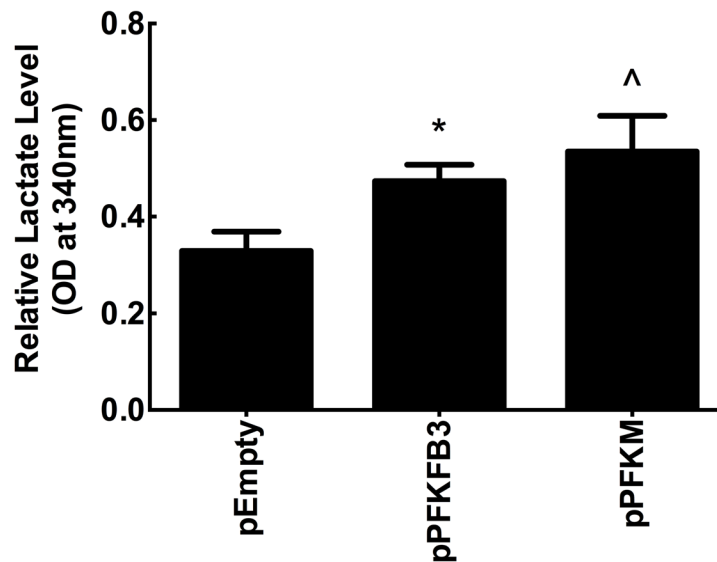
Figure 4.6. The level of lactate increases in glycolytic enzymes over-expressing cells. MDA-MB-231 cells were transfected with either an empty plasmid (pEmpty), or with plasmids encoding PFKM or PFKFB3, and cultured for 3 days in standard 10 mM glucose containing DMEM. The level of lactate in the supernatant was determined using a colorimetric (OD, optical density) assay. Lactate production was increased by 44% and 62% in PFKFB3 and PFKM plasmid transfected cells, compared to cells transfected with an empty plasmid. The data are representative of three independent experiments and the significance is indicated relative to empty plasmid transfected cells: (^, $p \leq 0.05$; *, $p \leq 0.01$).

PFKFB3 and PFKM expressing plasmids in 10 mM glucose medium, respectively **(Figure 4.6)**. Collectively these data support the observations from the original siRNA screens, and show that MYXV growth is positively correlated with glycolytic activity in a transformed human cell.

4.2.4   The effect of silencing of pyruvate dehydrogenase kinase 3 (PDK3) on MYXV replication

In normal cells, PDC catalyzes the conversion of glycolysis-generated pyruvate to acetyl-CoA, which then shuttles to the TCA cycle. The activity of PDC is regulated by

127

PDK, where phosphorylation leads to inhibition of PDC. There are four isotypes of PDK, PDK1-PDK4, in humans. Our screens showed that siRNA silencing of PDK3 increased MYXV replication in MDA-MB-231 cells, suggesting that increased shuttling of pyruvate to the TCA cycle creates a favorable condition for virus replication. We confirmed the results of our screen by using independent siRNAs that knockdown PDK3 in MDA-MB-231 cells. RT-PCR showed that siRNA concentration of 10nM or more achieved a near complete silencing of PDK3 after 3 days of transfection without any effect on cell viability **(Figure 4.7A and B)**. β-galactosidase and virus yield assays showed that the replication of vMYX-lacZ increased by 2.7 and 3.6 fold, respectively, in MDA-MB-231 cells that were transfected with 20nM PDK3 siRNA for 3 days **(Figure 4.7C and D)**. The level of lactate remained unchanged, while that of ATP increased by 50% in 5nM and by ~100% in 10nM and 20nM PDK3 siRNA transfected cells in 17.5mM glucose-containing DMEM **(Figure 4.8)**. These results suggest that increased glycolytic activity, which results in enhanced carbon flux to the TCA cycle, enhances the replication of MYXV.

4.2.5   MYXV infection of MDA-MB-231 cells does not affect lactate production

The above studies demonstrated that the degree of replication of MYXV is affected by the activity of glycolysis. To examine the effect of MYXV infection on the glycolytic activity of MDA-MB-231 cells, lactate levels were measured and compared with non-infected and VACV infected cells. The results showed that the level of lactate is not affected by MYXV infection in these cancer cells **(Figure 4.9)**. Even though previous studies showed that MYXV is able to increase lactate levels in primary cells, the virus may not need to enhance glycolysis in cancer cells with over-active glycolysis.
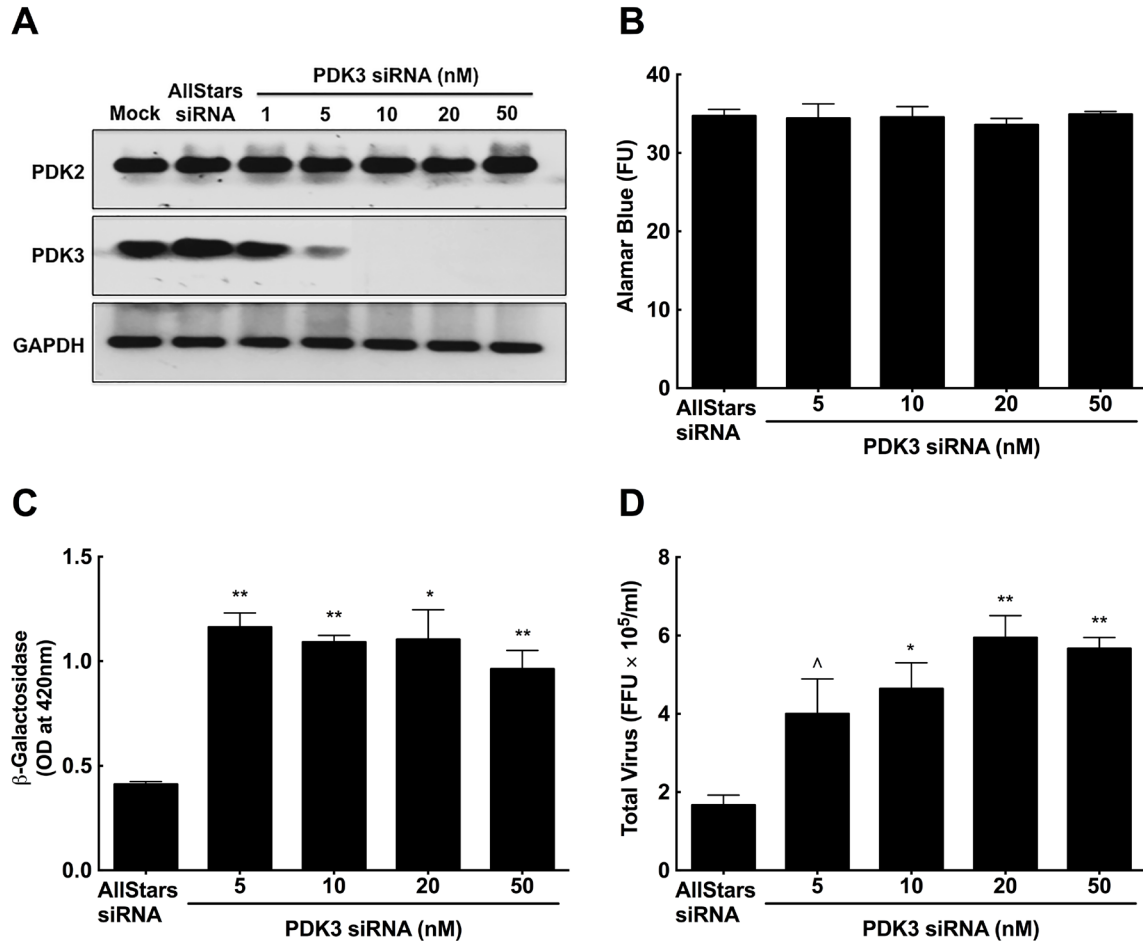
Figure 4.7. siRNA knockdown of pyruvate dehydrogenase kinase 3 (PDK3) increases the replication of MYXV. MDA-MB-231 cells were transfected with PDK2, PDK3 or AllStars negative control siRNA for 3 days and then lysed and RT-PCR used to measure silencing of the respective transcripts (Panel A). The transfected cells were also screened for viability using an Alamar blue assay (fluorescence units, FU) (B) or infected with MYXV for 48h at multiplicities of infection (MOI) of 1 for β-galactosidase assay (C) and for virus yield (D). The data are representative of three independent experiments.
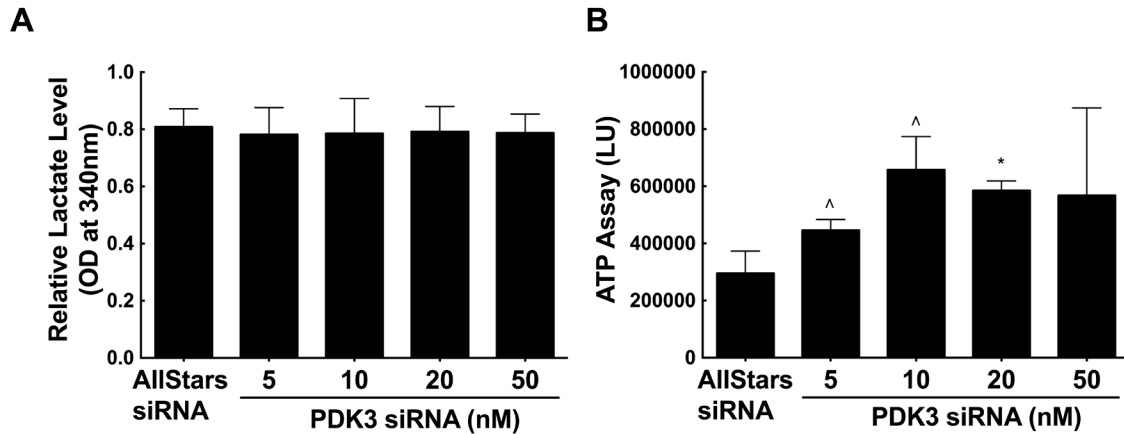
Figure 4.8. The effect of siRNA silencing of PDK3 on lactate and ATP levels. MDA-MB-231 cells were transfected for 24h with the indicated concentrations of PDK3 siRNA and the effects on the concentrations of lactate in the media (A) and ATP in the cell lysates (B) were determined using colorimetric (OD, optical density) and luminescence (LU, luminescence unit) assays, respectively. Although siRNA silencing of PDK3 does not change lactate production, it increased the levels of ATP. The data are representative of three independent experiments and the significance is indicated relative to AllStars negative control siRNA transfected cells: ($^\wedge$, $p \leq 0.05$; **, $p \leq 0.001$).
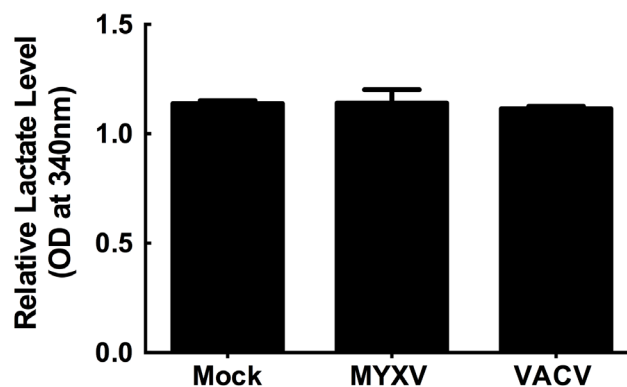
Figure 4.9. MYXV or VACV infection does not change the level of lactate in MDA-MB-231 cells. MDA-MB-231 cells were mock infected or infected with vMYX-lacZ or VACV (WR) at multiplicity of infection of 1 for 48h. The media was collected and lactate level was determined by measuring optical density (OD) in a colorimetric assay. The data are representative of three independent experiments.

4.2.6 siRNA screen hits of the cell cycle control system

The cell cycle is known to play an important role in modulating MYXV replication, as illustrated by studies showing that the MYXV M-T5 protein promotes p27 degradation and exit from the G0/G1 checkpoint (371). It is thus perhaps not surprising that a striking pattern of siRNA hits was observed amongst genes linked to, or regulating the cell cycle **(Table 4.1)**. Interventions that might promote the transition into G1, or inhibit passage from G1 into S-phase, in uninfected cells, consistently stimulated MYXV growth, whereas knocking down genes that regulate passage throughout the rest of the cell cycle consistently decreased virus growth **(Table 4.1)**. For example E2F5 appears to suppress expression of genes required for entry into G1 (538) and its knockdown stimulates MYXV growth. Similarly, Cdk6 regulates progression out of G1 in MDA-MB-231 cells through hyperphosphorylation of retinoblastoma protein and release of activator E2Fs (539), and also by catalyzing the assembly of the pre-replicative complex during G1 (540). Our screen detected proviral siRNA hits in both CDK6 and its regulatory binding partner cyclin D2 (CCND2) (541). The process of "DNA licensing" in G1 also requires that the Mcm proteins to be incorporated into a hexameric MCM2-7 helicase (540), and siRNAs targeting one of these genes (MCM2) also stimulated MYXV growth. Finally, another proviral siRNA hit was also detected in cyclin H (CCNH) a protein linked to many cellular activities including regulation of Cdk4/6 by forming a Cdk-activating kinase complex with Cdk7 and MAT1 (542).

In contrast, MYXV growth was inhibited by siRNAs targeting genes affecting or regulating subsequent events in the cell cycle. For example, the NPAT gene is required for S-phase histone expression and cell cycle progression (543) and siRNAs targeting

NPAT were highly inhibitory. Two of the siRNA pools were toxic for MDA-MB-231 cells (WEE1 and PLK1). Wee1 and Plk1 comprise a regulatory triad with Cdc2 (also called Cdk1), and inhibiting the expression of either Wee1 or Plk1 within this negative feedback loop, might be expected to improperly promote the G2-M transition by releasing Cdc2/Cdk1 from Wee1 inhibition (544). We also noted that knocking down genes involved in regulating the DNA damage checkpoints had deleterious effects on virus growth (although an important *caveat* is that MDA-MB-231 cells encode a mutated p53 gene which complicates the interpretation of signaling patterns (545, 546)). For example, DNA protein kinase (PRKDC) normally phosphorylates RPA2 in the presence

Table 4.1. Hits detected in the cell cycle using the DAVID algorithm

Gene Symbol	Gene name	SSMD[‡]
E2F5	E2F transcription factor 5, p130-binding	6.67
MCM2	minichromosome maintenance complex component 2	5.95
CDK6	cyclin-dependent kinase 6	5.89
LOC646096	protein kinase CHK2-like; CHK2 checkpoint homolog (*S. pombe*); similar to hCG1983233	5.70
CCNH	cyclin H	5.39
CCND2	cyclin D2	4.68
ANAPC13	anaphase promoting complex subunit 13	3.86
BUB1B	budding uninhibited by benzimidazoles 1 homolog beta (yeast)	-4.42
PRKDC	similar to protein kinase, DNA-activated, catalytic polypeptide; protein kinase, DNA-activated, catalytic polypeptide	-4.85
CDC25B	cell division cycle 25 homolog B (*S. pombe*)	-5.26
PLK1	polo-like kinase 1 (Drosophila) – TOXIC	-6.45
TTK	TTK protein kinase	-7.88
CHEK1	CHK1 checkpoint homolog (*S. pombe*)	-8.21
STAG2	stromal antigen 2	-8.89
WEE1	WEE1 homolog (*S. pombe*) – TOXIC	-9.57

[‡]Strictly standardized mean difference (SSMD).

of DNA damage and delays S-phase progression and mitotic entry (547), interfering with this system by knocking down PRKDC inhibited MYXV growth. Additional antiviral hits were seen in CHEK1 (also called CHK1) and a downstream effector, CDC25B. When activated by DNA damage signals, Chk1 phosphorylates (and inhibits) Cdc25B (548), stabilizing the phosphorylated form of Cdc2/Cdk1, and favouring G2 arrest. (Using siRNAs to inhibit WEE1 and CHK1 during S-phase also causes unscheduled DNA replication and chromosome breaks and could deplete cells of dNTPs (549).) Adding further to the complexity, Cdc25B, Cdc2/Cdk1, and Plk1 form another regulatory triad (550, 551), that when perturbed can promote aberrant mitosis (548). These data suggest that defective regulation of events outside of G1 creates a situation deleterious to MYXV growth. This hypothesis can perhaps be extended by noting that knocking down two genes required by the spindle assembly checkpoint, TTK (also called Mps1) (552) and BUB1B (553), also inhibits MYXV growth, although siRNAs directed against TPR (a component of the nuclear pore that is specifically required to assemble the mitotic spindle checkpoint complex (554)) seemed to stimulate virus growth. Some of these effects may be related to the fact that cap-dependent translation is inhibited in mitotic cells (555) or to regulation of the APC complex (553, 556). However, further studies are needed to clarify the situation.

4.2.7 MYXV replication is increased in cells arrested at G1-phase of the cell cycle

The analysis of the cell cycle hits of our siRNA screens, which is described above, led us to test the hypothesis that MYVX replication is favored in cells when they are initially encountered occupying the G1 (or the G1/S boundary) portion of the cell cycle. First we tested whether treating cells with the Cdk4/6 inhibitor PD-0332991 (557)
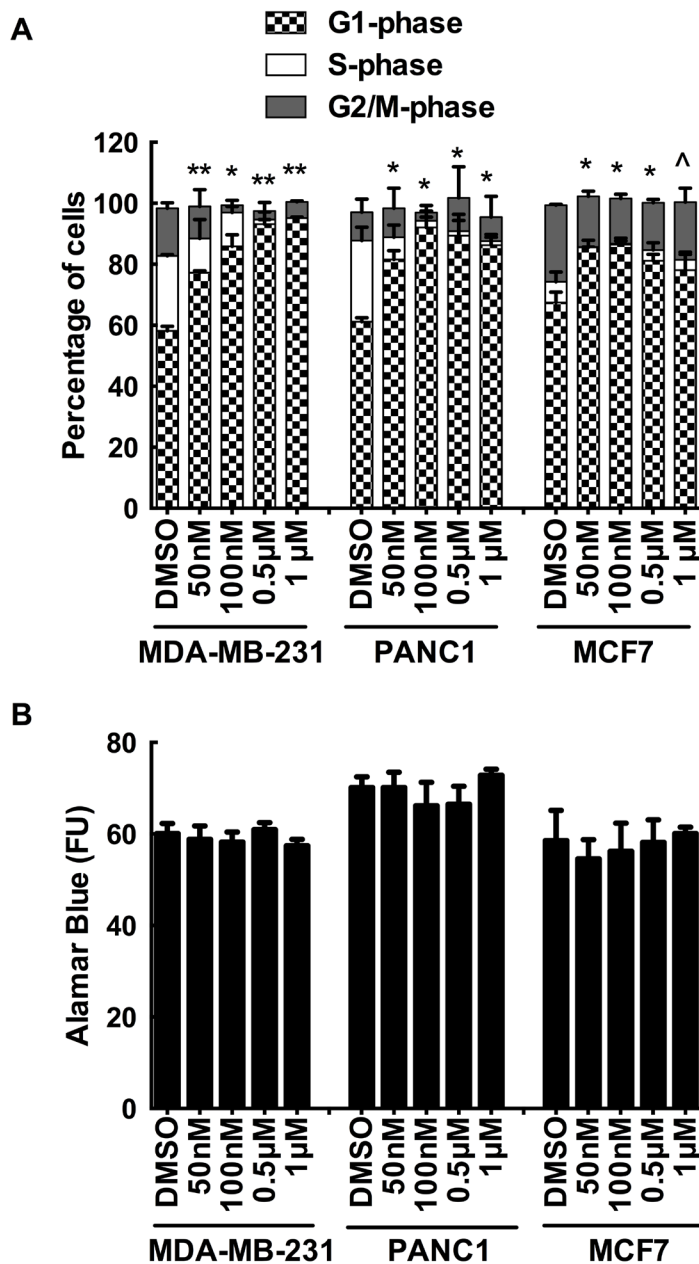
Figure 4.10. The CDK4/6 inhibitor, PD-0332991, induces G1 arrest without toxicity. MDA-MB-231, PANC1, and MCF7 cells were treated with the indicated doses of PD-0332991 for 24hr, trypsinized, stained with propidium iodide, and flow cytometry used to determine the distribution of cells across the cell cycle. Low (50nM) doses of the drug significantly increased the proportion of G1 phase MDA-MB-231 and PANC1 cells and (to a lesser extent) also increased the proportion of G1-phase MCF7 cells (A) without significant toxicity (B). The data are representative of three independent experiments and significance is indicated as described above.
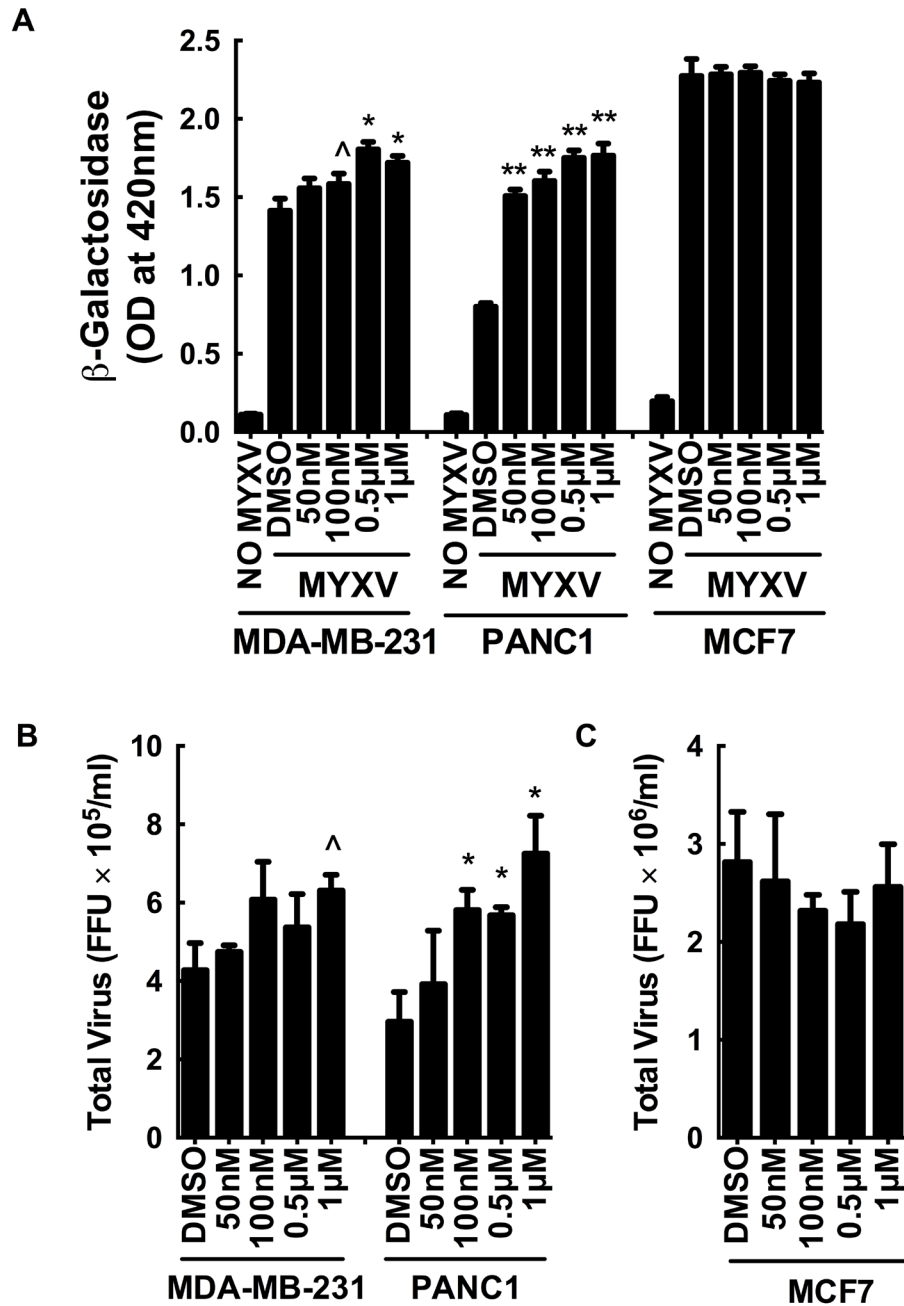
Figure 4.11. Inhibiting cell cycling with the CDK4/6 inhibitor, PD-0332991, enhances MYXV growth in some cancer cell lines. MDA-MB-231, PANC1, and MCF7 cells were treated with the indicated doses of PD-0332991 for 24hr and infected with MYXV for 48h and assayed for virus-encoded β-galactosidase and focus formation. PD-0332991 significantly enhanced MYXV growth in PANC1 and MDA-MB-231 cells, relative to the solvent controls, but had no effect on MCF7 cells (panels A-C). The data are representative of three independent experiments and significance is indicated as described above.

would produce the same proviral effects seen with siRNAs targeting CDK6. Such treatments should stabilize cells in G1, and this was tested by flow cytometric measurement of the DNA content in three different kinds of PD-0332991-treated cells: MDA-MB-231, PANC1 and MCF7 **(Figure 4.10A)**. These cells were also then tested to measure the effects of PD-0332991 on MYXV growth, and the effects of the siRNA targeting CDK6 were duplicated in MDA-MB-231 and PANC1 cells. Applying 1µM PD-0332991 to MDA-MB-231 cells (twice the IC$_{50}$ (557)) increased the proportion of cells in G1 from 58% to 95% and enhanced MYXV growth by about 30% **(Figure 4.11A and B)**. A similar effect was seen in PANC1 cells **(Figure 11A and B)**. The drug did not enhance MYXV growth in MCF7 cells, although PD-0332991 also had a lesser effect upon the proportion of G1 cells **(Figure 4.10A, Figure 4.11A and C)**. MCF7 cells are also far more supportive of MYXV growth, than are MDA-MB-231 and PANC1 cells, suggesting that the cell cycle may not be a factor that limits virus growth in these cells. If we assume that PD-0332991 is a specific inhibitor of Cdk4/6, these studies support the hypothesis that the G1 phase of the cell cycle is more advantageous for virus growth.

4.2.8 The effect of siRNA silencing of the accessory subunit of human DNA primase on cell cycle and MYXV replication

We also wanted to test how well MYXV grows when cells are stabilized in S-phase, but this is complicated by the fact that most S-phase inhibitors poison DNA replication and thus also directly inhibit virus replication. However, we had noted that siRNA silencing of PRIM2 expression also inhibited MYXV growth **(Table S2)**, and this provided another way of exploring how progression through the cell cycle affects MYXV growth. The mammalian DNA primase is a heterodimer composed of a catalytic subunit
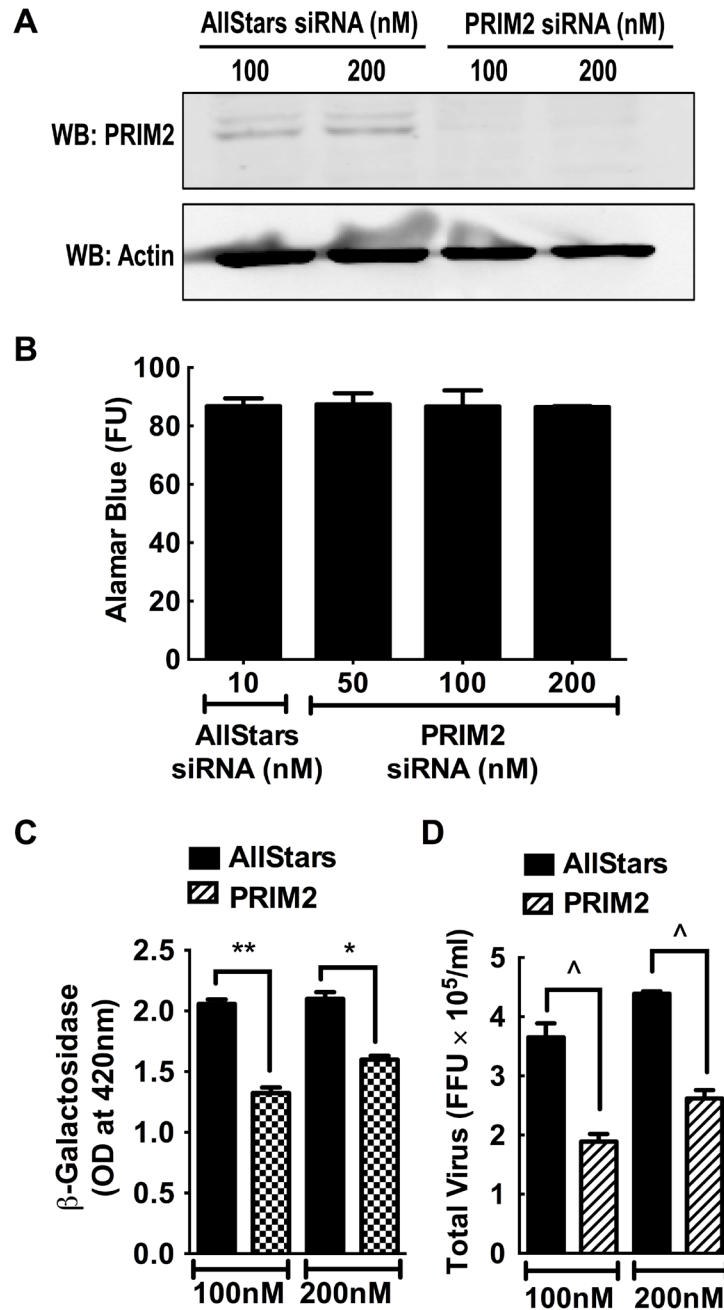
Figure 4.12. PRIM2 modulates MYXV growth in MDA-MB-231 cells. MDA-MB-231 cells were transfected with control or PRIM2 siRNA for 72h and then a Western blot was used to show PRIM2 knockdown (A). A three-day treatment with PRIM2 siRNA also caused a significant reduction in MYXV growth (MOI=0.1, 48h) as judged by β-galactosidase (B) and plaque assays (C). The data are representative of three independent experiments and significance is indicated as described above.
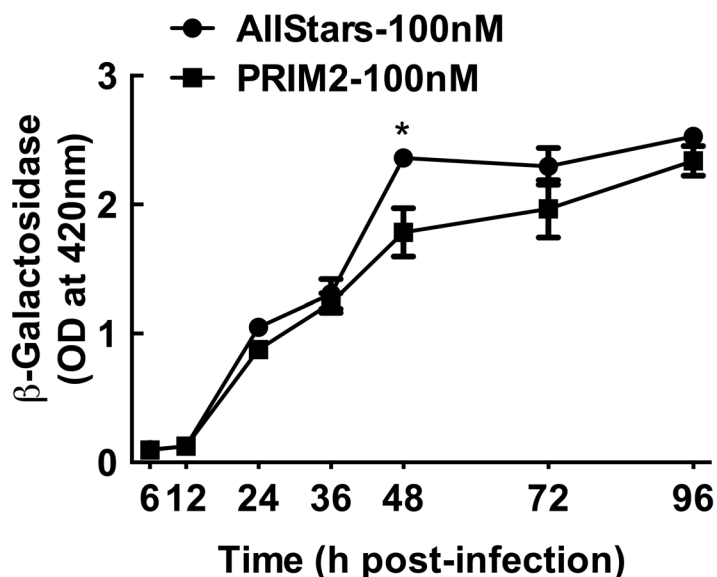
Figure 4.13. The growth kinetics of vMYX-LacZ in PRIM2 siRNA transfected cells. MDA-MB-231 cells were transfected with the indicated concentrations of AllStars or PRIM2 siRNAs for 72h. Then the cells were infected with vMYX-LacZ at MOI of 1. At the indicated time points after infection, the cells were lysed and β-galactosidase activity was determined. For PRIM2 siRNA transfected cells, the most significant reduction in virus replication was observed at 48h post infection. The data are representative of three independent experiments and the significance is indicated relative to AllStars negative control siRNA transfected cells: (*, $p \leq 0.01$).

(PRIM1) and an accessory subunit (PRIM2) (558-560). In *S. pombe*, disrupting primase function activates the Chk1 checkpoint response (561) and we suspected that this effect might also be observed in human cells. Independent experiments confirmed that siRNA silencing of PRIM2 **(Figure 4.12A)** caused a 25-40% decrease in MYXV growth as demonstrated by both β-galactosidase **(Figure 4.12C)** and plaque assays **(Figure 4.12D)** although the degree of reduction in virus replication is reduced as time of infection is advanced beyond 48h **(Figure 4.13)**. We also observed that inhibiting PRIM2 function had no negative effects on cell survival at doses up to 200 nM **(Figure 4.12B)** while increasing the proportion of cells in S-phase **(Figure 4.14)**. This is consistent with

knocking down PRIM2 causing a delay in S-phase progression, and supports the hypothesis that MYXV grows best when cells are occupying the G1 or the G1/S part of the cell cycle.
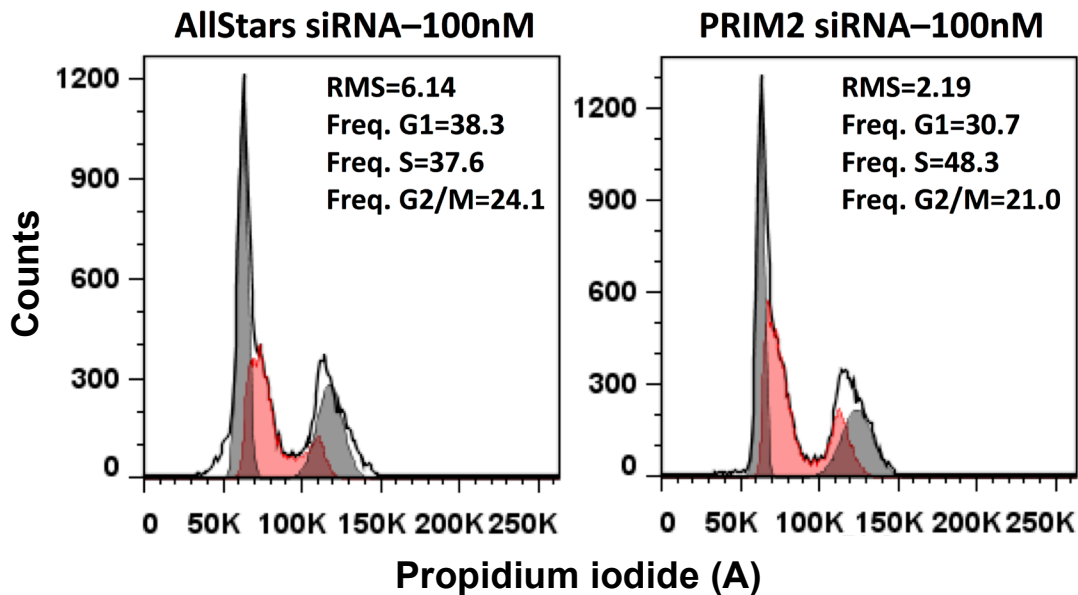
Figure 4.14. siRNA silencing of PRIM2 increases the proportion of cells in S-phase of the cell cycle. MDA-MB-231 cells were transfected with AllStars control or PRIM2 siRNA for 72h. Propidium iodide staining and flow cytometry showed that siRNA silencing of PRIM2 produced a 10% increase in the proportion of S-phase cells at the expense of G1- and G2/M-phase cells. The curve which corresponds to S-phase cells is shaded in red. The data are representative of three independent experiments.

These conclusions are complicated by one further observation. We had assumed that since poxviruses encode their own DNA primase (the VACV D5 protein exhibits a helicase-primase activity (55)), there would be no reason to expect that cellular PRIM2 would play any direct role in virus DNA replication. However, as a check on this

assumption, we transfected cells with a plasmid encoding a myc-tagged version of PRIM2 (none of the available antibodies were suitable for use in imaging applications) and then monitored the distribution of the protein in mock- and MYXV-infected cells. In the absence of virus, PRIM2 was mostly distributed throughout the cytoplasm, with some small amount of nuclear staining, but curiously appears to be recruited to factories in MYXV-infected cells **(Figure 4.15)**. This may not have any significance, as many DNA-binding proteins are recruited to virus factories (summarized in (562)), but we cannot exclude the possibility that PRIM2 also serves a more direct role in supporting MYXV growth.

4.2.9   The effect of G2-phase arrest on MYXV replication

Sulforaphane (SFN), which is a naturally occurring substance found in cruciferous vegetables, has antiviral and chemotherapeutic potentials. Its antiviral activities involve various mechanisms including induction of antioxidant responses, which have been shown to play a protective role in respiratory syncytial virus induced lung injury and experimental herpes encephalitis (563, 564). The anticancer effects of SFN also involve diverse mechanisms (565). One of them is through induction of G2/M arrest and apoptosis in prostate cancer cells by decreasing the levels of Cdc25B, Cdc25C and cyclin B1 as well as by keeping Cdk1 in its inactive state (566).

To determine the effect of G2/M-phase arrest on MYXV replication, we screened for cancer cell lines that undergo G2/M arrest with SFN treatment. We found that treatment of MCF7 cells with 25μM SFN for 24h increased G2/M-phase cells from 23.5% to 43.2% while reducing the proportion of G1 and S-phase cells without significant toxicity **(Figure 4.16A and B)**. Infection of MCF7 cells, which are pre-treated
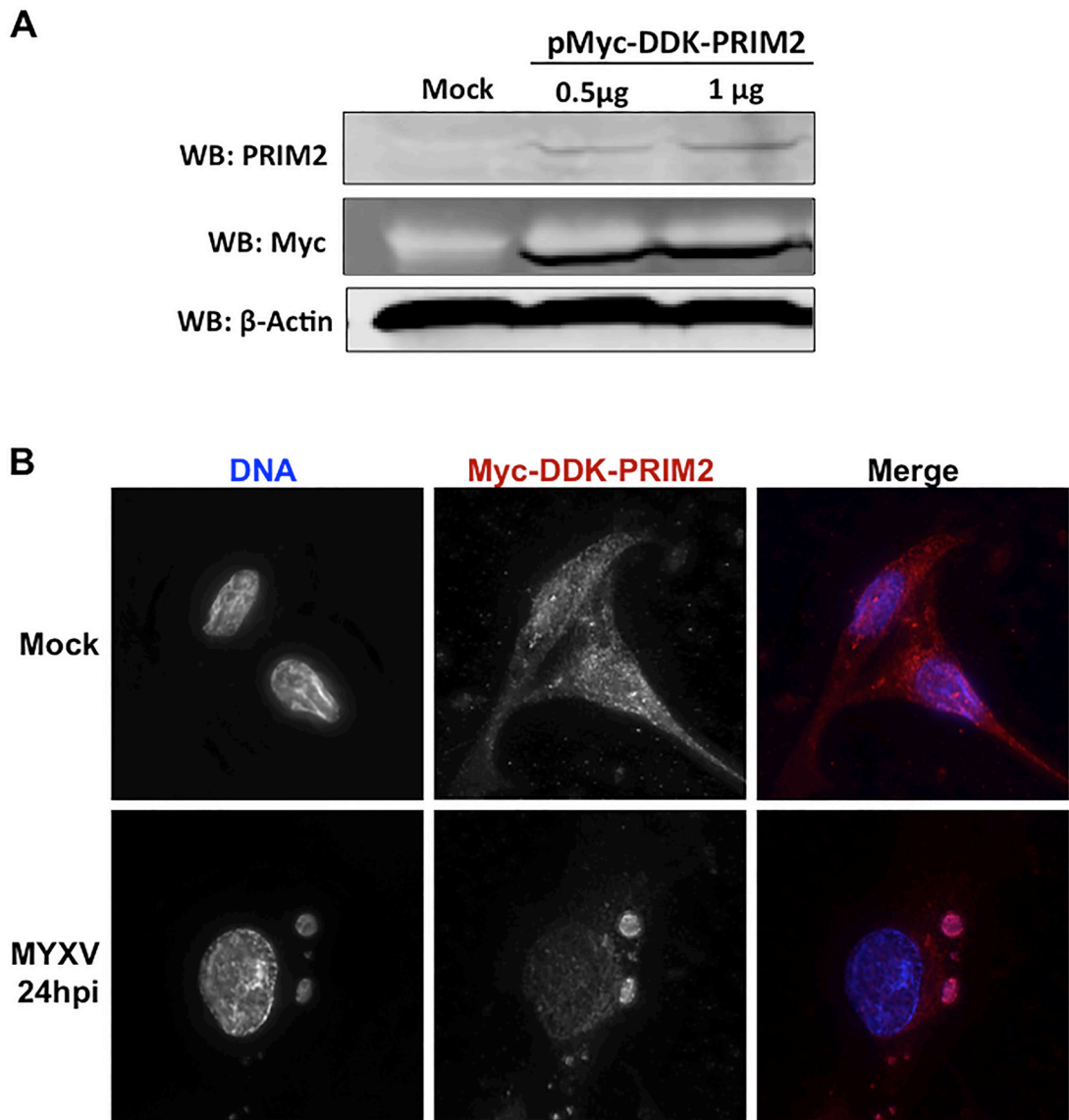
Figure 4.15. PRIM2 relocates to virus factories. A plasmid encoding a myc- and DDK-tagged form of PRIM2 was transfected into MDA-MB-231 cells where it can be over-expressed as judged by a Western blot (A). The cells were infected with vMYX-LacZ at MOI of 5 for 24h followed by fixation and staining for DNA and myc-DDK-PRIM2. PRIM2 appears to relocate to MYXV factories. The data are representative of three independent experiments.

with SFN for 24h, with vMYX-LacZ at MOI of 1, in the presence of the drug, resulted in a 75% reduction in the activity of virus encoded β-galactosidase activity, suggesting a reduction in virus replication **(Figure 4.16D)**. We also found a 25% reduction in the viability of cells following 72h of treatment with 25μM SFN **(Figure 4.16C)**, suggesting reduced cell viability could be a contributing factor for the reduction in virus replication. However, the reduction in the proportion of G1 cells and/or the increase in G2/M-phase cells may also play a role in the reduction of virus replication since the magnitude of reduction in virus replication (75%) is much higher than the reduction in cell viability (25%) with SFN treatment. SFN could also use other mechanisms to exert its anti-MYXV activity.

Our screens showed that siRNA knockdown of ANAPC13, the gene encoding APC subunit 13, increased the replication of MYXV **(Table 4.1)**. We tested the effect of inhibiting the activity of APC, and hence arresting cells in mid-mitosis, on MYXV replication by using a prodrug of Tosyl-L-Arginine Methyl Ester (proTAME), a small chemical inhibitor of APC (567). Even though, we observed a significant reduction in virus replication in cells treated with proTAME, the prodrug was found to be very toxic to the cells we tested. This suggests that the effect of the drug on virus replication could be indirectly resulting from a significant reduction in the number of viable cells that support virus replication **(Figure 4.17)**.
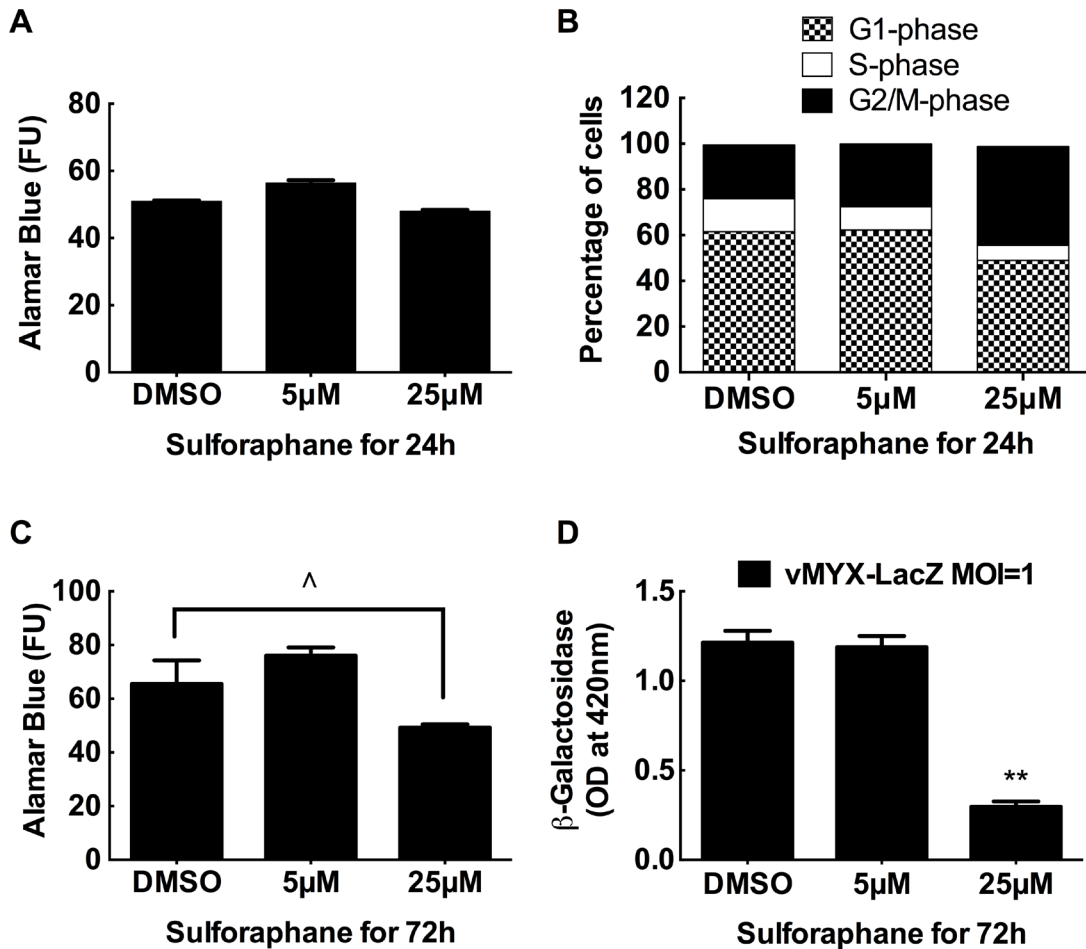
Figure 4.16. The effect of sulforaphane treatment and G2/M-phase arrest on MYXV replication. MCF7 cells were treated with the indicated concentrations of sulforaphane for 24h. Cell viability was determined by using a fluorescence based (FU, fluorescence unit) Alamar blue assay (A) and cell cycle analysis was performed using flow cytometry by staining the cells with propidium iodide (B). The viability of cells treated with sulforaphane for 72h was determined using Alamar blue assay (C). Sulforaphane treated cells were infected with vMYX-LacZ at multiplicity of infection (MOI) of 1 for 48h, in the presence of the drug, and virus replication was determined by measuring optical density in a β-galactosidase activity assay (D). The data are representative of three independent experiments and the significance is indicated relative to DMSO (vehicle) treated cells: $((^\wedge, p \leq 0.05; ^{**}, p \leq 0.001)$.

Figure 4.17. Produrg of Tosyl-L-Arginine Methyl Ester (proTAME) is toxic to cells. MDA-MB-231 cells were treated with proTAME for 24h and infected with vMYX-LacZ at multiplicity of infection (MOI) of 1 for 48h in the presence of the prodrug. Cell viability was determined after 72h of treatment using a fluorescence based Alamar blue assay (A). Virus replication was determined by measuring absorbance (OD, optical density) in a β-galactosidase assay (B). The data are representative of two independent experiments.

4.2.10 Enhancing oncolysis by manipulating the cell cycle control system

Finally, we also examined whether these studies might produce methods for improving virus killing of tumour cells. We hypothesized that combining a drug causing G1-phase growth arrest, PD-0332991, with MYXV infection would cause enhanced oncolysis. By itself, treating MDA-MB-231 cells with up to 1μM PD-0332991 for 4 days caused only a small (but not significant) reduction in cell viability, while infecting these cells with MYXV (at MOI=1) for 3 or 4 days killed 15-20% of the cells relative to uninfected and non-treated controls **(Figure 4.18)**. The amount of cell killing was further enhanced by ~20% either by simultaneous exposure of the cells to PD-0332991 and MYXV for 4 days, or by pre-treating the cells with PD-0332991 for a day followed by

A MDA-MB-231 Cells

B PANC1

C MCF7
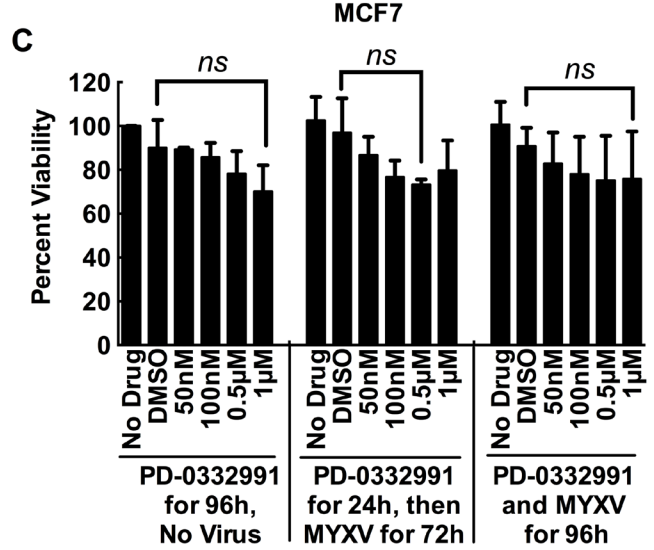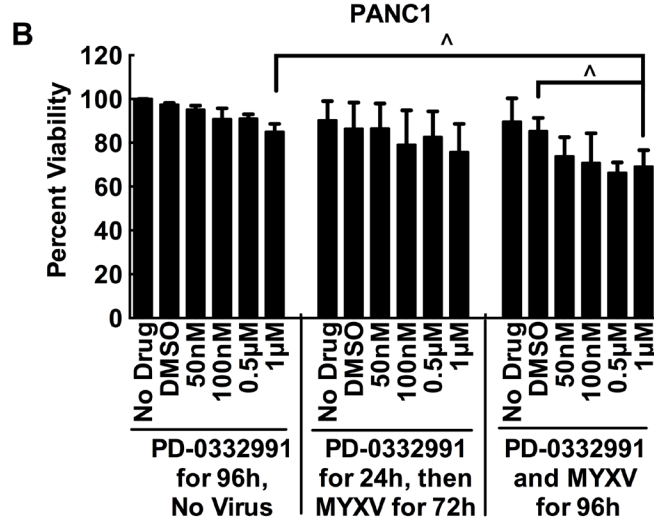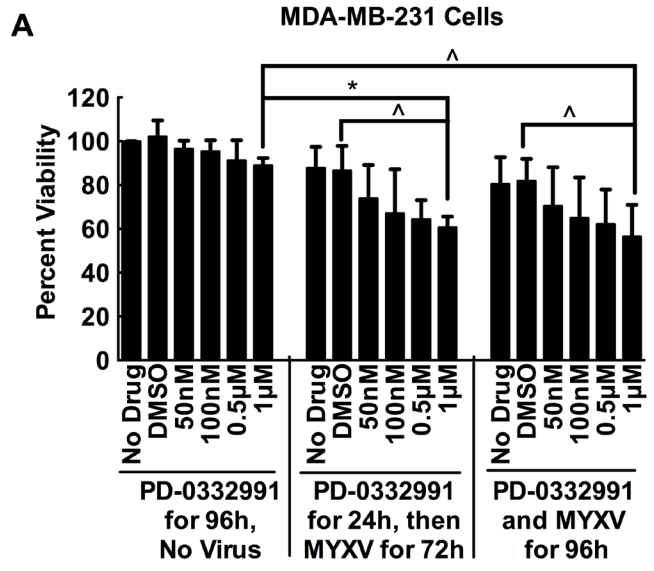
Figure 4.18. Treating cells with CDK4/6 inhibitor, PD-0332991, enhances the oncolytic activity of MYXV. MDA-MB-231 (A), PANC1 (B) and MCF7 (C) cells were treated with the indicated concentrations PD-0332991 alone for four days, or pre-treated with PD-0332991 for 24h and then infected with MYXV for three days (MOI=1), or they were simultaneously infected and treated with drug and virus for four days. Drug treatment appeared to reduce cell viability, but not enough to achieve significance. However, the effects of drug and virus appeared to be additive in MDA-MB-231 cells, with the combination treatment killing ~40% of the cells compared to the 10-15% killing caused by virus alone. The effect is also seen in PANC1 cells but not in MCF7 cells. The data combine the results of three independent experiments, each employing three replicates.

3 days of MYXV exposure **(Figure 4.18A)**. A similar effect was seen using PANC1 cells, albeit significance was obtained only if the cells were exposed to virus for 4 days **(Figure 4.18B)**. In contrast, these effects were not seen using PD-0332991-treated MCF7 cells, which as we have previously noted do not show the same drug-induced changes in the cell cycle that are seen in MDA-MB-231 or PANC1 cells **(Figure 4.10)**. Overall, these results suggest that MYXV oncolytic activity could be modestly enhanced by co-treatment with a class of chemotherapeutic drugs that promote accumulation of cells in G1-phase, although this effect will likely be seen only in selected cancer cells.

4.3   SUMMARY AND BRIEF DISCUSSION

Our screens identified a number of hits in glycolysis and the cell cycle control system. Further independent experiments demonstrated that increasing the glycolytic activity of cells enhances MYXV growth. Even though MYXV does not increase glycolysis in cancer cells, such as MDA-MB-231 cells, that already have high glycolytic activity, inhibiting glycolysis, on the other hand, results in a significant reduction in virus

replication. Our experiments also found that increased flux of glycolytic end products into the TCA cycle, and hence resulting in increased ATP production, also promotes MYXV replication. Studies have also demonstrated that MYXV tropism to cancer cells correlates with the level of Akt activity (119). Since Akt is one of the major regulators of glycolysis, as discussed in Chapter 1, our findings provide further insights into why Akt activity affects MYXV tropism.

Our screens identified several hits in the cell cycle control system. Analysis of the hits and independent small chemical inhibition experiments showed that cells in G1 or G1/S boundary support virus replication better than cells arrested in the other phases of the cell cycle. We have also showed that this observation can be exploited to enhance the oncolytic potential of MYXV in culture by combining the virus with a drug that results in G1-phase arrest.

CHAPTER 5: THE EFFECT OF POXVIRUS INFECTION ON CELLULAR CHROMATIN

The data presented in this chapter are part of an unpublished work.

I performed all the experiments discussed in this chapter except infection of cells with ΔF1L-VACV, which was performed by Ninad Mehta.

I would like to thank Dr. Michael Hendzel for generously providing reagents including D5 and W8 cell lines as well as for his invaluable comments and suggestions.

5.1 INTRODUCTION

As described in section 1.3.3, various families of viruses undergo extensive interactions with their cellular hosts' epigenetic mechanisms. Cells use their epigenetic tools to suppress virus replication and activate antiviral immunity. On the other hand, viruses exploit cellular epigenetic mechanisms to benefit their replication through inhibition of innate antiviral immunity and induction of pro-proliferative states. Moreover, viruses modulate chromatin-modifying complexes to promote viral gene expression and genome replication. Deciphering the interaction between viruses and the cellular epigenetic mechanisms has not only helped to further our understanding of epigenetics but also it has helped to identify potential targets for antiviral drugs.

A number of microarray and high-throughput sequencing studies were conducted to analyze cellular transcriptome changes during poxvirus infection (568-570). Most of these studies focused on members of the *orthopoxvirus* genus, such as VACV, cowpox and monkeypox viruses. In the case of VACV, a general pattern of changes in the cellular transcriptome was detected from the microarray and sequencing studies despite some variations in the results. The expression levels of a large number of cellular genes were reduced during VACV infection, especially at later time points after infection (569, 570). On the other hand, there were a few classes of genes that were up regulated throughout infection, including various types of histones and genes involved in intracellular signal transduction (568-570). The expression levels of the remainders of the genes were unchanged. In contrast, a microarray study for transriptome alterations during MYXV infection showed that only a small number of genes were either up- or down-regulated

149

while the vast majority of the genes remained unchanged, suggesting differential regulation of host gene expression between VACV and MYXV (571).

Currently, there are no published studies that have examined the interaction between poxviruses and the cellular chromatin regulation system. Our interest in studying the interaction between poxviruses and the cellular chromatin originated from a project that focused on studying the role of DNA-binding poxvirus proteins in modulating the DNA damage response and the G2/M checkpoint of the cell cycle, which is a major hit of our RNAi screens. In the study, we observed that one of the predicted DNA-binding VACV proteins, E5R, has two BEN domains (572). BEN domains are recently discovered DNA-binding protein domains, which are found in several animal and DNA virus proteins (572). Studies showed that BEN domain-containing proteins are involved in chromatin regulation and transcriptional suppression (573, 574). As a result we examined the effect of VACV infection on the repressive chromatin in the presence and absence of E5R (ΔE5R-VACV). This experiment showed that VACV infection enhanced markers of the repressive chromatin, although the presence or absence of E5R did not make any difference **(Figure S2 in the Appendix)**. Based on this interesting observation, we decided to study the interactions between poxviruses and the repressive chromatin in greater detail. In this study we analyzed how cellular chromatin dynamics changes during VACV infection. We specifically investigated the status of the repressive chromatin during infection with a focus on H3K9 and H4K20 methylation. We also determined whether VACV modulates the chromatin to reduce the expression of cellular genes during infection.

5.2   RESULTS

5.2.1   VACV infection increases the levels of markers of the repressive chromatin

The repressive chromatin is characterized by a compact structure and enrichment with H3K9me3, H4K20me3 and H3K27me3 (575, 576). These markers are abundant both at constitutive and facultative heterochromatin domains. To examine the effect of VACV infection on the amount and distribution of H3K9me3, BSC40 cells were infected with wild-type VACV (strain WR) and immunofluorescence and flow cytometry studies were conducted at various time points after infection. Infected cells demonstrated a global increase in the intensity of nuclear H3K9me3 staining as well as enhancement of H3K9me3 foci in the nucleus **(Figure 5.1)**. These levels increased throughout infection going from almost the same as uninfected cells at 3h post-infection to a ~ 2.5 fold increase at 6h post-infection and plateauing at a ~ 4 fold higher level at 9 – 12h post-infection. A direct comparison of H3K9me3 differences between infected and uninfected cells is shown in **Figure 5.2**.

To examine whether the increase in HK9me3 levels in VACV-WR infected cells occurs throughout the nucleus (i.e. both at high intensity foci and low intensity regions) or it is confined to high intensity foci only, we measured a pixel-by-pixel intensity of H3K9me3 along a line drawn across the longest diameter of the cells. The results indicated that VACV-infected cells demonstrated an increase H3K9me3 intensity both at high-intensity foci and low-intensity regions of the nucleus compared to non-infected cells **(Figure 5.3A-F)**. In contrast, the overall DAPI intensity appeared to be similar between infected and non-infected cells although infected cells showed more uniform DAPI intensity across the nuclei than non-infected cells **(Figure 5.3G-L)**.
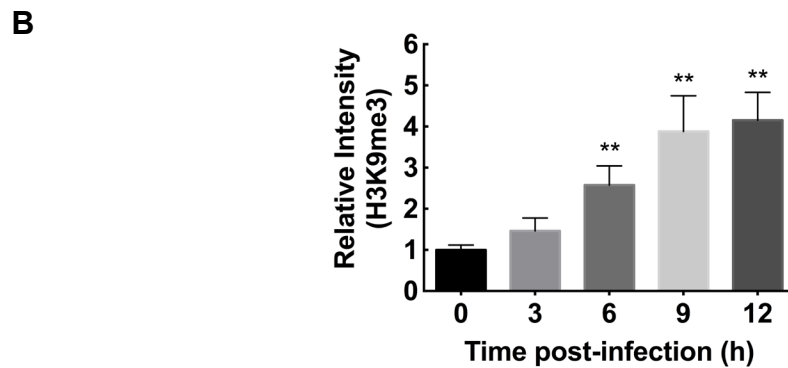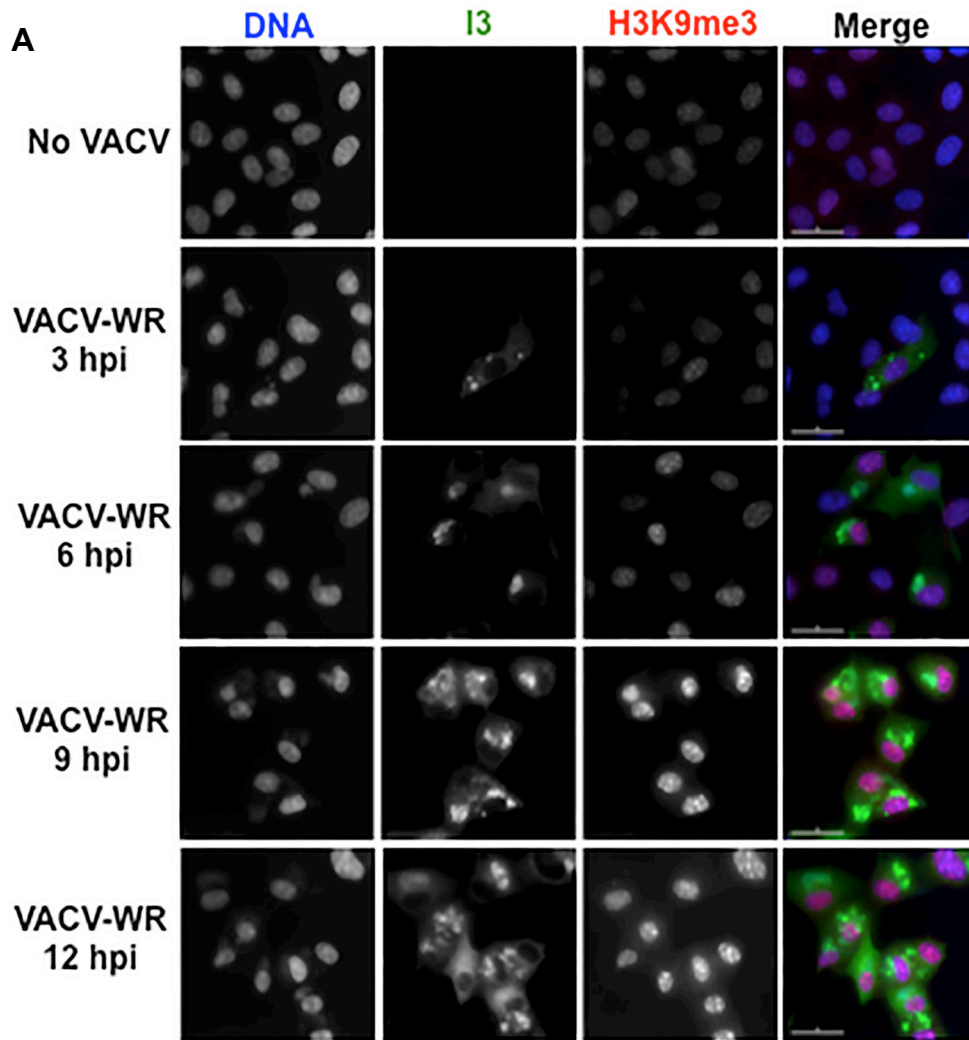
Figure 5.1. Infection of cells with VACV-WR increases H3K9me3 levels. (A) BSC40 cells were infected with VACV-WR at MOI of 5 for the indicated time points. Then the cells were fixed and stained for H3K9me3 and I3 using specific antibodies. DNA was stained with DAPI. (B) Intensity of nuclear H3K9me3 level was quantified using Image J. (A) shows a representative sample and (B) shows mean and SD of three independent experiments. (**, $p \leq 0.001$).

152
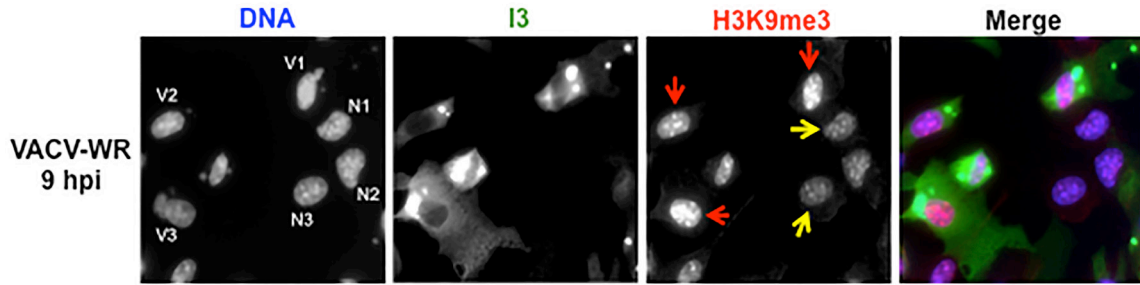
Figure 5.2. Side-by-side comparison of H3K9me3 levels in VACV-WR infected and non-infected cells. BSC40 cells were infected with VACV-WR at MOI of 0.5 for 9h. The cells were then fixed and stained for H3K9me3 and I3. DAPI was used to stain DNA. Red arrows indicate infected cells and yellow arrows indicate non-infected cells. N1-3, non-infected cells; V1-3, VACV-WR infected cells.

To corroborate the results of the immunofluorescence findings, flow cytometry analysis of H3K9me3 levels was performed **(Figure 5.4)**. In mock-infected samples, 3% of cells showed high levels of H3K9me3. In contrast, infected cells, as detected by staining for VACV I3, showed increased levels of H3K9me3. Among the infected cells 48.2 %, 49.8 %, 64 % and 84 % showed high H3K9me3 levels at 3, 6, 9 and 12h post-infection, respectively. These findings confirm that VACV infection increases H3K9me3 levels.

The repressive chromatin is enriched with H4K20me3, which is downstream of H3K9 tri-methylation by SUV39H1/2 in the genesis of heterochromatin **(Figure 1.10)** (576, 577). To ascertain if VACV infection alters the levels of the repressive chromatin, I monitored the levels of H4K20me3 following infection by immunofluorescence microscopy. Infection with VACV resulted in a global increase in the intensity and distribution of H4K20me3 foci. Quantification of the nuclear H4K20me3 levels showed a ~ 4 fold increase in the levels of H4K20me3 at 9h post-infection relative to uninfected
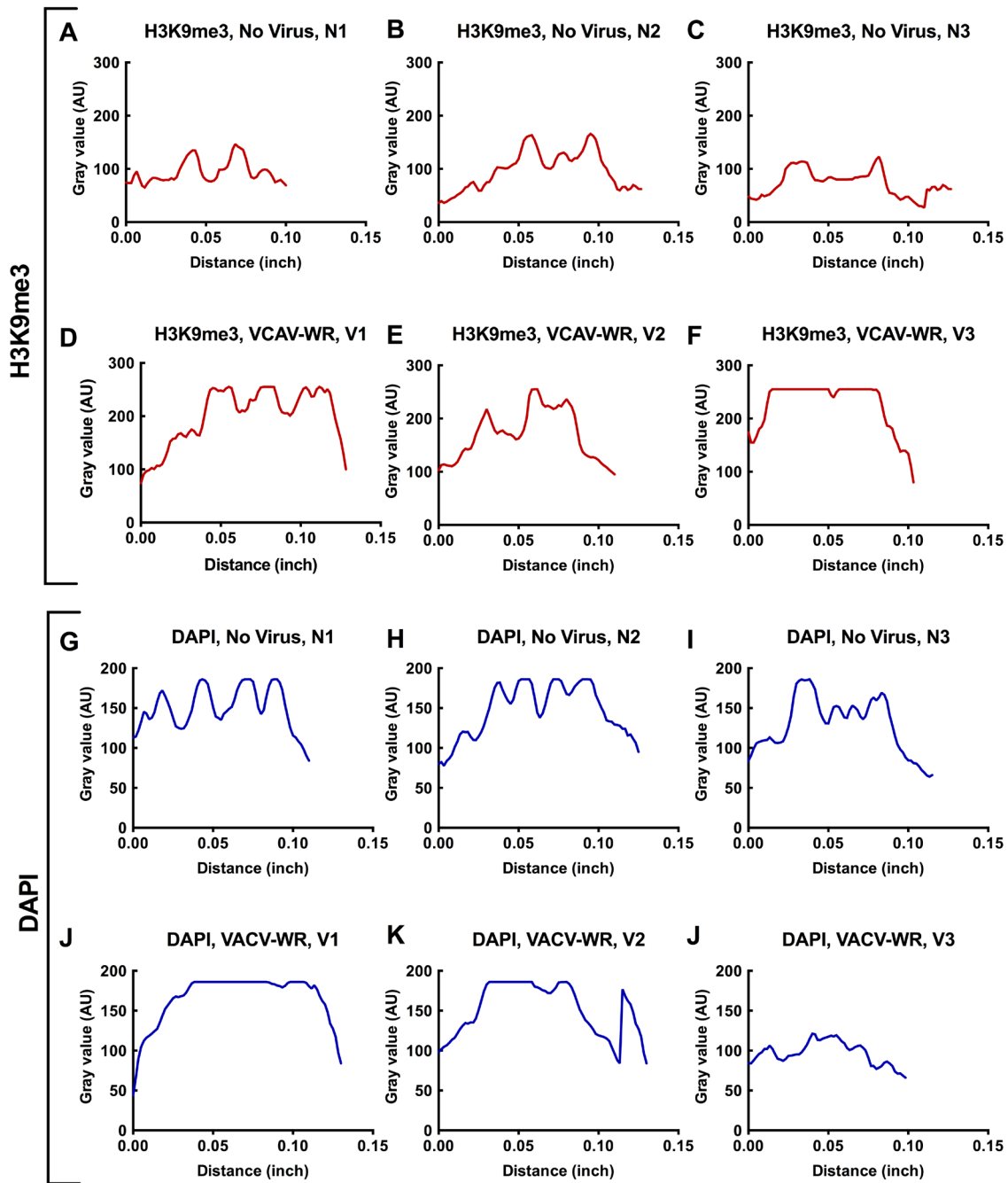
Figure 5.3. Intensity variations of H3K9me3 and DAPI along the longest diameters of cells. A line was drawn along the longest diameter of the cells indicated in Figure 5.2. and the intensities of H3K9me3 and DAPI were measured along the lines using the plot profile of Image J. N1-3 and V1-3 represent non-infected cells and VACV-WR infected BSC40 cells, shown in Figure 5.2.

154

cells **(Figure 5.4)**. Taken together these results demonstrate that infection of BSC40 cells with VACV increases the levels and distribution of markers of the repressive chromatin, with maximum effect observed ~ 9h post-infection.
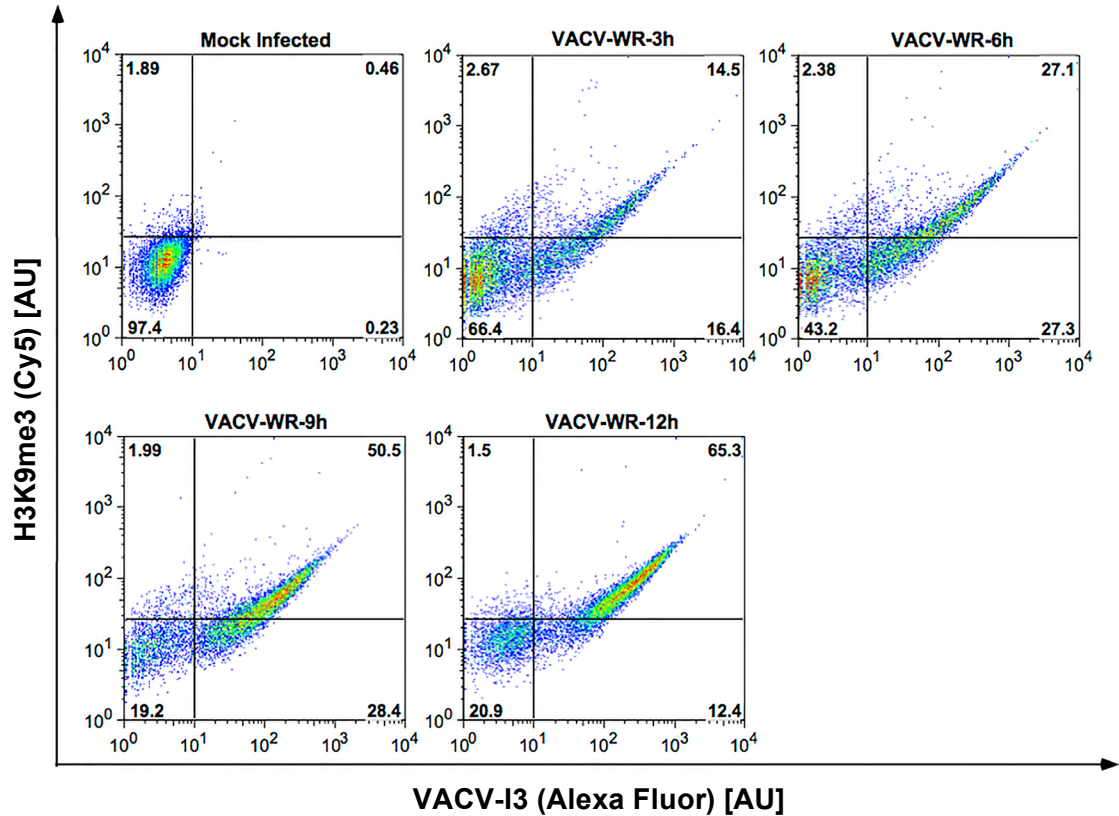
Figure 5.4. The percentage of cells with high levels of H3K9me3 increases with VACV-WR infection. BSC40 cells were infected with VACV-WR at MOI of 10 for the indicated time points. The cells were then trypsinized, fixed and permeablized. H3K9me3 and I3 were stained using specific antibodies and flow cytometry analysis was performed. Flow Jo software was used for gating and analysis. The figure shows a representative sample of three independent experiments.

155
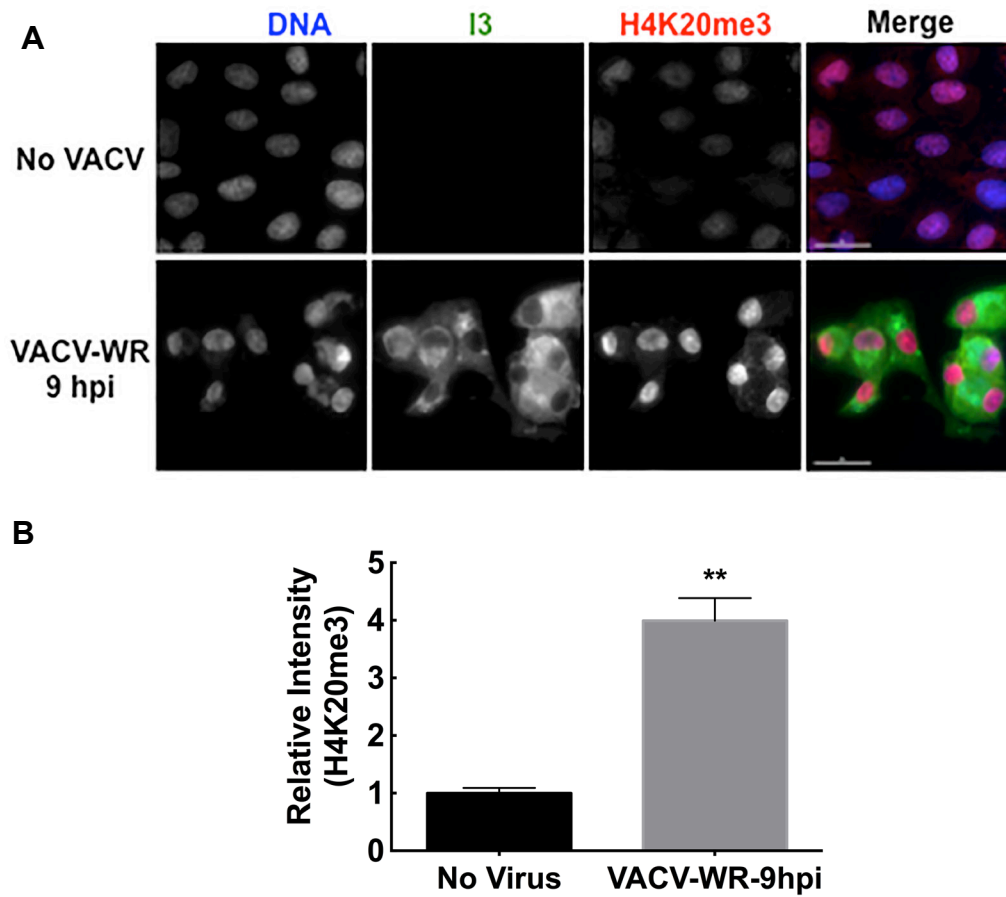
Figure 5.5. VACV-WR infected cells have high levels of H4K20me3 compared to non-infected cells. BSC40 cells were infected with VACV-WR at MOI of 5 for 9h. The cells were fixed, stained with antibodies specific for H4K20me3 and I3 and immunofluorescence microscopy was performed (A). H4K20me3 intensity was analyzed using Image J (B). (A) is a representative sample of three independent experiments while (B) indicates the means and SD of three independent experiments. (**, $p \leq 0.001$).

5.2.2 Increased H3K9me3 and H4K20me3 was observed with other orthopoxviruses, but not leporipoxviruses

I examined whether the alterations of the repressive chromatin observed in VACV-WR infected cells were also detected in cells infected with other members of the *poxviridae* family. I started by performing an experiment where I infected BSC40 cells with another strain of VACV (Copenhagen, VACV-Cop) or another member of the orthopoxviruses, CPXV (strain Brighton). At 9h post-infection, I fixed cells and measured both the changes in H3K9me3 (Figure 5.5) and H4K20me3 (Figure 5.6). Similar to the observation with VACV-WR, both VACV-Cop and CPXV increased the levels of H3K9me3 and H4K20me3 relative to that of uninfected cells. The level of H3K9me3 increased by ~ 5 and ~ 4 fold in VACV-Cop and CPXV infected BSC40 cells, respectively, relative to uninfected cells **(Figure 5.6)**. Similarly, a 5.5 and 4-fold increase in the levels of H4K20me3 were detected in VACV-Cop and CPXV infected BSC40 cells, respectively **(Figure 5.7)**. VACV-WR infection increased H4K20me3 levels by 4 fold **(Figure 5.7)**.

I also examined whether the leporipoxviruses MYXV and SFV are able to alter H3K9me3 and H4K20me3 levels. In contrast to the observations with VACV and CPXV, leporipoxviruses did not significantly change the levels of H3K9me3 **(Figure 5.8)** and H4K20me3 **(Figure 5.9)** 9h after infection compared to mock-infected cells. These results suggest that members of the *orthopoxvirus* genus are able to enhance the level and distribution of the repressive chromatin while members of the *leporipoxvirus* genus are not able to do so, although a number of other species should be examined in each genus.
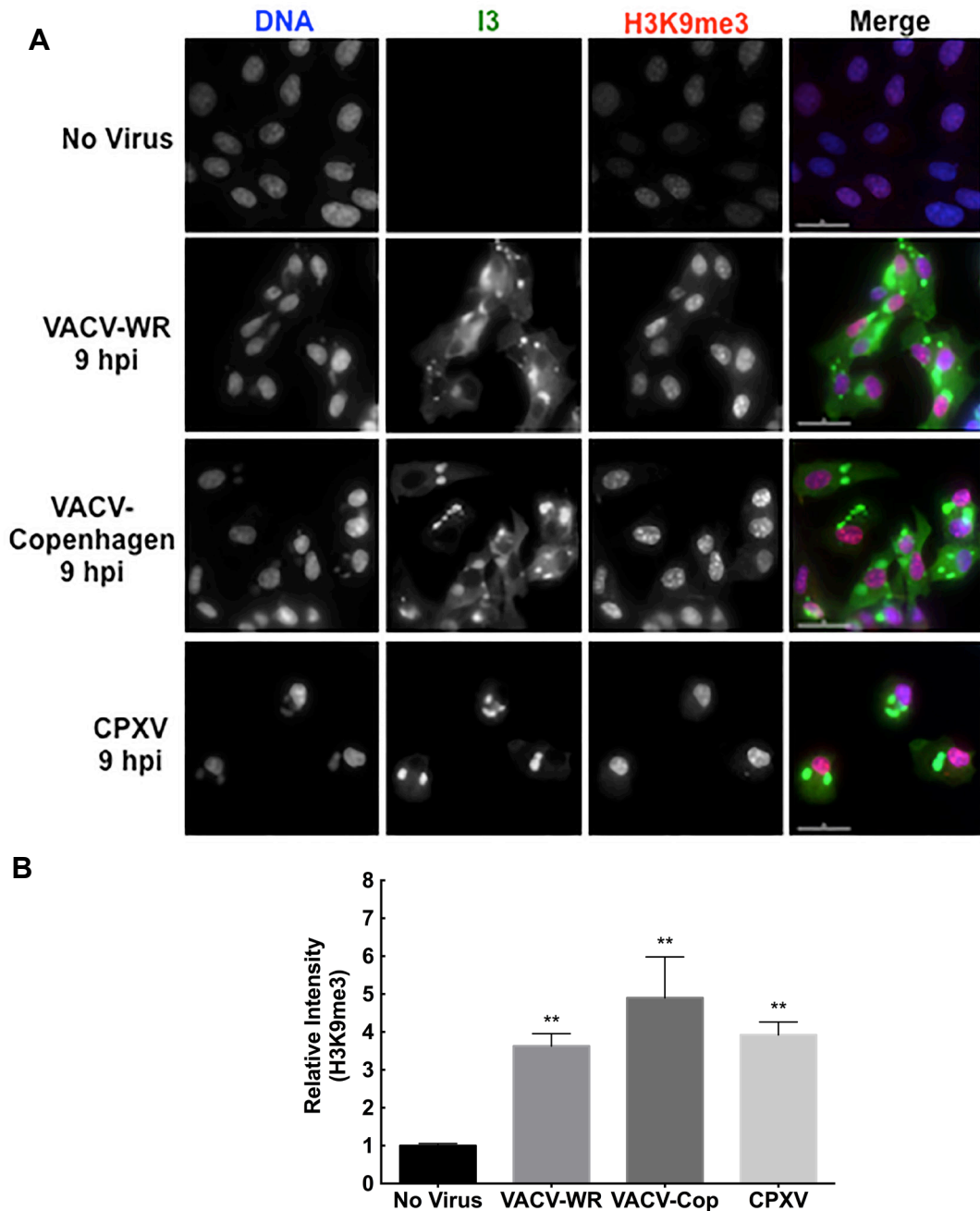
Figure 5.6. H3K9me3 levels in *orthopoxvirus* infected BSC40 cells. BSC40 cells wee infected with VACV-WR, VACV-Copenhagen or CPXV for 9h. Then H3K9me3 and I3 staining was performed using specific antibodies. Nuclei were stained with DAPI. Intensities of H3K9me3 staining were determined by Image J. (A) is representative sample and (B) is the mean and SD of three independent experiments. The images for the controls (No Virus and VACV-WR 9 hpi) are also shown in Figures 5.8 and 5.10. (**, $p \leq 0.001$).

A

B
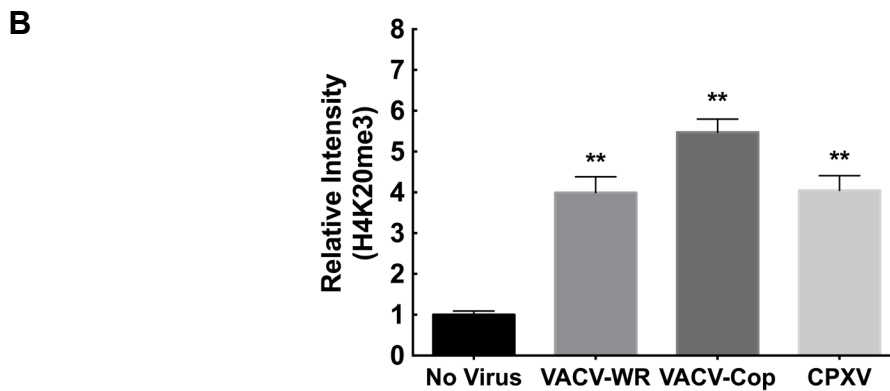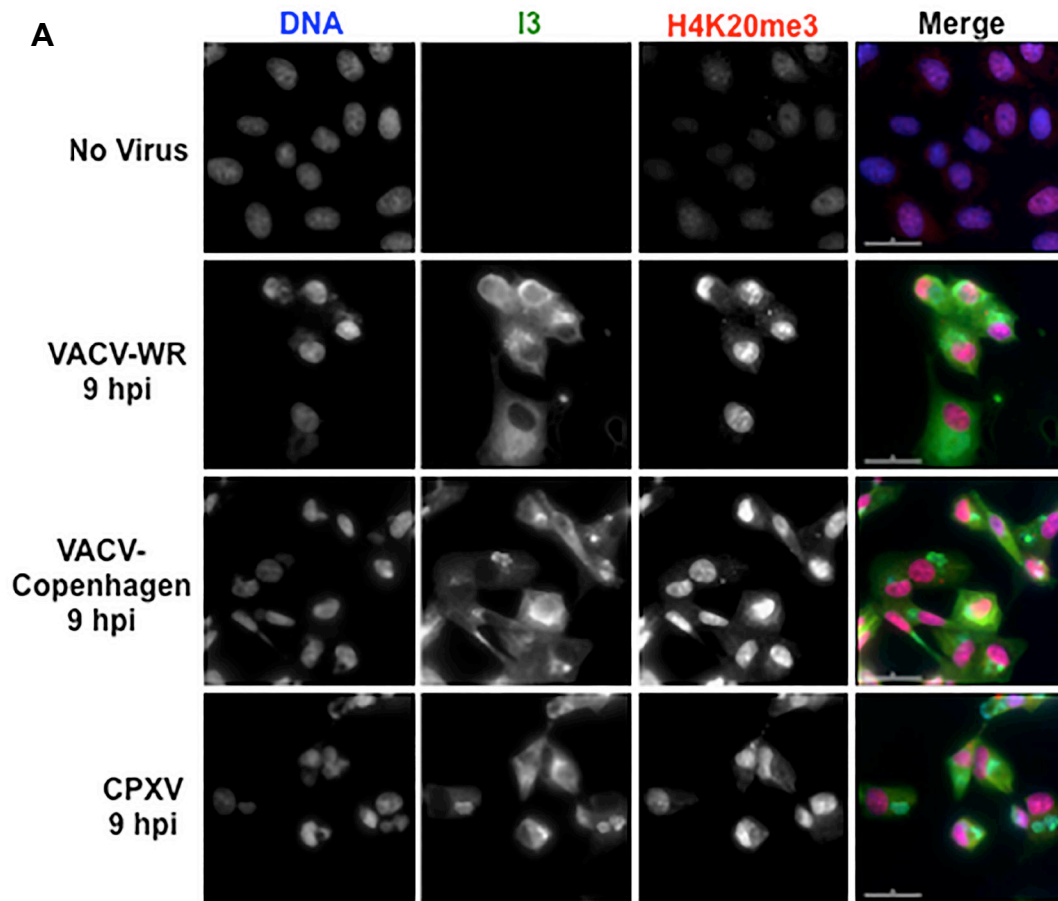
Figure 5.7. Enhancement of H4K20me3 staining in *orthopoxvirus* infected BSC40 cells. Following infection of BSC40 cells with VACV-WR, VACV-Copenhagen or CPXV for 9h, the cells were fixed and stained for H4K20me3 and I3. DNA was stained with DAPI. Nuclear intensities of H4K20me3 were determined by Image J. (A) is representative sample and (B) is the mean and SD of three independent experiments. The images for the controls (No Virus and VACV-WR 9 hpi) are also shown in Figure 5.9. (**, $p \leq 0.001$).

159
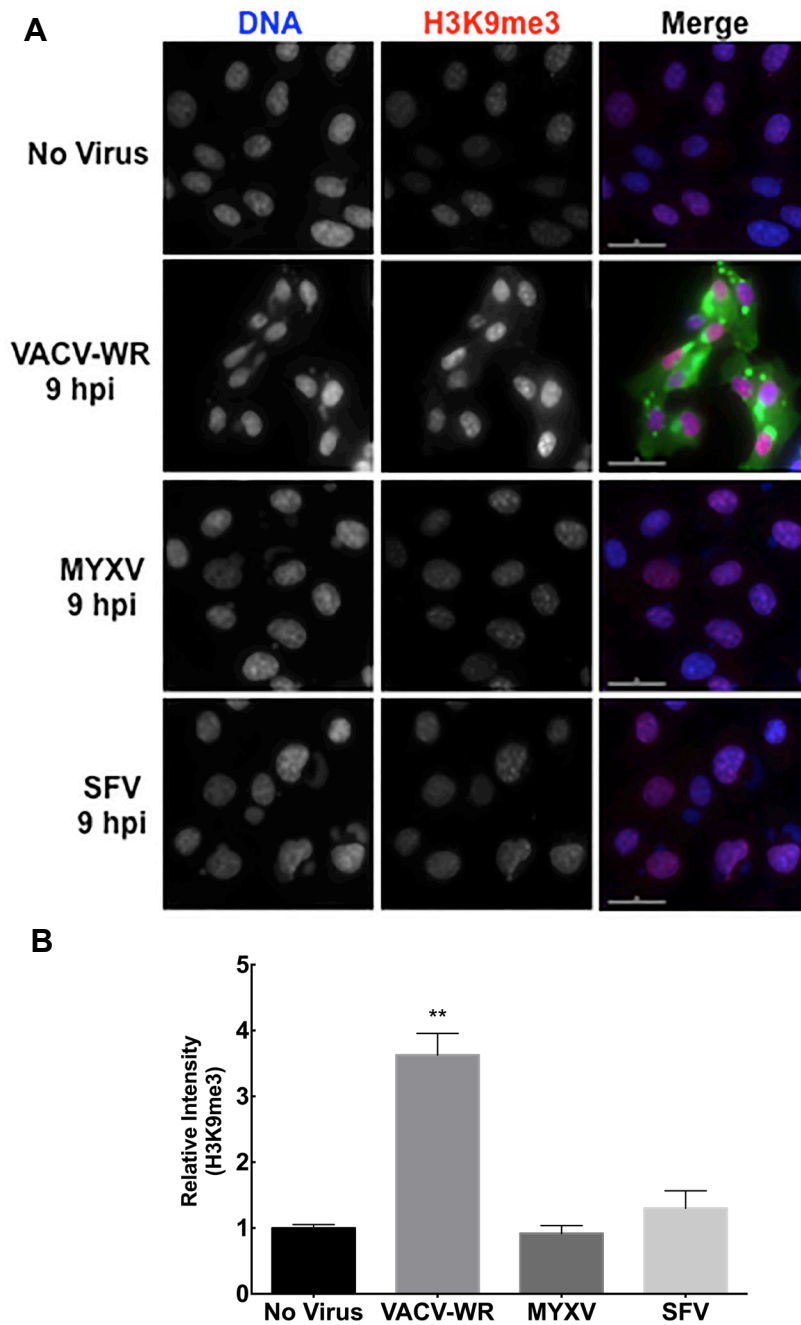
Figure 5.8. MYXV or SFV infection does not increase H3K9me3 levels. Confluent BSC40 cells were infected with VACV-WR, MYXV or SFV for 9h. Then H3K9me3 and I3 staining was performed using specific antibodies. DNA was stained with DAPI. Image J was used to measure global nuclear H3K9me3 intensities. (A) is a representative sample and (B) shows the mean and SD of three independent experiments. The images for the controls (No Virus and VACV-WR 9 hpi) are also shown in Figures 5.6 and 5.10. (**, $p \leq 0.001$).
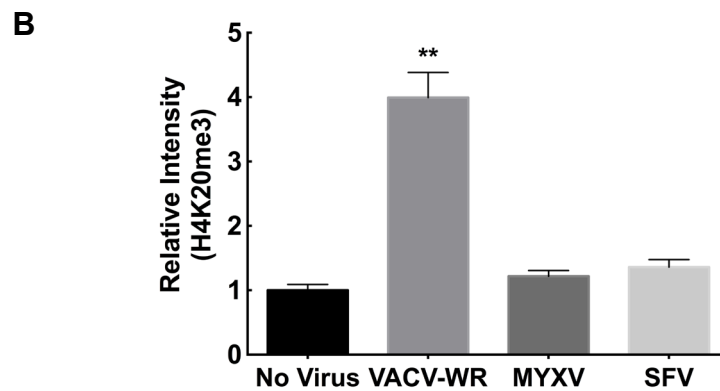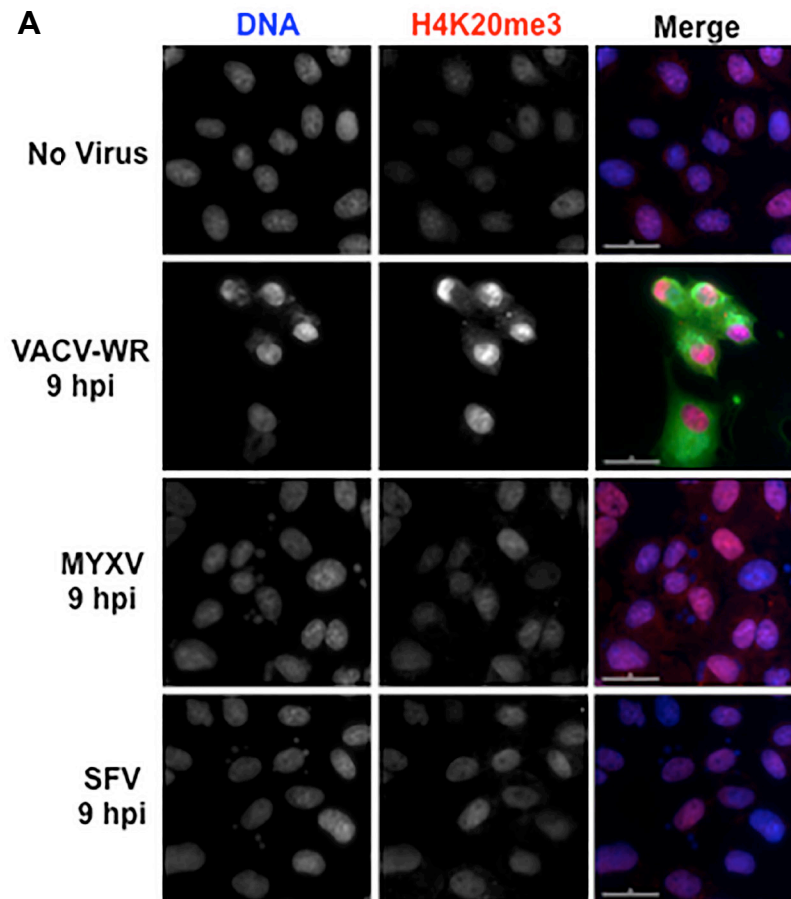
Figure 5.9. H4K20me3 levels in MYXV or SFV infected cells. BSC40 cells were infected with VACV-WR, MYXV or SFV for 9h. Following fixation and permeablization, the cells were stained for H4K20me3 and I3 using specific antibodies. DAPI was used to stain DNA. Intensities of H4K20me3 staining were determined by Image J. (A) is representative sample and (B) is the mean and SD of three independent experiments. The images for the controls (No Virus and VACV-WR 9 hpi) are also shown in Figures 5.7. (**, $p \leq 0.001$).

5.2.3 Enhancement of the repressive chromatin is dependent on the expression of early genes of VACV, but not late genes

Next I determined which step in the life cycle of VACV is necessary and/or sufficient to increase H3K9me3 levels in infected cells. Ultraviolet (UV) light-inactivated VACV is able to bind cellular receptors and enter into cells; however, it is not able to start early gene expression, which normally occurs in the virion core particle (578, 579). To examine whether the process of entry and delivery of virion proteins alone is enough to induce H3K9 tri-methylation, BSC40 cells were infected with UV-inactivated VACV-WR for 9h. Complete UV inactivation was confirmed with the absence of I3 in BSC40 cells that were infected with UV-inactivated VACV **(Figure 5.10A)**. Immunofluorescence staining for H3K9me3 showed that infection with UV-inactivated VACV-WR did not significantly change H3K9me3 levels compared to mock-infection suggesting that viral transcription is necessary for the induction of the repressive chromatin **(Figure 5.10)**.

As described in section 1.1.1, VACV gene expression occurs in a sequential fashion with early gene expression occurring before DNA replication and late gene expression occurring only after DNA replication (570, 580). If DNA replication is inhibited there will be no late gene expression. AraC is a DNA-damaging agent, which inhibits VACV DNA replication and late gene expression (581, 582). The araC we used in this study also inhibited late gene (A3L) but not early gene (I3L) expression **(Figure S3 in the Appendix)**. To examine whether early gene expression is sufficient or late gene expression is necessary to induce the repressive chromatin, BSC40 cells were treated with an inhibitory concentration of araC (80 μg/mL) starting from 2h after infection, the point

at which a significant amount of early gene products are made (51). During VACV infection late gene production normally starts after 2h of infection (51).
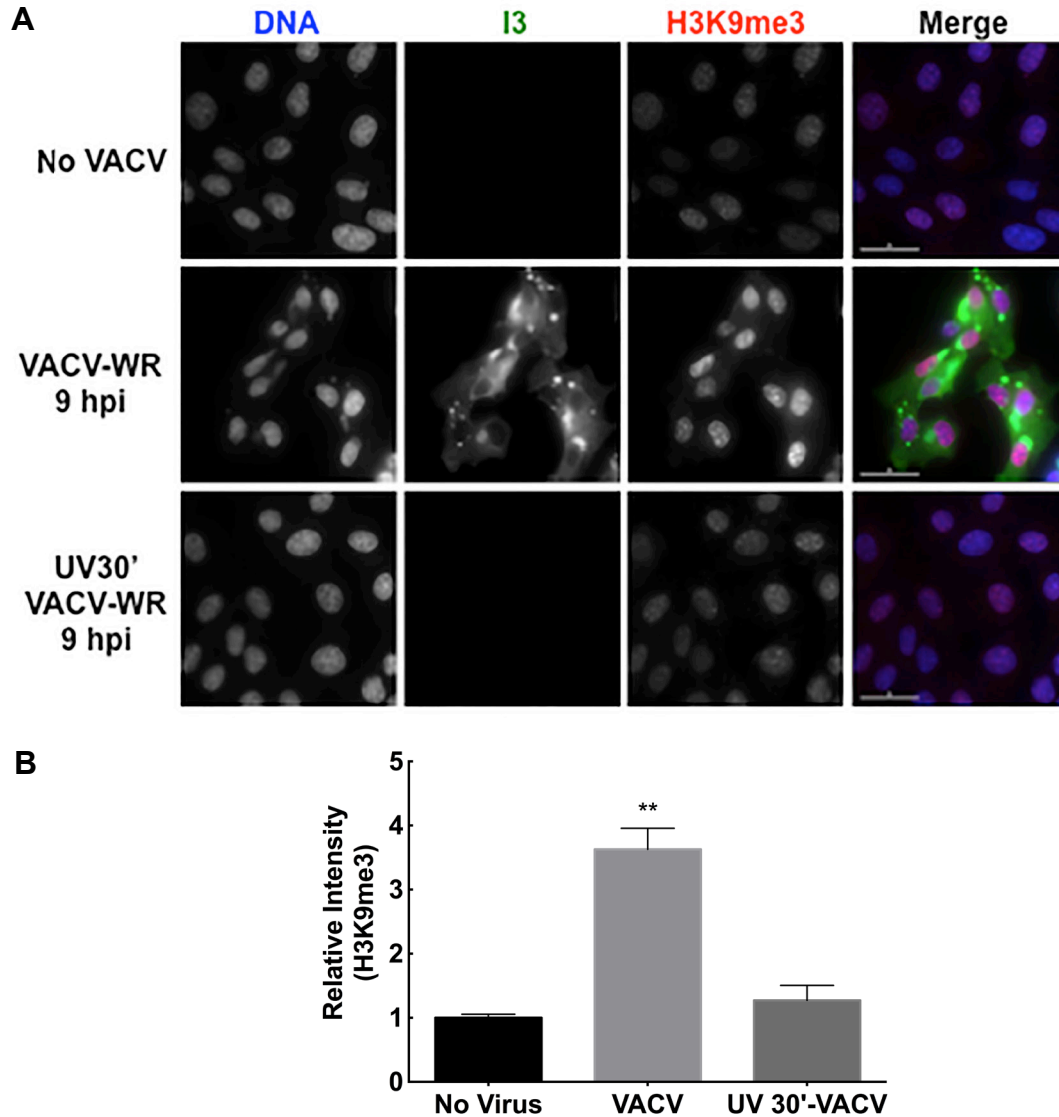
Figure 5.10. UV-irradiated VACV-WR does not increase H3K9me3 levels. BSC40 cells were infected with VACV-WR, or UV-inactivated VACV-WR for 9h. Then they were fixed and stained for H3K9me3 and I3 using specific antibodies. DNA was stained with DAPI. Intensities of H3K9me3 staining were calculated by Image J. (A) is a representative sample and (B) shows the mean and SD of three independent experiments. Virus was UV inactivated for 30 min (UV30′). The images for the controls (No Virus and VACV-WR 9 hpi) are also shown in Figures 5.6 and 5.8. (**, $p \leq 0.001$).
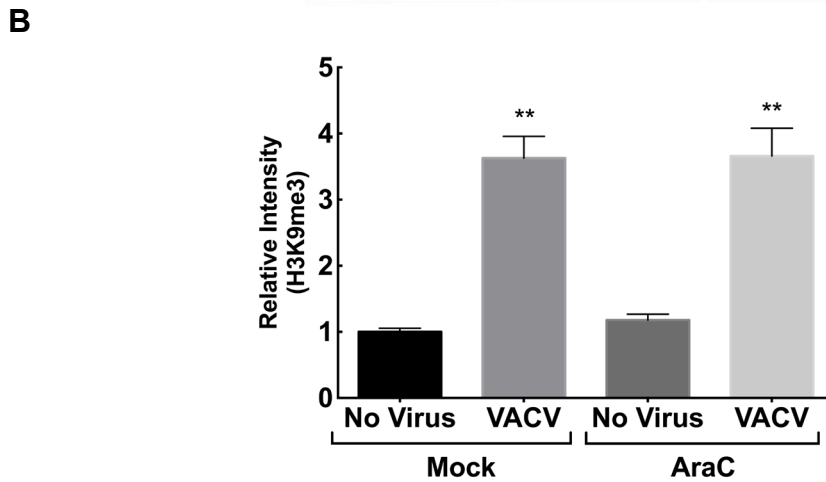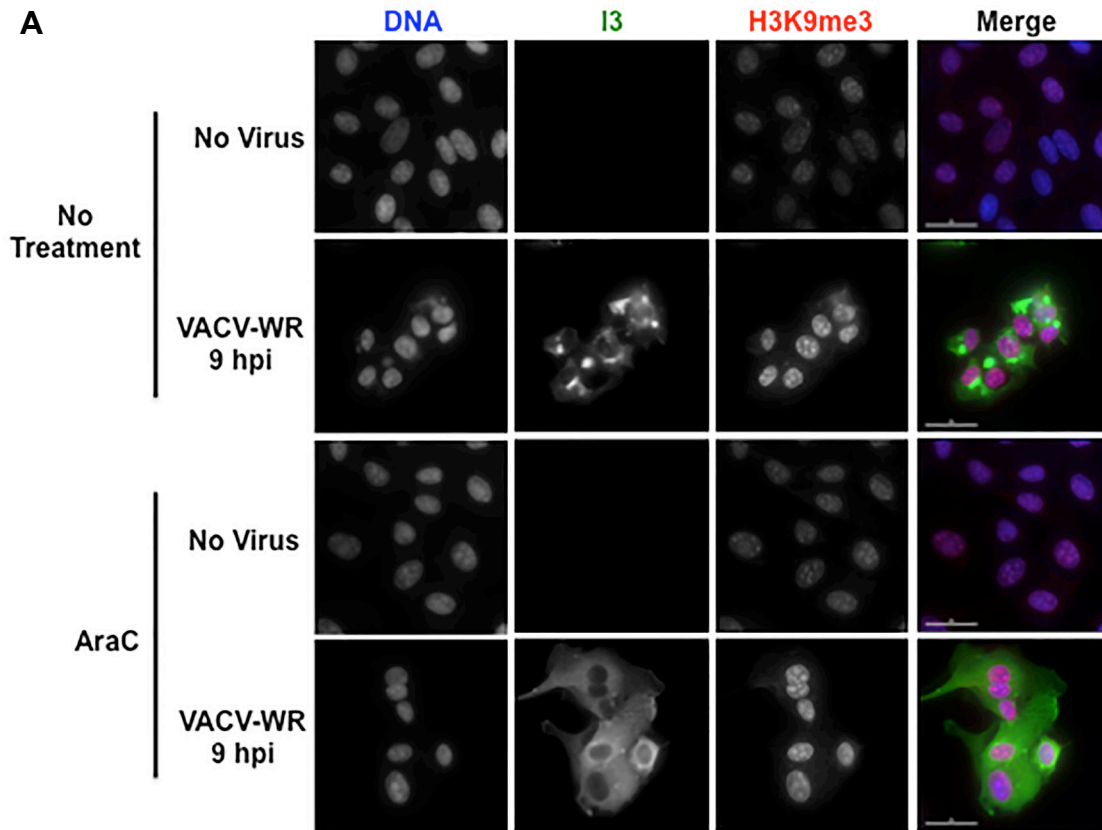
Figure 5.11. The effect of treatment of cells with araC on H3K9me3 levels. BSC40 cells were mock-infected or infected with VACV-WR for 2h. Then the cells were treated with 80μg/mL of araC for 7h. After a total of 9h of infection, the cells were fixed and stained for H3K9me3 and I3 using specific antibodies. DNA was stained with DAPI. Intensities of H3K9me3 were measured by Image J. (A) is a representative sample and (B) shows the mean and SD of three independent experiments. (**, $p \leq 0.001$).

Immunofluorescence staining showed that cells treated with araC were able to express I3, an early VACV protein **(Figure 5.11A)**. Treatment of non-infected cells with araC did not change the level of H3K9me3 compared to mock-treated non-infected cells **(Figure 5.11)**. AraC treatment of BSC40 cells starting from 2h after infection with VACV-WR resulted in a ~3.7 fold increase in H3K9me3 levels compared to araC-treated non-infected cells. This increment was comparable to the amount induced by VACV-WR in the absence of araC **(Figure. 5.11)**. These results suggest that early gene expression is sufficient for the induction of H3K9me3, a marker for the repressive chromatin, without the need for late gene expression.

To examine whether increased tri-methylation of H3K9 occurs due to synthesis of a new protein(s) or activation of an already synthesized protein(s), cycloheximide was used to inhibit protein synthesis (583). H3K9me3 levels were determined in three groups of BSC40 cells: mock-treated, cells pretreated with cycloheximide for 30 min prior to infection and then infected in the presence of the drug or cells treated with the drug 2h after infection. All the groups had VACV-WR infected and non-infected controls. At 9h post-infection, the cells were fixed and stained for H3K9me3 and I3. The results indicated that cells that were pretreated with cycloheximide failed to express I3 while cells treated with the drug 2h after infection expressed I3 **(Figure 5.12A)**. Cycloheximide treatment alone did not change the level of H3K9me3 in the absence of infection **(Figure 5.12)**. However, cells treated with cycloheximide after early genes were expressed (2h post infection) showed a 2.6 fold increase in the level of H3K9me3 compared to non-infected cells **(Figure 5.12)**. This level was comparable to the increase in H3K9me3

A

		DNA	I3	H3K9me3	Merge
No Treatment	No Virus				
	VACV-WR 9 hpi				
Cycloheximide at 2h pi, for 7h	No Virus				
	VACV-WR 9 hpi				
Cycloheximide at 30min pre-infection, for 9h	No Virus				
	VACV-WR 9 hpi				

B

Cycloheximide 300μg/mL

None   At 2h pi   At 30' pre-inf

Relative Intensity (H3K9me3)

Mock VACV Mock VACV Mock VACV
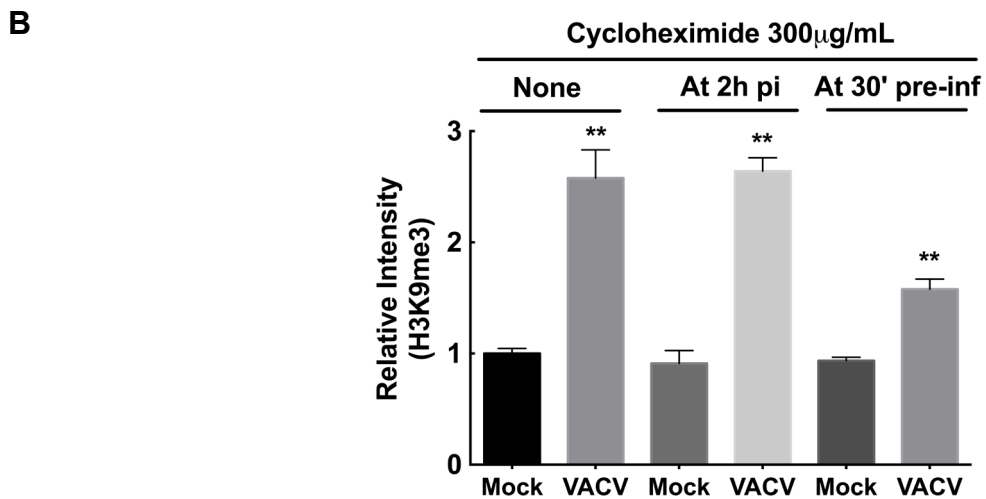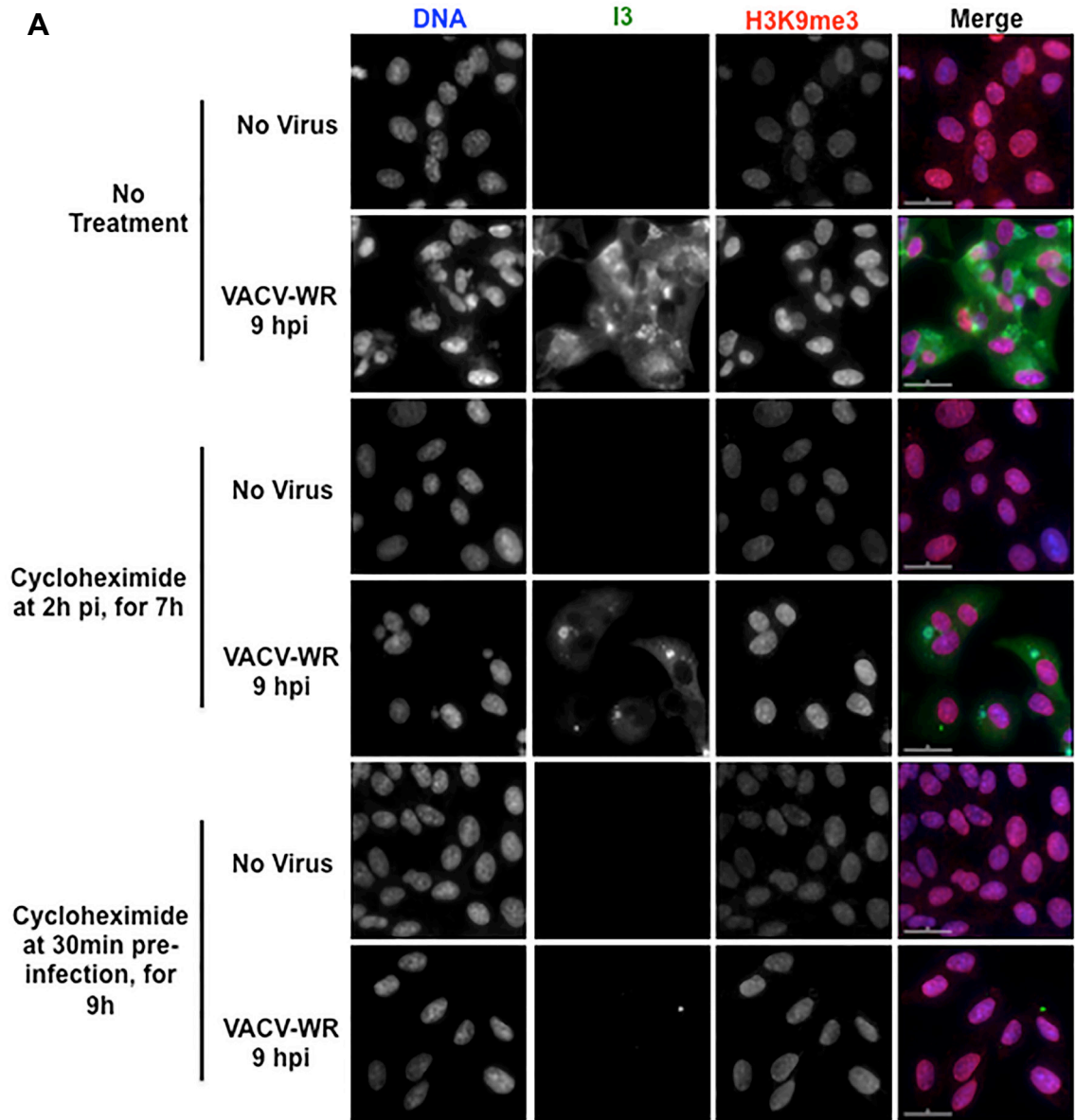
Figure 5.12. H3K9me3 enrichment does not require cellular protein synthesis. Monolayers of BSC40 cells were dived into three groups. Cells in the first group were mock-treated and mock infected or infected with VACV-WR for 9h. Cells in the second group were mock infected or infected with VACV-WR for 2h then they were treated with cycloheximide for 7h. Cells in the third group were pretreated with cycloheximide for 30 min and then infected with VACV-WR for 9h in the presence of the drug. H3K9me3 and I3 staining was performed using specific antibodies. DNA was stained with DAPI. Intensities of H3K9me3 staining were determined by Image J. (A) is a representative sample and (B) is the mean and SD of three independent experiments. (**, *p ≤ 0.001*).

levels (~2.6 fold) observed in mock-treated VACV infected cells **(Figure 5.12)**. On the other hand, pretreated cells showed a modest 57.8% increase in the level of H3K9me3 during VACV infection compared to pre-treated non-infected cells. These results suggest that a new cellular protein synthesis may not be required for the enhancement of H3K9me3 levels during infection as far as VACV early genes are expressed. However, a caveat to these experiments is that a cellular gene that might be synthesized in the first 2h of infection could be responsible for the increment in H3K9me3 levels. These experiments also confirm the results of the araC treatment studies described above.

5.2.4 SUV39H1/2 play a role in increasing the levels of H3K9me3 during VACV infection

In mammalian cells, there are six different HKMTs that are able to di- or tri-methylate H3K9me (467). Each of these HKMTs has substrate specificity as well as an affinity for certain domains within the chromatin. SUV39H1 and SUV39H2 (SUV39H1/2) are the most studied H3K9 HKMTs. They are able to di- or tri-methylate a mono-methylated H3K9 and they are predominantly involved in the generation of

constitutive heterochromatin (584, 585). However, they are also able to enrich the euchromatin region with H3K9me2 and H3K9me3 in response to various stimuli including double-strand DNA breaks and retinoblastoma mediated regulation of the cell cycle (466, 586).

As the results described in previous sections showed, VACV infection increases the level H3K9me3 in the nuclei of infected cells. This enhanced methylation could be mediated by one or more HKMTs that are able to tri-methylate H3 at K9. I determined whether SUV39H1/2 play a role in increasing the tri-methylation of H3K9 during VACV infection by examining H3K9me3 levels in SUV39H1 and SUV39H2 double null immortalized mouse embryonic fibroblast cells (D5) and their wild type counterparts (W8) (503).

D5 and W8 cells were mock infected or infected with VACV-WR and immunofluorescence staining was performed. At 9h after infection of W8 cells, the level of H3K9me3 increased by 3.2 fold compared to non-infected W8 cells **(Figure 5.13)**. On the other hand, H3K9me3 level did not show a significant difference between non-infected and VACV-WR infected D5 cells **(Figure 5.13)**. These findings suggest that SUV39H1 and/or SUV39H2 play a significant role in enhancement of tri-methylation of H3K9 during VACV infection.
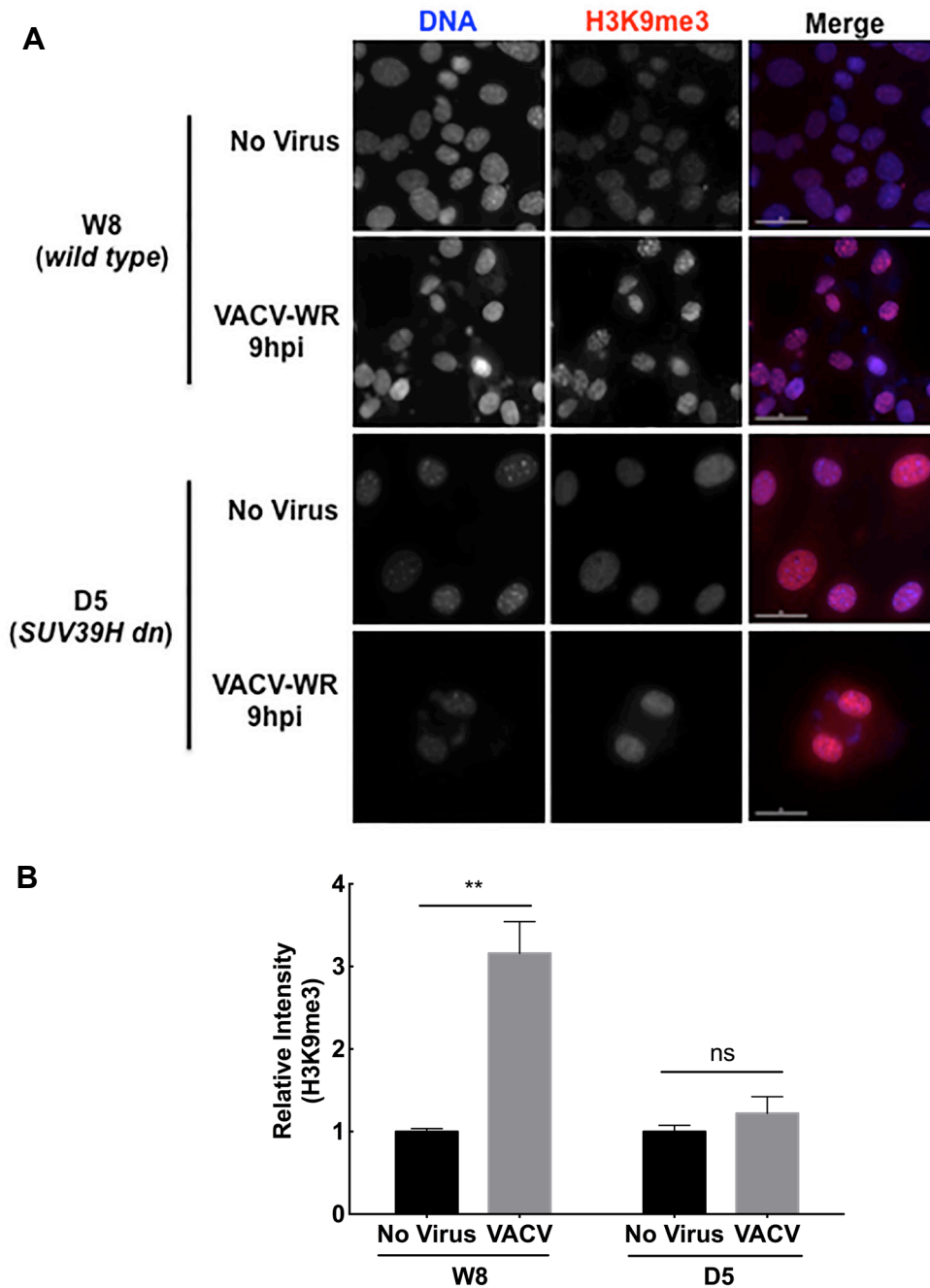
Figure 5.13. VACV infection does not result in increased levels of H3K9me3 in SUV39H double null (D5) cells. SUV39H1/2 double null (dn) mouse embryonic fibroblasts (D5) and their wild type counterparts (W8) were infected with VACV-WR. After a total of 9h of infection, the cells were fixed and stained for H3K9me3 and I3 using specific antibodies. DNA was stained with DAPI. Intensities of H3K9me3 were measured by Image J. D5 cells have larger nuclei likely due to their inability to make constitutive heterochromatin. (A) is a representative sample and (B) shows the mean and SD of three independent experiments. (**, $p \leq 0.001$).

5.2.5 VACV-WR replication is reduced in SUV39H double null (D5) cells

To determine whether SUV39H1/2 mediated H3K9 tri-methylation is important for the replication of VACV-WR *in vitro*, the growth kinetics of the virus was compared between W8 and D5 cells. The results indicated that VACV-WR grew more efficiently in W8 than D5 cells with a 3 and 2.7 fold higher levels of PFUs at 48 and 60h post-infection, respectively **(Figure 5.14)**. The findings of this experiment suggest that SUV39H mediated generation of H3K9me3 is important for VACV-WR replication since in its absence the level of replication is reduced. However, the difference in the growth kinetics is only modest suggesting generation of the repressive chromatin during VACV infection is not very critical for VACV replication in culture.
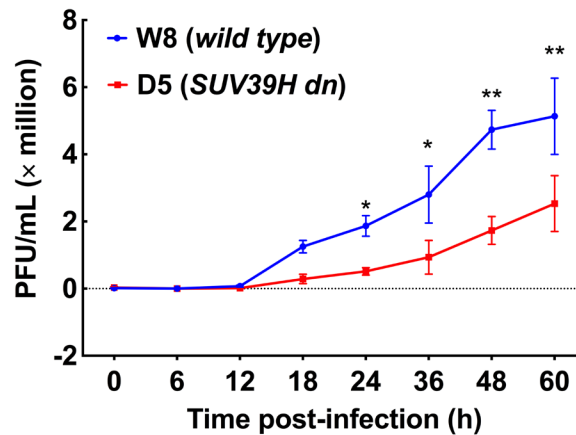
Figure 5.14. VACV infection is reduced in SUV39H double null (D5) cells. SUV39H1/2 double null mouse embryonic fibroblasts (D5) and their wild type counterparts (W8) were infected with VACV-WR at MOI of 5. The cells and their supernatants were collected at the indicated time points. Intracellular virions were released with 3 cycles of freeze-thawing and used to infect monolayers of BSC40 cells. Then plaques were counted following crystal violet staining. The data presented is a representative sample of three independent experiments performed in triplicate. (*, $p \leq 0.01$; **, $p \leq 0.001$).

5.2.6 VACV-WR cannot effectively down-regulate cellular gene expression in SUV39H double null (D5) cells

A number of microarray and high-throughput sequencing studies were previously carried out to determine how the cellular transcriptome is altered during VACV infection (568-570). According to these studies, a significant number of transcripts are down-regulated during infection. On the other hand, only a small number of transcripts are up-regulated. The studies also indicated that the level of up- or down-regulation and the specific types of genes affected are cell type dependent (568-570). One of these studies, published by Guerra *et al.* (2003), indicated that cellular genes could be grouped into 6 clusters based on transcriptional activity during VACV infection of HeLa cells (568). The first group is genes that are up-regulated throughout infection. Another group, which represents the majority of genes examined, are those that are down-regulated throughout infection. Yet another class incorporates genes that are up-regulated early in infection (2h) but then down-regulated later in infection (6h and 16h).

Even though the mechanism through which VACV infection reduces the transcript levels of the majority of cellular genes is not clearly understood, one or both of the following mechanisms could be involved: transcriptional and/or post-transcriptional suppression. Previous studies have suggested that VACV undergoes post-transcriptional regulation of both viral and cellular mRNAs through its decapping enzymes [D9 (an early protein) and D10 (a late protein)], which remove the 5′ caps of mRNAs resulting in their degradation (587, 588). However, it is also possible that VACV infection can suppress the transcriptional activity of cells, in addition to post-transcriptional decapping and degradation of transcripts.
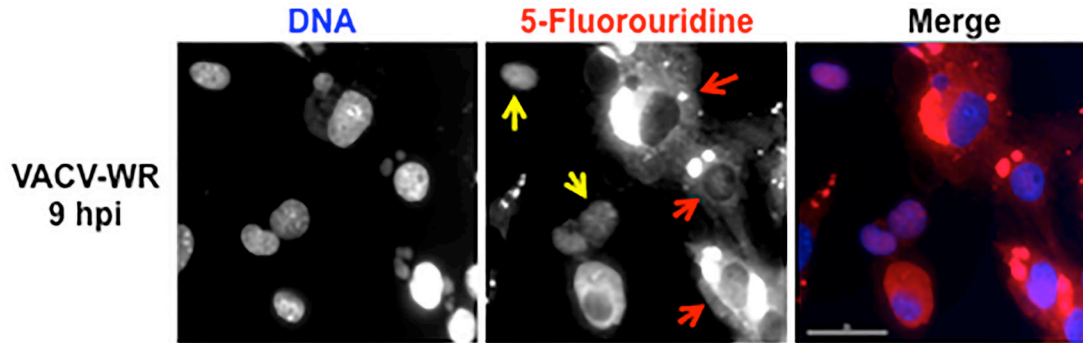
Figure 5.15. 5-fluorouridine incorporation assay. BSC40 cells were infected with VACV-WR at MOI of 5. At 9h post-infection the cells were treated with 1mM 5-fluorouridine for 15 min and subsequently fixed and stained for 5-fluorouridine using an anti-BrdU antibody, which cross-reacts with 5-fluorouridine. DNA was counterstained with DAPI. Red arrows indicate VACV infected cells while non-infected cells are pointed with yellow arrows. Image is a representative sample a two independent experiments.

Incorporation of 5-fluoruridine into nascent transcripts can be used to qualitatively assess transcriptional activity (515, 516, 589). I performed immunofluorescence studies of 5-fluorouridine uptake to determine if VACV infection leads to a reduction in the transcriptional activity of cells. At 9h post-infection, nuclear 5-fluoruridine uptake is diminished while a significant level of uptake took place in viral factories **(Figure 5.15)**. This suggests that VACV infection results in a reduction in cellular transcriptional activity and nascent RNA formation in VACV-infected cells in favor of viral transcription. Based on these observations, I hypothesized that VACV infection associated enhancement of the repressive chromatin is involved in the reduction of cellular transcriptional activity.

To test this hypothesis, the following genes were selected from some of the gene clusters described previously (568), and mentioned above: five genes (CASP3, SRSF2,

XPO1, EEF2 and CCD1) from the class of genes that were down-regulated throughout infection, two genes (WASF1 and FAM169) from up-regulated genes class and two (APEX2 and PIH1D1) from unchanged genes class. Next, W8 and D5 cells were mock infected or infected with VACV-WR. At various times post-infection (2, 6 or 9h), total RNA was isolated and following cDNA synthesis, real time RT-PCR was performed for selected genes using gene-specific primers.

The results indicated that some of the genes I selected did not fall in the same cluster as the original experiments, which were performed in HeLa cells (568). This is expected since previous studies have showed that regulation of specific genes during VACV infection is cell type-dependent, despite a general pattern of down-regulation of gene expression (568-570). However, the results of my experiments give a valuable insight into the differential regulation of cellular gene expression during VACV infection in cells that lack SUV39H1/2. During VACV infection of W8 cells, the expression levels of APEX2, CASP3, FAM169A and SRSF2 remained unchanged **(Figure 5.16)**. On the other hand EEF2, WASF1 and XPO1 were down-regulated throughout infection and PIH1D1 and CCD1were down-regulated at 9 and 2h post-infection, respectively **(Figure 5.16)**. None of the examined genes was found to be up-regulated during VACV infection of W8 cells. Similarly, in D5 cells, CCD1, FAM169A, SRSF2 and WASF1 did not show a change in their expression during infection **(Figure 5.16)**. However, APEX2 was up-regulated at 2 and 6h post-infection, while CASP3 and XPO1 were up-regulated at 6 and 9h post-infection **(Figure 5.16)**. Two genes (EEF2 and PIH1D1) were up-regulated early but they were down-regulated at later time points.
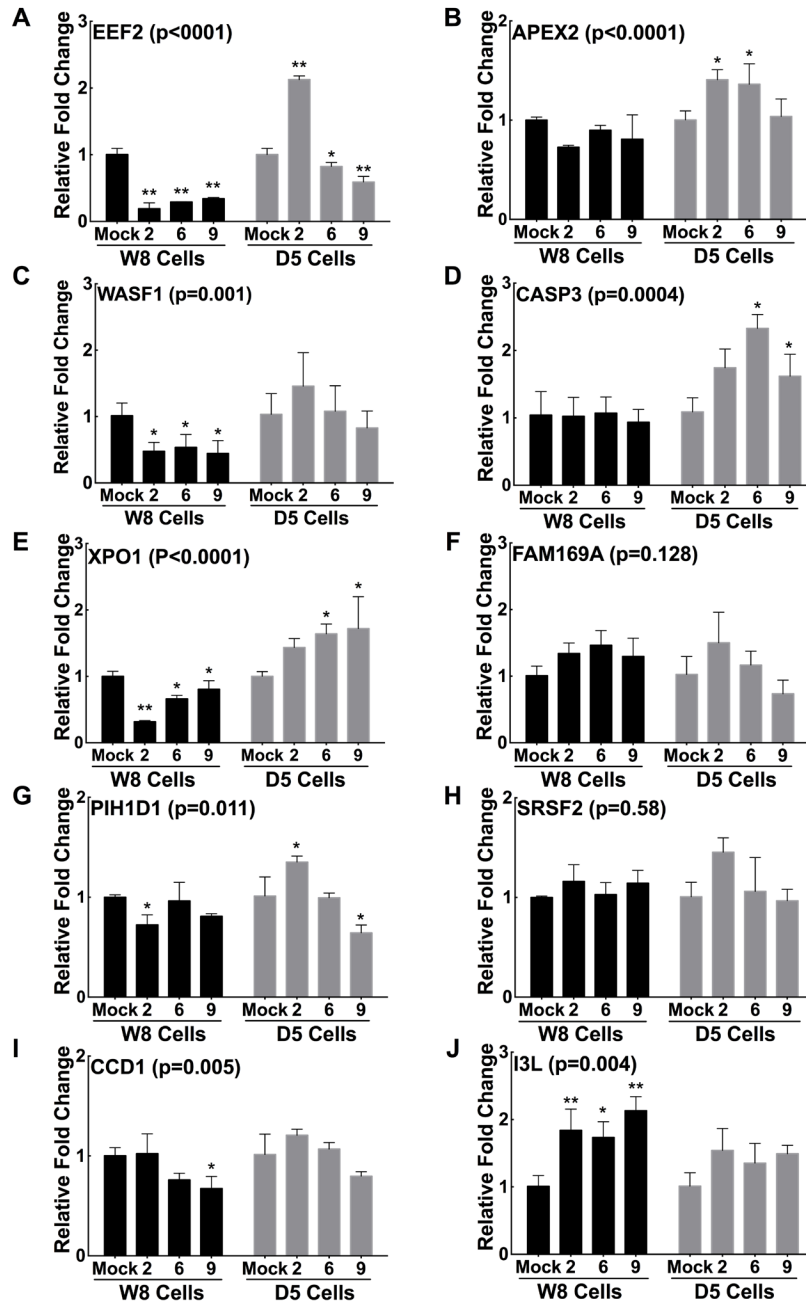
Figure 5.16. Real time RT-PCR for mRNAs of selected cellular genes. SUV39H1/2 double null mouse embryonic fibroblasts (D5) and their wild type counterparts (W8) were infected with VACV-WR. At the indicated time points after infection, total RNA was isolated and cDNA was synthesized. Then real time RT-PCR was performed using gene-specific primers. Statistical analysis was conducted using two-way ANOVA followed by Sidak's multiple comparison test. The indicated p-values are for comparisons of gene expression between D5 and W8 cells. Panels on the left side represent genes down-regulated in W8 cells at least at one time point.

The changes in the expression levels of the genes were also compared between W8 and D5 cells using two-way ANOVA **(Figure 5.16)**. The results showed that three genes (APEX2, CASP3, and XPO1) that were unchanged or down-regulated in W8 cells were up regulated in D5 cells. In contrast, two genes (WASF1 and EEF2) that were down-regulated throughout infection in W8 cells became unchanged or up-regulated at a certain time point during infection in D5 cells. None of the examined genes was unchanged in W8 cells and became down-regulated in D5 cells.

Overall, in W8 cells, 60% of the examined genes showed a statistically significant reduction in their expression at one or more time point after infection while none of the genes showed up-regulation. On the contrary in D5 cells, only 20 % of the examined genes were down-regulated at one or more time point post-infection while 50% of the genes showed up-regulated expression at one or more time point after infection. Even though the magnitudes of these changes are modest, the general pattern suggests that SUV39H1/2 mediated generation of repressive chromatin contributes to the down-regulation of cellular genes during VACV infection.

5.2.7 Identification of specific VACV gene(s) responsible for enhancing the repressive chromatin in infected cells

As the results in the previous sections showed, VACV infection leads to enhancement of H3K9me3 levels in SUV39H1/2 dependent manner. Moreover, the results of araC and cycloheximide treatment experiments suggested that expression of early viral genes is sufficient to increase H3K9 tri-methylation. Out of the ~200 VACV- WR genes, 118 are designated as early genes (46). To identify the gene(s) responsible for the increment in H3K9me3, I used a large deletion mutant of the WR strain of VACV that is available in

Table 5.1. List of genes deleted in XY-dBID-VACV

Gene	Temporal	MYXV Homolog	Function	Ref.	Ruled out
N1L	Early/Late	M146R	Virulence, anti-apoptotic, NFκB	(590-592)	
N2L	Early	None	Nuclear IRF3 inhibitor, virulence	(593)	✔
M1L	Early	M148R	ANK-like protein	(25)	
M2L	Early	M154L	ER-protein, NFκB inhibition	(594)	
K1L	Early	None	ANK-like, NFκB and IFN response blocker	(595-597)	✔ (?)
K2L	Early	M151R	Inhibits cell-cell fusion, serine protease inhibitor	(598)	
K3L	Early	M156R	IFN resistance gene	(599, 600)	
K4L		M22L	Phospholipase D-like protein, DNA nicking-joining enzyme	(601, 602)	
VACWR036 (Fragment)		None	Putative monoglyceride lipase	(25)	
VACWR037/ K5L		None	Putative monoglyceride lipase	(25)	
K6L		M042L	Putative monoglyceride lipase	(25)	
K7R		M136R	Virulence factor, NFκB and IRF3 inhibition	(603, 604)	
F1L	Early	None	BCL2-containing anti-apoptotic protein	(506, 605-607)	✔
F2L	Early	M012L	dUTPase (dUTP to dUMP)	(608, 609)	
F3L	Late	M014L/ M140R	kelch-like protein, host immune suppression	(610)	
F4L	Early	M015L	Ribonucleotide reductase, small subunit	(52, 109)	✔

IFN-interferon, IRF3-interferone response factor 3, ANK-ankyrin, ER-endoplasmic reticulum, dUTPase-deoxyuridine 5'-triphosphate nucleotidohydrolase, dUTP- deoxyuridine 5'-triphosphate, dUMP- deoxyuridine 5'-monophosphate

the laboratory, with the hope that unlike wild-type VACV, this virus would not be capable of altering the repressive chromatin. XY-dBID-VACV was generated by substituting 11 kb of viral DNA between N1L and F4L with LacZ gene (611). In comparison to wild-type VACV, this virus lacks 16 genes, which are listed in Table 5.1.

To examine the level of H3K9me3 and H4K20me3, BSC40 cells were infected with XY-dBID-VACV or VACV-WR for 9h. Specific antibodies were then used to stain for H3K9me3, H4K20me3 and I3. The results indicated that while VACV-WR resulted in a 3.6 and 4 fold increase in the levels of H3K9me3 and H4K20me3, respectively, XY-dBID-VACV did not result in a significant change in the levels of both markers compared to non-infected cells **(Figure 5.17 and 5.18)**. Since XY-dBID-VACV replicates less efficiently compared to wild type strains, it could be that XY-dBID-VACV infection requires longer period than wild-type VACV to result in alteration in methylation patterns. To examine this, H3K9me3 levels were determined at later times in infection. Similar to the observations at 9h post-infection, I found that at 18h post-infection, XY-dBID-VACV infected cells did not show any significant change in the levels of H3K9me3 compared to non-infected cells **(Figure 5.19 and 5.20)**. On the other hand, H3K9me3 levels continued to rise from 2.3 fold at 9h post infection to ~2.7 fold at 18h post-infection in VACV-WR infected cells **(Figure 5.19 and 5.20)**. MYXV, which also replicates less efficiently compared to VACV-WR, did not show a significant change in H3K9me3 levels both at 9 and 18h post-infection compared to non-infected cells. These results suggest that both XY-dBID-VACV and MYXV are not able to induce the repressive chromatin at any time point after infection. Moreover, the genes responsible

for increasing the repressive chromatin during VACV infection are mapped to the 11 kb region deleted in XY-dBID-VACV.
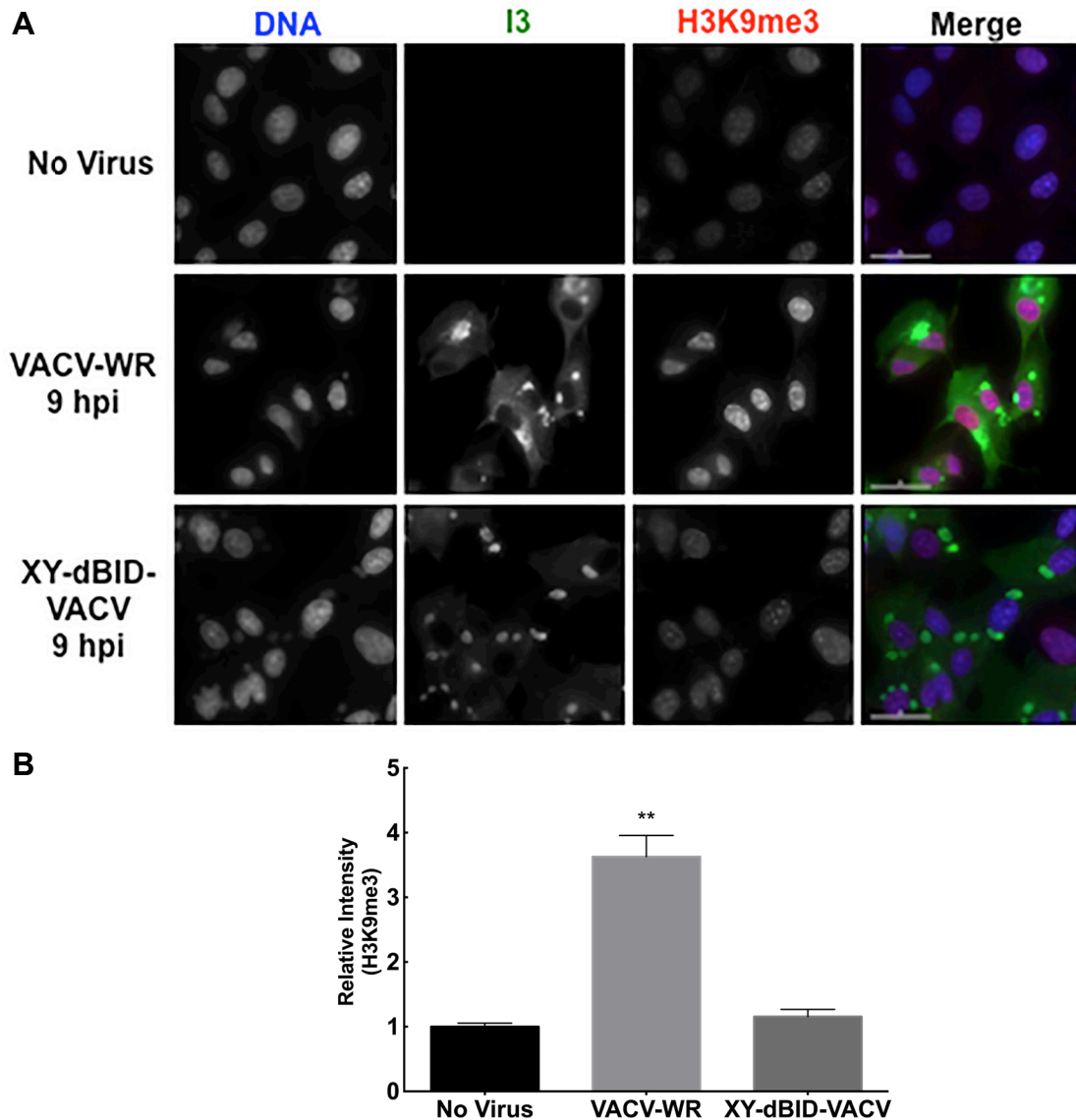
Figure 5.17. XY-dBID-VACV infection does not enhance H3k9me3 levels. BSC40 cells were mock infected or infected with VACV-WR or XY-dBID-VACV, which has an 11 kb deletion. After 9h of infection, the cells were fixed and stained for H3K9me3 and I3 using specific antibodies. DNA was stained with DAPI. Intensities of H3K9me3 were measured by Image J. (A) is a representative sample and (B) shows the mean and SD of three independent experiments. (**, $p \leq 0.001$).
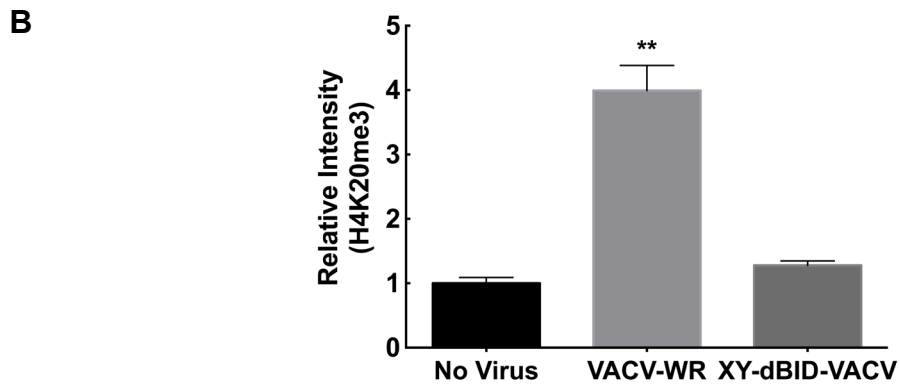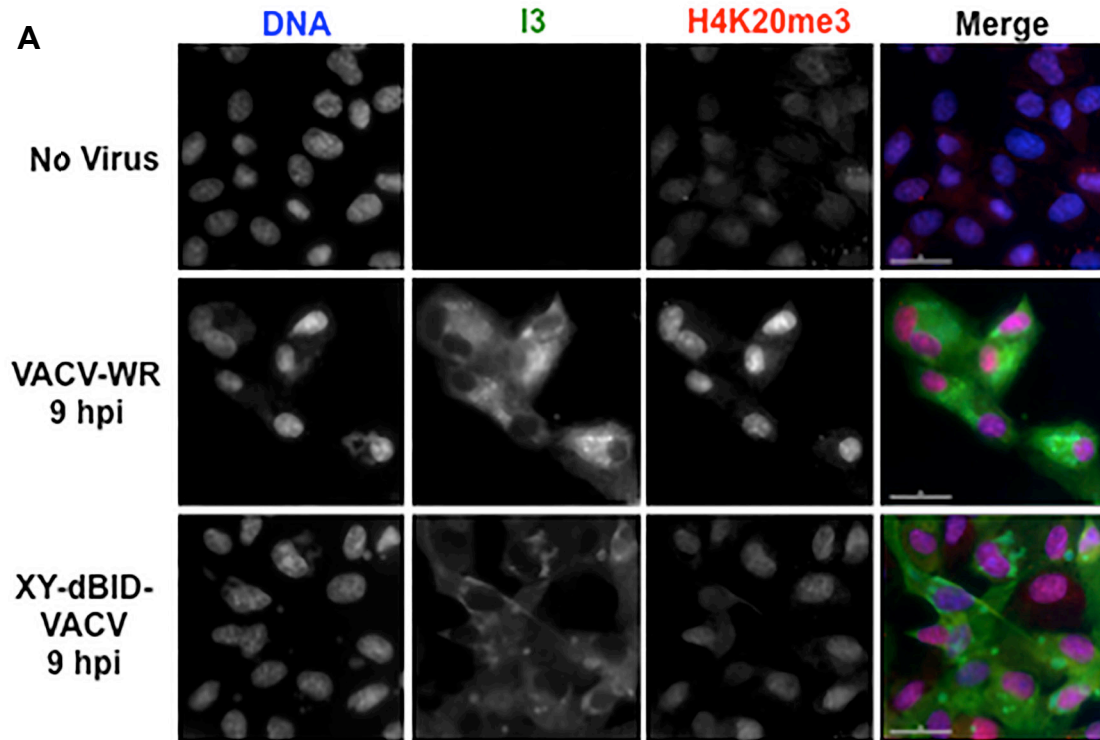
Figure 5.18. H4K20me3 levels do not increase in XY-dBID-VACV infected cells. Monolayers of BSC40 cells were infected with VACV-WR or XY-dBID-VACV for 9h. Then the cells were fixed and stained for H3K9me3 and I3 using specific antibodies. DNA was stained with DAPI. Mock infected cells were used as controls. Intensities of H3K9me3 were measured by Image J. (A) is a representative sample and (B) shows the mean and SD of three independent experiments. (**, $p \leq 0.001$).
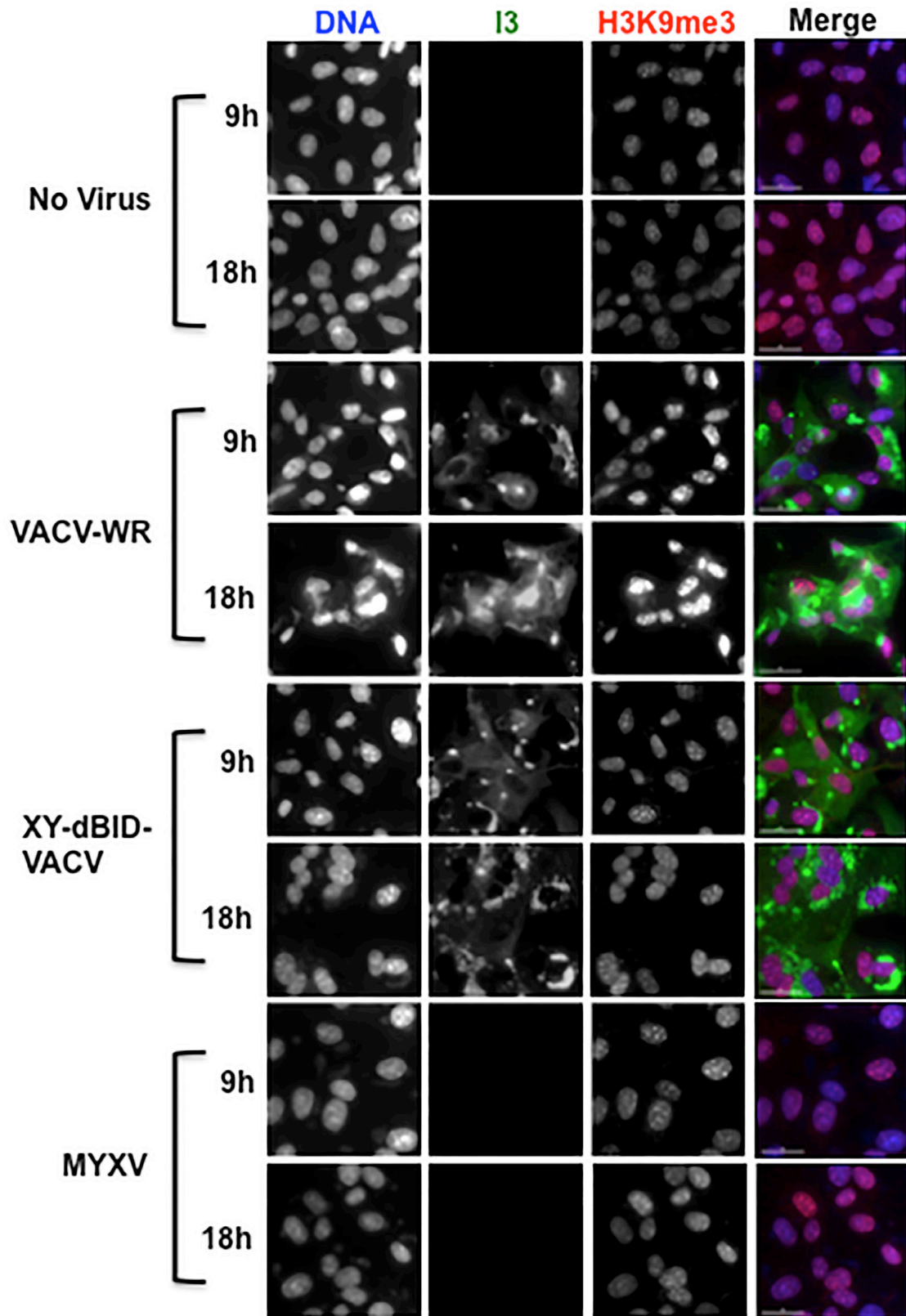
Figure 5.19. XY-dBID-VACV or MYXV infected cells do not show increment in H3K9me3 levels both at earlier and later time points. BSC40 cells were mock infected or infected with VACV-WR or XY-dBID-VACV or MYXV. At 9 and 18h post-infection the cells were fixed and stained for H3K9me3 and I3 using specific antibodies. A representative sample of three experiments is shown.
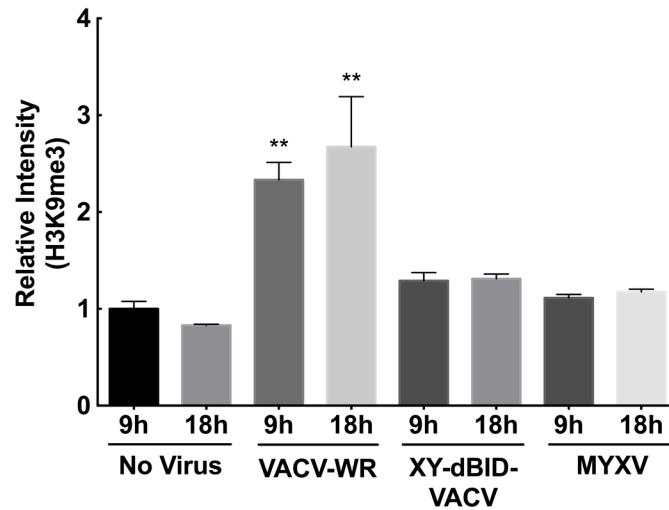
Figure 5.20. Quantification of H3K9me3 intensities at advanced time points after infection. BSC40 cells were infected with VACV-WR, XY-dBID-VACV or MYXV for 9 and 18h. The cells were then fixed and stained for H3K9me3 and I3 using specific antibodies. DNA was stained with DAPI. Total nuclear intensities of H3K9me3 were measured by Image J. Data shows the mean and SD of three independent experiments. (**, $p \leq 0.001$). A representative immunofluorescence image is shown in Figure 5.18.

As mentioned above, I rationalize that the gene(s) responsible for VACV-induced alterations in the repressive chromatin would map in the 11 kb region deleted in XY-dBID-VACV, which encodes for 16 genes with various functions (Table 5.1). Moreover, since MYXV does not increase the levels of H3K9me3 and H4K20me3, I would predict that the gene(s) responsible for increasing the repressive chromatin would not have a

MYXV homolog. Five of the genes (N2L, K1L, VACWR036, VACWR037 and F1L) do not have a MYXV homologue and almost all of them are expressed early (except F3L).

Four genes, including three that do no have a MYXV homologue, were examined independently using available single-gene mutants of VACV (ΔN2L-VACV (507), ΔF1L-VACV (606), and ΔF4L-VACV (109)) or over-expression plasmids (K1L). The results showed that all of the single-gene mutants led to H3K9me3 enhancement comparable to that of wild type strains **(Images S4 – S6 in the Appendix)**. Moreover, overexpression of K1L in XY-dBID-VACV infected cells did not result in enhancement of H3K9me3 **(Image S7 in the Appendix)**. The results suggest that none of these four genes are able to enhance the formation of the repressive chromatin independently. As a result, examination of the rest of the genes is recommended.

5.3   SUMMARY AND BRIEF DISCUSSION

Several studies have identified ample interactions between the cellular epigenetic mechanisms and various families of viruses. However, these interactions have not been investigated in poxviruses. In this study, I examined the effect of poxvirus infection on the repressive chromatin. Members of the *orthopoxvirus* genus, such as VACV and CPXV, increased the nuclear levels of H3K9me3 and H4K20me3, which are markers of the repressive chromatin. In contrast leporipoxviruses including MYXV and SFV did not alter the levels of these markers in infected cells. In the case of VACV, a significant enhancement in the nuclear levels of H3K9me3 was observed starting from 6h post-infection and plateauing between 9 and 12h after infection.

According to several previous studies, VACV infection leads to a reduction in cellular gene expression and it was shown that virus-encoded decapping enzymes play a

role in this process. This study also showed that VACV infection leads to a reduction in the transcriptional activity of infected cells. As discussed in chapter 1, one of the mechanisms through which cells regulate gene expression is by using epigenetic mechanisms including histone methylation. As a result, it is possible that the induction of the repressive chromatin during VACV infection could be another mechanism, in addition to decapping of cellular mRNAs, through which VACV down regulates cellular gene expression. This hypothesis is supported by the preliminary real-time RT-PCR studies discussed in section 5.2.6 that showed differential regulation of cellular gene expression between SUV39H double null cell lines and their wild-type counterparts. Even though my studies have not identified the viral protein(s) responsible for altering the levels of the repressive chromatin, the protein(s) is/are expected to be expressed in the first 2h of infection. It is also very likely that the protein maps to the 11 kb region of VACV genome, which is deleted in XY-dBID-VACV.

The results of this study give insight into poxviral regulation of the cellular chromatin. Further studies would be able to consolidate our understanding of the mechanisms involved in the process and also would help us identify possible targets for anti-poxvirus drug development.

CHAPTER 6: DISCUSSION AND FUTURE DIRECTION

In this research project, I investigated the interaction between poxviruses and their cellular hosts. I, in collaboration with my colleagues, identified more than 1000 candidate human host cell factors that modulate the replication of MYXV in human breast cancer cells using large-scale siRNA screens. Based on the results of the screens, I also described the role of glycolysis and the cell cycle control system in MYXV replication. Furthermore, I studied the effect of poxvirus infection on the repressive chromatin. In this chapter, the results of these studies are summarized and discussed in the context of our current knowledge. Future research directions are also suggested.

6.1 Identification of human cellular factors that modulate MYXV replication

Poxviruses replicate and transmit efficiently by actively modulating the structural and functional components of their cellular hosts through the large number of proteins they encode. On the other hand, hosts also utilize several mechanisms, both at cellular and organismal levels, to circumvent virus replication. This evolutionary struggle is the basis for poxvirus-host interactions.

As one of the most studied virus families, several poxvirus-host interactions have been described. Various independent studies have identified mechanisms used by poxviruses to modulate host antiviral immunity, apoptosis, cell proliferation and metabolism, among others. These discoveries have been accelerated in the last decade due to the availability of large-scale RNAi libraries and high throughput screening technologies. For example, RNAi screens have identified the role of AMPK in VACV entry (236) and that of the nuclear pore complex protein, Nup62, in virus morphogenesis (231).

In this study, we conducted kinome screens and the first genome-wide siRNA screen for MYXV to identify cellular factors that influence MYXV replication and to further our understanding of poxvirus-host interactions. In order to successfully perform the screens, we developed our screening methods using rigorous optimization procedures. We used MDA-MB-231 cells due to their intermediate level of permissiveness to MYXV, which proved to be important to identify factors that changed virus replication either positively or negatively within the dynamic range of our reporter detection system. Our reporter system utilized a virus encoded β-galactosidase enzyme, which is expressed late in infection. We confirmed that the activity of virus-encoded β-galactosidase corresponds to actual virus yield. A shortcoming of the system, however, was its inability to efficiently identify cellular factors that impact the late events of virus replication cycle including assembly and egress. For example, a cellular gene, which might inhibit assembly without any effect on preceding events, including the expression of β-galactosidase, could be considered a non-hit. As a result, our results accurately reflect those cellular factors that impact pre-assembly events of the MYXV replication cycle.

6.1.1 Cellular factors identified by kinome screens

After we optimized our transfection system, we conducted kinome test screens. Our kinome screens, which used a library of 986 pooled siRNAs that target human kinases and phosphatases, identified 70 proviral and 26 antiviral genes. Pathways enriched with these genes included those that were previously known to play a role in MYXV and/or other poxvirus replication, such as chemokine and cytokine mediated signaling pathways, MAPK pathways and apoptosis. Studies have shown that poxviruses, including MYXV, undergo extensive interactions with the mediators of antiviral

immunity including cytokines and chemokines, and as a result it is not surprising to identify hits that belong to these pathways (241).

Poxviruses also encode several growth factors that signal through one or more of the three MAPK pathways: Erk1/2, p38 and Jnk (612-615). Moreover, MAPK pathways were shown to be crucial for VACV replication and the expression of VACV-encoded foreign genes (615-617). Our screens showed similar results to these observations seen in VACV. For example, silencing of phosphatases, DUSP5 and DUSP6, which dephosphorylate and inhibit the Erk1/2 MAPK pathway increased MYXV replication indicating a positive role played by the pathway in MYXV replication **(Table S1)**. Studies have also showed that VRK-2 phosphorylates and inhibits scaffold proteins, Jip1 and Ksr1, which promote the activation of Jnk and Erk1, respectively (618, 619). Our screens and independent experiments demonstrated that siRNA silencing of VRK2 promoted MYXV replication **(Table S1 and Figure S1)**. This further validates the positive role of the Erk1/2 MAPK pathway in MYXV replication even though VRK-2 is a multifunctional kinase.

In contrast to our findings, the Erk1/2 MAPK pathway was shown to play a fundamental role in activating the IFN system and inhibiting MYXV replication in non-permissive MEFs (120, 620). The reason why activation of the Erk1/2 MAPK pathway in MDA-MB-231 cells led to increased MYXV replication, while its activation in MEFs showed the opposite effect, is not clearly understood. However, this might be a consequence of a dysfunctional IFN system in MDA-MB-231 cells as it was previously demonstrated by significantly reduced activation of IFN effectors, such as 2'5'-oligoadenylate synthetase, in IFN-α2a treated MDA-MB-231 cells (621). To decipher the

exact role played by the three MAPK pathways, small chemical inhibitors of the various kinases and phosphatases involved in the pathways as well as primary cells with intact MAPK pathway regulation need to be utilized in future experiments.

Our kinome screens also identified novel pathways, such as glycolysis, whose role in MYXV infection was not previously described. Based on the results of our kinome test screens, which identified both previously known and novel cellular factors, we considered our screening methods to be optimal and decided to perform whole genome screens.

6.1.2   Cellular factors identified by a whole-genome siRNA screen

We performed a two-step screen, which we named primary and validation, to identify hits of the whole genome screen. The primary screen involved more than 21000 genes, which included all of the known protein-coding genes of the human genome, and identified 1588 hits. These hits, hits of our kinome screens that were not identified in the primary screen and housekeeping non-hits were rescreened in a validation screen using similar siRNAs and screening methods. We believed rescreening the hits of the primary screen would help to minimize false identification rates by reducing both systemic and random errors. The final hits of the whole genome screens included 711 antiviral genes and 333 proviral genes. These represent 4.8% of the genes in the human genome. A whole genome screen performed for VACV identified a similar number of 1106 genes (231). Moreover, a druggable genome screen for VACV, which included 6719 human druggable genes, identified a total of 302 hits, i.e. ~4.5% of the screened genes (233). Overall these results suggest that 4.5% − 5% of the protein-coding genes in the human

genome influence the replication of poxviruses although more data is needed for other members of the *Poxviridae* family.

The most striking difference between our screen and the published VACV screens is that our screen identified more than twice as many antiviral genes as proviral genes while both VACV screens identified nearly equal numbers of proviral and antiviral hits. Even though the exact reason for this observation is not understood, I predict that human cells, which are naturally resistant to MYXV infection, might have much more restriction factors against MYXV than VACV, which is able to infect most human cell types. To test this prediction, it would be important to perform a similar large-scale screen for MYXV in rabbit cells, which are naturally permissive to MYXV infection.

To get a rough estimate on the reproducibility of our results, we determined the proportion of our hits that would be identified by independently designed siRNAs. We screened a custom-made siRNA library that had a pool of 4 different siRNAs targeting each gene of 59 hits (30 proviral and 29 antiviral genes) and 29 non-hits randomly selected from the results of our whole genome validation screen. Assuming that genes repeatedly identified as hits by several independent screens are true positives, our custom siRNA library screen predicted a ~25% true positivity rate for our hits while the predicted true negativity rate for the non-hits was close to 75%. Even though the negative predictive value for the non-hits appears to be very high, it is realistic because any randomly selected gene has a very high probability of being one of the ~ 95% of genes in the human genome that do not influence poxvirus replication, as described above. On the other hand, the positive predictive value for the hits appears to be high compared to gene-level reproducibility rates observed for similar independent siRNA screens for VACV,

which is <10%, as described in section 1.2. Gene-level reproducibility rates of large-scale siRNA screens performed for other viruses were also lower than our rates. The reason for this may be that all of our screens were performed using the same cell line, virus strain and transfection system, while the screens for VACV and other viruses were performed by different groups independently, using different cell lines and transfection systems. I predict a screen performed using a different cell line and MYXV strain would result in a lower reproducibility rate that is on par with the values observed for other viruses.

We also conducted a toxicity screen to identify those siRNAs that indirectly inhibit virus replication by inducing cell death. The toxicity screen was performed using the validation screen library and identified 32 toxic siRNAs. Most of these siRNAs target several genes that belong to the ubiquitin-proteasome system. Given the central role of this pathway in various important cellular functions, it is expected that inhibition of the pathway ultimately triggers programmed cell death. It is due to this effect that chemical inhibitors of the pathway, such as bortezomib, are used for the treatment of hematologic malignancies (622).

We performed a pathway enrichment analysis of our whole genome screen hits using DAVID and PANTHER algorithms. Similar to our kinome screens, chemokine and cytokine mediated signaling pathways and MAPK pathways were enriched with the hits of the whole genome screen. Moreover, oxidative stress response pathways and the cell cycle control system were among the top pathway-hits of our whole genome screen. Even though the whole genome screen hits included most of the glycolytic hits of the kinome screens, glycolysis, as a pathway, was not included among the top pathway hits of our whole genome screen.

Interestingly, we observed that the oxidative stress response pathway was enriched with antiviral hits of our whole genome screen. It was previously shown that MYXV and SFV encode catalytically inactive homologs of superoxide dismutase 1 (SOD1) gene, which is suggested to play a role in interfering with the oxidative stress response of infected cells (623). Wild-type strains of MYXV and SFV increased intracellular superoxide levels, promoted cell growth and inhibited apoptosis compared to strains with deleted SOD1 homologs, indicating the importance of an optimal level of oxidative stress in achieving an intracellular environment that is favorable for MYXV and SFV replication (623). Future studies that focus on the hits of the oxidative stress response pathways would further our understanding of the role of this pathway in poxvirus replication.

Overall, our screens identified ~1000 hits that modulate the replication of MYXV in a human malignant breast cancer cell line. As expected from any screen, all of these hits would not be true positives. However, according to our prediction a quarter of these genes would have a very high probability of being true positives. Moreover, the validity of a subset of these hits was ascertained based on previous work described in the literature, as described above, and independent confirmation experiments that we performed. We believe that our gene and pathway hits will serve as an excellent starting point for future studies that focus on poxvirus-host interactions, anti-poxvirus drug target identification and poxvirus-based oncolytic virotherapy.

6.2 Comparisons between the hits of our screens and that of large-scale RNAi screens for VACV

I conducted a pairwise comparison of our genome-wide screen hits with that of previous VACV druggable genome or genome-wide screens **(Table 1.2)**. Mercer *et al.* (2012), identified 188 proviral hits with a druggable genome screen for VACV (234). A pairwise comparison analysis of these hits and that of our whole genome screen identified 11 common hits (i.e. 3.3% of the provial hits of the whole genome screen). Close to half of these hits belong to the proteasome system, which was shown by Mercer *et al.* to play a role in VACV uncoating. Further testing is needed to determine whether the proteasome system might play a similar role in MYXV life cycle, since most of our siRNAs that target the proteasome were toxic.

A whole genome siRNA screen conducted by Sivan *et al.* (2013) for human cellular factors that modulate VACV replication identified 576 proviral and 530 antiviral hits (231). A pairwise comparison of these hits with the results of our screen identified 12 and 22 common proviral and antiviral hits, respectively. This represents 3.6% and 3.1% of the proviral and antiviral hits of the whole genome screen conducted in this project, respectively. Sivan *et al.*'s screen identified six proviral genes that belong to the nuclear pore complex, which were confirmed to play a role in viral morphogenesis with further studies. Even though none of the six nucleoproteins were identified in our whole genome screen, another nuclear pore protein, Nup188, was found to be a proviral hit in our screen. The role of the nuclear pore complex in MYXV replication needs further investigation.

191

The degree of overlap between the hits of our whole genome screen and a druggable genome screen for VACV performed by Beard *et al.* (2015) identified 3 common genes for both antiviral and proviral hits. This corresponds to <1% of the hits of our screens.

Filone *et al*. (2014) identified 34 proviral hits with a stringent shRNA screen for VACV host factors (235). Based on their screens, the authors described the positive role of heat shock transcription factor 1 (HSF-1) and its target genes in VACV replication. Pairwise comparison between the 34 hits of the screen and the 1044 hits of our whole genome screen identified only one common hit (cyclin nucleotide gated beta 3, CNGB3). Even though HSF-1 was not identified as a hit in our screens, two heat shock proteins (heat shock 22 kDa protein 8/ HSPB8 and heat shock protein, alpha-crystallin-related, B9/ HSPB9) were shown to be proviral. This observation needs further investigation to determine the role of heat shock proteins in the replication of MYXV, and other leporipoxviruses.

In addition to the gene-level comparisons described above, I conducted a functional class enrichment analysis of the hits of our screen and that of the aforementioned VACV screens using DAVID's GOTERM_BP_FAT functional annotation tool. The degree of overlap between the hit-enriched functional classes of our screen, Mercer *et al*.'s screen and Beard *et al*.' screen was 7 – 13%. Cell cycle, regulation of protein kinase activity and regulation of transferase activity are some of the processes that were enriched with hits of the three screens. The functional class overlap between Sivan *et al*.'s screen and the other screens was very low.

The above analyses indicated low gene-level overlaps between hits of our whole genome screen and other large-scale VACV RNAi screens, in a pairwise comparison. However, the functional class overlap was higher, suggesting these viruses, which belong to the same family, interact with similar cellular functions to successfully complete their replication cycles. My analyses also suggest that cellular functions that were shown to play a role in VACV replication, such as heat shock proteins and nuclear pore complex proteins, might also play a similar role in MYXV replication, although further experiments need to be performed. The findings of my analyses are comparable to that of previous meta-analyses of the results of large-scale RNAi screens for HIV and influenza virus, as described in section 1.2.

6.3 The replication of MYXV is influenced by the glycolytic activity of cells

Glycolysis is a central component of the energy metabolism network of cells. Its end product, pyruvate, is converted into acetyl-CoA, which shuttles to the TCA cycle and oxidative phosphorylation leading to the production of energy in the form of ATP. Glycolysis also produces several intermediates, which are crucial inputs for metabolic pathways that produce nucleotides, amino acids, fatty acids and other lipids. Moreover, glycolytic intermediates are involved in regulating oxidative stress by generating NADPH, which is needed to produce important reducing agents (624).

Several studies have uncovered important interactions between viruses and the cellular energy metabolism network. Glycolysis, fatty acid synthesis and glutaminolysis are the major metabolic pathways that are frequently modulated by viruses (250). Activation of these pathways, which leads to the production of energy and biosynthetic intermediates, creates an intracellular environment that is favorable for virus replication.

VACV infection of cells results in metabolic outcomes that appear to be paradoxical: on one hand, VACV replicates well in the absence of glucose, while on the other hand it activates HIF-1, a major activator of glycolysis (307, 309). VACV does not increase glycolytic activity in infected cells; however, it increases glutaminolyis and fatty acid synthesis (306, 307). Similarly, inhibition of glutaminolysis or fatty acid synthesis significantly reduces virus replication (306, 307). The paradox lies in the fact that VACV encodes C16, which leads to stabilization and activation of HIF-1 and its downstream glycolytic enzymes and glucose transporters in normoxic conditions (308, 309). The reason why HIF-1 is up-regulated during VACV infection despite a lack of dependence on glycolysis is not known at the moment.

There are limited studies that examined the effect of MYXV infection on energy metabolism. The only study conducted more than 60 years ago demonstrated that inoculation of chorioallantoic cells with MYXV enhanced lactate production, suggesting increased glycolysis during infection (310).

Our kinome and whole genome screens identified a number of glycolytic enzymes as hits. Two isoforms of PFK-1 (PFKL and PFKM), which catalyzes the rate-limiting step of glycolysis (conversion of F6P to F1,6BP), were identified as proviral hits; i.e. siRNA silencing of the genes reduced virus replication. Likewise, an isoform of PFKFB, an enzyme that leads to the production of F2,6BP from F6P, was also shown to be a proviral hit. F2,6BP is a major allosteric activator of PFK-1 (625). In contrast, siRNA silencing of FBP1, a gene encoding an enzyme that reverses the reaction catalyzed by PFK-1, resulted in increased MYXV replication, suggesting an antiviral role of the

enzyme. Taken together the findings suggested a positive role of glycolysis in MYXV replication.

We confirmed that siRNA silencing of PFK-1 reduced MYXV replication by using independently designed siRNAs that target PFKL. Further confirmation was achieved by demonstrating a reduction in MYXV replication with a competitive chemical inhibitor of glycolysis, 2DG. Our experiments also showed that increasing glycolytic activity of cells by over-expressing key glycolytic enzymes, such as PFK-1 and PFKFB, resulted in increased replication of MYXV in an optimal glucose environment. In both settings we used lactate and ATP measurements as markers of glycolytic activity. Over all, these results showed that the activity of glycolysis influences the replication of MYXV.

Given the importance of glycolysis in supplying biosynthetic intermediates for the generation of various macromolecules, it may not be surprising that MYXV replicates well in cells with increased glycolytic activity. It is interesting that, while almost all orthopoxviruses encode homologs of C16 (VACV Copenhagen ORF B22R), MYXV does not encode any C16 homolog, suggesting a different form of metabolic regulation in MYXV and possibly other leporipoxvirus-infected cells. Future experiments should examine the importance of glutaminolysis and fatty acid synthesis in MYXV replication using chemical inhibitors of these processes.

According to our experiments, infection of MDA-MB-231 cells with either MYXV or VACV did not alter lactate levels, indicating that both viruses do not enhance glycolytic activity in these cancer cells. For VACV, this finding confirms previous observations that VACV infection does not increase lactate production in infected cells

(308). However, previous studies showed that MYXV infection increased lactate production in primary cells (310). The reason that MYXV infection did not increase lactate production in MDA-MB-231 cells could be related to the fact that these cancer cells already have high basal glycolytic activity, as it was previously demonstrated by higher PFKL levels and lactate production compared to less aggressive breast cancer cell lines, such as MCF7, and primary cells (255).

Enhanced glycolytic activity, despite the presence of abundant oxygen (aerobic glycolysis or the Warburg effect), is a common phenomenon of cancer cells (260, 262, 263). As a result, to determine the effect of MYXV infection on the glycolytic activity of infected cells, future experiments should be conducted using primary rabbit cells (non-rabbit primary cells are not permissive to MYXV) that have intact metabolic regulation. Moreover, using these types of cells, it would be possible to perform a global analysis of metabolomics and carbon flux studies to get an important insight into the regulation of the entire energy metabolic process during MYXV infection, and to compare the findings with that of VACV.

Our screens and independent experiments also showed that MYXV replicates better when PDK3 is silenced. PDK3 is an isoform of a kinase that phosphorylates and inhibits PDC, blocking the conversion of glycolysis-derived pyruvate to acetyl-CoA (626). These data, taken together with the data on the key glycolytic enzymes, suggests that MYXV better replicates in cells that demonstrate increased glycolysis, where there is enhanced metabolism of glucose towards pyruvate and acetyl-CoA. At this point, we do not know whether the TCA cycle is kept active during MYXV infection primarily by carbon-flux from glycolysis or by substrates such as α-ketoglutarate, which could be

derived through glutaminolysis, in a similar way as VACV. Metabolomics and carbon flux studies described above, as well as glutamine deprivation and chemical inhibition of glutaminolysis would help to clarify these questions.

One of the most interesting features of MYXV is its ability to specifically replicate in some human cancer cells, despite its inability to do so in primary cells. Studies showed that MYXV ankyrin-repeat protein MT5 is a crucial determinant factor for MYXV tropism in human cancer cells through its interactions with cellular Akt (119, 371, 521, 523, 627, 628). Further studies also identified that the level of phosphorylation and activation of endogenous Akt determine the degree of permissiveness of cancer cells to MYXV (119). As described above, most cancer cells reprogram their metabolism towards aerobic glycolysis, which is primarily mediated by Akt (534). I predict that the degree of activation of glycolysis in cancer cells also determines MYXV tropism. This could be tested with simple correlation experiments where lactate levels of a panel of cancer cells is determined and plotted against the degree of replication of MYXV in the cells. Examining this correlation would have an important clinical utility. If and when MYXV is used for oncolytic virotherapy, it would be possible to predict patients' response to treatment by determining *in situ* glycolytic activity of malignant masses using positron emission tomography (PET) scans that measure glycolytic activity (629).

In general, our screens and independent experiments have demonstrated the importance of glycolysis in MYXV replication. Moreover, the possibility of differential regulation of the cellular energy metabolism between different genera of the *Poxviridae* family has also been suggested. Further understanding of the interactions between poxviruses and the cellular energy metabolism will help to identify anti-poxvirus drug

targets as well as to increase the efficiency of targeted use of these viruses for oncolytic applications.

6.4 Cells arrested at G1 or G1/S boundary of the cell cycle create a favorable environment for MYXV replication

The cell cycle control system ascertains the successful completion of important milestones in a particular phase of the cell cycle prior to transitioning to the next phase. Signaling pathways and regulatory networks of the cell cycle control system regulate the cell cycle at three important checkpoints: restriction checkpoint in late G1, G2/M-checkpoint in late G2 and spindle checkpoint in mid-mitosis.

Viruses undergo interactions with the components of the cell cycle control system to deregulate the cell cycle (366). Depending on their needs, viruses can induce cells to enter into the cell cycle from resting G0-phase or they can arrest them at a particular phase of the cell cycle. For example, small DNA viruses induce cells to enter into the cell cycle so that they can use cellular nucleotide and DNA-replication machineries. In contrast, large DNA viruses, which encode for enzymes involved in nucleotide synthesis and DNA replication, can arrest cells in G1 to prevent cellular competition for substrates. Viruses can also block entry into mitosis so that the cellular cytoskeleton and other organelles remain intact to benefit viruses.

Similar to other families of viruses, poxviruses interact with the cell cycle control system in a species-specific manner. MYXV, for example, induces entry of cells, which are synchronized at G0/G1, into the cell cycle through M-T5 mediated activation of a cullin-3 ubiquitin ligase, which leads to ubiquitin-proteasome based degradation of p27 (371). After entry into the cell cycle, the cells have been observed to accumulate in S-

and G2/M-phases of the cell cycle (please see below for explanations on the shortcomings of this experiment). Likewise, VACV also induces rapid entry of infected cells into the cell cycle (373). In contrast, SFV does not affect the regulation of the cell cycle. A few species of poxviruses, such as Orf virus and crocodile poxvirus, encode a catalytically inactive homolog of APC11, which is called PACR (412, 413). PACR, which is lacking in leporipoxviruses and orthopoxviruses, gets incorporated into the APC and blocks its functions (412, 413).

The cell cycle control system was one of the top hits of our whole-genome screens, where 15 genes of the system were identified as hits using the DAVID algorithm **(Table 4.1)**. Mapping of theses hits on the pathways and networks of the cell cycle control system revealed an interesting pattern. siRNA silencing of genes that encode proteins involved in regulation of early and late G1 phases of the cell cycle, such as Cdk6, Cyclin D2 and E2F5, increased the replication of MYXV. In contrast, knocking down of genes that encode proteins regulating the G2/M-checkpoint, such as Wee1, Plk1, Chk1 and Cdc25B, reduced MYXV replication. At a glance this appears to be counterintuitive since silencing of either promoters or inhibitors of cyclin B-Cdk2 complex appear to inhibit MYXV. However, a close examination reveals that the proteins at this control system function in a feedback loop, as a result silencing of one of the proteins leads to the deregulation of the other (630). The screens also found that siRNA silencing of APC13 enhanced MYXV replication. In general these results suggest that arresting cells in early and late G1 phases of the cell cycle results in increased MYXV replication. A similar result is also expected by blocking the activity of APC. On the

other hand, blocking the progression of cells through the G2/M-checkpoint appears to inhibit the cell cycle.

To confirm the patterns we observed from the cell cycle hits of the siRNA screens, we performed independent experiments where we used small chemical inhibitors to induce cell cycle arrest at various phases of the cell cycle. A Cdk4/6 inhibitor (PD0332991), a G2/M inhibitor (SFN) and an APC inhibitor (proTAME) were used for these purposes. PD0332991 significantly increased the proportion of G1-phase cells in two cell lines (MDA-MB-231 and PANC1) without significant toxicity, while it achieved a modest increase in G1-phase cells in MCF7 cells. MYXV replication increased in the former two cell lines while it was not affected in the later with PD0332991 treatment, indicating better replication of MYXV in cells arrested at G1. These findings conform to the results of our screens.

The reason why MYXV replicates better in cells arrested at G1 phase of the cell cycle is not currently known. MYXV encodes a number of enzymes that are involved in nucleotide biosynthesis and also expresses its own polymerases (26). Since cells are not actively replicating their DNA during G1-phase of the cell cycle, this phase could be suitable for MYXV replication to avoid cellular competition for substrates needed to synthesize nucleotides and DNA. A similar phenomenon was observed in herpesviruses and a similar mechanism has been proposed (631). Another mechanism might involve the interplay between the cell cycle control system and cellular energy metabolism (632). Evidence suggests that glycolytic activity and lactate production is high in G1-phase than the other phases of the cell cycle in colon cancer cells (633). If glycolysis is active in G1 cells, it creates a favorable condition for MYXV replication as described above. To test

if a similar phenomenon is observed in the cell lines used in this study, cells could be arrested at various phases of the cell cycle using chemical inhibitors and/or fractionated into various phases using fluorescence-activated cell sorting (FACS), and their metabolic signatures could be examined using metabolomics and carbon flux studies.

As described above, a previous study demonstrated that MYXV promoted the entry of resting cells into the cell cycle by counteracting the activity of p27 (371). The study also showed that most of these cells were ultimately arrested at S-phase or G2/M-phase of the cell cycle. In the study, cell cycle analysis of the infected cells was performed by propidium iodide (PI) staining of DNA and flow cytometry between 6h and 48h of infection. A shortcoming to this method is that as post-infection time increases, viral DNA accumulates, increasing the total cellular DNA content. This leads to a failure in differentiating S- and G2-phase cells from virus-infected cells with high DNA content, suggesting a possible mischaracterization of MYXV infected cells as S- or G2-phase cells. As a result, I propose using other techniques, such as measurement of the levels of cyclins, transcription factors and downstream targets as well as the activity of Cdks, to accurately determine the patterns of cell cycle deregulation during MYXV infection. Moreover, the fucci (fluorescent ubiquitination-based cell cycle indicator) system can also be used for more accurate results (634).

In contrast, treatment of cells with SFN achieved G2/M arrest without significant toxicity in the first 24h of treatment; however, continued treatment induced significant cell death in later time points. MYXV replication was reduced in much higher proportion than the reduction in viability in SFN treated cells. Even though this might suggest that MYXV replication is reduced in cells arrested at late G2-phase of the cell cycle, the non-

specificity of SFN and its toxicities warrant further studies. Similarly, proTAME was also found to be too toxic to draw any conclusion on its effects on MYXV replication. Future studies should focus on using more specific and less toxic chemical inhibitors of the cell cycle control system. Moreover, RNAi methods could also be used to achieve these effects with more specificity and less toxicity.

We examined whether the cell cycle results of our screens and independent experiments could be utilized to optimize the oncolytic potential of MYXV. Our results indicted that MYXV growth was enhanced in cells that were arrested at G1-phase of the cell cycle with the treatment of PD0332991. The oncolytic activity of the virus and/or the drug were examined after 3-4 days and indicated that the virus-drug combination resulted in more significant cell killing than either the virus or the drug alone. PD0332991 (Palbociclib) is currently in 63 recruiting, active or completed clinical trials (https://clinicaltrials.gov accessed at the end of May 2015). Consequently, our results suggest that a combination therapy of MYXV and a G1 inhibitor, such as PD0332991, could enhance the oncolytic potential of MYXV. Based on our results, I predict that a combination of MYXV and S-phase inhibitors (most of the current chemotherapeutic agents) or G2/M-checkpoint inhibitors would have a negative effect on MYXV growth and reduce its oncolytic potentials. Futures studies should be performed to ascertain that these results could be replicated in animal models as well as in clinical trials.

Overall, a clear understanding of the mechanisms that govern the interactions between poxviruses and the cell cycle control system will help to identify antipoxvirus drug targets and to enhance the oncolytic potentials of these viruses, as described above.

6.5   Orthopoxviruses modulate the cellular repressive chromatin

One of the research projects, which studied poxvirus-host interactions, in my laboratory focused on understanding the role of DNA-binding VACV proteins on various cellular processes such as DNA-damage response and cellular chromatin regulation. In this project, I studied the effect of poxvirus infection of cells on the repressive chromatin.

Chromatin modification is one of the epigenetic systems that cells use to regulate various cellular processes including gene expression and replication. Several studies have demonstrated the interactions between the cellular chromatin and a number of viruses (recently reviewed in (475)).

Cells use their chromatin systems to inhibit virus infection **(Figure 1.11)**. Some of these systems include depositing repressive chromatin on viral genomes leading to inhibition of viral gene expression and genome replication. Cells also utilize their chromatin-modifying mechanisms to regulate the expression of genes that encode for pattern recognition receptors and mediators of antiviral immunity. In contrast viruses also manipulate the cellular chromatin system to benefit their replication **(Figure 1.11)**. Certain viruses control various phases of their replication cycle, such as latency and persistence, by using the cellular chromatin. Others modulate the chromatin system to inhibit the expression of antiviral genes and also to promote cell proliferation.

Even though poxviruses replicate in the cytoplasm, studies have indicated the presence of an interaction between the nucleus and virus factories. For example, cellular topoisomerase II and the YY1 transcription factor are recruited to VACV factories while VACV N2L is transported to the nucleus (562, 593, 635). These studies establish the possibility of more nucleus-virus factory interactions. It is likely that some of these

interactions could be involved in modulating the cellular chromatin system. Despite these possibilities, the interaction between poxviruses and the cellular chromatin system has not been a focus of investigations.

In this study, I described the changes associated with the cellular repressive chromatin during poxvirus infection. At least two strains of VACV and CPXV induced the formation of repressive chromatin in infected cells. Markers of the repressive chromatin, H3K9me3 and H4K20me3, increased starting from 6h of infection and plateaued between 9h and 12h post-infection. In contrast, leporipoxviruses, such as MYXV and SFV, did not alter the levels of these markers. These results suggest that orthopoxviruses increase the nuclear repressive chromatin, while leporipoxviruses do not.

The reason for the differential regulation of the cellular repressive chromatin in VACV or MYXV infected cells could be related to the differences in cellular gene expression patterns observed between the two viruses, as described below.

A number of genome-scale microarray and RNA-seq studies were conducted to determine the alterations in the transcriptome of VACV infected cells (568-570). Despite the variations observed based on the cells used in these studies, the results showed that a significantly large number of cellular genes were down-regulated during VACV infection. Similarly, a large number of genes were unchanged, while a small number of genes were up-regulated. A microarray study was also performed to examine the expression patterns of cellular genes during infection of ovine bone marrow derived dendritic cells with an attenuated MYXV strain (SG33) (571). The results indicated that at 3h post-infection, the expression of most cellular genes was unchanged; however, at 8h post-infection, 390 genes showed a change in their expression profile with 233 up-

regulated and 157 down-regulated genes. According to the study, it appears that most of the 15000 genes examined by the microarray experiment remained unchanged. Accordingly, these studies demonstrated that VACV infection leads to a wide spread inhibition of cellular gene expression, unlike MYXV where the expression of most genes remains unchanged. A shortcoming to this conclusion is that the number of MYXV-based studies is limited and also the change in the transcriptome could be different in rabbit cells, which are the natural hosts of MYXV. As a result, additional transcriptome studies of MYXV-infected rabbit cells should be performed and analyzed in the future.

Experiments described in section 5.5 gave a preliminary indication that VACV could manipulate the repressive chromatin to achieve a general reduction in the expression of cellular genes. More robust studies need to be performed in the future to confirm these observations. The studies could involve comparisons of genome-wide transcriptome analyses in VACV-infected cells that are able to induce repressive chromatin and those that are not able to do so. Similar comparisons could also be performed between VACV deletion mutants such as XY-dBID-VACV, which do not enhance the repressive chromatin, and wild-type VACV strains.

My studies have also identified preliminary features of the mechanism(s) involved in the induction of the repressive chromatin during VACV infection. The results indicated that early gene expression, but not late gene expression, is necessary for the induction of H3K9me3 and H4K20me3. Moreover, the mechanism does not involve synthesis of a new cellular protein. It most likely involves the activation of cellular chromatin modifying enzymes and/or redirecting these enzymes to chromatin domains where repressive methylation reactions are carried out. It has also been showed that the

increased tri-methylation of H3K9 during VACV infection is mediated by SUV39H1/2, since VACV was not able to induce H3K9me3 in cells that have double-deletions of these KMTs. Future studies need to examine the roles of the remaining KMTs that are able to tri-methylate H3 at K9 by utilizing siRNA silencing of the genes encoding the KMTs, specific small molecule inhibitors or cell lines with KMT knockouts.

This study also showed that a large deletion mutant of VACV (XY-dBID-VACV), which has an 11 kbp deletion between N1L and F4L, was not able to increase the levels of H3K9me3 and H4K20me3 in infected cells. As a result, this virus could be used to identify the gene(s) responsible for modulating the cellular repressive chromatin. Among the 16 genes represented in the deleted region, I examined and ruled out F1L, F4L, and N2L. In future studies, single-gene deletion mutants need to be generated for all the remaining genes represented in the region to identify the responsible gene(s) and to describe the exact mechanism used by VACV and other orthopoxviruses to modulate the cellular chromatin. Moreover, components of the mechanism could be targeted to generate anti-poxvirus drugs.

6.6 Conclusion

This research project aimed at furthering our understanding of poxvirus-host interactions. Using high throughput siRNA screening technologies, we identified >1000 cellular host factors that modulate the replication of MYXV. Based on these factors, we described the effect of the cellular glycolytic activity on MYXV replication and also showed that MYXV replicates better in G1-phase cells. Furthermore, we also demonstrated a mechanism that can be used to enhance the oncolytic potential of MYXV by combining the virus with a drug that causes G1 arrest. In the last part of the project,

we also described, for the first time, the interaction between poxviruses and the cellular repressive chromatin.

Overall, the findings of this research project demonstrate the power of genome-scale studies in gaining deeper insights into the interactions between viruses and the various intracellular molecular networks that form signaling pathways and define functional processes and intracellular domains. These insights, without a doubt, will help us to further our knowledge of viruses as well as cells and also will give us the capacity to exploit them for biomedical and clinical applications.

REFERENCES

1.   **Barquet N, Domingo P.** 1997. Smallpox: the triumph over the most terrible of the ministers of death. Ann Intern Med **127:**635-642.
2.   **Breman JG, Arita I.** 1980. The confirmation and maintenance of smallpox eradication. N Engl J Med **303:**1263-1273.
3.   **Verardi PH, Titong A, Hagen CJ.** 2012. A vaccinia virus renaissance: new vaccine and immunotherapeutic uses after smallpox eradication. Hum Vaccin Immunother **8:**961-970.
4.   **Chan WM, Rahman MM, McFadden G.** 2013. Oncolytic myxoma virus: the path to clinic. Vaccine **31:**4252-4258.
5.   **Van Vliet K, Mohamed MR, Zhang L, Villa NY, Werden SJ, Liu J, McFadden G.** 2009. Poxvirus proteomics and virus-host protein interactions. Microbiol Mol Biol Rev **73:**730-749.
6.   **Haller SL, Peng C, McFadden G, Rothenburg S.** 2014. Poxviruses and the evolution of host range and virulence. Infect Genet Evol **21:**15-40.
7.   **Moss B.** 2001. Poxviridae: the viruses and their replication, p 2849-2884. *In* Fields BN, Knipe DM, Howley PM, Griffin DE (ed), Fields Virology, 4th ed. Lippincott Williams & Wilkins, Philadelphia.
8.   **Cyrklaff M, Risco C, Fernandez JJ, Jimenez MV, Esteban M, Baumeister W, Carrascosa JL.** 2005. Cryo-electron tomography of vaccinia virus. Proc Natl Acad Sci U S A **102:**2772-2777.
9.   **Hollinshead M, Vanderplasschen A, Smith GL, Vaux DJ.** 1999. Vaccinia virus intracellular mature virions contain only one lipid membrane. J Virol **73:**1503-1517.
10. **Blasco R, Moss B.** 1991. Extracellular vaccinia virus formation and cell-to-cell virus transmission are prevented by deletion of the gene encoding the 37,000-Dalton outer envelope protein. J Virol **65:**5910-5920.
11. **Smith GL, Vanderplasschen A, Law M.** 2002. The formation and function of extracellular enveloped vaccinia virus. J Gen Virol **83:**2915-2931.
12. **Schmidt FI, Bleck CK, Mercer J.** 2012. Poxvirus host cell entry. Curr Opin Virol **2:**20-27.
13. **Ulaeto D, Grosenbach D, Hruby DE.** 1996. The vaccinia virus 4c and A-type inclusion proteins are specific markers for the intracellular mature virus particle. J Virol **70:**3372-3377.
14. **Chang SJ, Chang YX, Izmailyan R, Tang YL, Chang W.** 2010. Vaccinia virus A25 and A26 proteins are fusion suppressors for mature virions and determine strain-specific virus entry pathways into HeLa, CHO-K1, and L cells. J Virol **84:**8422-8432.
15. **Peters D, Mueller G.** 1963. The Fine Structure of the DNA-Containing Core of Vaccinia Virus. Virology **21:**267-269.
16. **Condit RC, Moussatche N, Traktman P.** 2006. In a nutshell: structure and assembly of the vaccinia virion. Adv Virus Res **66:**31-124.
17. **Moussatche N, Condit RC.** 2015. Fine structure of the vaccinia virion determined by controlled degradation and immunolocalization. Virology **475:**204-218.

18. **Chung CS, Chen CH, Ho MY, Huang CY, Liao CL, Chang W.** 2006. Vaccinia virus proteome: identification of proteins in vaccinia virus intracellular mature virion particles. J Virol **80:**2127-2140.
19. **Yoder JD, Chen TS, Gagnier CR, Vemulapalli S, Maier CS, Hruby DE.** 2006. Pox proteomics: mass spectrometry analysis and identification of Vaccinia virion proteins. Virol J **3:**10.
20. **Resch W, Hixson KK, Moore RJ, Lipton MS, Moss B.** 2007. Protein composition of the vaccinia virus mature virion. Virology **358:**233-247.
21. **Baroudy BM, Venkatesan S, Moss B.** 1982. Incompletely base-paired flip-flop terminal loops link the two DNA strands of the vaccinia virus genome into one uninterrupted polynucleotide chain. Cell **28:**315-324.
22. **Wittek R, Moss B.** 1980. Tandem repeats within the inverted terminal repetition of vaccinia virus DNA. Cell **21:**277-284.
23. **Wittek R, Cooper JA, Barbosa E, Moss B.** 1980. Expression of the vaccinia virus genome: analysis and mapping of mRNAs encoded within the inverted terminal repetition. Cell **21:**487-493.
24. **Lefkowitz EJ, Wang C, Upton C.** 2006. Poxviruses: past, present and future. Virus Res **117:**105-118.
25. **Goebel SJ, Johnson GP, Perkus ME, Davis SW, Winslow JP, Paoletti E.** 1990. The complete DNA sequence of vaccinia virus. Virology **179:**247-266, 517-263.
26. **Cameron C, Hota-Mitchell S, Chen L, Barrett J, Cao JX, Macaulay C, Willer D, Evans D, McFadden G.** 1999. The complete DNA sequence of myxoma virus. Virology **264:**298-318.
27. **Upton C, Slack S, Hunter AL, Ehlers A, Roper RL.** 2003. Poxvirus orthologous clusters: toward defining the minimum essential poxvirus genome. J Virol **77:**7590-7600.
28. **Gubser C, Hue S, Kellam P, Smith GL.** 2004. Poxvirus genomes: a phylogenetic analysis. J Gen Virol **85:**105-117.
29. **Moss B.** 2013. Poxviridae, p 2 volumes (xx, 2456, I-2482 pages). *In* Fields BN, Knipe DM, Howley PM (ed), Fields virology, 6th ed. Wolters Kluwer Health/Lippincott Williams & Wilkins, Philadelphia.
30. **Moss B.** 2012. Poxvirus cell entry: how many proteins does it take? Viruses **4:**688-707.
31. **Carter GC, Law M, Hollinshead M, Smith GL.** 2005. Entry of the vaccinia virus intracellular mature virion and its interactions with glycosaminoglycans. J Gen Virol **86:**1279-1290.
32. **Townsley AC, Weisberg AS, Wagenaar TR, Moss B.** 2006. Vaccinia virus entry into cells via a low-pH-dependent endosomal pathway. J Virol **80:**8899-8908.
33. **Vanderplasschen A, Hollinshead M, Smith GL.** 1998. Intracellular and extracellular vaccinia virions enter cells by different mechanisms. J Gen Virol **79 (Pt 4):**877-887.
34. **Lin CL, Chung CS, Heine HG, Chang W.** 2000. Vaccinia virus envelope H3L protein binds to cell surface heparan sulfate and is important for intracellular

mature virion morphogenesis and virus infection in vitro and in vivo. J Virol **74:**3353-3365.

35. **Hsiao JC, Chung CS, Chang W.** 1999. Vaccinia virus envelope D8L protein binds to cell surface chondroitin sulfate and mediates the adsorption of intracellular mature virions to cells. J Virol **73:**8750-8761.

36. **Chung CS, Hsiao JC, Chang YS, Chang W.** 1998. A27L protein mediates vaccinia virus interaction with cell surface heparan sulfate. J Virol **72:**1577-1585.

37. **Chiu WL, Lin CL, Yang MH, Tzou DL, Chang W.** 2007. Vaccinia virus 4c (A26L) protein on intracellular mature virus binds to the extracellular cellular matrix laminin. J Virol **81:**2149-2157.

38. **Mercer J, Helenius A.** 2008. Vaccinia virus uses macropinocytosis and apoptotic mimicry to enter host cells. Science **320:**531-535.

39. **Huang CY, Lu TY, Bair CH, Chang YS, Jwo JK, Chang W.** 2008. A novel cellular protein, VPEF, facilitates vaccinia virus penetration into HeLa cells through fluid phase endocytosis. J Virol **82:**7988-7999.

40. **Roberts KL, Breiman A, Carter GC, Ewles HA, Hollinshead M, Law M, Smith GL.** 2009. Acidic residues in the membrane-proximal stalk region of vaccinia virus protein B5 are required for glycosaminoglycan-mediated disruption of the extracellular enveloped virus outer membrane. J Gen Virol **90:**1582-1591.

41. **Law M, Carter GC, Roberts KL, Hollinshead M, Smith GL.** 2006. Ligand-induced and nonfusogenic dissolution of a viral membrane. Proc Natl Acad Sci U S A **103:**5989-5994.

42. **Villa NY, Bartee E, Mohamed MR, Rahman MM, Barrett JW, McFadden G.** 2010. Myxoma and vaccinia viruses exploit different mechanisms to enter and infect human cancer cells. Virology **401:**266-279.

43. **Roberts KL, Smith GL.** 2008. Vaccinia virus morphogenesis and dissemination. Trends Microbiol **16:**472-479.

44. **Moss B, Ahn BY, Amegadzie B, Gershon PD, Keck JG.** 1991. Cytoplasmic transcription system encoded by vaccinia virus. J Biol Chem **266:**1355-1358.

45. **Pennington TH.** 1974. Vaccinia virus polypeptide synthesis: sequential appearance and stability of pre- and post-replicative polypeptides. J Gen Virol **25:**433-444.

46. **Yang Z, Reynolds SE, Martens CA, Bruno DP, Porcella SF, Moss B.** 2011. Expression profiling of the intermediate and late stages of poxvirus replication. J Virol **85:**9899-9908.

47. **Carter GC, Rodger G, Murphy BJ, Law M, Krauss O, Hollinshead M, Smith GL.** 2003. Vaccinia virus cores are transported on microtubules. J Gen Virol **84:**2443-2458.

48. **Katsafanas GC, Moss B.** 2007. Colocalization of transcription and translation within cytoplasmic poxvirus factories coordinates viral expression and subjugates host functions. Cell Host Microbe **2:**221-228.

49. **Golini F, Kates JR.** 1985. A soluble transcription system derived from purified vaccinia virions. J Virol **53:**205-213.

50. **Rohrmann G, Moss B.** 1985. Transcription of vaccinia virus early genes by a template-dependent soluble extract of purified virions. J Virol **56:**349-355.
51. **Baldick CJ, Jr., Moss B.** 1993. Characterization and temporal regulation of mRNAs encoded by vaccinia virus intermediate-stage genes. J Virol **67:**3515-3527.
52. **Slabaugh M, Roseman N, Davis R, Mathews C.** 1988. Vaccinia virus-encoded ribonucleotide reductase: sequence conservation of the gene for the small subunit and its amplification in hydroxyurea-resistant mutants. J Virol **62:**519-527.
53. **Weir JP, Moss B.** 1983. Nucleotide sequence of the vaccinia virus thymidine kinase gene and the nature of spontaneous frameshift mutations. J Virol **46:**530-537.
54. **Bray G, Brent TP.** 1972. Deoxyribonucleoside 5'-triphosphate pool fluctuations during the mammalian cell cycle. Biochim Biophys Acta **269:**184-191.
55. **De Silva FS, Lewis W, Berglund P, Koonin EV, Moss B.** 2007. Poxvirus DNA primase. Proc Natl Acad Sci U S A **104:**18724-18729.
56. **Kerr SM, Smith GL.** 1989. Vaccinia virus encodes a polypeptide with DNA ligase activity. Nucleic Acids Res **17:**9039-9050.
57. **Moyer RW, Graves RL.** 1981. The mechanism of cytoplasmic orthopoxvirus DNA replication. Cell **27:**391-401.
58. **Moss B.** 2013. Poxvirus DNA replication. Cold Spring Harb Perspect Biol **5**.
59. **Merchlinsky M, Moss B.** 1989. Resolution of vaccinia virus DNA concatemer junctions requires late-gene expression. J Virol **63:**1595-1603.
60. **Garcia AD, Moss B.** 2001. Repression of vaccinia virus Holliday junction resolvase inhibits processing of viral DNA into unit-length genomes. J Virol **75:**6460-6471.
61. **Garcia AD, Aravind L, Koonin EV, Moss B.** 2000. Bacterial-type DNA holliday junction resolvases in eukaryotic viruses. Proc Natl Acad Sci U S A **97:**8926-8931.
62. **Joklik WK, Becker Y.** 1964. The Replication and Coating of Vaccinia DNA. J Mol Biol **10:**452-474.
63. **Duteyrat JL, Gelfi J, Bertagnoli S.** 2006. Ultrastructural study of myxoma virus morphogenesis. Arch Virol **151:**2161-2180.
64. **Morgan C, Wyckoff RW.** 1950. The electron microscopy of fowl pox virus within the chorioallantoic membrane. J Immunol **65:**285-295.
65. **Gaylord WH, Jr., Melnick JL.** 1953. Intracellular forms of pox viruses as shown by the electron microscope (Vaccinia, Ectromelia, Molluscum Contagiosum). J Exp Med **98:**157-172.
66. **Morgan C, Ellison SA, Rose HM, Moore DH.** 1954. Structure and development of viruses observed in the electron microscope. II. Vaccinia and fowl pox viruses. J Exp Med **100:**301-310.
67. **Chlanda P, Carbajal MA, Cyrklaff M, Griffiths G, Krijnse-Locker J.** 2009. Membrane rupture generates single open membrane sheets during vaccinia virus assembly. Cell Host Microbe **6:**81-90.

68.   **Heuser J.** 2005. Deep-etch EM reveals that the early poxvirus envelope is a single membrane bilayer stabilized by a geodetic "honeycomb" surface coat. J Cell Biol **169:**269-283.
69.   **Szajner P, Weisberg AS, Lebowitz J, Heuser J, Moss B.** 2005. External scaffold of spherical immature poxvirus particles is made of protein trimers, forming a honeycomb lattice. J Cell Biol **170:**971-981.
70.   **Moss B.** 2015. Poxvirus membrane biogenesis. Virology doi:10.1016/j.virol.2015.02.003.
71.   **Bisht H, Weisberg AS, Szajner P, Moss B.** 2009. Assembly and disassembly of the capsid-like external scaffold of immature virions during vaccinia virus morphogenesis. J Virol **83:**9140-9150.
72.   **Moss B, Rosenblum EN.** 1973. Letter: Protein cleavage and poxvirus morphogenesis: tryptic peptide analysis of core precursors accumulated by blocking assembly with rifampicin. J Mol Biol **81:**267-269.
73.   **Tooze J, Hollinshead M, Reis B, Radsak K, Kern H.** 1993. Progeny vaccinia and human cytomegalovirus particles utilize early endosomal cisternae for their envelopes. Eur J Cell Biol **60:**163-178.
74.   **Hiller G, Weber K.** 1985. Golgi-derived membranes that contain an acylated viral polypeptide are used for vaccinia virus envelopment. J Virol **55:**651-659.
75.   **Schmelz M, Sodeik B, Ericsson M, Wolffe EJ, Shida H, Hiller G, Griffiths G.** 1994. Assembly of vaccinia virus: the second wrapping cisterna is derived from the trans Golgi network. J Virol **68:**130-147.
76.   **Sanderson CM, Hollinshead M, Smith GL.** 2000. The vaccinia virus A27L protein is needed for the microtubule-dependent transport of intracellular mature virus particles. J Gen Virol **81:**47-58.
77.   **Ward BM.** 2005. Visualization and characterization of the intracellular movement of vaccinia virus intracellular mature virions. J Virol **79:**4755-4763.
78.   **Arakawa Y, Cordeiro JV, Way M.** 2007. F11L-mediated inhibition of RhoA-mDia signaling stimulates microtubule dynamics during vaccinia virus infection. Cell Host Microbe **1:**213-226.
79.   **Arakawa Y, Cordeiro JV, Schleich S, Newsome TP, Way M.** 2007. The release of vaccinia virus from infected cells requires RhoA-mDia modulation of cortical actin. Cell Host Microbe **1:**227-240.
80.   **Irwin CR, Evans DH.** 2012. Modulation of the myxoma virus plaque phenotype by vaccinia virus protein F11. J Virol **86:**7167-7179.
81.   **Boulanger D, Smith T, Skinner MA.** 2000. Morphogenesis and release of fowlpox virus. J Gen Virol **81:**675-687.
82.   **Meiser A, Sancho C, Krijnse Locker J.** 2003. Plasma membrane budding as an alternative release mechanism of the extracellular enveloped form of vaccinia virus from HeLa cells. J Virol **77:**9931-9942.
83.   **Garcia-Arriaza J, Esteban M.** 2014. Enhancing poxvirus vectors vaccine immunogenicity. Hum Vaccin Immunother **10:**2235-2244.
84.   **Moss B.** 2013. Reflections on the early development of poxvirus vectors. Vaccine **31:**4220-4222.

85. **Moroziewicz D, Kaufman HL.** 2005. Gene therapy with poxvirus vectors. Curr Opin Mol Ther **7:**317-325.
86. **Panicali D, Paoletti E.** 1982. Construction of poxviruses as cloning vectors: insertion of the thymidine kinase gene from herpes simplex virus into the DNA of infectious vaccinia virus. Proc Natl Acad Sci U S A **79:**4927-4931.
87. **Mackett M, Smith GL, Moss B.** 1982. Vaccinia virus: a selectable eukaryotic cloning and expression vector. Proc Natl Acad Sci U S A **79:**7415-7419.
88. **Mackett M, Smith GL, Moss B.** 1984. General method for production and selection of infectious vaccinia virus recombinants expressing foreign genes. J Virol **49:**857-864.
89. **Legrand FA, Verardi PH, Jones LA, Chan KS, Peng Y, Yilma TD.** 2004. Induction of potent humoral and cell-mediated immune responses by attenuated vaccinia virus vectors with deleted serpin genes. J Virol **78:**2770-2779.
90. **Wright PF, Mestecky J, McElrath MJ, Keefer MC, Gorse GJ, Goepfert PA, Moldoveanu Z, Schwartz D, Spearman PW, El Habib R, Spring MD, Zhu Y, Smith C, Flores J, Weinhold KJ, National Institutes of A, Infectious Diseases AVEG.** 2004. Comparison of systemic and mucosal delivery of 2 canarypox virus vaccines expressing either HIV-1 genes or the gene for rabies virus G protein. J Infect Dis **189:**1221-1231.
91. **Mwau M, Cebere I, Sutton J, Chikoti P, Winstone N, Wee EG, Beattie T, Chen YH, Dorrell L, McShane H, Schmidt C, Brooks M, Patel S, Roberts J, Conlon C, Rowland-Jones SL, Bwayo JJ, McMichael AJ, Hanke T.** 2004. A human immunodeficiency virus 1 (HIV-1) clade A vaccine in clinical trials: stimulation of HIV-specific T-cell responses by DNA and recombinant modified vaccinia virus Ankara (MVA) vaccines in humans. J Gen Virol **85:**911-919.
92. **Hanke T, Goonetilleke N, McMichael AJ, Dorrell L.** 2007. Clinical experience with plasmid DNA- and modified vaccinia virus Ankara-vectored human immunodeficiency virus type 1 clade A vaccine focusing on T-cell induction. J Gen Virol **88:**1-12.
93. **Cebere I, Dorrell L, McShane H, Simmons A, McCormack S, Schmidt C, Smith C, Brooks M, Roberts JE, Darwin SC, Fast PE, Conlon C, Rowland-Jones S, McMichael AJ, Hanke T.** 2006. Phase I clinical trial safety of DNA- and modified virus Ankara-vectored human immunodeficiency virus type 1 (HIV-1) vaccines administered alone and in a prime-boost regime to healthy HIV-1-uninfected volunteers. Vaccine **24:**417-425.
94. **Kreijtz JH, Goeijenbier M, Moesker FM, van den Dries L, Goeijenbier S, De Gruyter HL, Lehmann MH, Mutsert G, van de Vijver DA, Volz A, Fouchier RA, van Gorp EC, Rimmelzwaan GF, Sutter G, Osterhaus AD.** 2014. Safety and immunogenicity of a modified-vaccinia-virus-Ankara-based influenza A H5N1 vaccine: a randomised, double-blind phase 1/2a clinical trial. Lancet Infect Dis **14:**1196-1207.
95. **Hui EP, Taylor GS, Jia H, Ma BB, Chan SL, Ho R, Wong WL, Wilson S, Johnson BF, Edwards C, Stocken DD, Rickinson AB, Steven NM, Chan AT.** 2013. Phase I trial of recombinant modified vaccinia ankara encoding

Epstein-Barr viral tumor antigens in nasopharyngeal carcinoma patients. Cancer Res **73:**1676-1688.

96. **Gulley J, Chen AP, Dahut W, Arlen PM, Bastian A, Steinberg SM, Tsang K, Panicali D, Poole D, Schlom J, Michael Hamilton J.** 2002. Phase I study of a vaccine using recombinant vaccinia virus expressing PSA (rV-PSA) in patients with metastatic androgen-independent prostate cancer. Prostate **53:**109-117.

97. **Taylor GS, Jia H, Harrington K, Lee LW, Turner J, Ladell K, Price DA, Tanday M, Matthews J, Roberts C, Edwards C, McGuigan L, Hartley A, Wilson S, Hui EP, Chan AT, Rickinson AB, Steven NM.** 2014. A recombinant modified vaccinia ankara vaccine encoding Epstein-Barr Virus (EBV) target antigens: a phase I trial in UK patients with EBV-positive cancer. Clin Cancer Res **20:**5009-5022.

98. **Siegel R, DeSantis C, Virgo K, Stein K, Mariotto A, Smith T, Cooper D, Gansler T, Lerro C, Fedewa S, Lin C, Leach C, Cannady RS, Cho H, Scoppa S, Hachey M, Kirch R, Jemal A, Ward E.** 2012. Cancer treatment and survivorship statistics, 2012. CA Cancer J Clin **62:**220-241.

99. **Chiocca EA.** 2002. Oncolytic viruses. Nat Rev Cancer **2:**938-950.

100. **Garber K.** 2006. China approves world's first oncolytic virus therapy for cancer treatment. J Natl Cancer Inst **98:**298-300.

101. **Lun X, Yang W, Alain T, Shi ZQ, Muzik H, Barrett JW, McFadden G, Bell J, Hamilton MG, Senger DL, Forsyth PA.** 2005. Myxoma virus is a novel oncolytic virus with significant antitumor activity against experimental human gliomas. Cancer Res **65:**9982-9990.

102. **Lun XQ, Jang JH, Tang N, Deng H, Head R, Bell JC, Stojdl DF, Nutt CL, Senger DL, Forsyth PA, McCart JA.** 2009. Efficacy of systemically administered oncolytic vaccinia virotherapy for malignant gliomas is enhanced by combination therapy with rapamycin or cyclophosphamide. Clin Cancer Res **15:**2777-2788.

103. **Yu YA, Galanis C, Woo Y, Chen N, Zhang Q, Fong Y, Szalay AA.** 2009. Regression of human pancreatic tumor xenografts in mice after a single systemic injection of recombinant vaccinia virus GLV-1h68. Mol Cancer Ther **8:**141-151.

104. **Woo Y, Kelly KJ, Stanford MM, Galanis C, Chun YS, Fong Y, McFadden G.** 2008. Myxoma virus is oncolytic for human pancreatic adenocarcinoma cells. Ann Surg Oncol **15:**2329-2335.

105. **Zhang Q, Yu YA, Wang E, Chen N, Danner RL, Munson PJ, Marincola FM, Szalay AA.** 2007. Eradication of solid human breast tumors in nude mice with an intravenously injected light-emitting oncolytic vaccinia virus. Cancer Res **67:**10038-10046.

106. **Gentschev I, Stritzker J, Hofmann E, Weibel S, Yu YA, Chen N, Zhang Q, Bullerdiek J, Nolte I, Szalay AA.** 2009. Use of an oncolytic vaccinia virus for the treatment of canine breast cancer in nude mice: preclinical development of a therapeutic agent. Cancer Gene Ther **16:**320-328.

107. **Kirn DH, Thorne SH.** 2009. Targeted and armed oncolytic poxviruses: a novel multi-mechanistic therapeutic class for cancer. Nat Rev Cancer **9:**64-71.
108. **Rahman MM, Madlambayan GJ, Cogle CR, McFadden G.** 2010. Oncolytic viral purging of leukemic hematopoietic stem and progenitor cells with Myxoma virus. Cytokine Growth Factor Rev **21:**169-175.
109. **Gammon DB, Gowrishankar B, Duraffour S, Andrei G, Upton C, Evans DH.** 2010. Vaccinia virus-encoded ribonucleotide reductase subunits are differentially required for replication and pathogenesis. PLoS Pathog **6:**e1000984.
110. **McCart JA, Ward JM, Lee J, Hu Y, Alexander HR, Libutti SK, Moss B, Bartlett DL.** 2001. Systemic cancer therapy with a tumor-selective vaccinia virus mutant lacking thymidine kinase and vaccinia growth factor genes. Cancer Res **61:**8751-8757.
111. **Kim JH, Oh JY, Park BH, Lee DE, Kim JS, Park HE, Roh MS, Je JE, Yoon JH, Thorne SH, Kirn D, Hwang TH.** 2006. Systemic armed oncolytic and immunologic therapy for cancer with JX-594, a targeted poxvirus expressing GM-CSF. Mol Ther **14:**361-370.
112. **Park BH, Hwang T, Liu TC, Sze DY, Kim JS, Kwon HC, Oh SY, Han SY, Yoon JH, Hong SH, Moon A, Speth K, Park C, Ahn YJ, Daneshmand M, Rhee BG, Pinedo HM, Bell JC, Kirn DH.** 2008. Use of a targeted oncolytic poxvirus, JX-594, in patients with refractory primary or metastatic liver cancer: a phase I trial. Lancet Oncol **9:**533-542.
113. **Heo J, Reid T, Ruo L, Breitbach CJ, Rose S, Bloomston M, Cho M, Lim HY, Chung HC, Kim CW, Burke J, Lencioni R, Hickman T, Moon A, Lee YS, Kim MK, Daneshmand M, Dubois K, Longpre L, Ngo M, Rooney C, Bell JC, Rhee BG, Patt R, Hwang TH, Kirn DH.** 2013. Randomized dose-finding clinical trial of oncolytic immunotherapeutic vaccinia JX-594 in liver cancer. Nat Med **19:**329-336.
114. **Hwang TH, Moon A, Burke J, Ribas A, Stephenson J, Breitbach CJ, Daneshmand M, De Silva N, Parato K, Diallo JS, Lee YS, Liu TC, Bell JC, Kirn DH.** 2011. A mechanistic proof-of-concept clinical trial with JX-594, a targeted multi-mechanistic oncolytic poxvirus, in patients with metastatic melanoma. Mol Ther **19:**1913-1922.
115. **Fenner F.** 1959. Myxomatosis. Br Med Bull **15:**240-245.
116. **Kerr PJ.** 2012. Myxomatosis in Australia and Europe: a model for emerging infectious diseases. Antiviral Res **93:**387-415.
117. **Fenner F.** 2000. Adventures with poxviruses of vertebrates. FEMS Microbiol Rev **24:**123-133.
118. **Lun X, Alain T, Zemp FJ, Zhou H, Rahman MM, Hamilton MG, McFadden G, Bell J, Senger DL, Forsyth PA.** 2010. Myxoma virus virotherapy for glioma in immunocompetent animal models: optimizing administration routes and synergy with rapamycin. Cancer Res **70:**598-608.
119. **Wang G, Barrett JW, Stanford M, Werden SJ, Johnston JB, Gao X, Sun M, Cheng JQ, McFadden G.** 2006. Infection of human cancer cells with myxoma

virus requires Akt activation via interaction with a viral ankyrin-repeat host range factor. Proc Natl Acad Sci U S A **103:**4640-4645.

120. **Wang F, Ma Y, Barrett JW, Gao X, Loh J, Barton E, Virgin HW, McFadden G.** 2004. Disruption of Erk-dependent type I interferon induction breaks the myxoma virus species barrier. Nat Immunol **5:**1266-1274.

121. **Stojdl DF, Lichty B, Knowles S, Marius R, Atkins H, Sonenberg N, Bell JC.** 2000. Exploiting tumor-specific defects in the interferon pathway with a previously unknown oncolytic virus. Nat Med **6:**821-825.

122. **Irwin CR, Favis NA, Agopsowicz KC, Hitt MM, Evans DH.** 2013. Myxoma virus oncolytic efficiency can be enhanced through chemical or genetic disruption of the actin cytoskeleton. PLoS One **8:**e84134.

123. **Handa Y, Durkin CH, Dodding MP, Way M.** 2013. Vaccinia virus F11 promotes viral spread by acting as a PDZ-containing scaffolding protein to bind myosin-9A and inhibit RhoA signaling. Cell Host Microbe **14:**51-62.

124. **Irwin CR, Farmer A, Willer DO, Evans DH.** 2012. In-fusion(R) cloning with vaccinia virus DNA polymerase. Methods Mol Biol **890:**23-35.

125. **Geng L, Xin W, Huang DW, Feng G.** 2006. A universal cloning vector using vaccinia topoisomerase I. Mol Biotechnol **33:**23-28.

126. **Damon I.** 2013. Poxviruses, p 2 volumes (xx, 2456, I-2482 pages). *In* Fields BN, Knipe DM, Howley PM (ed), Fields virology, 6th ed, vol 2. Wolters Kluwer Health/Lippincott Williams & Wilkins, Philadelphia.

127. **Shchelkunov SN.** 2012. Orthopoxvirus genes that mediate disease virulence and host tropism. Adv Virol **2012:**524743.

128. **Goldstein JA, Neff JM, Lane JM, Koplan JP.** 1975. Smallpox vaccination reactions, prophylaxis, and therapy of complications. Pediatrics **55:**342-347.

129. **Henderson DA.** 1999. Smallpox: clinical and epidemiologic features. Emerg Infect Dis **5:**537-539.

130. **Breman JG, Henderson DA.** 2002. Diagnosis and management of smallpox. N Engl J Med **346:**1300-1308.

131. **Baxby D.** 1977. The origins of vaccinia virus. J Infect Dis **136:**453-455.

132. **Breman JG.** 2000. Monkeypox: an Emerging Infection for Humans, p xv, 218 p. *In* Scheld WM, Armstrong D, Hughes JM, American Society for Microbiology. (ed), Emerging infections 4. American Society for Microbiology, Washington, D.C.

133. **Vorou RM, Papavassiliou VG, Pierroutsakos IN.** 2008. Cowpox virus infection: an emerging health threat. Curr Opin Infect Dis **21:**153-156.

134. **Blackford S, Roberts DL, Thomas PD.** 1993. Cowpox infection causing a generalized eruption in a patient with atopic dermatitis. Br J Dermatol **129:**628-629.

135. **Pelkonen PM, Tarvainen K, Hynninen A, Kallio ER, Henttonen K, Palva A, Vaheri A, Vapalahti O.** 2003. Cowpox with severe generalized eruption, Finland. Emerg Infect Dis **9:**1458-1461.

136. **Abrahao JS, Campos RK, Trindade Gde S, Guimaraes da Fonseca F, Ferreira PC, Kroon EG.** 2015. Outbreak of severe zoonotic vaccinia virus infection, southeastern Brazil. Emerg Infect Dis **21:**695-698.

137. **Leung AK.** 2015. The natural history of molluscum contagiosum in children. Lancet Infect Dis **15:**136-137.
138. **Enserink M.** 2003. Infectious diseases. U.S. monkeypox outbreak traced to Wisconsin pet dealer. Science **300:**1639.
139. **Arita I.** 2014. Discovery of forgotten variola specimens at the National Institutes of Health in the USA. Expert Rev Anti Infect Ther **12:**1419-1421.
140. **Meltzer MI, Damon I, LeDuc JW, Millar JD.** 2001. Modeling potential responses to smallpox as a bioterrorist weapon. Emerg Infect Dis **7:**959-969.
141. **Magee WC, Hostetler KY, Evans DH.** 2005. Mechanism of inhibition of vaccinia virus DNA polymerase by cidofovir diphosphate. Antimicrob Agents Chemother **49:**3153-3162.
142. **Yang G, Pevear DC, Davies MH, Collett MS, Bailey T, Rippen S, Barone L, Burns C, Rhodes G, Tohan S, Huggins JW, Baker RO, Buller RL, Touchette E, Waller K, Schriewer J, Neyts J, DeClercq E, Jones K, Hruby D, Jordan R.** 2005. An orally bioavailable antipoxvirus compound (ST-246) inhibits extracellular virus formation and protects mice from lethal orthopoxvirus Challenge. J Virol **79:**13139-13149.
143. **Duraffour S, Lorenzo MM, Zoller G, Topalis D, Grosenbach D, Hruby DE, Andrei G, Blasco R, Meyer H, Snoeck R.** 2015. ST-246 is a key antiviral to inhibit the viral F13L phospholipase, one of the essential proteins for orthopoxvirus wrapping. J Antimicrob Chemother doi:10.1093/jac/dku545.
144. **Fire A, Xu S, Montgomery MK, Kostas SA, Driver SE, Mello CC.** 1998. Potent and specific genetic interference by double-stranded RNA in Caenorhabditis elegans. Nature **391:**806-811.
145. **Izant JG, Weintraub H.** 1984. Inhibition of thymidine kinase gene expression by anti-sense RNA: a molecular approach to genetic analysis. Cell **36:**1007-1015.
146. **Fire A, Albertson D, Harrison SW, Moerman DG.** 1991. Production of antisense RNA leads to effective and specific inhibition of gene expression in C. elegans muscle. Development **113:**503-514.
147. **Nellen W, Lichtenstein C.** 1993. What makes an mRNA anti-sense-itive? Trends Biochem Sci **18:**419-423.
148. **Holoch D, Moazed D.** 2015. RNA-mediated epigenetic regulation of gene expression. Nat Rev Genet **16:**71-84.
149. **Szweykowska-Kulinska Z, Jarmolowski A, Figlerowicz M.** 2003. RNA interference and its role in the regulation of eucaryotic gene expression. Acta Biochim Pol **50:**217-229.
150. **Volpe TA, Kidner C, Hall IM, Teng G, Grewal SI, Martienssen RA.** 2002. Regulation of heterochromatic silencing and histone H3 lysine-9 methylation by RNAi. Science **297:**1833-1837.
151. **Moazed D.** 2009. Small RNAs in transcriptional gene silencing and genome defence. Nature **457:**413-420.
152. **Malone CD, Hannon GJ.** 2009. Small RNAs as guardians of the genome. Cell **136:**656-668.
153. **Buhler M, Moazed D.** 2007. Transcription and RNAi in heterochromatic gene silencing. Nat Struct Mol Biol **14:**1041-1048.

154. **Lecellier CH, Dunoyer P, Arar K, Lehmann-Che J, Eyquem S, Himber C, Saib A, Voinnet O.** 2005. A cellular microRNA mediates antiviral defense in human cells. Science **308:**557-560.
155. **Umbach JL, Cullen BR.** 2009. The role of RNAi and microRNAs in animal virus replication and antiviral immunity. Genes Dev **23:**1151-1164.
156. **Ipsaro JJ, Joshua-Tor L.** 2015. From guide to target: molecular insights into eukaryotic RNA-interference machinery. Nat Struct Mol Biol **22:**20-28.
157. **Meister G.** 2013. Argonaute proteins: functional insights and emerging roles. Nat Rev Genet **14:**447-459.
158. **Jinek M, Doudna JA.** 2009. A three-dimensional view of the molecular machinery of RNA interference. Nature **457:**405-412.
159. **Simon B, Kirkpatrick JP, Eckhardt S, Reuter M, Rocha EA, Andrade-Navarro MA, Sehr P, Pillai RS, Carlomagno T.** 2011. Recognition of 2'-O-methylated 3'-end of piRNA by the PAZ domain of a Piwi protein. Structure **19:**172-180.
160. **Cai X, Hagedorn CH, Cullen BR.** 2004. Human microRNAs are processed from capped, polyadenylated transcripts that can also function as mRNAs. RNA **10:**1957-1966.
161. **Graves P, Zeng Y.** 2012. Biogenesis of mammalian microRNAs: a global view. Genomics Proteomics Bioinformatics **10:**239-245.
162. **Lee Y, Ahn C, Han J, Choi H, Kim J, Yim J, Lee J, Provost P, Radmark O, Kim S, Kim VN.** 2003. The nuclear RNase III Drosha initiates microRNA processing. Nature **425:**415-419.
163. **Gregory RI, Yan KP, Amuthan G, Chendrimada T, Doratotaj B, Cooch N, Shiekhattar R.** 2004. The Microprocessor complex mediates the genesis of microRNAs. Nature **432:**235-240.
164. **Denli AM, Tops BB, Plasterk RH, Ketting RF, Hannon GJ.** 2004. Processing of primary microRNAs by the Microprocessor complex. Nature **432:**231-235.
165. **Zhang H, Kolb FA, Brondani V, Billy E, Filipowicz W.** 2002. Human Dicer preferentially cleaves dsRNAs at their termini without a requirement for ATP. EMBO J **21:**5875-5885.
166. **Hutvagner G, McLachlan J, Pasquinelli AE, Balint E, Tuschl T, Zamore PD.** 2001. A cellular function for the RNA-interference enzyme Dicer in the maturation of the let-7 small temporal RNA. Science **293:**834-838.
167. **Bohnsack MT, Czaplinski K, Gorlich D.** 2004. Exportin 5 is a RanGTP-dependent dsRNA-binding protein that mediates nuclear export of pre-miRNAs. RNA **10:**185-191.
168. **Maniataki E, Mourelatos Z.** 2005. A human, ATP-independent, RISC assembly machine fueled by pre-miRNA. Genes Dev **19:**2979-2990.
169. **Meister G, Landthaler M, Patkaniowska A, Dorsett Y, Teng G, Tuschl T.** 2004. Human Argonaute2 mediates RNA cleavage targeted by miRNAs and siRNAs. Mol Cell **15:**185-197.
170. **Liu J, Carmell MA, Rivas FV, Marsden CG, Thomson JM, Song JJ, Hammond SM, Joshua-Tor L, Hannon GJ.** 2004. Argonaute2 is the catalytic engine of mammalian RNAi. Science **305:**1437-1441.

171. **Rehwinkel J, Behm-Ansmant I, Gatfield D, Izaurralde E.** 2005. A crucial role for GW182 and the DCP1:DCP2 decapping complex in miRNA-mediated gene silencing. RNA **11:**1640-1647.
172. **Eulalio A, Huntzinger E, Izaurralde E.** 2008. GW182 interaction with Argonaute is essential for miRNA-mediated translational repression and mRNA decay. Nat Struct Mol Biol **15:**346-353.
173. **Ding XC, Grosshans H.** 2009. Repression of C. elegans microRNA targets at the initiation level of translation requires GW182 proteins. EMBO J **28:**213-222.
174. **Lewis BP, Burge CB, Bartel DP.** 2005. Conserved seed pairing, often flanked by adenosines, indicates that thousands of human genes are microRNA targets. Cell **120:**15-20.
175. **Lewis BP, Shih IH, Jones-Rhoades MW, Bartel DP, Burge CB.** 2003. Prediction of mammalian microRNA targets. Cell **115:**787-798.
176. **Ghildiyal M, Seitz H, Horwich MD, Li C, Du T, Lee S, Xu J, Kittler EL, Zapp ML, Weng Z, Zamore PD.** 2008. Endogenous siRNAs derived from transposons and mRNAs in Drosophila somatic cells. Science **320:**1077-1081.
177. **Okamura K, Balla S, Martin R, Liu N, Lai EC.** 2008. Two distinct mechanisms generate endogenous siRNAs from bidirectional transcription in Drosophila melanogaster. Nat Struct Mol Biol **15:**998.
178. **Watanabe T, Totoki Y, Toyoda A, Kaneda M, Kuramochi-Miyagawa S, Obata Y, Chiba H, Kohara Y, Kono T, Nakano T, Surani MA, Sakaki Y, Sasaki H.** 2008. Endogenous siRNAs from naturally formed dsRNAs regulate transcripts in mouse oocytes. Nature **453:**539-543.
179. **Tam OH, Aravin AA, Stein P, Girard A, Murchison EP, Cheloufi S, Hodges E, Anger M, Sachidanandam R, Schultz RM, Hannon GJ.** 2008. Pseudogene-derived small interfering RNAs regulate gene expression in mouse oocytes. Nature **453:**534-538.
180. **Babiarz JE, Ruby JG, Wang Y, Bartel DP, Blelloch R.** 2008. Mouse ES cells express endogenous shRNAs, siRNAs, and other Microprocessor-independent, Dicer-dependent small RNAs. Genes Dev **22:**2773-2785.
181. **Okamura K, Lai EC.** 2008. Endogenous small interfering RNAs in animals. Nat Rev Mol Cell Biol **9:**673-678.
182. **Zamore PD, Tuschl T, Sharp PA, Bartel DP.** 2000. RNAi: double-stranded RNA directs the ATP-dependent cleavage of mRNA at 21 to 23 nucleotide intervals. Cell **101:**25-33.
183. **Brennecke J, Aravin AA, Stark A, Dus M, Kellis M, Sachidanandam R, Hannon GJ.** 2007. Discrete small RNA-generating loci as master regulators of transposon activity in Drosophila. Cell **128:**1089-1103.
184. **Muerdter F, Olovnikov I, Molaro A, Rozhkov NV, Czech B, Gordon A, Hannon GJ, Aravin AA.** 2012. Production of artificial piRNAs in flies and mice. RNA **18:**42-52.
185. **Nishimasu H, Ishizu H, Saito K, Fukuhara S, Kamatani MK, Bonnefond L, Matsumoto N, Nishizawa T, Nakanaga K, Aoki J, Ishitani R, Siomi H,**

Siomi MC, Nureki O. 2012. Structure and function of Zucchini endoribonuclease in piRNA biogenesis. Nature **491:**284-287.

186. **Ipsaro JJ, Haase AD, Knott SR, Joshua-Tor L, Hannon GJ.** 2012. The structural biochemistry of Zucchini implicates it as a nuclease in piRNA biogenesis. Nature **491:**279-283.

187. **Kawaoka S, Izumi N, Katsuma S, Tomari Y.** 2011. 3' end formation of PIWI-interacting RNAs in vitro. Mol Cell **43:**1015-1022.

188. **Saito K, Sakaguchi Y, Suzuki T, Suzuki T, Siomi H, Siomi MC.** 2007. Pimet, the Drosophila homolog of HEN1, mediates 2'-O-methylation of Piwi-interacting RNAs at their 3' ends. Genes Dev **21:**1603-1608.

189. **Aravin AA, Sachidanandam R, Bourc'his D, Schaefer C, Pezic D, Toth KF, Bestor T, Hannon GJ.** 2008. A piRNA pathway primed by individual transposons is linked to de novo DNA methylation in mice. Mol Cell **31:**785-799.

190. **Aravin AA, Bourc'his D.** 2008. Small RNA guides for de novo DNA methylation in mammalian germ cells. Genes Dev **22:**970-975.

191. **Klenov MS, Lavrov SA, Stolyarenko AD, Ryazansky SS, Aravin AA, Tuschl T, Gvozdev VA.** 2007. Repeat-associated siRNAs cause chromatin silencing of retrotransposons in the Drosophila melanogaster germline. Nucleic Acids Res **35:**5430-5438.

192. **Wang SH, Elgin SC.** 2011. Drosophila Piwi functions downstream of piRNA production mediating a chromatin-based transposon silencing mechanism in female germ line. Proc Natl Acad Sci U S A **108:**21164-21169.

193. **Mohr SE, Smith JA, Shamu CE, Neumuller RA, Perrimon N.** 2014. RNAi screening comes of age: improved techniques and complementary approaches. Nat Rev Mol Cell Biol **15:**591-600.

194. **Pei Y, Tuschl T.** 2006. On the art of identifying effective and specific siRNAs. Nat Methods **3:**670-676.

195. **Elbashir SM, Harborth J, Lendeckel W, Yalcin A, Weber K, Tuschl T.** 2001. Duplexes of 21-nucleotide RNAs mediate RNA interference in cultured mammalian cells. Nature **411:**494-498.

196. **Kim DH, Behlke MA, Rose SD, Chang MS, Choi S, Rossi JJ.** 2005. Synthetic dsRNA Dicer substrates enhance RNAi potency and efficacy. Nat Biotechnol **23:**222-226.

197. **Amarzguioui M, Lundberg P, Cantin E, Hagstrom J, Behlke MA, Rossi JJ.** 2006. Rational design and in vitro and in vivo delivery of Dicer substrate siRNA. Nat Protoc **1:**508-517.

198. **Paddison PJ, Caudy AA, Bernstein E, Hannon GJ, Conklin DS.** 2002. Short hairpin RNAs (shRNAs) induce sequence-specific silencing in mammalian cells. Genes Dev **16:**948-958.

199. **Matsukura S, Jones PA, Takai D.** 2003. Establishment of conditional vectors for hairpin siRNA knockdowns. Nucleic Acids Res **31:**e77.

200. **An DS, Xie Y, Mao SH, Morizono K, Kung SK, Chen IS.** 2003. Efficient lentiviral vectors for short hairpin RNA delivery into human cells. Hum Gene Ther **14:**1207-1212.

201. **Kittler R, Putz G, Pelletier L, Poser I, Heninger AK, Drechsel D, Fischer S, Konstantinova I, Habermann B, Grabner H, Yaspo ML, Himmelbauer H, Korn B, Neugebauer K, Pisabarro MT, Buchholz F.** 2004. An endoribonuclease-prepared siRNA screen in human cells identifies genes essential for cell division. Nature **432:**1036-1040.

202. **Yang D, Buchholz F, Huang Z, Goga A, Chen CY, Brodsky FM, Bishop JM.** 2002. Short RNA duplexes produced by hydrolysis with Escherichia coli RNase III mediate effective RNA interference in mammalian cells. Proc Natl Acad Sci U S A **99:**9942-9947.

203. **Surendranath V, Theis M, Habermann BH, Buchholz F.** 2013. Designing efficient and specific endoribonuclease-prepared siRNAs. Methods Mol Biol **942:**193-204.

204. **Spagnou S, Miller AD, Keller M.** 2004. Lipidic carriers of siRNA: differences in the formulation, cellular uptake, and delivery with plasmid DNA. Biochemistry **43:**13348-13356.

205. **Brazas RM, Hagstrom JE.** 2005. Delivery of small interfering RNA to mammalian cells in culture by using cationic lipid/polymer-based transfection reagents. Methods Enzymol **392:**112-124.

206. **Timmons L, Fire A.** 1998. Specific interference by ingested dsRNA. Nature **395:**854.

207. **Parsons BD, Schindler A, Evans DH, Foley E.** 2009. A direct phenotypic comparison of siRNA pools and multiple individual duplexes in a functional assay. PLoS One **4:**e8471.

208. **Boutros M, Ahringer J.** 2008. The art and design of genetic screens: RNA interference. Nat Rev Genet **9:**554-566.

209. **Campeau E, Gobeil S.** 2011. RNA interference in mammals: behind the screen. Brief Funct Genomics **10:**215-226.

210. **Sigoillot FD, King RW.** 2011. Vigilance and validation: Keys to success in RNAi screening. ACS Chem Biol **6:**47-60.

211. **Jackson AL, Burchard J, Schelter J, Chau BN, Cleary M, Lim L, Linsley PS.** 2006. Widespread siRNA "off-target" transcript silencing mediated by seed region sequence complementarity. RNA **12:**1179-1187.

212. **Schmidt EE, Pelz O, Buhlmann S, Kerr G, Horn T, Boutros M.** 2013. GenomeRNAi: a database for cell-based and in vivo RNAi phenotypes, 2013 update. Nucleic Acids Res **41:**D1021-1026.

213. **Echeverri CJ, Beachy PA, Baum B, Boutros M, Buchholz F, Chanda SK, Downward J, Ellenberg J, Fraser AG, Hacohen N, Hahn WC, Jackson AL, Kiger A, Linsley PS, Lum L, Ma Y, Mathey-Prevot B, Root DE, Sabatini DM, Taipale J, Perrimon N, Bernards R.** 2006. Minimizing the risk of reporting false positives in large-scale RNAi screens. Nat Methods **3:**777-779.

214. **Kondo S, Booker M, Perrimon N.** 2009. Cross-species RNAi rescue platform in Drosophila melanogaster. Genetics **183:**1165-1173.

215. **Buehler E, Chen YC, Martin S.** 2012. C911: A bench-level control for sequence specific siRNA off-target effects. PLoS One **7:**e51942.

216. **Huang da W, Sherman BT, Lempicki RA.** 2009. Systematic and integrative analysis of large gene lists using DAVID bioinformatics resources. Nat Protoc **4:**44-57.

217. **Huang da W, Sherman BT, Lempicki RA.** 2009. Bioinformatics enrichment tools: paths toward the comprehensive functional analysis of large gene lists. Nucleic Acids Res **37:**1-13.

218. **Thomas PD, Campbell MJ, Kejariwal A, Mi H, Karlak B, Daverman R, Diemer K, Muruganujan A, Narechania A.** 2003. PANTHER: a library of protein families and subfamilies indexed by function. Genome Res **13:**2129-2141.

219. **Mi H, Lazareva-Ulitsky B, Loo R, Kejariwal A, Vandergriff J, Rabkin S, Guo N, Muruganujan A, Doremieux O, Campbell MJ, Kitano H, Thomas PD.** 2005. The PANTHER database of protein families, subfamilies, functions and pathways. Nucleic Acids Res **33:**D284-288.

220. **Vinayagam A, Hu Y, Kulkarni M, Roesel C, Sopko R, Mohr SE, Perrimon N.** 2013. Protein complex-based analysis framework for high-throughput data sets. Sci Signal **6:**rs5.

221. **Brass AL, Dykxhoorn DM, Benita Y, Yan N, Engelman A, Xavier RJ, Lieberman J, Elledge SJ.** 2008. Identification of host proteins required for HIV infection through a functional genomic screen. Science **319:**921-926.

222. **Konig R, Zhou Y, Elleder D, Diamond TL, Bonamy GM, Irelan JT, Chiang CY, Tu BP, De Jesus PD, Lilley CE, Seidel S, Opaluch AM, Caldwell JS, Weitzman MD, Kuhen KL, Bandyopadhyay S, Ideker T, Orth AP, Miraglia LJ, Bushman FD, Young JA, Chanda SK.** 2008. Global analysis of host-pathogen interactions that regulate early-stage HIV-1 replication. Cell **135:**49-60.

223. **Zhou H, Xu M, Huang Q, Gates AT, Zhang XD, Castle JC, Stec E, Ferrer M, Strulovici B, Hazuda DJ, Espeseth AS.** 2008. Genome-scale RNAi screen for host factors required for HIV replication. Cell Host Microbe **4:**495-504.

224. **Hao L, Sakurai A, Watanabe T, Sorensen E, Nidom CA, Newton MA, Ahlquist P, Kawaoka Y.** 2008. Drosophila RNAi screen identifies host genes important for influenza virus replication. Nature **454:**890-893.

225. **Konig R, Stertz S, Zhou Y, Inoue A, Hoffmann HH, Bhattacharyya S, Alamares JG, Tscherne DM, Ortigoza MB, Liang Y, Gao Q, Andrews SE, Bandyopadhyay S, De Jesus P, Tu BP, Pache L, Shih C, Orth A, Bonamy G, Miraglia L, Ideker T, Garcia-Sastre A, Young JA, Palese P, Shaw ML, Chanda SK.** 2010. Human host factors required for influenza virus replication. Nature **463:**813-817.

226. **Karlas A, Machuy N, Shin Y, Pleissner KP, Artarini A, Heuer D, Becker D, Khalil H, Ogilvie LA, Hess S, Maurer AP, Muller E, Wolff T, Rudel T, Meyer TF.** 2010. Genome-wide RNAi screen identifies human host factors crucial for influenza virus replication. Nature **463:**818-822.

227. **Su WC, Chen YC, Tseng CH, Hsu PW, Tung KF, Jeng KS, Lai MM.** 2013. Pooled RNAi screen identifies ubiquitin ligase Itch as crucial for influenza A virus release from the endosome during virus entry. Proc Natl Acad Sci U S A **110:**17516-17521.

228. **Tai AW, Benita Y, Peng LF, Kim SS, Sakamoto N, Xavier RJ, Chung RT.** 2009. A functional genomic screen identifies cellular cofactors of hepatitis C virus replication. Cell Host Microbe **5:**298-307.

229. **Li Q, Brass AL, Ng A, Hu Z, Xavier RJ, Liang TJ, Elledge SJ.** 2009. A genome-wide genetic screen for host factors required for hepatitis C virus propagation. Proc Natl Acad Sci U S A **106:**16410-16415.

230. **Lupberger J, Zeisel MB, Xiao F, Thumann C, Fofana I, Zona L, Davis C, Mee CJ, Turek M, Gorke S, Royer C, Fischer B, Zahid MN, Lavillette D, Fresquet J, Cosset FL, Rothenberg SM, Pietschmann T, Patel AH, Pessaux P, Doffoel M, Raffelsberger W, Poch O, McKeating JA, Brino L, Baumert TF.** 2011. EGFR and EphA2 are host factors for hepatitis C virus entry and possible targets for antiviral therapy. Nat Med **17:**589-595.

231. **Sivan G, Martin SE, Myers TG, Buehler E, Szymczyk KH, Ormanoglu P, Moss B.** 2013. Human genome-wide RNAi screen reveals a role for nuclear pore proteins in poxvirus morphogenesis. Proc Natl Acad Sci U S A **110:**3519-3524.

232. **Moser TS, Sabin LR, Cherry S.** 2010. RNAi screening for host factors involved in Vaccinia virus infection using Drosophila cells. J Vis Exp doi:10.3791/2137.

233. **Beard PM, Griffiths SJ, Gonzalez O, Haga IR, Pechenick Jowers T, Reynolds DK, Wildenhain J, Tekotte H, Auer M, Tyers M, Ghazal P, Zimmer R, Haas J.** 2014. A loss of function analysis of host factors influencing Vaccinia virus replication by RNA interference. PLoS One **9:**e98431.

234. **Mercer J, Snijder B, Sacher R, Burkard C, Bleck CK, Stahlberg H, Pelkmans L, Helenius A.** 2012. RNAi screening reveals proteasome- and Cullin3-dependent stages in vaccinia virus infection. Cell Rep **2:**1036-1047.

235. **Filone CM, Caballero IS, Dower K, Mendillo ML, Cowley GS, Santagata S, Rozelle DK, Yen J, Rubins KH, Hacohen N, Root DE, Hensley LE, Connor J.** 2014. The master regulator of the cellular stress response (HSF1) is critical for orthopoxvirus infection. PLoS Pathog **10:**e1003904.

236. **Moser TS, Jones RG, Thompson CB, Coyne CB, Cherry S.** 2010. A kinome RNAi screen identified AMPK as promoting poxvirus entry through the control of actin dynamics. PLoS Pathog **6:**e1000954.

237. **Bushman FD, Malani N, Fernandes J, D'Orso I, Cagney G, Diamond TL, Zhou H, Hazuda DJ, Espeseth AS, Konig R, Bandyopadhyay S, Ideker T, Goff SP, Krogan NJ, Frankel AD, Young JA, Chanda SK.** 2009. Host cell factors in HIV replication: meta-analysis of genome-wide studies. PLoS Pathog **5:**e1000437.

238. **Chou YC, Lai MM, Wu YC, Hsu NC, Jeng KS, Su WC.** 2015. Variations in genome-wide RNAi screens: lessons from influenza research. J Clin Bioinforma **5:**2.

239. **Hao L, He Q, Wang Z, Craven M, Newton MA, Ahlquist P.** 2013. Limited agreement of independent RNAi screens for virus-required host genes owes more to false-negative than false-positive factors. PLoS Comput Biol **9:**e1003235.

240. **Kilcher S, Schmidt FI, Schneider C, Kopf M, Helenius A, Mercer J.** 2014. siRNA screen of early poxvirus genes identifies the AAA+ ATPase D5 as the virus genome-uncoating factor. Cell Host Microbe **15:**103-112.

241. **Seet BT, Johnston JB, Brunetti CR, Barrett JW, Everett H, Cameron C, Sypula J, Nazarian SH, Lucas A, McFadden G.** 2003. Poxviruses and immune evasion. Annu Rev Immunol **21:**377-423.

242. **Taylor JM, Barry M.** 2006. Near death experiences: poxvirus regulation of apoptotic death. Virology **344:**139-150.

243. **Soares JA, Leite FG, Andrade LG, Torres AA, De Sousa LP, Barcelos LS, Teixeira MM, Ferreira PC, Kroon EG, Souto-Padron T, Bonjardim CA.** 2009. Activation of the PI3K/Akt pathway early during vaccinia and cowpox virus infections is required for both host survival and viral replication. J Virol **83:**6883-6899.

244. **Sabourdy F, Casteignau A, Gelfi J, Deceroi S, Delverdier M, Messud-Petit FL.** 2004. Tumorigenic poxviruses: growth factors in a viral context? J Gen Virol **85:**3597-3606.

245. **Menendez JA, Lupu R.** 2007. Fatty acid synthase and the lipogenic phenotype in cancer pathogenesis. Nat Rev Cancer **7:**763-777.

246. **Semenza GL.** 2008. Hypoxia-inducible factor 1 and cancer pathogenesis. IUBMB Life **60:**591-597.

247. **Nomura DK, Long JZ, Niessen S, Hoover HS, Ng SW, Cravatt BF.** 2010. Monoacylglycerol lipase regulates a fatty acid network that promotes cancer pathogenesis. Cell **140:**49-61.

248. **Locasale JW, Grassian AR, Melman T, Lyssiotis CA, Mattaini KR, Bass AJ, Heffron G, Metallo CM, Muranen T, Sharfi H, Sasaki AT, Anastasiou D, Mullarky E, Vokes NI, Sasaki M, Beroukhim R, Stephanopoulos G, Ligon AH, Meyerson M, Richardson AL, Chin L, Wagner G, Asara JM, Brugge JS, Cantley LC, Vander Heiden MG.** 2011. Phosphoglycerate dehydrogenase diverts glycolytic flux and contributes to oncogenesis. Nat Genet **43:**869-874.

249. **Rochfort S.** 2005. Metabolomics reviewed: a new "omics" platform technology for systems biology and implications for natural products research. J Nat Prod **68:**1813-1820.

250. **Sanchez EL, Lagunoff M.** 2015. Viral activation of cellular metabolism. Virology doi:10.1016/j.virol.2015.02.038.

251. **Berg JM, Tymoczko JL, Stryer L, Stryer L.** 2007. Biochemistry, 6th ed. W. H. Freeman, New York.

252. **Lunt SY, Vander Heiden MG.** 2011. Aerobic glycolysis: meeting the metabolic requirements of cell proliferation. Annu Rev Cell Dev Biol **27:**441-464.

253. **Weber G.** 1977. Enzymology of cancer cells (second of two parts). N Engl J Med **296:**541-551.

254. **Marshall MJ, Goldberg DM, Neal FE, Millar DR.** 1978. Enzymes of glucose metabolism in carcinoma of the cervix and endometrium of the human uterus. Br J Cancer **37:**990-1001.

255. **Zancan P, Sola-Penna M, Furtado CM, Da Silva D.** 2010. Differential expression of phosphofructokinase-1 isoforms correlates with the glycolytic efficiency of breast cancer cells. Mol Genet Metab **100:**372-378.

256. **Van Schaftingen E, Hers HG.** 1981. Phosphofructokinase 2: the enzyme that forms fructose 2,6-bisphosphate from fructose 6-phosphate and ATP. Biochem Biophys Res Commun **101:**1078-1084.

257. **Van Schaftingen E, Jett MF, Hue L, Hers HG.** 1981. Control of liver 6-phosphofructokinase by fructose 2,6-bisphosphate and other effectors. Proc Natl Acad Sci U S A **78:**3483-3486.

258. **Van Schaftingen E, Hue L, Hers HG.** 1980. Fructose 2,6-bisphosphate, the probably structure of the glucose- and glucagon-sensitive stimulator of phosphofructokinase. Biochem J **192:**897-901.

259. **Racker E.** 1974. History of the Pasteur effect and its pathobiology. Mol Cell Biochem **5:**17-23.

260. **Gatenby RA, Gillies RJ.** 2004. Why do cancers have high aerobic glycolysis? Nat Rev Cancer **4:**891-899.

261. **Cornell NW, Lund P, Krebs HA.** 1974. The effect of lysine on gluconeogenesis from lactate in rat hepatocytes. Biochem J **142:**327-337.

262. **Pedersen PL.** 1978. Tumor mitochondria and the bioenergetics of cancer cells. Prog Exp Tumor Res **22:**190-274.

263. **Moreno-Sanchez R, Rodriguez-Enriquez S, Marin-Hernandez A, Saavedra E.** 2007. Energy metabolism in tumor cells. FEBS J **274:**1393-1418.

264. **Warburg O, Wind F, Negelein E.** 1927. The Metabolism of Tumors in the Body. J Gen Physiol **8:**519-530.

265. **Hennipman A, Smits J, van Oirschot B, van Houwelingen JC, Rijksen G, Neyt JP, Van Unnik JA, Staal GE.** 1987. Glycolytic enzymes in breast cancer, benign breast disease and normal breast tissue. Tumour Biol **8:**251-263.

266. **Hennipman A, van Oirschot BA, Smits J, Rijksen G, Staal GE.** 1988. Glycolytic enzyme activities in breast cancer metastases. Tumour Biol **9:**241-248.

267. **Yalcin A, Telang S, Clem B, Chesney J.** 2009. Regulation of glucose metabolism by 6-phosphofructo-2-kinase/fructose-2,6-bisphosphatases in cancer. Exp Mol Pathol **86:**174-179.

268. **Wang T, Marquardt C, Foker J.** 1976. Aerobic glycolysis during lymphocyte proliferation. Nature **261:**702-705.

269. **Brand KA, Hermfisse U.** 1997. Aerobic glycolysis by proliferating cells: a protective strategy against reactive oxygen species. FASEB J **11:**388-395.

270. **Wood T.** 1986. Physiological functions of the pentose phosphate pathway. Cell Biochem Funct **4:**241-247.

271. **Kruger NJ, von Schaewen A.** 2003. The oxidative pentose phosphate pathway: structure and organisation. Curr Opin Plant Biol **6:**236-246.

272. **Seagroves TN, Ryan HE, Lu H, Wouters BG, Knapp M, Thibault P, Laderoute K, Johnson RS.** 2001. Transcription factor HIF-1 is a necessary mediator of the pasteur effect in mammalian cells. Mol Cell Biol **21:**3436-3444.

273. **Lum JJ, Bui T, Gruber M, Gordan JD, DeBerardinis RJ, Covello KL, Simon MC, Thompson CB.** 2007. The transcription factor HIF-1alpha plays a critical role in the growth factor-dependent regulation of both aerobic and anaerobic glycolysis. Genes Dev **21:**1037-1049.

274. **Jaakkola P, Mole DR, Tian YM, Wilson MI, Gielbert J, Gaskell SJ, von Kriegsheim A, Hebestreit HF, Mukherji M, Schofield CJ, Maxwell PH, Pugh CW, Ratcliffe PJ.** 2001. Targeting of HIF-alpha to the von Hippel-Lindau ubiquitylation complex by O2-regulated prolyl hydroxylation. Science **292:**468-472.

275. **Ivan M, Kondo K, Yang H, Kim W, Valiando J, Ohh M, Salic A, Asara JM, Lane WS, Kaelin WG, Jr.** 2001. HIFalpha targeted for VHL-mediated destruction by proline hydroxylation: implications for O2 sensing. Science **292:**464-468.

276. **Maxwell PH, Wiesener MS, Chang GW, Clifford SC, Vaux EC, Cockman ME, Wykoff CC, Pugh CW, Maher ER, Ratcliffe PJ.** 1999. The tumour suppressor protein VHL targets hypoxia-inducible factors for oxygen-dependent proteolysis. Nature **399:**271-275.

277. **Cockman ME, Masson N, Mole DR, Jaakkola P, Chang GW, Clifford SC, Maher ER, Pugh CW, Ratcliffe PJ, Maxwell PH.** 2000. Hypoxia inducible factor-alpha binding and ubiquitylation by the von Hippel-Lindau tumor suppressor protein. J Biol Chem **275:**25733-25741.

278. **Semenza GL, Roth PH, Fang HM, Wang GL.** 1994. Transcriptional regulation of genes encoding glycolytic enzymes by hypoxia-inducible factor 1. J Biol Chem **269:**23757-23763.

279. **O'Rourke JF, Pugh CW, Bartlett SM, Ratcliffe PJ.** 1996. Identification of hypoxically inducible mRNAs in HeLa cells using differential-display PCR. Role of hypoxia-inducible factor-1. Eur J Biochem **241:**403-410.

280. **Kim JW, Tchernyshyov I, Semenza GL, Dang CV.** 2006. HIF-1-mediated expression of pyruvate dehydrogenase kinase: a metabolic switch required for cellular adaptation to hypoxia. Cell Metab **3:**177-185.

281. **Deprez J, Vertommen D, Alessi DR, Hue L, Rider MH.** 1997. Phosphorylation and activation of heart 6-phosphofructo-2-kinase by protein kinase B and other protein kinases of the insulin signaling cascades. J Biol Chem **272:**17269-17275.

282. **Vander Heiden MG, Plas DR, Rathmell JC, Fox CJ, Harris MH, Thompson CB.** 2001. Growth factors can influence cell growth and survival through effects on glucose metabolism. Mol Cell Biol **21:**5899-5912.

283. **Zhang W, Patil S, Chauhan B, Guo S, Powell DR, Le J, Klotsas A, Matika R, Xiao X, Franks R, Heidenreich KA, Sajan MP, Farese RV, Stolz DB, Tso P, Koo SH, Montminy M, Unterman TG.** 2006. FoxO1 regulates multiple metabolic pathways in the liver: effects on gluconeogenic, glycolytic, and lipogenic gene expression. J Biol Chem **281:**10105-10117.

284. **Hudson CC, Liu M, Chiang GG, Otterness DM, Loomis DC, Kaper F, Giaccia AJ, Abraham RT.** 2002. Regulation of hypoxia-inducible factor 1alpha expression and function by the mammalian target of rapamycin. Mol Cell Biol **22:**7004-7014.

285. **Jiang BH, Jiang G, Zheng JZ, Lu Z, Hunter T, Vogt PK.** 2001. Phosphatidylinositol 3-kinase signaling controls levels of hypoxia-inducible factor 1. Cell Growth Differ **12:**363-369.

286. **Osthus RC, Shim H, Kim S, Li Q, Reddy R, Mukherjee M, Xu Y, Wonsey D, Lee LA, Dang CV.** 2000. Deregulation of glucose transporter 1 and glycolytic gene expression by c-Myc. J Biol Chem **275:**21797-21800.

287. **Dang CV, Le A, Gao P.** 2009. MYC-induced cancer cell energy metabolism and therapeutic opportunities. Clin Cancer Res **15:**6479-6483.

288. **Green DR, Chipuk JE.** 2006. p53 and metabolism: Inside the TIGAR. Cell **126:**30-32.

289. **Bensaad K, Tsuruta A, Selak MA, Vidal MN, Nakano K, Bartrons R, Gottlieb E, Vousden KH.** 2006. TIGAR, a p53-inducible regulator of glycolysis and apoptosis. Cell **126:**107-120.

290. **Munger J, Bajad SU, Coller HA, Shenk T, Rabinowitz JD.** 2006. Dynamics of the cellular metabolome during human cytomegalovirus infection. PLoS Pathog **2:**e132.

291. **Landini MP.** 1984. Early enhanced glucose uptake in human cytomegalovirus-infected cells. J Gen Virol **65 (Pt 7):**1229-1232.

292. **Yu Y, Maguire TG, Alwine JC.** 2011. Human cytomegalovirus activates glucose transporter 4 expression to increase glucose uptake during infection. J Virol **85:**1573-1580.

293. **Vastag L, Koyuncu E, Grady SL, Shenk TE, Rabinowitz JD.** 2011. Divergent effects of human cytomegalovirus and herpes simplex virus-1 on cellular metabolism. PLoS Pathog **7:**e1002124.

294. **Munger J, Bennett BD, Parikh A, Feng XJ, McArdle J, Rabitz HA, Shenk T, Rabinowitz JD.** 2008. Systems-level metabolic flux profiling identifies fatty acid synthesis as a target for antiviral therapy. Nat Biotechnol **26:**1179-1186.

295. **Delgado T, Sanchez EL, Camarda R, Lagunoff M.** 2012. Global metabolic profiling of infection by an oncogenic virus: KSHV induces and requires lipogenesis for survival of latent infection. PLoS Pathog **8:**e1002866.

296. **Delgado T, Carroll PA, Punjabi AS, Margineantu D, Hockenbery DM, Lagunoff M.** 2010. Induction of the Warburg effect by Kaposi's sarcoma herpesvirus is required for the maintenance of latently infected endothelial cells. Proc Natl Acad Sci U S A **107:**10696-10701.

297. **Xiao L, Hu ZY, Dong X, Tan Z, Li W, Tang M, Chen L, Yang L, Tao Y, Jiang Y, Li J, Yi B, Li B, Fan S, You S, Deng X, Hu F, Feng L, Bode AM, Dong Z, Sun LQ, Cao Y.** 2014. Targeting Epstein-Barr virus oncoprotein LMP1-mediated glycolysis sensitizes nasopharyngeal carcinoma to radiation therapy. Oncogene **33:**4568-4578.

298. **Thai M, Graham NA, Braas D, Nehil M, Komisopoulou E, Kurdistani SK, McCormick F, Graeber TG, Christofk HR.** 2014. Adenovirus E4ORF1-induced MYC activation promotes host cell anabolic glucose metabolism and virus replication. Cell Metab **19:**694-701.

299. **Diamond DL, Syder AJ, Jacobs JM, Sorensen CM, Walters KA, Proll SC, McDermott JE, Gritsenko MA, Zhang Q, Zhao R, Metz TO, Camp DG, 2nd, Waters KM, Smith RD, Rice CM, Katze MG.** 2010. Temporal proteome and

lipidome profiles reveal hepatitis C virus-associated reprogramming of hepatocellular metabolism and bioenergetics. PLoS Pathog **6:**e1000719.

300. **Ripoli M, D'Aprile A, Quarato G, Sarasin-Filipowicz M, Gouttenoire J, Scrima R, Cela O, Boffoli D, Heim MH, Moradpour D, Capitanio N, Piccoli C.** 2010. Hepatitis C virus-linked mitochondrial dysfunction promotes hypoxia-inducible factor 1 alpha-mediated glycolytic adaptation. J Virol **84:**647-660.

301. **Ramiere C, Rodriguez J, Enache LS, Lotteau V, Andre P, Diaz O.** 2014. Activity of hexokinase is increased by its interaction with hepatitis C virus protein NS5A. J Virol **88:**3246-3254.

302. **Klemperer H.** 1961. Glucose breakdown in chick embryo cells infected with influenza virus. Virology **13:**68-77.

303. **Ritter JB, Wahl AS, Freund S, Genzel Y, Reichl U.** 2010. Metabolic effects of influenza virus infection in cultured animal cells: Intra- and extracellular metabolite profiling. BMC Syst Biol **4:**61.

304. **Chan EY, Sutton JN, Jacobs JM, Bondarenko A, Smith RD, Katze MG.** 2009. Dynamic host energetics and cytoskeletal proteomes in human immunodeficiency virus type 1-infected human primary CD4 cells: analysis by multiplexed label-free mass spectrometry. J Virol **83:**9283-9295.

305. **Hollenbaugh JA, Munger J, Kim B.** 2011. Metabolite profiles of human immunodeficiency virus infected CD4+ T cells and macrophages using LC-MS/MS analysis. Virology **415:**153-159.

306. **Greseth MD, Traktman P.** 2014. De novo fatty acid biosynthesis contributes significantly to establishment of a bioenergetically favorable environment for vaccinia virus infection. PLoS Pathog **10:**e1004021.

307. **Fontaine KA, Camarda R, Lagunoff M.** 2014. Vaccinia virus requires glutamine but not glucose for efficient replication. J Virol **88:**4366-4374.

308. **Mazzon M, Castro C, Roberts LD, Griffin JL, Smith GL.** 2015. A role for vaccinia virus protein C16 in reprogramming cellular energy metabolism. J Gen Virol **96:**395-407.

309. **Mazzon M, Peters NE, Loenarz C, Krysztofinska EM, Ember SW, Ferguson BJ, Smith GL.** 2013. A mechanism for induction of a hypoxic response by vaccinia virus. Proc Natl Acad Sci U S A **110:**12444-12449.

310. **Kun E, Smith MH.** 1950. Effect of infectious myxoma virus on glycolysis of chorioallantoic membrane of chick embryo. Proc Soc Exp Biol Med **73:**628-631.

311. **Courtney RJ, Steiner SM, Benyesh-Melnick M.** 1973. Effects of 2-deoxy-D-glucose on herpes simplex virus replication. Virology **52:**447-455.

312. **Radsak KD, Weder D.** 1981. Effect of 2-deoxy-D-glucose on cytomegalovirus-induced DNA synthesis in human fibroblasts. J Gen Virol **57:**33-42.

313. **Fontaine KA, Sanchez EL, Camarda R, Lagunoff M.** 2015. Dengue virus induces and requires glycolysis for optimal replication. J Virol **89:**2358-2366.

314. **McClure J, Margineantu DH, Sweet IR, Polyak SJ.** 2014. Inhibition of HIV by Legalon-SIL is independent of its effect on cellular metabolism. Virology **449:**96-103.

315. **Santamaria D, Ortega S.** 2006. Cyclins and CDKS in development and cancer: lessons from genetically modified mice. Front Biosci **11:**1164-1188.
316. **Alberts B, Johnson, A, Lewis J, et at. .** 2008. Mitosis, Molecular biology of the cell, 5th ed. Garland Science, New York.
317. **Hartwell LH, Weinert TA.** 1989. Checkpoints: controls that ensure the order of cell cycle events. Science **246:**629-634.
318. **Johnson A, Skotheim JM.** 2013. Start and the restriction point. Curr Opin Cell Biol **25:**717-723.
319. **Stark GR, Taylor WR.** 2004. Analyzing the G2/M checkpoint. Methods Mol Biol **280:**51-82.
320. **Hauf S.** 2013. The spindle assembly checkpoint: progress and persistent puzzles. Biochem Soc Trans **41:**1755-1760.
321. **Malumbres M.** 2014. Cyclin-dependent kinases. Genome Biol **15:**122.
322. **Asghar U, Witkiewicz AK, Turner NC, Knudsen ES.** 2015. The history and future of targeting cyclin-dependent kinases in cancer therapy. Nat Rev Drug Discov **14:**130-146.
323. **Bretones G, Delgado MD, Leon J.** 2015. Myc and cell cycle control. Biochim Biophys Acta **1849:**506-516.
324. **Sherr CJ, Roberts JM.** 1999. CDK inhibitors: positive and negative regulators of G1-phase progression. Genes Dev **13:**1501-1512.
325. **Pavletich NP.** 1999. Mechanisms of cyclin-dependent kinase regulation: structures of Cdks, their cyclin activators, and Cip and INK4 inhibitors. J Mol Biol **287:**821-828.
326. **Russo AA, Tong L, Lee JO, Jeffrey PD, Pavletich NP.** 1998. Structural basis for inhibition of the cyclin-dependent kinase Cdk6 by the tumour suppressor p16INK4a. Nature **395:**237-243.
327. **Jeffrey PD, Tong L, Pavletich NP.** 2000. Structural basis of inhibition of CDK-cyclin complexes by INK4 inhibitors. Genes Dev **14:**3115-3125.
328. **Denicourt C, Dowdy SF.** 2004. Cip/Kip proteins: more than just CDKs inhibitors. Genes Dev **18:**851-855.
329. **LaBaer J, Garrett MD, Stevenson LF, Slingerland JM, Sandhu C, Chou HS, Fattaey A, Harlow E.** 1997. New functional activities for the p21 family of CDK inhibitors. Genes Dev **11:**847-862.
330. **Cheng M, Olivier P, Diehl JA, Fero M, Roussel MF, Roberts JM, Sherr CJ.** 1999. The p21(Cip1) and p27(Kip1) CDK 'inhibitors' are essential activators of cyclin D-dependent kinases in murine fibroblasts. EMBO J **18:**1571-1583.
331. **Tang HY, Zhao K, Pizzolato JF, Fonarev M, Langer JC, Manfredi JJ.** 1998. Constitutive expression of the cyclin-dependent kinase inhibitor p21 is transcriptionally regulated by the tumor suppressor protein p53. J Biol Chem **273:**29156-29163.
332. **Duronio RJ, Xiong Y.** 2013. Signaling pathways that control cell proliferation. Cold Spring Harb Perspect Biol **5:**a008904.
333. **Waters CM, Littlewood TD, Hancock DC, Moore JP, Evan GI.** 1991. c-myc protein expression in untransformed fibroblasts. Oncogene **6:**797-805.
334. **Littlewood TD, Evan GI.** 1990. The role of myc oncogenes in cell growth and differentiation. Adv Dent Res **4:**69-79.

335. **Kerkhoff E, Houben R, Loffler S, Troppmair J, Lee JE, Rapp UR.** 1998. Regulation of c-myc expression by Ras/Raf signalling. Oncogene **16:**211-216.
336. **Kato JY, Matsuoka M, Strom DK, Sherr CJ.** 1994. Regulation of cyclin D-dependent kinase 4 (cdk4) by cdk4-activating kinase. Mol Cell Biol **14:**2713-2721.
337. **Lolli G, Johnson LN.** 2005. CAK-Cyclin-dependent Activating Kinase: a key kinase in cell cycle control and a target for drugs? Cell Cycle **4:**572-577.
338. **Weinberg RA.** 1995. The retinoblastoma protein and cell cycle control. Cell **81:**323-330.
339. **Duronio RJ, O'Farrell PH, Xie JE, Brook A, Dyson N.** 1995. The transcription factor E2F is required for S phase during Drosophila embryogenesis. Genes Dev **9:**1445-1455.
340. **Wu CL, Classon M, Dyson N, Harlow E.** 1996. Expression of dominant-negative mutant DP-1 blocks cell cycle progression in G1. Mol Cell Biol **16:**3698-3706.
341. **Lundberg AS, Weinberg RA.** 1998. Functional inactivation of the retinoblastoma protein requires sequential modification by at least two distinct cyclin-cdk complexes. Mol Cell Biol **18:**753-761.
342. **Bracken AP, Ciro M, Cocito A, Helin K.** 2004. E2F target genes: unraveling the biology. Trends Biochem Sci **29:**409-417.
343. **Muller D, Bouchard C, Rudolph B, Steiner P, Stuckmann I, Saffrich R, Ansorge W, Huttner W, Eilers M.** 1997. Cdk2-dependent phosphorylation of p27 facilitates its Myc-induced release from cyclin E/cdk2 complexes. Oncogene **15:**2561-2576.
344. **Sheaff RJ, Groudine M, Gordon M, Roberts JM, Clurman BE.** 1997. Cyclin E-CDK2 is a regulator of p27Kip1. Genes Dev **11:**1464-1478.
345. **Kato J.** 1999. Induction of S phase by G1 regulatory factors. Front Biosci **4:**D787-792.
346. **Zhu H, Nie L, Maki CG.** 2005. Cdk2-dependent Inhibition of p21 stability via a C-terminal cyclin-binding motif. J Biol Chem **280:**29282-29288.
347. **Ohtsubo M, Theodoras AM, Schumacher J, Roberts JM, Pagano M.** 1995. Human cyclin E, a nuclear protein essential for the G1-to-S phase transition. Mol Cell Biol **15:**2612-2624.
348. **Girard F, Strausfeld U, Fernandez A, Lamb NJ.** 1991. Cyclin A is required for the onset of DNA replication in mammalian fibroblasts. Cell **67:**1169-1179.
349. **Voitenleitner C, Fanning E, Nasheuer HP.** 1997. Phosphorylation of DNA polymerase alpha-primase by cyclin A-dependent kinases regulates initiation of DNA replication in vitro. Oncogene **14:**1611-1615.
350. **Voitenleitner C, Rehfuess C, Hilmes M, O'Rear L, Liao PC, Gage DA, Ott R, Nasheuer HP, Fanning E.** 1999. Cell cycle-dependent regulation of human DNA polymerase alpha-primase activity by phosphorylation. Mol Cell Biol **19:**646-656.
351. **Woo RA, Poon RY.** 2003. Cyclin-dependent kinases and S phase control in mammalian cells. Cell Cycle **2:**316-324.

352. **Stark GR, Taylor WR.** 2006. Control of the G2/M transition. Mol Biotechnol **32:**227-248.

353. **Hagting A, Karlsson C, Clute P, Jackman M, Pines J.** 1998. MPF localization is controlled by nuclear export. EMBO J **17:**4127-4138.

354. **Porter LA, Donoghue DJ.** 2003. Cyclin B1 and CDK1: nuclear localization and upstream regulators. Prog Cell Cycle Res **5:**335-347.

355. **Parker LL, Piwnica-Worms H.** 1992. Inactivation of the p34cdc2-cyclin B complex by the human WEE1 tyrosine kinase. Science **257:**1955-1957.

356. **McGowan CH, Russell P.** 1993. Human Wee1 kinase inhibits cell division by phosphorylating p34cdc2 exclusively on Tyr15. EMBO J **12:**75-85.

357. **Hoffmann I, Karsenti E.** 1994. The role of cdc25 in checkpoints and feedback controls in the eukaryotic cell cycle. J Cell Sci Suppl **18:**75-79.

358. **Lammer C, Wagerer S, Saffrich R, Mertens D, Ansorge W, Hoffmann I.** 1998. The cdc25B phosphatase is essential for the G2/M phase transition in human cells. J Cell Sci **111 (Pt 16):**2445-2453.

359. **Harper JW, Elledge SJ.** 2007. The DNA damage response: ten years after. Mol Cell **28:**739-745.

360. **Page AM, Hieter P.** 1999. The anaphase-promoting complex: new subunits and regulators. Annu Rev Biochem **68:**583-609.

361. **Visintin R, Prinz S, Amon A.** 1997. CDC20 and CDH1: a family of substrate-specific activators of APC-dependent proteolysis. Science **278:**460-463.

362. **Rudner AD, Murray AW.** 2000. Phosphorylation by Cdc28 activates the Cdc20-dependent activity of the anaphase-promoting complex. J Cell Biol **149:**1377-1390.

363. **Yu H.** 2002. Regulation of APC-Cdc20 by the spindle checkpoint. Curr Opin Cell Biol **14:**706-714.

364. **Thornton BR, Toczyski DP.** 2003. Securin and B-cyclin/CDK are the only essential targets of the APC. Nat Cell Biol **5:**1090-1094.

365. **Hauf S, Waizenegger IC, Peters JM.** 2001. Cohesin cleavage by separase required for anaphase and cytokinesis in human cells. Science **293:**1320-1323.

366. **Nascimento R, Costa H, Parkhouse RM.** 2012. Virus manipulation of cell cycle. Protoplasma **249:**519-528.

367. **Bagga S, Bouchard MJ.** 2014. Cell cycle regulation during viral infection. Methods Mol Biol **1170:**165-227.

368. **Gearhart TL, Bouchard MJ.** 2010. The hepatitis B virus X protein modulates hepatocyte proliferation pathways to stimulate viral replication. J Virol **84:**2675-2686.

369. **Gearhart TL, Bouchard MJ.** 2011. The hepatitis B virus HBx protein modulates cell cycle regulatory proteins in cultured primary human hepatocytes. Virus Res **155:**363-367.

370. **Wang T, Zhao R, Wu Y, Kong D, Zhang L, Wu D, Li C, Zhang C, Yu Z, Jin X.** 2011. Hepatitis B virus induces G1 phase arrest by regulating cell cycle genes in HepG2.2.15 cells. Virol J **8:**231.

371. **Johnston JB, Wang G, Barrett JW, Nazarian SH, Colwill K, Moran M, McFadden G.** 2005. Myxoma virus M-T5 protects infected cells from the

stress of cell cycle arrest through its interaction with host cell cullin-1. J Virol **79:**10750-10763.

372. **Wali A, Strayer DS.** 1999. Comparative effects of virulent and avirulent poxviruses on cell cycle progression. Exp Mol Pathol **66:**31-38.

373. **Wali A, Strayer DS.** 1999. Infection with vaccinia virus alters regulation of cell cycle progression. DNA Cell Biol **18:**837-843.

374. **Grce M, Mravak-Stipetic M.** 2014. Human papillomavirus-associated diseases. Clin Dermatol **32:**253-258.

375. **Scheffner M, Werness BA, Huibregtse JM, Levine AJ, Howley PM.** 1990. The E6 oncoprotein encoded by human papillomavirus types 16 and 18 promotes the degradation of p53. Cell **63:**1129-1136.

376. **Werness BA, Levine AJ, Howley PM.** 1990. Association of human papillomavirus types 16 and 18 E6 proteins with p53. Science **248:**76-79.

377. **Huibregtse JM, Scheffner M, Howley PM.** 1993. Cloning and expression of the cDNA for E6-AP, a protein that mediates the interaction of the human papillomavirus E6 oncoprotein with p53. Mol Cell Biol **13:**775-784.

378. **Scheffner M, Huibregtse JM, Howley PM.** 1994. Identification of a human ubiquitin-conjugating enzyme that mediates the E6-AP-dependent ubiquitination of p53. Proc Natl Acad Sci U S A **91:**8797-8801.

379. **Dyson N, Howley PM, Munger K, Harlow E.** 1989. The human papilloma virus-16 E7 oncoprotein is able to bind to the retinoblastoma gene product. Science **243:**934-937.

380. **Davies R, Hicks R, Crook T, Morris J, Vousden K.** 1993. Human papillomavirus type 16 E7 associates with a histone H1 kinase and with p107 through sequences necessary for transformation. J Virol **67:**2521-2528.

381. **Zerfass K, Levy LM, Cremonesi C, Ciccolini F, Jansen-Durr P, Crawford L, Ralston R, Tommasino M.** 1995. Cell cycle-dependent disruption of E2F-p107 complexes by human papillomavirus type 16 E7. J Gen Virol **76 (Pt 7):**1815-1820.

382. **Boyer SN, Wazer DE, Band V.** 1996. E7 protein of human papilloma virus-16 induces degradation of retinoblastoma protein through the ubiquitin-proteasome pathway. Cancer Res **56:**4620-4624.

383. **Felsani A, Mileo AM, Paggi MG.** 2006. Retinoblastoma family proteins as key targets of the small DNA virus oncoproteins. Oncogene **25:**5277-5285.

384. **He Y, Xu K, Keiner B, Zhou J, Czudai V, Li T, Chen Z, Liu J, Klenk HD, Shu YL, Sun B.** 2010. Influenza A virus replication induces cell cycle arrest in G0/G1 phase. J Virol **84:**12832-12840.

385. **Jiang W, Wang Q, Chen S, Gao S, Song L, Liu P, Huang W.** 2013. Influenza A virus NS1 induces G0/G1 cell cycle arrest by inhibiting the expression and activity of RhoA protein. J Virol **87:**3039-3052.

386. **Yuan X, Wu J, Shan Y, Yao Z, Dong B, Chen B, Zhao Z, Wang S, Chen J, Cong Y.** 2006. SARS coronavirus 7a protein blocks cell cycle progression at G0/G1 phase via the cyclin D3/pRb pathway. Virology **346:**74-85.

387. **Surjit M, Liu B, Chow VT, Lal SK.** 2006. The nucleocapsid protein of severe acute respiratory syndrome-coronavirus inhibits the activity of cyclin-cyclin-

dependent kinase complex and blocks S phase progression in mammalian cells. J Biol Chem **281:**10669-10681.

388. **Yuan X, Yao Z, Wu J, Zhou Y, Shan Y, Dong B, Zhao Z, Hua P, Chen J, Cong Y.** 2007. G1 phase cell cycle arrest induced by SARS-CoV 3a protein via the cyclin D3/pRb pathway. Am J Respir Cell Mol Biol **37:**9-19.

389. **Huang SY, Hsieh MJ, Chen CY, Chen YJ, Chen JY, Chen MR, Tsai CH, Lin SF, Hsu TY.** 2012. Epstein-Barr virus Rta-mediated transactivation of p21 and 14-3-3sigma arrests cells at the G1/S transition by reducing cyclin E/CDK2 activity. J Gen Virol **93:**139-149.

390. **Ueda R, Sugiura T, Kume S, Ichikawa A, Larsen S, Miyoshi H, Hiramatsu H, Nagatsuka Y, Arai F, Suzuki Y, Hirabayashi Y, Fukuda T, Honda A.** 2013. A novel single virus infection system reveals that influenza virus preferentially infects cells in g1 phase. PLoS One **8:**e67011.

391. **Hobbs WE, 2nd, DeLuca NA.** 1999. Perturbation of cell cycle progression and cellular gene expression as a function of herpes simplex virus ICP0. J Virol **73:**8245-8255.

392. **Song B, Yeh KC, Liu J, Knipe DM.** 2001. Herpes simplex virus gene products required for viral inhibition of expression of G1-phase functions. Virology **290:**320-328.

393. **Hume AJ, Kalejta RF.** 2009. Regulation of the retinoblastoma proteins by the human herpesviruses. Cell Div **4:**1.

394. **Davy C, Doorbar J.** 2007. G2/M cell cycle arrest in the life cycle of viruses. Virology **368:**219-226.

395. **Li H, Baskaran R, Krisky DM, Bein K, Grandi P, Cohen JB, Glorioso JC.** 2008. Chk2 is required for HSV-1 ICP0-mediated G2/M arrest and enhancement of virus growth. Virology **375:**13-23.

396. **Li L, Gu B, Zhou F, Chi J, Wang F, Peng G, Xie F, Qing J, Feng D, Lu S, Yao K.** 2011. Human herpesvirus 6 suppresses T cell proliferation through induction of cell cycle arrest in infected cells in the G2/M phase. J Virol **85:**6774-6783.

397. **Li L, Gu B, Zhou F, Chi J, Feng D, Xie F, Wang F, Ma C, Li M, Wang J, Yao K.** 2014. Cell cycle perturbations induced by human herpesvirus 6 infection and their effect on virus replication. Arch Virol **159:**365-370.

398. **Schleimann MH, Hoberg S, Solhoj Hansen A, Bundgaard B, Witt CT, Kofod-Olsen E, Hollsberg P.** 2014. The DR6 protein from human herpesvirus-6B induces p53-independent cell cycle arrest in G2/M. Virology **452-453:**254-263.

399. **Romani B, Engelbrecht S.** 2009. Human immunodeficiency virus type 1 Vpr: functions and molecular interactions. J Gen Virol **90:**1795-1805.

400. **Li G, Park HU, Liang D, Zhao RY.** 2010. Cell cycle G2/M arrest through an S phase-dependent mechanism by HIV-1 viral protein R. Retrovirology **7:**59.

401. **He J, Choe S, Walker R, Di Marzio P, Morgan DO, Landau NR.** 1995. Human immunodeficiency virus type 1 viral protein R (Vpr) arrests cells in the G2 phase of the cell cycle by inhibiting p34cdc2 activity. J Virol **69:**6705-6711.

402. **Goh WC, Manel N, Emerman M.** 2004. The human immunodeficiency virus Vpr protein binds Cdc25C: implications for G2 arrest. Virology **318:**337-349.

403. **Huard S, Elder RT, Liang D, Li G, Zhao RY.** 2008. Human immunodeficiency virus type 1 Vpr induces cell cycle G2 arrest through Srk1/MK2-mediated phosphorylation of Cdc25. J Virol **82:**2904-2917.
404. **Matsuda N, Tanaka H, Yamazaki S, Suzuki J, Tanaka K, Yamada T, Masuda M.** 2006. HIV-1 Vpr induces G2 cell cycle arrest in fission yeast associated with Rad24/14-3-3-dependent, Chk1/Cds1-independent Wee1 upregulation. Microbes Infect **8:**2736-2744.
405. **Yuan H, Kamata M, Xie YM, Chen IS.** 2004. Increased levels of Wee-1 kinase in G(2) are necessary for Vpr- and gamma irradiation-induced G(2) arrest. J Virol **78:**8183-8190.
406. **Goh WC, Rogel ME, Kinsey CM, Michael SF, Fultz PN, Nowak MA, Hahn BH, Emerman M.** 1998. HIV-1 Vpr increases viral expression by manipulation of the cell cycle: a mechanism for selection of Vpr in vivo. Nat Med **4:**65-71.
407. **Poon B, Grovit-Ferbas K, Stewart SA, Chen IS.** 1998. Cell cycle arrest by Vpr in HIV-1 virions and insensitivity to antiretroviral agents. Science **281:**266-269.
408. **Zimmerman ES, Sherman MP, Blackett JL, Neidleman JA, Kreis C, Mundt P, Williams SA, Warmerdam M, Kahn J, Hecht FM, Grant RM, de Noronha CM, Weyrich AS, Greene WC, Planelles V.** 2006. Human immunodeficiency virus type 1 Vpr induces DNA replication stress in vitro and in vivo. J Virol **80:**10407-10418.
409. **Fehr AR, Yu D.** 2013. Control the host cell cycle: viral regulation of the anaphase-promoting complex. J Virol **87:**8818-8825.
410. **Fehr AR, Gualberto NC, Savaryn JP, Terhune SS, Yu D.** 2012. Proteasome-dependent disruption of the E3 ubiquitin ligase anaphase-promoting complex by HCMV protein pUL21a. PLoS Pathog **8:**e1002789.
411. **Fehr AR, Yu D.** 2011. Human cytomegalovirus early protein pUL21a promotes efficient viral DNA synthesis and the late accumulation of immediate-early transcripts. J Virol **85:**663-674.
412. **Mo M, Fleming SB, Mercer AA.** 2009. Cell cycle deregulation by a poxvirus partial mimic of anaphase-promoting complex subunit 11. Proc Natl Acad Sci U S A **106:**19527-19532.
413. **Mo M, Fleming SB, Mercer AA.** 2010. Orf virus cell cycle regulator, PACR, competes with subunit 11 of the anaphase promoting complex for incorporation into the complex. J Gen Virol **91:**3010-3015.
414. **Kornberg RD.** 1974. Chromatin structure: a repeating unit of histones and DNA. Science **184:**868-871.
415. **Kornberg RD.** 1977. Structure of chromatin. Annu Rev Biochem **46:**931-954.
416. **Eickbush TH, Moudrianakis EN.** 1978. The histone core complex: an octamer assembled by two sets of protein-protein interactions. Biochemistry **17:**4955-4964.
417. **Luger K, Mader AW, Richmond RK, Sargent DF, Richmond TJ.** 1997. Crystal structure of the nucleosome core particle at 2.8 A resolution. Nature **389:**251-260.

418. **Whitlock JP, Jr., Simpson RT.** 1976. Removal of histone H1 exposes a fifty base pair DNA segment between nucleosomes. Biochemistry **15:**3307-3314.
419. **Harshman SW, Young NL, Parthun MR, Freitas MA.** 2013. H1 histones: current perspectives and challenges. Nucleic Acids Res **41:**9593-9609.
420. **Widom J, Finch JT, Thomas JO.** 1985. Higher-order structure of long repeat chromatin. EMBO J **4:**3189-3194.
421. **Song F, Chen P, Sun D, Wang M, Dong L, Liang D, Xu RM, Zhu P, Li G.** 2014. Cryo-EM study of the chromatin fiber reveals a double helix twisted by tetranucleosomal units. Science **344:**376-380.
422. **Arents G, Moudrianakis EN.** 1995. The histone fold: a ubiquitous architectural motif utilized in DNA compaction and protein dimerization. Proc Natl Acad Sci U S A **92:**11170-11174.
423. **Baxevanis AD, Arents G, Moudrianakis EN, Landsman D.** 1995. A variety of DNA-binding and multimeric proteins contain the histone fold motif. Nucleic Acids Res **23:**2685-2691.
424. **Campos EI, Reinberg D.** 2009. Histones: annotating chromatin. Annu Rev Genet **43:**559-599.
425. **Passarge E.** 1979. Emil Heitz and the concept of heterochromatin: longitudinal chromosome differentiation was recognized fifty years ago. Am J Hum Genet **31:**106-115.
426. **Mayer WE, Uinuk-Ool T, Tichy H, Gartland LA, Klein J, Cooper MD.** 2002. Isolation and characterization of lymphocyte-like cells from a lamprey. Proc Natl Acad Sci U S A **99:**14350-14355.
427. **Fox MH, Arndt-Jovin DJ, Jovin TM, Baumann PH, Robert-Nicoud M.** 1991. Spatial and temporal distribution of DNA replication sites localized by immunofluorescence and confocal microscopy in mouse fibroblasts. J Cell Sci **99 (Pt 2):**247-253.
428. **Ahmad K, Henikoff S.** 2001. Centromeres are specialized replication domains in heterochromatin. J Cell Biol **153:**101-110.
429. **Grewal SI, Jia S.** 2007. Heterochromatin revisited. Nat Rev Genet **8:**35-46.
430. **Luger K, Dechassa ML, Tremethick DJ.** 2012. New insights into nucleosome and chromatin structure: an ordered state or a disordered affair? Nat Rev Mol Cell Biol **13:**436-447.
431. **Venkatesh S, Workman JL.** 2015. Histone exchange, chromatin structure and the regulation of transcription. Nat Rev Mol Cell Biol **16:**178-189.
432. **Swygert SG, Peterson CL.** 2014. Chromatin dynamics: interplay between remodeling enzymes and histone modifications. Biochim Biophys Acta **1839:**728-736.
433. **Murr R.** 2010. Interplay between different epigenetic modifications and mechanisms. Adv Genet **70:**101-141.
434. **Sadakierska-Chudy A, Kostrzewa RM, Filip M.** 2015. A comprehensive view of the epigenetic landscape part I: DNA methylation, passive and active DNA demethylation pathways and histone variants. Neurotox Res **27:**84-97.
435. **Franklin SG, Zweidler A.** 1977. Non-allelic variants of histones 2a, 2b and 3 in mammals. Nature **266:**273-275.

436. **Talbert PB, Henikoff S.** 2010. Histone variants--ancient wrap artists of the epigenome. Nat Rev Mol Cell Biol **11:**264-275.
437. **Ahmad K, Henikoff S.** 2002. The histone variant H3.3 marks active chromatin by replication-independent nucleosome assembly. Mol Cell **9:**1191-1200.
438. **McKittrick E, Gafken PR, Ahmad K, Henikoff S.** 2004. Histone H3.3 is enriched in covalent modifications associated with active chromatin. Proc Natl Acad Sci U S A **101:**1525-1530.
439. **Van Hooser AA, Ouspenski, II, Gregson HC, Starr DA, Yen TJ, Goldberg ML, Yokomori K, Earnshaw WC, Sullivan KF, Brinkley BR.** 2001. Specification of kinetochore-forming chromatin by the histone H3 variant CENP-A. J Cell Sci **114:**3529-3542.
440. **Kouzarides T.** 2007. Chromatin modifications and their function. Cell **128:**693-705.
441. **Turner BM.** 2005. Reading signals on the nucleosome with a new nomenclature for modified histones. Nat Struct Mol Biol **12:**110-112.
442. **Waterborg JH.** 2002. Dynamics of histone acetylation in vivo. A function for acetylation turnover? Biochem Cell Biol **80:**363-378.
443. **Zentner GE, Henikoff S.** 2013. Regulation of nucleosome dynamics by histone modifications. Nat Struct Mol Biol **20:**259-266.
444. **Bauer WR, Hayes JJ, White JH, Wolffe AP.** 1994. Nucleosome structural changes due to acetylation. J Mol Biol **236:**685-690.
445. **Anderson JD, Lowary PT, Widom J.** 2001. Effects of histone acetylation on the equilibrium accessibility of nucleosomal DNA target sites. J Mol Biol **307:**977-985.
446. **Dion MF, Altschuler SJ, Wu LF, Rando OJ.** 2005. Genomic characterization reveals a simple histone H4 acetylation code. Proc Natl Acad Sci U S A **102:**5501-5506.
447. **Lee DY, Hayes JJ, Pruss D, Wolffe AP.** 1993. A positive role for histone acetylation in transcription factor access to nucleosomal DNA. Cell **72:**73-84.
448. **Nightingale KP, Wellinger RE, Sogo JM, Becker PB.** 1998. Histone acetylation facilitates RNA polymerase II transcription of the Drosophila hsp26 gene in chromatin. EMBO J **17:**2865-2876.
449. **Tamburini BA, Tyler JK.** 2005. Localized histone acetylation and deacetylation triggered by the homologous recombination pathway of double-strand DNA repair. Mol Cell Biol **25:**4903-4913.
450. **Vogelauer M, Rubbi L, Lucas I, Brewer BJ, Grunstein M.** 2002. Histone acetylation regulates the time of replication origin firing. Mol Cell **10:**1223-1233.
451. **Zeng L, Zhou MM.** 2002. Bromodomain: an acetyl-lysine binding domain. FEBS Lett **513:**124-128.
452. **Muller S, Filippakopoulos P, Knapp S.** 2011. Bromodomains as therapeutic targets. Expert Rev Mol Med **13:**e29.
453. **Banerjee T, Chakravarti D.** 2011. A peek into the complex realm of histone phosphorylation. Mol Cell Biol **31:**4858-4873.

454. **Rogakou EP, Pilch DR, Orr AH, Ivanova VS, Bonner WM.** 1998. DNA double-stranded breaks induce histone H2AX phosphorylation on serine 139. J Biol Chem **273:**5858-5868.
455. **Thiriet C, Hayes JJ.** 2005. Chromatin in need of a fix: phosphorylation of H2AX connects chromatin to DNA repair. Mol Cell **18:**617-622.
456. **Ziv Y, Bielopolski D, Galanty Y, Lukas C, Taya Y, Schultz DC, Lukas J, Bekker-Jensen S, Bartek J, Shiloh Y.** 2006. Chromatin relaxation in response to DNA double-strand breaks is modulated by a novel ATM- and KAP-1 dependent pathway. Nat Cell Biol **8:**870-876.
457. **Black JC, Van Rechem C, Whetstine JR.** 2012. Histone lysine methylation dynamics: establishment, regulation, and biological impact. Mol Cell **48:**491-507.
458. **Rea S, Eisenhaber F, O'Carroll D, Strahl BD, Sun ZW, Schmid M, Opravil S, Mechtler K, Ponting CP, Allis CD, Jenuwein T.** 2000. Regulation of chromatin structure by site-specific histone H3 methyltransferases. Nature **406:**593-599.
459. **Jenuwein T, Laible G, Dorn R, Reuter G.** 1998. SET domain proteins modulate chromatin domains in eu- and heterochromatin. Cell Mol Life Sci **54:**80-93.
460. **Del Rizzo PA, Trievel RC.** 2011. Substrate and product specificities of SET domain methyltransferases. Epigenetics **6:**1059-1067.
461. **Ernst J, Kellis M.** 2010. Discovery and characterization of chromatin states for systematic annotation of the human genome. Nat Biotechnol **28:**817-825.
462. **Ciabrelli F, Cavalli G.** 2014. Chromatin-Driven Behavior of Topologically Associating Domains. J Mol Biol doi:10.1016/j.jmb.2014.09.013.
463. **Peters AH, Mermoud JE, O'Carroll D, Pagani M, Schweizer D, Brockdorff N, Jenuwein T.** 2002. Histone H3 lysine 9 methylation is an epigenetic imprint of facultative heterochromatin. Nat Genet **30:**77-80.
464. **Trojer P, Reinberg D.** 2007. Facultative heterochromatin: is there a distinctive molecular signature? Mol Cell **28:**1-13.
465. **Margueron R, Reinberg D.** 2011. The Polycomb complex PRC2 and its mark in life. Nature **469:**343-349.
466. **Ayrapetov MK, Gursoy-Yuzugullu O, Xu C, Xu Y, Price BD.** 2014. DNA double-strand breaks promote methylation of histone H3 on lysine 9 and transient formation of repressive chromatin. Proc Natl Acad Sci U S A **111:**9169-9174.
467. **Wu H, Min J, Lunin VV, Antoshenko T, Dombrovski L, Zeng H, Allali-Hassani A, Campagna-Slater V, Vedadi M, Arrowsmith CH, Plotnikov AN, Schapira M.** 2010. Structural biology of human H3K9 methyltransferases. PLoS One **5:**e8570.
468. **Dambacher S, Hahn M, Schotta G.** 2013. The compact view on heterochromatin. Cell Cycle **12:**2925-2926.
469. **Saksouk N, Simboeck E, Dejardin J.** 2015. Constitutive heterochromatin formation and transcription in mammals. Epigenetics Chromatin **8:**3.
470. **Tachibana M, Ueda J, Fukuda M, Takeda N, Ohta T, Iwanari H, Sakihama T, Kodama T, Hamakubo T, Shinkai Y.** 2005. Histone methyltransferases

G9a and GLP form heteromeric complexes and are both crucial for methylation of euchromatin at H3-K9. Genes Dev **19:**815-826.

471. **Schultz DC, Ayyanathan K, Negorev D, Maul GG, Rauscher FJ, 3rd.** 2002. SETDB1: a novel KAP-1-associated histone H3, lysine 9-specific methyltransferase that contributes to HP1-mediated silencing of euchromatic genes by KRAB zinc-finger proteins. Genes Dev **16:**919-932.

472. **Falandry C, Fourel G, Galy V, Ristriani T, Horard B, Bensimon E, Salles G, Gilson E, Magdinier F.** 2010. CLLD8/KMT1F is a lysine methyltransferase that is important for chromosome segregation. J Biol Chem **285:**20234-20241.

473. **Kaustov L, Ouyang H, Amaya M, Lemak A, Nady N, Duan S, Wasney GA, Li Z, Vedadi M, Schapira M, Min J, Arrowsmith CH.** 2011. Recognition and specificity determinants of the human cbx chromodomains. J Biol Chem **286:**521-529.

474. **Lomberk G, Wallrath L, Urrutia R.** 2006. The Heterochromatin Protein 1 family. Genome Biol **7:**228.

475. **Li S, Kong L, Yu X, Zheng Y.** 2014. Host-virus interactions: from the perspectives of epigenetics. Rev Med Virol **24:**223-241.

476. **Knipe DM, Lieberman PM, Jung JU, McBride AA, Morris KV, Ott M, Margolis D, Nieto A, Nevels M, Parks RJ, Kristie TM.** 2013. Snapshots: chromatin control of viral infection. Virology **435:**141-156.

477. **Josse T, Mokrani-Benhelli H, Benferhat R, Shestakova E, Mansuroglu Z, Kakanakou H, Billecocq A, Bouloy M, Bonnefoy E.** 2012. Association of the interferon-beta gene with pericentromeric heterochromatin is dynamically regulated during virus infection through a YY1-dependent mechanism. Nucleic Acids Res **40:**4396-4411.

478. **Han X, Li X, Yue SC, Anandaiah A, Hashem F, Reinach PS, Koziel H, Tachado SD.** 2012. Epigenetic regulation of tumor necrosis factor alpha (TNFalpha) release in human macrophages by HIV-1 single-stranded RNA (ssRNA) is dependent on TLR8 signaling. J Biol Chem **287:**13778-13786.

479. **Pignatti PF, Cassai E.** 1980. Analysis of herpes simplex virus nucleoprotein complexes extracted from infected cells. J Virol **36:**816-828.

480. **Deshmane SL, Fraser NW.** 1989. During latency, herpes simplex virus type 1 DNA is associated with nucleosomes in a chromatin structure. J Virol **63:**943-947.

481. **Oh J, Fraser NW.** 2008. Temporal association of the herpes simplex virus genome with histone proteins during a lytic infection. J Virol **82:**3530-3537.

482. **Wang QY, Zhou C, Johnson KE, Colgrove RC, Coen DM, Knipe DM.** 2005. Herpesviral latency-associated transcript gene promotes assembly of heterochromatin on viral lytic-gene promoters in latent infection. Proc Natl Acad Sci U S A **102:**16055-16059.

483. **Kwiatkowski DL, Thompson HW, Bloom DC.** 2009. The polycomb group protein Bmi1 binds to the herpes simplex virus 1 latent genome and maintains repressive histone marks during latency. J Virol **83:**8173-8181.

484. **Kent JR, Zeng PY, Atanasiu D, Gardner J, Fraser NW, Berger SL.** 2004. During lytic infection herpes simplex virus type 1 is associated with histones

bearing modifications that correlate with active transcription. J Virol **78:**10178-10186.

485. **Huang J, Kent JR, Placek B, Whelan KA, Hollow CM, Zeng PY, Fraser NW, Berger SL.** 2006. Trimethylation of histone H3 lysine 4 by Set1 in the lytic infection of human herpes simplex virus 1. J Virol **80:**5740-5746.

486. **Lieberman PM.** 2013. Keeping it quiet: chromatin control of gammaherpesvirus latency. Nat Rev Microbiol **11:**863-875.

487. **Wu SY, Lee AY, Hou SY, Kemper JK, Erdjument-Bromage H, Tempst P, Chiang CM.** 2006. Brd4 links chromatin targeting to HPV transcriptional silencing. Genes Dev **20:**2383-2396.

488. **Lee AY, Chiang CM.** 2009. Chromatin adaptor Brd4 modulates E2 transcription activity and protein stability. J Biol Chem **284:**2778-2786.

489. **Favre M, Breitburd F, Croissant O, Orth G.** 1977. Chromatin-like structures obtained after alkaline disruption of bovine and human papillomaviruses. J Virol **21:**1205-1209.

490. **Ilves I, Kivi S, Ustav M.** 1999. Long-term episomal maintenance of bovine papillomavirus type 1 plasmids is determined by attachment to host chromosomes, which Is mediated by the viral E2 protein and its binding sites. J Virol **73:**4404-4412.

491. **Skiadopoulos MH, McBride AA.** 1998. Bovine papillomavirus type 1 genomes and the E2 transactivator protein are closely associated with mitotic chromatin. J Virol **72:**2079-2088.

492. **Jang MK, Kwon D, McBride AA.** 2009. Papillomavirus E2 proteins and the host BRD4 protein associate with transcriptionally active cellular chromatin. J Virol **83:**2592-2600.

493. **Baxter MK, McPhillips MG, Ozato K, McBride AA.** 2005. The mitotic chromosome binding activity of the papillomavirus E2 protein correlates with interaction with the cellular chromosomal protein, Brd4. J Virol **79:**4806-4818.

494. **Schweiger MR, You J, Howley PM.** 2006. Bromodomain protein 4 mediates the papillomavirus E2 transcriptional activation function. J Virol **80:**4276-4285.

495. **Chen HS, Lu F, Lieberman PM.** 2013. Epigenetic regulation of EBV and KSHV latency. Curr Opin Virol **3:**251-259.

496. **Knipe DM, Cliffe A.** 2008. Chromatin control of herpes simplex virus lytic and latent infection. Nat Rev Microbiol **6:**211-221.

497. **Lusic M, Giacca M.** 2015. Regulation of HIV-1 latency by chromatin structure and nuclear architecture. J Mol Biol **427:**688-694.

498. **Hasan UA, Zannetti C, Parroche P, Goutagny N, Malfroy M, Roblot G, Carreira C, Hussain I, Muller M, Taylor-Papadimitriou J, Picard D, Sylla BS, Trinchieri G, Medzhitov R, Tommasino M.** 2013. The human papillomavirus type 16 E7 oncoprotein induces a transcriptional repressor complex on the Toll-like receptor 9 promoter. J Exp Med **210:**1369-1387.

499. **Andrisani OM.** 2013. Deregulation of epigenetic mechanisms by the hepatitis B virus X protein in hepatocarcinogenesis. Viruses **5:**858-872.

500. **Yang L, He J, Chen L, Wang G.** 2009. Hepatitis B virus X protein upregulates expression of SMYD3 and C-MYC in HepG2 cells. Med Oncol **26:**445-451.
501. **Edelstein LC, Micheva-Viteva S, Phelan BD, Dougherty JP.** 2009. Short communication: activation of latent HIV type 1 gene expression by suberoylanilide hydroxamic acid (SAHA), an HDAC inhibitor approved for use to treat cutaneous T cell lymphoma. AIDS Res Hum Retroviruses **25:**883-887.
502. **Reuse S, Calao M, Kabeya K, Guiguen A, Gatot JS, Quivy V, Vanhulle C, Lamine A, Vaira D, Demonte D, Martinelli V, Veithen E, Cherrier T, Avettand V, Poutrel S, Piette J, de Launoit Y, Moutschen M, Burny A, Rouzioux C, De Wit S, Herbein G, Rohr O, Collette Y, Lambotte O, Clumeck N, Van Lint C.** 2009. Synergistic activation of HIV-1 expression by deacetylase inhibitors and prostratin: implications for treatment of latent infection. PLoS One **4:**e6093.
503. **Peters AH, O'Carroll D, Scherthan H, Mechtler K, Sauer S, Schofer C, Weipoltshammer K, Pagani M, Lachner M, Kohlmaier A, Opravil S, Doyle M, Sibilia M, Jenuwein T.** 2001. Loss of the Suv39h histone methyltransferases impairs mammalian heterochromatin and genome stability. Cell **107:**323-337.
504. **Hamid R, Rotshteyn Y, Rabadi L, Parikh R, Bullock P.** 2004. Comparison of alamar blue and MTT assays for high through-put screening. Toxicol In Vitro **18:**703-710.
505. **Opgenorth A, Graham K, Nation N, Strayer D, McFadden G.** 1992. Deletion analysis of two tandemly arranged virulence genes in myxoma virus, M11L and myxoma growth factor. J Virol **66:**4720-4731.
506. **Wasilenko ST, Banadyga L, Bond D, Barry M.** 2005. The vaccinia virus F1L protein interacts with the proapoptotic protein Bak and inhibits Bak activation. J Virol **79:**14031-14043.
507. **Desaulniers MA, University of Alberta. Department of Medical Microbiology and Immunology.** The vaccinia virus N2 protein associates with karyopherins a2 and a4 and reduces the turnover rate of karyopherin a2.
508. **Smallwood SE, Rahman MM, Smith DW, McFadden G.** 2010. Myxoma virus: propagation, purification, quantification, and storage. Curr Protoc Microbiol **Chapter 14:**Unit 14A 11.
509. **Schmittgen TD, Livak KJ.** 2008. Analyzing real-time PCR data by the comparative C(T) method. Nat Protoc **3:**1101-1108.
510. **Strauss WM.** 2001. Preparation of genomic DNA from mammalian tissue. Curr Protoc Mol Biol **Chapter 2:**Unit2 2.
511. **Almeida A, Bolanos JP, Moncada S.** 2010. E3 ubiquitin ligase APC/C-Cdh1 accounts for the Warburg effect by linking glycolysis to cell proliferation. Proc Natl Acad Sci U S A **107:**738-741.
512. **Rintoul JL, Wang J, Gammon DB, van Buuren NJ, Garson K, Jardine K, Barry M, Evans DH, Bell JC.** 2011. A selectable and excisable marker system for the rapid creation of recombinant poxviruses. PLoS One **6:**e24643.

513. **Falkner FG, Moss B.** 1988. Escherichia coli gpt gene provides dominant selection for vaccinia virus open reading frame expression vectors. J Virol **62:**1849-1854.

514. **Lundholm L, Mohme-Lundholm E, Vamos N.** 1963. Lactic acid assay with L(plus)lactic acid dehydrogenase from rabbit muscle. Acta Physiol Scand **58:**243-249.

515. **Bleoo S, Sun X, Hendzel MJ, Rowe JM, Packer M, Godbout R.** 2001. Association of human DEAD box protein DDX1 with a cleavage stimulation factor involved in 3'-end processing of pre-MRNA. Mol Biol Cell **12:**3046-3059.

516. **Boisvert FM, Kruhlak MJ, Box AK, Hendzel MJ, Bazett-Jones DP.** 2001. The transcription coactivator CBP is a dynamic component of the promyelocytic leukemia nuclear body. J Cell Biol **152:**1099-1106.

517. **Zhang XD, Ferrer M, Espeseth AS, Marine SD, Stec EM, Crackower MA, Holder DJ, Heyse JF, Strulovici B.** 2007. The use of strictly standardized mean difference for hit selection in primary RNA interference high-throughput screening experiments. J Biomol Screen **12:**497-509.

518. **Zhang XD, Lacson R, Yang R, Marine SD, McCampbell A, Toolan DM, Hare TR, Kajdas J, Berger JP, Holder DJ, Heyse JF, Ferrer M.** 2010. The Use of SSMD-Based False Discovery and False Nondiscovery Rates in Genome-Scale RNAi Screens. J Biomol Screen doi:1087057110381919 [pii] 10.1177/1087057110381919.

519. **Birmingham A, Selfors LM, Forster T, Wrobel D, Kennedy CJ, Shanks E, Santoyo-Lopez J, Dunican DJ, Long A, Kelleher D, Smith Q, Beijersbergen RL, Ghazal P, Shamu CE.** 2009. Statistical methods for analysis of high-throughput RNA interference screens. Nat Methods **6:**569-575.

520. **Luc PV, Tempst P.** 2004. PINdb: a database of nuclear protein complexes from human and yeast. Bioinformatics **20:**1413-1415.

521. **Werden SJ, McFadden G.** 2008. The role of cell signaling in poxvirus tropism: the case of the M-T5 host range protein of myxoma virus. Biochim Biophys Acta **1784:**228-237.

522. **Spiesschaert B, McFadden G, Hermans K, Nauwynck H, Van de Walle GR.** 2011. The current status and future directions of myxoma virus, a master in immune evasion. Vet Res **42:**76.

523. **Werden SJ, Barrett JW, Wang G, Stanford MM, McFadden G.** 2007. M-T5, the ankyrin repeat, host range protein of myxoma virus, activates Akt and can be functionally replaced by cellular PIKE-A. J Virol **81:**2340-2348.

524. **Wang F, Barrett JW, Ma Y, Dekaban GA, McFadden G.** 2009. Induction of alpha/beta interferon by myxoma virus is selectively abrogated when primary mouse embryo fibroblasts become immortalized. J Virol **83:**5928-5932.

525. **Kim M, Williamson CT, Prudhomme J, Bebb DG, Riabowol K, Lee PW, Lees-Miller SP, Mori Y, Rahman MM, McFadden G, Johnston RN.** 2010. The viral tropism of two distinct oncolytic viruses, reovirus and myxoma virus, is modulated by cellular tumor suppressor gene status. Oncogene **29:**3990-3996.

526. **Cailleau R, Young R, Olive M, Reeves WJ, Jr.** 1974. Breast tumor cell lines from pleural effusions. J Natl Cancer Inst **53:**661-674.

527. **Reichard P.** 1988. Interactions between deoxyribonucleotide and DNA synthesis. Annu Rev Biochem **57:**349-374.

528. **Wright M, Grim J, Deshane J, Kim M, Strong TV, Siegal GP, Curiel DT.** 1997. An intracellular anti-erbB-2 single-chain antibody is specifically cytotoxic to human breast carcinoma cells overexpressing erbB-2. Gene Ther **4:**317-322.

529. **Tzahar E, Moyer JD, Waterman H, Barbacci EG, Bao J, Levkowitz G, Shelly M, Strano S, Pinkas-Kramarski R, Pierce JH, Andrews GC, Yarden Y.** 1998. Pathogenic poxviruses reveal viral strategies to exploit the ErbB signaling network. EMBO J **17:**5948-5963.

530. **Boutros M, Bras LP, Huber W.** 2006. Analysis of cell-based RNAi screens. Genome Biol **7:**R66.

531. **Bonvini P, Zorzi E, Basso G, Rosolen A.** 2007. Bortezomib-mediated 26S proteasome inhibition causes cell-cycle arrest and induces apoptosis in CD-30+ anaplastic large cell lymphoma. Leukemia **21:**838-842.

532. **Satheshkumar PS, Anton LC, Sanz P, Moss B.** 2009. Inhibition of the ubiquitin-proteasome system prevents vaccinia virus DNA replication and expression of intermediate and late genes. J Virol **83:**2469-2479.

533. **Teale A, Campbell S, Van Buuren N, Magee WC, Watmough K, Couturier B, Shipclark R, Barry M.** 2009. Orthopoxviruses require a functional ubiquitin-proteasome system for productive replication. J Virol **83:**2099-2108.

534. **Gottlob K, Majewski N, Kennedy S, Kandel E, Robey RB, Hay N.** 2001. Inhibition of early apoptotic events by Akt/PKB is dependent on the first committed step of glycolysis and mitochondrial hexokinase. Genes Dev **15:**1406-1418.

535. **Pedersen PL, Mathupala S, Rempel A, Geschwind JF, Ko YH.** 2002. Mitochondrial bound type II hexokinase: a key player in the growth and survival of many cancers and an ideal prospect for therapeutic intervention. Biochim Biophys Acta **1555:**14-20.

536. **Wallace DC.** 2005. Mitochondria and cancer: Warburg addressed. Cold Spring Harb Symp Quant Biol **70:**363-374.

537. **Bando H, Atsumi T, Nishio T, Niwa H, Mishima S, Shimizu C, Yoshioka N, Bucala R, Koike T.** 2005. Phosphorylation of the 6-phosphofructo-2-kinase/fructose 2,6-bisphosphatase/PFKFB3 family of glycolytic regulators in human cancer. Clin Cancer Res **11:**5784-5792.

538. **Chen HZ, Tsai SY, Leone G.** 2009. Emerging roles of E2Fs in cancer: an exit from cell cycle control. Nat Rev Cancer **9:**785-797.

539. **Cover CM, Hsieh SJ, Tran SH, Hallden G, Kim GS, Bjeldanes LF, Firestone GL.** 1998. Indole-3-carbinol inhibits the expression of cyclin-dependent kinase-6 and induces a G1 cell cycle arrest of human breast cancer cells independent of estrogen receptor signaling. J Biol Chem **273:**3838-3847.

540. **Bell SP, Dutta A.** 2002. DNA replication in eukaryotic cells. Annu Rev Biochem **71:**333-374.

541. **Sherr CJ.** 1995. D-type cyclins. Trends Biochem Sci **20:**187-190.
542. **Kaldis P.** 1999. The cdk-activating kinase (CAK): from yeast to mammals. Cell Mol Life Sci **55:**284-296.
543. **Gao G, Bracken AP, Burkard K, Pasini D, Classon M, Attwooll C, Sagara M, Imai T, Helin K, Zhao J.** 2003. NPAT expression is regulated by E2F and is essential for cell cycle progression. Mol Cell Biol **23:**2821-2833.
544. **Watanabe N, Arai H, Nishihara Y, Taniguchi M, Watanabe N, Hunter T, Osada H.** 2004. M-phase kinases induce phospho-dependent ubiquitination of somatic Wee1 by SCFbeta-TrCP. Proc Natl Acad Sci U S A **101:**4419-4424.
545. **Negrini M, Sabbioni S, Haldar S, Possati L, Castagnoli A, Corallini A, Barbanti-Brodano G, Croce CM.** 1994. Tumor and growth suppression of breast cancer cells by chromosome 17-associated functions. Cancer Res **54:**1818-1824.
546. **Reinhardt HC, Aslanian AS, Lees JA, Yaffe MB.** 2007. p53-deficient cells rely on ATM- and ATR-mediated checkpoint signaling through the p38MAPK/MK2 pathway for survival after DNA damage. Cancer Cell **11:**175-189.
547. **Liaw H, Lee D, Myung K.** 2011. DNA-PK-dependent RPA2 hyperphosphorylation facilitates DNA repair and suppresses sister chromatid exchange. PLoS One **6:**e21424.
548. **Loffler H, Rebacz B, Ho AD, Lukas J, Bartek J, Kramer A.** 2006. Chk1-dependent regulation of Cdc25B functions to coordinate mitotic events. Cell Cycle **5:**2543-2547.
549. **Sorensen CS, Syljuasen RG.** 2012. Safeguarding genome integrity: the checkpoint kinases ATR, CHK1 and WEE1 restrain CDK activity during normal DNA replication. Nucleic Acids Res **40:**477-486.
550. **Lobjois V, Froment C, Braud E, Grimal F, Burlet-Schiltz O, Ducommun B, Bouche JP.** 2011. Study of the docking-dependent PLK1 phosphorylation of the CDC25B phosphatase. Biochem Biophys Res Commun **410:**87-90.
551. **Lee HJ, Hwang HI, Jang YJ.** 2010. Mitotic DNA damage response: Polo-like kinase-1 is dephosphorylated through ATM-Chk1 pathway. Cell Cycle **9:**2389-2398.
552. **Lan W, Cleveland DW.** 2010. A chemical tool box defines mitotic and interphase roles for Mps1 kinase. J Cell Biol **190:**21-24.
553. **Lara-Gonzalez P, Scott MI, Diez M, Sen O, Taylor SS.** 2011. BubR1 blocks substrate recruitment to the APC/C in a KEN-box-dependent manner. J Cell Sci **124:**4332-4345.
554. **Lee SH, Sterling H, Burlingame A, McCormick F.** 2008. Tpr directly binds to Mad1 and Mad2 and is important for the Mad1-Mad2-mediated mitotic spindle checkpoint. Genes Dev **22:**2926-2931.
555. **Pyronnet S, Dostie J, Sonenberg N.** 2001. Suppression of cap-dependent translation in mitosis. Genes Dev **15:**2083-2093.
556. **Barford D.** 2011. Structural insights into anaphase-promoting complex function and mechanism. Philos Trans R Soc Lond B Biol Sci **366:**3605-3624.
557. **Finn RS, Dering J, Conklin D, Kalous O, Cohen DJ, Desai AJ, Ginther C, Atefi M, Chen I, Fowst C, Los G, Slamon DJ.** 2009. PD 0332991, a selective

cyclin D kinase 4/6 inhibitor, preferentially inhibits proliferation of luminal estrogen receptor-positive human breast cancer cell lines in vitro. Breast Cancer Res **11:**R77.

558. **Tseng BY, Ahlem CN.** 1982. DNA primase activity from human lymphocytes. Synthesis of oligoribonucleotides that prime DNA synthesis. J Biol Chem **257:**7280-7283.

559. **Yagura T, Kozu T, Seno T, Saneyoshi M, Hiraga S, Nagano H.** 1983. Novel form of DNA polymerase alpha associated with DNA primase activity of vertebrates. Detection with mouse stimulating factor. J Biol Chem **258:**13070-13075.

560. **Frick DN, Richardson CC.** 2001. DNA primases. Annu Rev Biochem **70:**39-80.

561. **Griffiths DJ, Liu VF, Nurse P, Wang TS.** 2001. Role of fission yeast primase catalytic subunit in the replication checkpoint. Mol Biol Cell **12:**115-128.

562. **Lin YC, Li J, Irwin CR, Jenkins H, DeLange L, Evans DH.** 2008. Vaccinia virus DNA ligase recruits cellular topoisomerase II to sites of viral replication and assembly. J Virol **82:**5922-5932.

563. **Cho HY, Imani F, Miller-DeGraff L, Walters D, Melendi GA, Yamamoto M, Polack FP, Kleeberger SR.** 2009. Antiviral activity of Nrf2 in a murine model of respiratory syncytial virus disease. Am J Respir Crit Care Med **179:**138-150.

564. **Schachtele SJ, Hu S, Lokensgard JR.** 2012. Modulation of experimental herpes encephalitis-associated neurotoxicity through sulforaphane treatment. PLoS One **7:**e36216.

565. **Lenzi M, Fimognari C, Hrelia P.** 2014. Sulforaphane as a promising molecule for fighting cancer. Cancer Treat Res **159:**207-223.

566. **Singh SV, Herman-Antosiewicz A, Singh AV, Lew KL, Srivastava SK, Kamath R, Brown KD, Zhang L, Baskaran R.** 2004. Sulforaphane-induced G2/M phase cell cycle arrest involves checkpoint kinase 2-mediated phosphorylation of cell division cycle 25C. J Biol Chem **279:**25813-25822.

567. **Zeng X, Sigoillot F, Gaur S, Choi S, Pfaff KL, Oh DC, Hathaway N, Dimova N, Cuny GD, King RW.** 2010. Pharmacologic inhibition of the anaphase-promoting complex induces a spindle checkpoint-dependent mitotic arrest in the absence of spindle damage. Cancer Cell **18:**382-395.

568. **Guerra S, Lopez-Fernandez LA, Pascual-Montano A, Munoz M, Harshman K, Esteban M.** 2003. Cellular gene expression survey of vaccinia virus infection of human HeLa cells. J Virol **77:**6493-6506.

569. **Rubins KH, Hensley LE, Relman DA, Brown PO.** 2011. Stunned silence: gene expression programs in human cells infected with monkeypox or vaccinia virus. PLoS One **6:**e15615.

570. **Yang Z, Bruno DP, Martens CA, Porcella SF, Moss B.** 2010. Simultaneous high-resolution analysis of vaccinia virus and host cell transcriptomes by deep RNA sequencing. Proc Natl Acad Sci U S A **107:**11513-11518.

571. **Top S, Foulon E, Pignolet B, Deplanche M, Caubet C, Tasca C, Bertagnoli S, Meyer G, Foucras G.** 2011. Infection of nonhost species dendritic cells in

vitro with an attenuated myxoma virus induces gene expression that predicts its efficacy as a vaccine vector. J Virol **85:**12982-12994.

572. **Abhiman S, Iyer LM, Aravind L.** 2008. BEN: a novel domain in chromatin factors and DNA viral proteins. Bioinformatics **24:**458-461.

573. **Dai Q, Ren A, Westholm JO, Serganov AA, Patel DJ, Lai EC.** 2013. The BEN domain is a novel sequence-specific DNA-binding domain conserved in neural transcriptional repressors. Genes Dev **27:**602-614.

574. **Sathyan KM, Shen Z, Tripathi V, Prasanth KV, Prasanth SG.** 2011. A BEN-domain-containing protein associates with heterochromatin and represses transcription. J Cell Sci **124:**3149-3163.

575. **Noma K, Allis CD, Grewal SI.** 2001. Transitions in distinct histone H3 methylation patterns at the heterochromatin domain boundaries. Science **293:**1150-1155.

576. **Regha K, Sloane MA, Huang R, Pauler FM, Warczok KE, Melikant B, Radolf M, Martens JH, Schotta G, Jenuwein T, Barlow DP.** 2007. Active and repressive chromatin are interspersed without spreading in an imprinted gene cluster in the mammalian genome. Mol Cell **27:**353-366.

577. **Schotta G, Lachner M, Sarma K, Ebert A, Sengupta R, Reuter G, Reinberg D, Jenuwein T.** 2004. A silencing pathway to induce H3-K9 and H4-K20 trimethylation at constitutive heterochromatin. Genes Dev **18:**1251-1262.

578. **Ramsey-Ewing A, Moss B.** 1998. Apoptosis induced by a postbinding step of vaccinia virus entry into Chinese hamster ovary cells. Virology **242:**138-149.

579. **Broyles SS.** 2003. Vaccinia virus transcription. J Gen Virol **84:**2293-2303.

580. **Moss B.** 1990. Regulation of vaccinia virus transcription. Annu Rev Biochem **59:**661-688.

581. **Taddie JA, Traktman P.** 1993. Genetic characterization of the vaccinia virus DNA polymerase: cytosine arabinoside resistance requires a variable lesion conferring phosphonoacetate resistance in conjunction with an invariant mutation localized to the 3'-5' exonuclease domain. J Virol **67:**4323-4336.

582. **Kufe DW, Major PP, Egan EM, Beardsley GP.** 1980. Correlation of cytotoxicity with incorporation of ara-C into DNA. J Biol Chem **255:**8997-8900.

583. **Ennis HL, Lubin M.** 1964. Cycloheximide: Aspects of Inhibition of Protein Synthesis in Mammalian Cells. Science **146:**1474-1476.

584. **Peters AH, Kubicek S, Mechtler K, O'Sullivan RJ, Derijck AA, Perez-Burgos L, Kohlmaier A, Opravil S, Tachibana M, Shinkai Y, Martens JH, Jenuwein T.** 2003. Partitioning and plasticity of repressive histone methylation states in mammalian chromatin. Mol Cell **12:**1577-1589.

585. **Lehnertz B, Ueda Y, Derijck AA, Braunschweig U, Perez-Burgos L, Kubicek S, Chen T, Li E, Jenuwein T, Peters AH.** 2003. Suv39h-mediated histone H3 lysine 9 methylation directs DNA methylation to major satellite repeats at pericentric heterochromatin. Curr Biol **13:**1192-1200.

586. **Nielsen SJ, Schneider R, Bauer UM, Bannister AJ, Morrison A, O'Carroll D, Firestein R, Cleary M, Jenuwein T, Herrera RE, Kouzarides T.** 2001. Rb targets histone H3 methylation and HP1 to promoters. Nature **412:**561-565.

587. **Parrish S, Resch W, Moss B.** 2007. Vaccinia virus D10 protein has mRNA decapping activity, providing a mechanism for control of host and viral gene expression. Proc Natl Acad Sci U S A **104:**2139-2144.
588. **Parrish S, Moss B.** 2007. Characterization of a second vaccinia virus mRNA-decapping enzyme conserved in poxviruses. J Virol **81:**12973-12978.
589. **McDonald D, Carrero G, Andrin C, de Vries G, Hendzel MJ.** 2006. Nucleoplasmic beta-actin exists in a dynamic equilibrium between low-mobility polymeric species and rapidly diffusing populations. J Cell Biol **172:**541-552.
590. **Aoyagi M, Zhai D, Jin C, Aleshin AE, Stec B, Reed JC, Liddington RC.** 2007. Vaccinia virus N1L protein resembles a B cell lymphoma-2 (Bcl-2) family protein. Protein Sci **16:**118-124.
591. **Cooray S, Bahar MW, Abrescia NG, McVey CE, Bartlett NW, Chen RA, Stuart DI, Grimes JM, Smith GL.** 2007. Functional and structural studies of the vaccinia virus virulence factor N1 reveal a Bcl-2-like anti-apoptotic protein. J Gen Virol **88:**1656-1666.
592. **Maluquer de Motes C, Cooray S, Ren H, Almeida GM, McGourty K, Bahar MW, Stuart DI, Grimes JM, Graham SC, Smith GL.** 2011. Inhibition of apoptosis and NF-kappaB activation by vaccinia protein N1 occur via distinct binding surfaces and make different contributions to virulence. PLoS Pathog **7:**e1002430.
593. **Ferguson BJ, Benfield CT, Ren H, Lee VH, Frazer GL, Strnadova P, Sumner RP, Smith GL.** 2013. Vaccinia virus protein N2 is a nuclear IRF3 inhibitor that promotes virulence. J Gen Virol **94:**2070-2081.
594. **Hinthong O, Jin XL, Shisler JL.** 2008. Characterization of wild-type and mutant vaccinia virus M2L proteins' abilities to localize to the endoplasmic reticulum and to inhibit NF-kappaB activation during infection. Virology **373:**248-262.
595. **Shisler JL, Jin XL.** 2004. The vaccinia virus K1L gene product inhibits host NF-kappaB activation by preventing IkappaBalpha degradation. J Virol **78:**3553-3560.
596. **Bradley RR, Terajima M.** 2005. Vaccinia virus K1L protein mediates host-range function in RK-13 cells via ankyrin repeat and may interact with a cellular GTPase-activating protein. Virus Res **114:**104-112.
597. **Meng X, Jiang C, Arsenio J, Dick K, Cao J, Xiang Y.** 2009. Vaccinia virus K1L and C7L inhibit antiviral activities induced by type I interferons. J Virol **83:**10627-10636.
598. **Zhou J, Sun XY, Fernando GJ, Frazer IH.** 1992. The vaccinia virus K2L gene encodes a serine protease inhibitor which inhibits cell-cell fusion. Virology **189:**678-686.
599. **Davies MV, Elroy-Stein O, Jagus R, Moss B, Kaufman RJ.** 1992. The vaccinia virus K3L gene product potentiates translation by inhibiting double-stranded-RNA-activated protein kinase and phosphorylation of the alpha subunit of eukaryotic initiation factor 2. J Virol **66:**1943-1950.
600. **Carroll K, Elroy-Stein O, Moss B, Jagus R.** 1993. Recombinant vaccinia virus K3L gene product prevents activation of double-stranded RNA-dependent,

initiation factor 2 alpha-specific protein kinase. J Biol Chem **268:**12837-12842.

601. **Eckert D, Williams O, Meseda CA, Merchlinsky M.** 2005. Vaccinia virus nicking-joining enzyme is encoded by K4L (VACWR035). J Virol **79:**15084-15090.

602. **Cao JX, Koop BF, Upton C.** 1997. A human homolog of the vaccinia virus HindIII K4L gene is a member of the phospholipase D superfamily. Virus Res **48:**11-18.

603. **Di Pilato M, Mejias-Perez E, Zonca M, Perdiguero B, Gomez CE, Trakala M, Nieto J, Najera JL, Sorzano CO, Combadiere C, Pantaleo G, Planelles L, Esteban M.** 2015. NFkappaB activation by modified vaccinia virus as a novel strategy to enhance neutrophil migration and HIV-specific T-cell responses. Proc Natl Acad Sci U S A **112:**E1333-1342.

604. **Benfield CT, Ren H, Lucas SJ, Bahsoun B, Smith GL.** 2013. Vaccinia virus protein K7 is a virulence factor that alters the acute immune response to infection. J Gen Virol **94:**1647-1657.

605. **Stewart TL, Wasilenko ST, Barry M.** 2005. Vaccinia virus F1L protein is a tail-anchored protein that functions at the mitochondria to inhibit apoptosis. J Virol **79:**1084-1098.

606. **Taylor JM, Quilty D, Banadyga L, Barry M.** 2006. The vaccinia virus protein F1L interacts with Bim and inhibits activation of the pro-apoptotic protein Bax. J Biol Chem **281:**39728-39739.

607. **Postigo A, Cross JR, Downward J, Way M.** 2006. Interaction of F1L with the BH3 domain of Bak is responsible for inhibiting vaccinia-induced apoptosis. Cell Death Differ **13:**1651-1662.

608. **Millns AK, Carpenter MS, DeLange AM.** 1994. The vaccinia virus-encoded uracil DNA glycosylase has an essential role in viral DNA replication. Virology **198:**504-513.

609. **Prichard MN, Kern ER, Quenelle DC, Keith KA, Moyer RW, Turner PC.** 2008. Vaccinia virus lacking the deoxyuridine triphosphatase gene (F2L) replicates well in vitro and in vivo, but is hypersensitive to the antiviral drug (N)-methanocarbathymidine. Virol J **5:**39.

610. **Froggatt GC, Smith GL, Beard PM.** 2007. Vaccinia virus gene F3L encodes an intracellular protein that affects the innate immune response. J Gen Virol **88:**1917-1921.

611. **Xiao-Dan Yao DHE.** 2004. Construction of Recombinant Vaccinia Viruses Using Leporipoxvirus-Catalyzed Recombination and Reactivation of Orthopoxvirus DNA. *In* Isaacs SN (ed), Vaccinia virus and poxvirology methods and protocols Humana Press, Totowa, N.J. http://dx.doi.org/10.1385/1592597890.

612. **Twardzik DR, Brown JP, Ranchalis JE, Todaro GJ, Moss B.** 1985. Vaccinia virus-infected cells release a novel polypeptide functionally related to transforming and epidermal growth factors. Proc Natl Acad Sci U S A **82:**5300-5304.

613. **Chang W, Upton C, Hu SL, Purchio AF, McFadden G.** 1987. The genome of Shope fibroma virus, a tumorigenic poxvirus, contains a growth factor gene

with sequence similarity to those encoding epidermal growth factor and transforming growth factor alpha. Mol Cell Biol **7:**535-540.

614. **Upton C, Macen JL, McFadden G.** 1987. Mapping and sequencing of a gene from myxoma virus that is related to those encoding epidermal growth factor and transforming growth factor alpha. J Virol **61:**1271-1275.

615. **Andrade AA, Silva PN, Pereira AC, De Sousa LP, Ferreira PC, Gazzinelli RT, Kroon EG, Ropert C, Bonjardim CA.** 2004. The vaccinia virus-stimulated mitogen-activated protein kinase (MAPK) pathway is required for virus multiplication. Biochem J **381:**437-446.

616. **Hu N, Yu R, Shikuma C, Shiramizu B, Ostrwoski MA, Yu Q.** 2009. Role of cell signaling in poxvirus-mediated foreign gene expression in mammalian cells. Vaccine **27:**2994-3006.

617. **de Magalhaes JC, Andrade AA, Silva PN, Sousa LP, Ropert C, Ferreira PC, Kroon EG, Gazzinelli RT, Bonjardim CA.** 2001. A mitogenic signal triggered at an early stage of vaccinia virus infection: implication of MEK/ERK and protein kinase A in virus multiplication. J Biol Chem **276:**38353-38360.

618. **Fernandez IF, Blanco S, Lozano J, Lazo PA.** 2010. VRK2 inhibits mitogen-activated protein kinase signaling and inversely correlates with ErbB2 in human breast cancer. Mol Cell Biol **30:**4687-4697.

619. **Blanco S, Sanz-Garcia M, Santos CR, Lazo PA.** 2008. Modulation of interleukin-1 transcriptional response by the interaction between VRK2 and the JIP1 scaffold protein. PLoS One **3:**e1660.

620. **Vilcek J.** 2004. Why are rabbits uniquely sensitive to myxoma virus? Cherchez l'interferon! Nat Immunol **5:**1205-1206.

621. **Robinson SP, Goldstein D, Witt PL, Borden EC, Jordan VC.** 1990. Inhibition of hormone-dependent and independent breast cancer cell growth in vivo and in vitro with the antiestrogen toremifene and recombinant human interferon-alpha 2. Breast Cancer Res Treat **15:**95-101.

622. **Teicher BA, Tomaszewski JE.** 2015. Proteasome Inhibitors. Biochem Pharmacol doi:10.1016/j.bcp.2015.04.008.

623. **Teoh ML, Turner PV, Evans DH.** 2005. Tumorigenic poxviruses up-regulate intracellular superoxide to inhibit apoptosis and promote cell proliferation. J Virol **79:**5799-5811.

624. **Winkler BS, DeSantis N, Solomon F.** 1986. Multiple NADPH-producing pathways control glutathione (GSH) content in retina. Exp Eye Res **43:**829-847.

625. **Mor I, Cheung EC, Vousden KH.** 2011. Control of glycolysis through regulation of PFK1: old friends and recent additions. Cold Spring Harb Symp Quant Biol **76:**211-216.

626. **Holness MJ, Sugden MC.** 2003. Regulation of pyruvate dehydrogenase complex activity by reversible phosphorylation. Biochem Soc Trans **31:**1143-1151.

627. **Mossman K, Lee SF, Barry M, Boshkov L, McFadden G.** 1996. Disruption of M-T5, a novel myxoma virus gene member of poxvirus host range superfamily, results in dramatic attenuation of myxomatosis in infected European rabbits. J Virol **70:**4394-4410.

628. **Werden SJ, Lanchbury J, Shattuck D, Neff C, Dufford M, McFadden G.** 2009. The myxoma virus m-t5 ankyrin repeat host range protein is a novel adaptor that coordinately links the cellular signaling pathways mediated by Akt and Skp1 in virus-infected cells. J Virol **83:**12068-12083.

629. **Satoh Y, Nambu A, Ichikawa T, Onishi H.** 2014. Whole-body total lesion glycolysis measured on fluorodeoxyglucose positron emission tomography/computed tomography as a prognostic variable in metastatic breast cancer. BMC Cancer **14:**525.

630. **Perry JA, Kornbluth S.** 2007. Cdc25 and Wee1: analogous opposites? Cell Div **2:**12.

631. **Flemington EK.** 2001. Herpesvirus lytic replication and the cell cycle: arresting new developments. J Virol **75:**4475-4481.

632. **Buchakjian MR, Kornbluth S.** 2010. The engine driving the ship: metabolic steering of cell proliferation and death. Nat Rev Mol Cell Biol **11:**715-727.

633. **Bao Y, Mukai K, Hishiki T, Kubo A, Ohmura M, Sugiura Y, Matsuura T, Nagahata Y, Hayakawa N, Yamamoto T, Fukuda R, Saya H, Suematsu M, Minamishima YA.** 2013. Energy management by enhanced glycolysis in G1-phase in human colon cancer cells in vitro and in vivo. Mol Cancer Res **11:**973-985.

634. **Sakaue-Sawano A, Kurokawa H, Morimura T, Hanyu A, Hama H, Osawa H, Kashiwagi S, Fukami K, Miyata T, Miyoshi H, Imamura T, Ogawa M, Masai H, Miyawaki A.** 2008. Visualizing spatiotemporal dynamics of multicellular cell-cycle progression. Cell **132:**487-498.

635. **Slezak K, Michalik M, Kowalczyk A, Rokita H.** 2004. YY1 is recruited to the cytoplasm of vaccinia virus-infected human macrophages by the Crm1 system. Virus Res **102:**177-184.
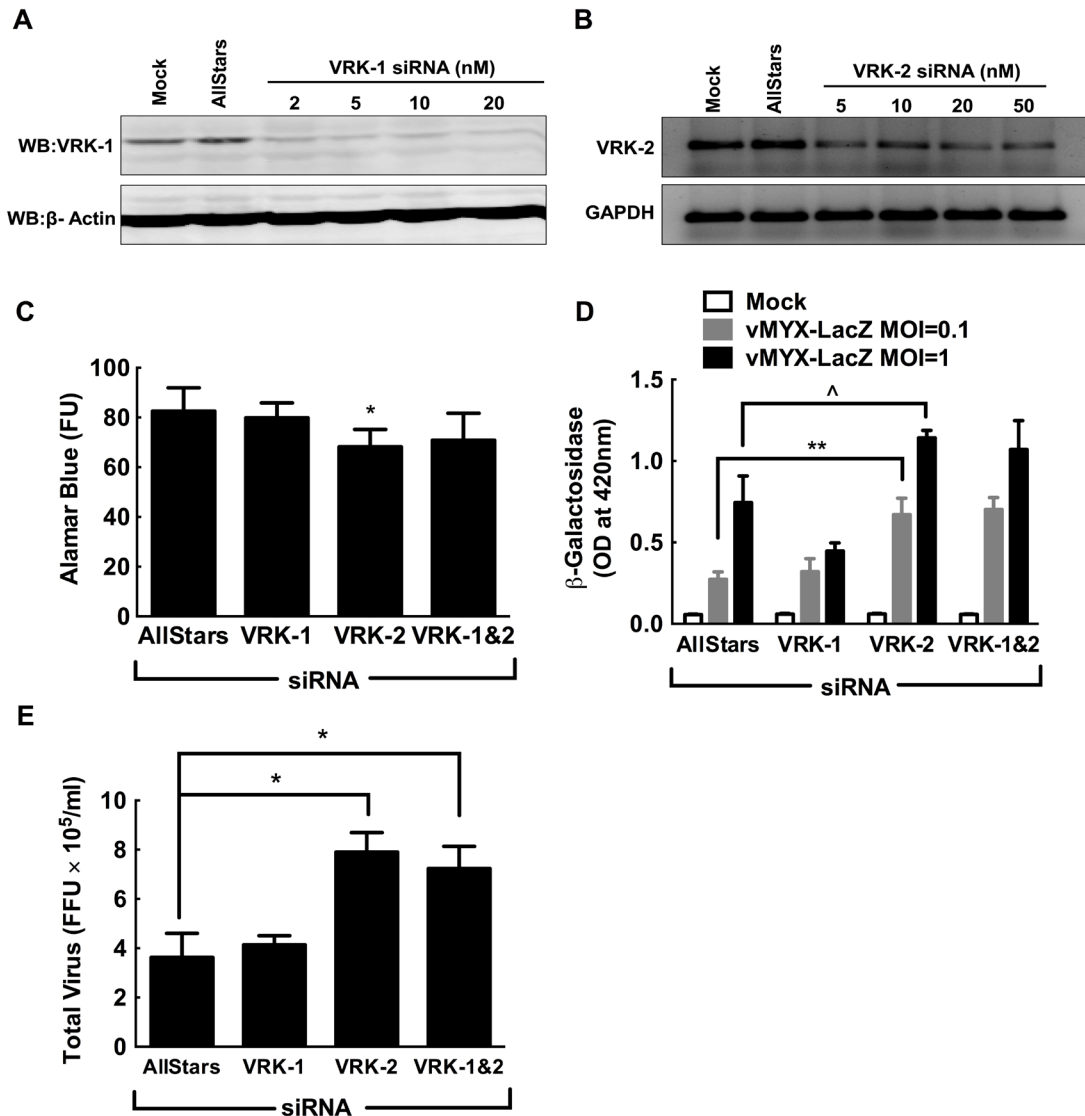
Figure S1. Silencing VRK-2 enhances MYXV replication in MDA-MB-231 cells. MDA-MB-231 cells were transfected with the indicated concentrations of siRNAs for 3 days and then assayed for the effects on VRK-1 (A) or VRK-2 (B) expression by western blotting or RT-PCR, respectively. Subsequent studies used 10nM AllStars and VRK-1 siRNAs and 50nM VRK-2 siRNA although one can detect a slight, but still significant ($p \leq 0.01$), reduction in the viability of cells transfected with 50nM VRK-2 siRNA (C). The cells were also treated with siRNAs for three days, infected with MYXV for 48h and assayed for virus growth using β-galactosidase (D) or plaque (E) assays. Knocking down VRK-2 significantly enhances MYXV growth, but the same effect is not seen in cells treated with siRNAs against VRK-1. The data are representative of three independent experiments. (^, $p \leq 0.05$; *, $p \leq 0.01$; **, $p \leq 0.001$).

A

E5R

GAPDH

VACV-WR   ΔE5R-VACV   rE5R-VACV

B

DNA | H3K9me3 | Merge

No Virus

VACV-WR
9 hpi

ΔE5R-VACV
9 hpi

rE5R-VACV
9 hpi

C

Relative Intensity (H3K9me3)

No Virus   VACV-WR   ΔE5R-VACV   rE5R-VACV

ns   *ns*
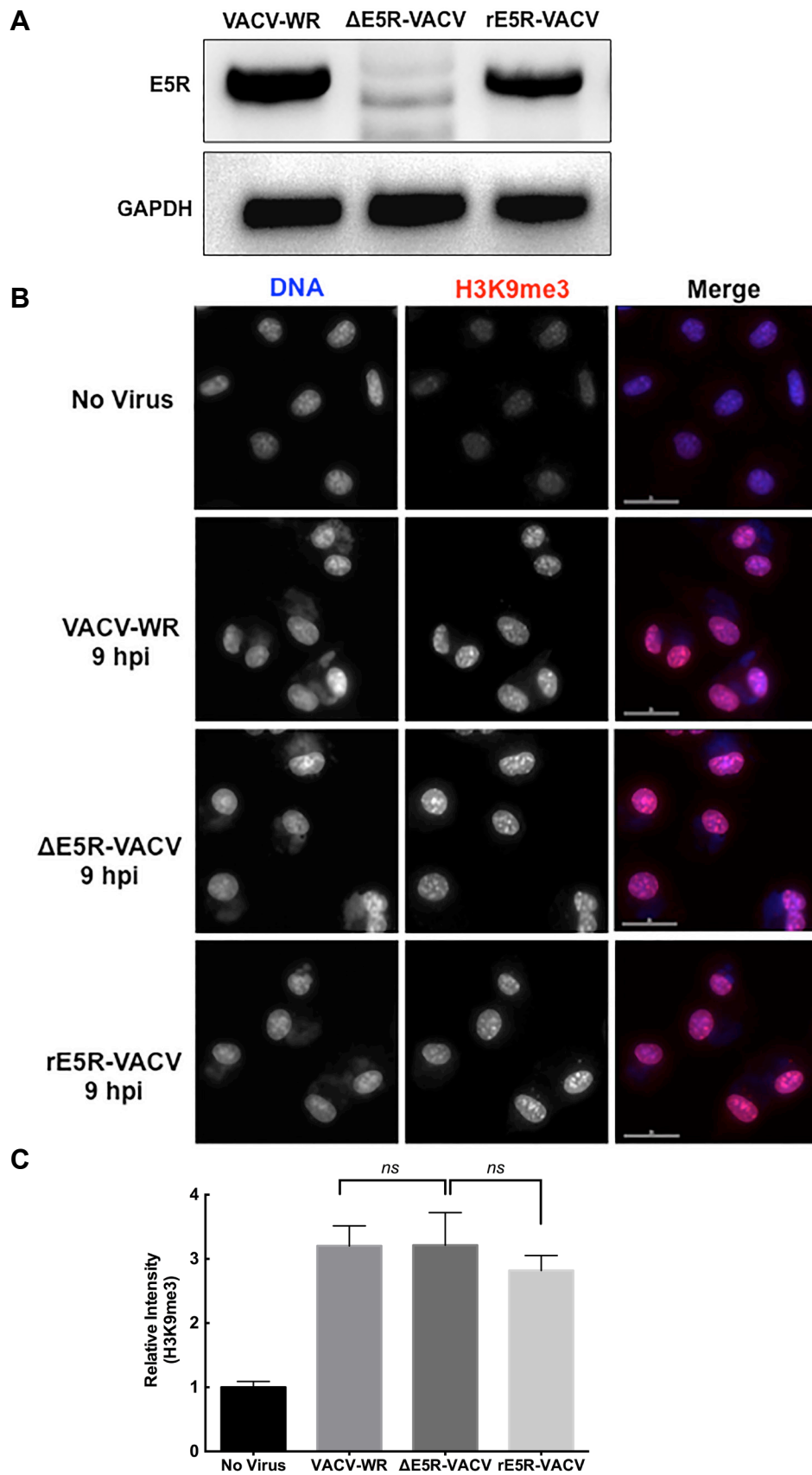
Figure S2. Deleting E5R gene does not change the effect of VACV- infection on H3K9me3. BSC40 cells were infected with VACV-WR, ΔE5R-VACV or rE5R-VACV at MOI of 5 for 9h. (A)Total DNA was extracted and PCR was performed using primers that are specific for E5R and GAPDH. (B) The cells were fixed, stained with antibodies specific for H3K9me3 and immunofluorescence microscopy was performed. DNA was counterstained with DAPI. (C) Total nuclear H3K9me3 intensity was measured by using Image J. Data shown in panels A and B are representative of three independent experiments while (C) shows the mean and standard deviation derived from three independent experiments. (*ns*, non-significant).
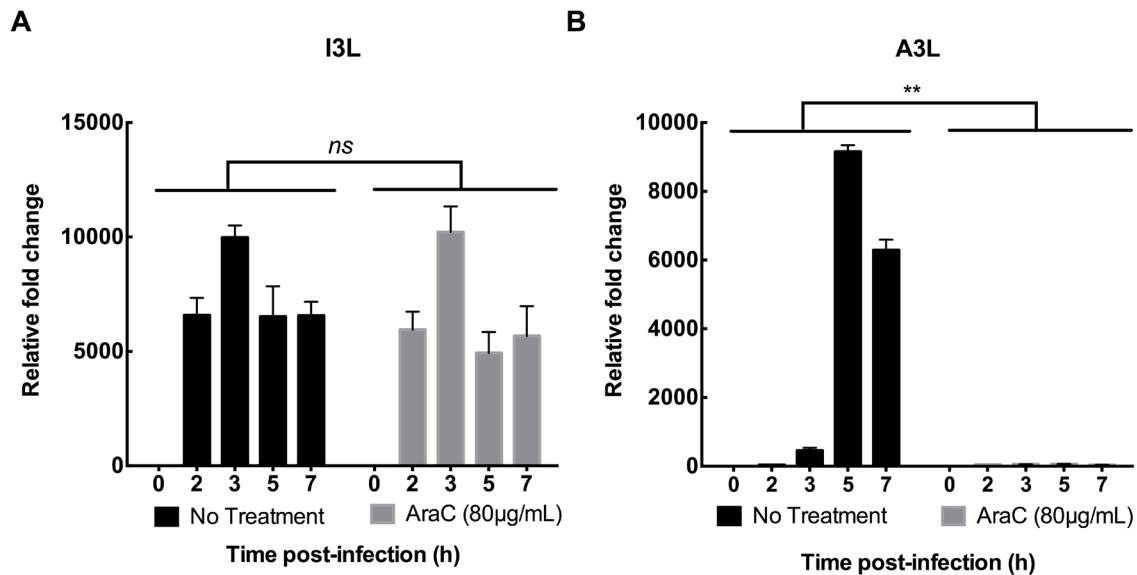
Figure S3. Cytosine arabinoside (araC) inhibits late gene, but not early gene, expression. BSC40 cells were infected with VACV-WR at MOI of 3. Ara C was added in the media one hour after infection. The cells were lyzed with Trizol at the indicated time points and total RNA was isolated. Following cDNA synthesis RT-PCR was performed using primers specific for I3L, an early gene (A), and A3L, a late gene, (B). Analysis was performed using $\Delta\Delta C_T$ method using GAPDH as a housekeeping gene. Data shown are representative of three independent experiments. (*ns*, non-significant; **, *p ≤0.001*).
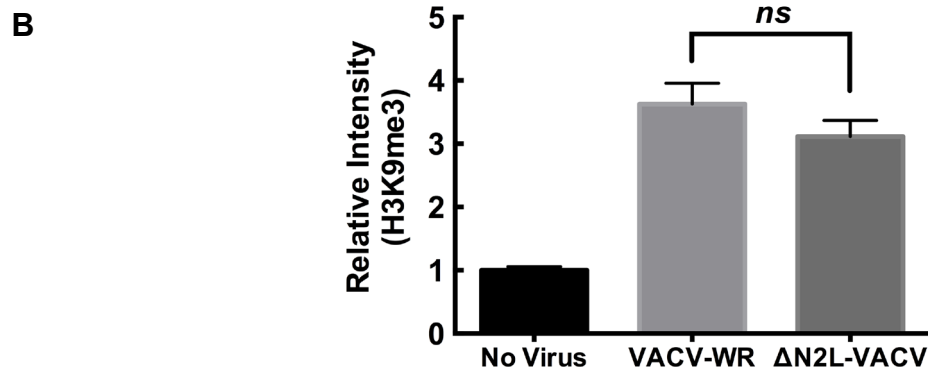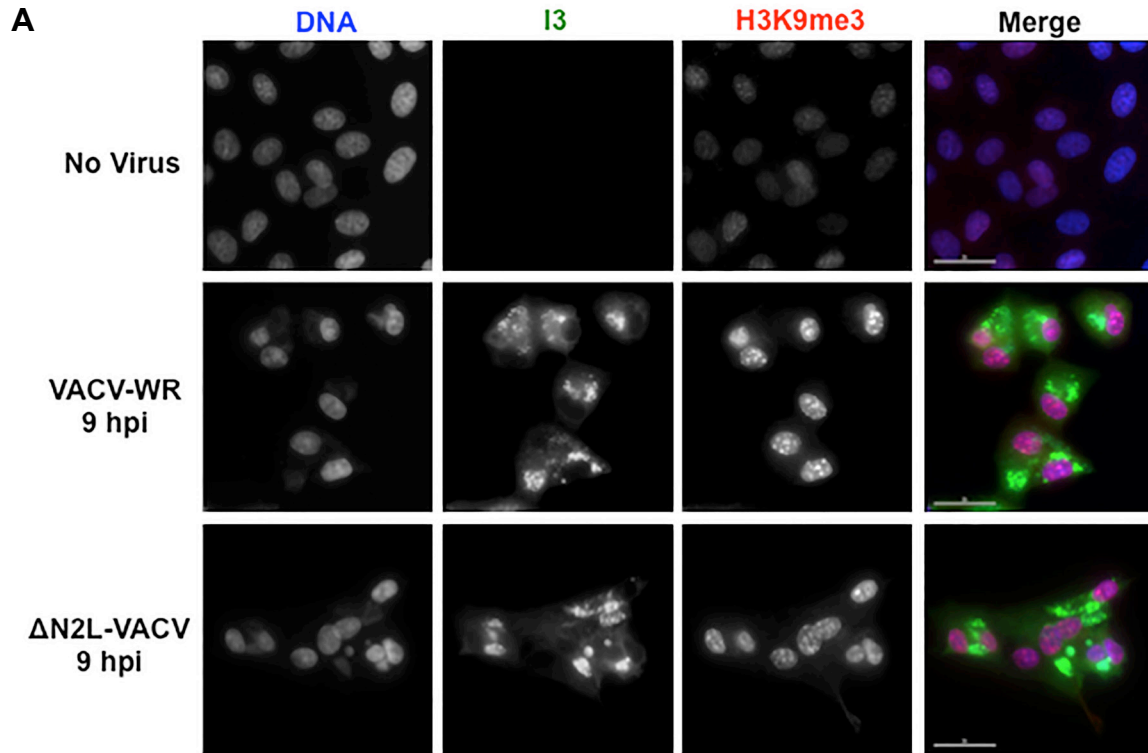
Figure S4. The effect of deleting N2L gene of VACV-WR on H3K9me3 levels. (A) BSC40 cells were infected with VACV-WR or ΔN2L-VACV at MOI of 5 for the indicated time points. Then the cells were fixed and stained for H3K9me3 and I3 using specific antibodies. DNA was counterstained with DAPI. (B) Intensity of nuclear H3K9me3 level was quantified using Image J. (A) shows a representative sample and (B) shows mean and SD of three independent experiments. (*ns*, non-significant).

A

	DNA	I3	H3K9me3	Merge
No Virus				
VACV-WR 9 hpi				
VACV-Cop 9 hpi				
ΔF1L-VACV 9 hpi				

B
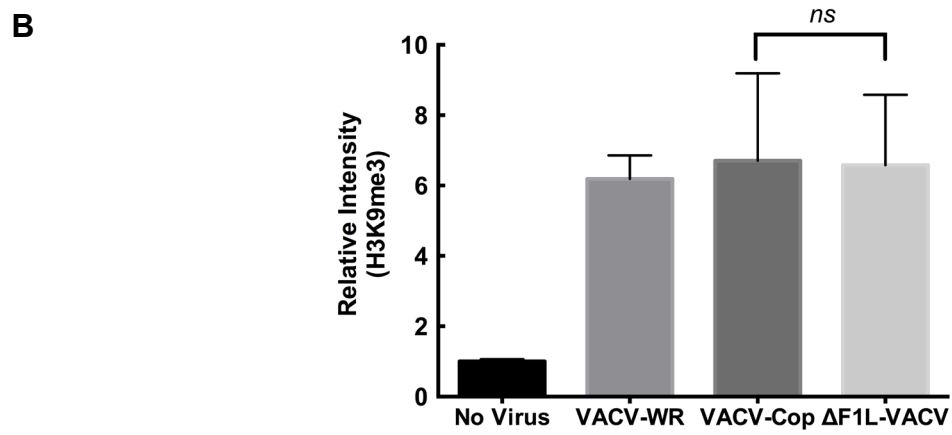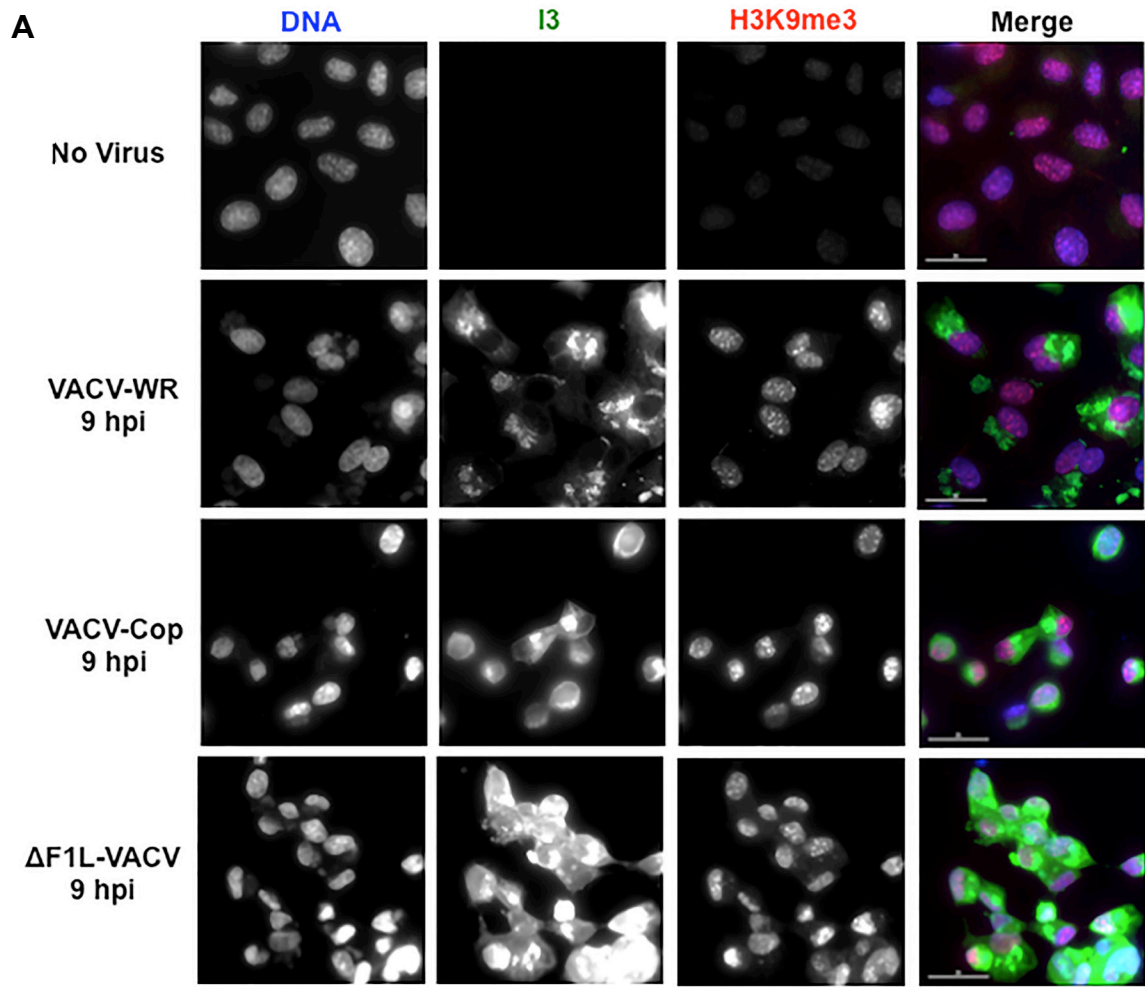
Figure S5. The effect of deleting F1L gene of VACV-Cop on H3K9me3 levels. (A) BSC40 cells were infected with VACV-WR, VACV-Cop or ΔF1L-VACV at MOI of 5 for 9h. Then the cells were fixed and stained for H3K9me3 and I3 using specific antibodies. DNA was counterstained with DAPI. (B) The nuclear intensity of H3K9me3 was quantified using Image J. (A) shows a representative sample and (B) shows mean and SD of three independent experiments. (*ns*, non-significant).
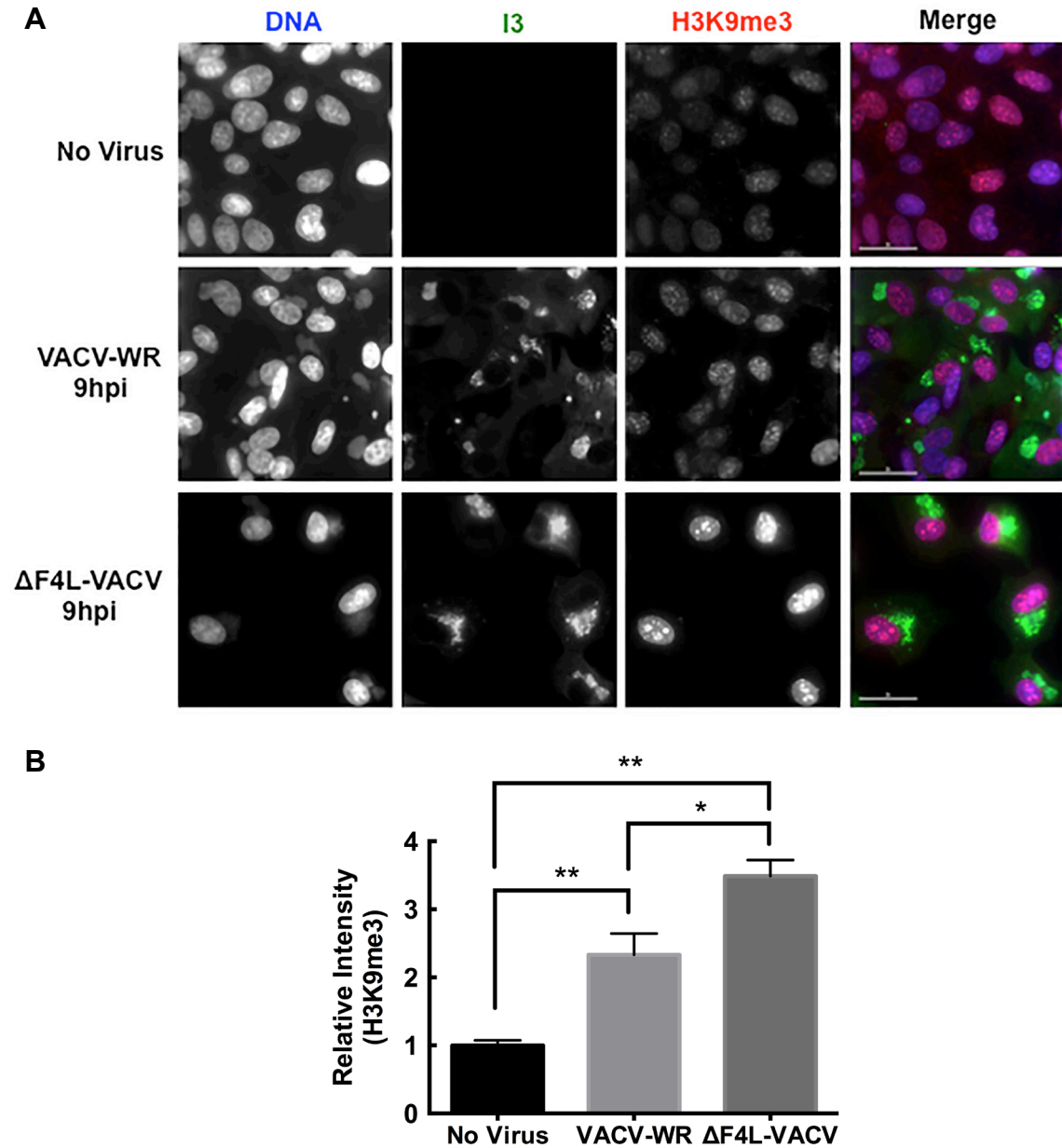
Figure S6. ΔF4L-VACV causes more H3K9me3 induction than VACV-WR in infected cells.
(A) BSC40 cells were infected with VACV-WR or ΔF4L-VACV at MOI of 5 for the indicated time points. Then the cells were fixed and stained for H3K9me3 and I3 using specific antibodies. DNA was counterstained with DAPI. (B) Intensity of nuclear H3K9me3 level was quantified using Image J. (A) shows a representative sample and (B) shows mean and SD of three independent experiments. (*, $p \leq 0.01$; **, $p \leq 0.001$).

A

	No Virus	VACV-WR		
	pControl	pControl	pmyc-K1	pK1-myc

WB: K1-myc   35 kDa

WB: β-actin

B

	DNA	K1L-myc	H3K9me3	Merge

Control plasmid
- No Virus
- VACV-WR 12 hpi
- XY-dBID-VCAV 12 hpi

pK1L-myc
- XY-dBID-VACV 12 hpi

C

ns

Relative Intensity (H3K9me3)

No Virus | VACV-WR | XY-dBID-VACV | XY-dBID-VACV
pControl | | | pK1L-myc

257
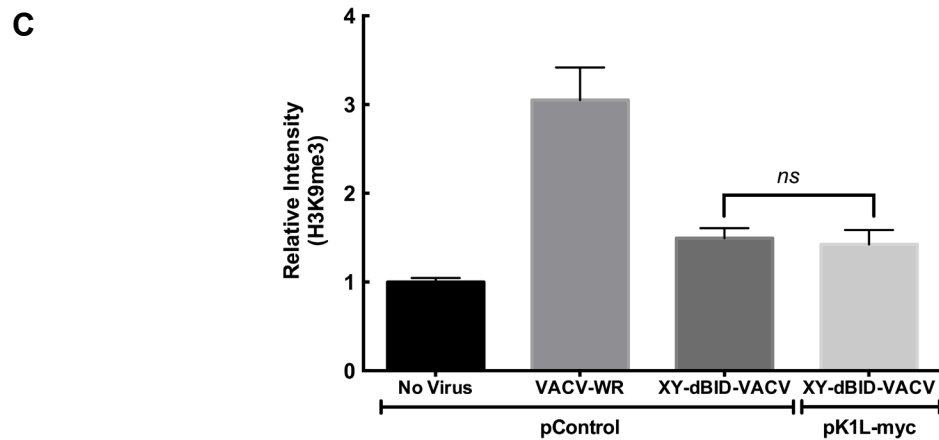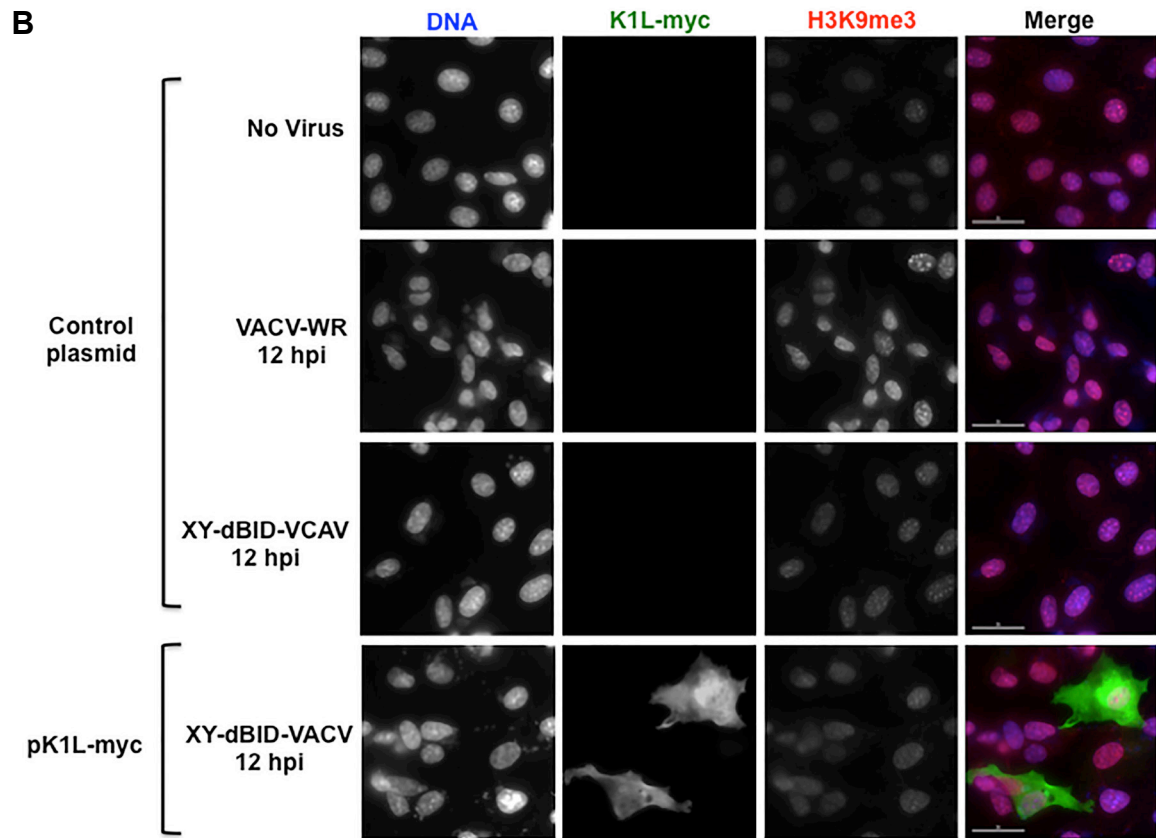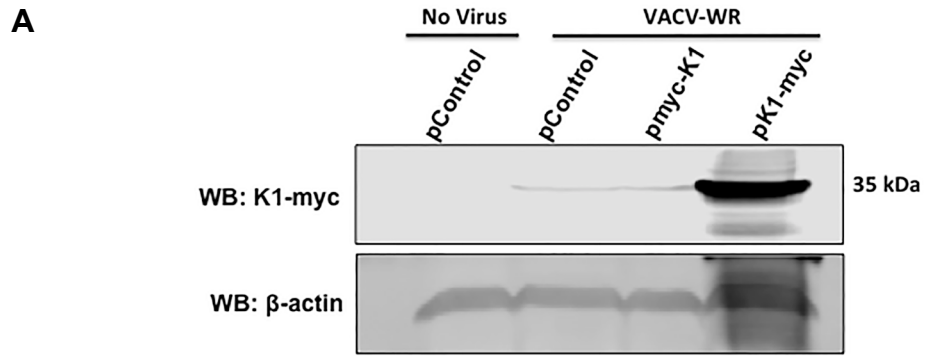
Figure S7. The effect of over-expression of VACV K1L in XY-dBID-VACV infected cells.
(A) BSC40 cells were transfected with an N- or C-terminal *myc* tagged K1L (*myc*-K1L or K1L-*myc*, respectively) under the early late poxvirus promoter, constructed in a TOPO vector, for 24h. Then the cells were lysed and Western blot was performed using the indicated primary antibodies. (B) BSC40 cells were infected with VACV-WR or XY-dBID-VACV at MOI of 5 for 2h, followed by transfection with pK1L-*myc* or control plasmid for 10h (a total of 12h of infection). Then the cells were fixed and stained for H3K9me3 and *myc* using specific antibodies. DNA was counterstained with DAPI. (B) Intensity of nuclear H3K9me3 level was quantified using Image J. (A) shows a representative sample and (B) shows mean and SD of three independent experiments. (*ns*, non-significant).

Table S1. List of gene-hits of the kinase and phosphatase (kinome) screens

RefSeq Accession Number	Gene Symbol	Gene ID	SSMD score in 1st Kinase and Phosphatase Screen	SSMD score in 2nd Kinase and Phosphatase Screen
Genes which decreased vMYX-LacZ replication when silenced with siRNAs				
NM_138981	MAPK10	5602	-9.96	-3.71
NM_004073	PLK3	1263	-9.47	-3.59
NM_001004056	GRK4	2868	-9.00	-3.54
NM_001486	GCKR	2646	-7.95	-4.97
NM_001381	DOK1	1796	-7.86	-4.44
NM_000222	KIT	3815	-7.56	-7.12
NM_002115	HK3	3101	-7.53	-3.02
NM_003390	WEE1	7465	-7.50	-4.89
NM_006218	PIK3CA	5290	-7.06	-4.07
NM_005248	FGR	2268	-6.93	-7.54
NM_001002021	PFKL	5211	-6.48	-3.38
NM_015568	PPP1R16B	26051	-6.31	-7.38
NM_031432	UCK1	83549	-6.11	-3.98
NM_033215	PPP1R3F	89801	-6.08	-6.80
NM_003837	FBP2	8789	-6.03	-5.57
NM_002480	PPP1R12A	4659	-5.89	-6.08
NM_002012	FHIT	2272	-5.80	-5.22
NM_014874	MFN2	9927	-5.80	-6.70
NM_000151	G6PC	2538	-5.80	-6.99
NM_138793	ENTPD8	124583	-5.73	-5.80
NM_000167	GK	2710	-5.72	-3.04
NM_004836	EIF2AK3	9451	-5.63	-3.57
NM_144648	FLJ32786	136332	-5.56	-3.18
NM_178003	PPP2R4	5524	-5.39	-4.61
NM_130436	DYRK1A	1859	-5.39	-6.42
NM_000289	PFKM	5213	-5.37	-5.32
NM_014678	KIAA0685	9701	-5.36	-5.54
XM_496065	ANP32F	440272	-5.33	-6.08
NM_033256	PPP1R14A	94274	-5.19	-3.83
NM_004538	NAP1L3	4675	-5.12	-6.32
NM_017726	PPP1R14D	54866	-5.10	-3.57
NM_021963	NAP1L2	4674	-5.03	-3.04
NM_032593	HINT2	84681	-5.02	-5.54
NM_004119	FLT3	2322	-5.01	-3.14
NM_004901	ENTPD4	9583	-4.97	-5.93
NM_002481	PPP1R12B	4660	-4.91	-3.53
NM_001776	ENTPD1	953	-4.89	-3.72
NM_018638	ETNK1	55500	-4.89	-4.02

RefSeq Accession Number	Gene Symbol	Gene ID	SSMD score in 1st Kinase and Phosphatase Screen	SSMD score in 2nd Kinase and Phosphatase Screen
NM_018401	STK32B	55351	-4.68	-3.43
NM_145687	MAP4K4	9448	-4.62	-3.1
NM_017771	PXK	54899	-4.54	-4.35
NM_001018066	NTRK2	4915	-4.52	-5.05
NM_139354	MATK	4145	-4.51	-2.95
NM_172083	CAMK2B	816	-4.50	-2.99
NM_001249	ENTPD5	957	-4.48	-4.64
NM_198585	UNQ2492	377841	-4.41	-4.55
NM_005204	MAP3K8	1326	-4.40	-4.57
XM_499479	LOC442731	442731	-4.40	-6.37
NM_012229	NT5C2	22978	-4.39	-3.25
NM_002031	FRK	2444	-4.36	-4.16
XM_372654	LOC390760	390760	-4.25	-4.56
XM_496862	LOC441215	441215	-4.25	-4.22
XM_497861	LOC339819	339819	-4.17	-3.29
NM_183246	PHACTR3	116154	-4.15	-5.57
NM_014721	C6orf56	9749	-4.14	-4.07
NM_005923	MAP3K5	4217	-4.06	-3.17
NM_001211	BUB1B	701	-3.99	-3.3
NM_002625	PFKFB1	5207	-3.94	-3.62
NM_001248	ENTPD3	956	-3.87	-5.79
NM_007314	ABL2	27	-3.83	-3.17
NM_138689	PPP1R14B	26472	-3.53	-3.90
NM_001033578	SGKL	23678	-3.47	-5.34
NM_181493	ITPA	3704	-3.42	-3.15
NM_004409	DMPK	1760	-3.29	-7.35
NM_001721	BMX	660	-3.23	-4.14
NM_005028	PIP5K2A	5305	-3.19	-3.8
NM_000788	DCK	1633	-3.09	-7.03
NM_003331	TYK2	7297	-3.07	-3.24
NM_016281	JIK	51347	-3.06	-4.92
NM_020666	CLK4	57396	-2.93	-5.4
Genes which increased vMYX-LacZ replication when silenced with siRNAs				
RefSeq Accession Number	**Gene Symbol**	**Gene ID**	**SSMD score in 1st Kinase and Phosphatase Screen**	**SSMD score in 2nd Kinase and Phosphatase Screen**
NM_000061	BTK	695	25.50	3.16
NM_002730	PRKACA	5566	21.71	14.88
NM_006296	VRK2	7444	12.87	5.81
NM_001743	CALM2	805	11.91	4.23
NM_032960	MAPKAPK2	9261	11.43	7.58
NM_006904	PRKDC	5591	11.40	3.88
NM_003384	VRK1	7443	9.11	3.2
NM_000245	MET	4233	8.85	5.83

NM_004570	PIK3C2G	5288	8.66	6.73
NM_017514	PLXNA3	55558	7.75	6
NM_007181	MAP4K1	11184	7.23	3.66
NM_054111	IHPK3	117283	6.61	2.98
NM_020168	PAK6	56924	6.46	5.42
NM_197972	NME7	29922	6.17	5.47
NM_005391	PDK3	5165	5.77	7.88
NM_130474	MADD	8567	5.64	6.06
NM_016231	NLK	51701	4.99	4.38
NM_020152	C21orf7	56911	4.24	4.1
NM_003463	PTP4A1	7803	4.13	4.63
NM_001259	CDK6	1021	4.12	6.88
NM_201284	EGFR	1956	4.08	3.12
NM_002513	NME3	4832	3.60	3.54
NM_201554	DGKA	1606	3.52	6.38
NM_002576	PAK1	5058	3.31	6.71
NM_000507	FBP1	2203	3.27	3.42
NM_031480	RIOK1	83732	2.94	9.29

SSMD = Strictly Standardized Mean Difference

Table S2. List of the final gene-hits of the whole genome screens

Genes which decreased vMYX-LacZ replication when silenced with siRNAs					
RefSeq Accession Number	**Gene Symbol**	**Gene ID**	**SSMD of the whole-genome validation screen**	**SSMD of custom library screen**	**Remark**
NM_033160	ZNF658	26149	-13.46	ND	ND
NM_006325	RAN	5901	-13.36	ND	ND
NM_022752	ZNF574	64763	-13.36	ND	ND
XM_375646	ZNF525	170958	-13.24	ND	ND
NM_152557	ZNF746	155061	-13.24	ND	ND
NM_000477	ALB	213	-13.18	ND	ND
XM_001130425	LOC645864	645864	-13.00	ND	ND
NM_153018	ZFP3	124961	-12.91	ND	ND
XM_939809	LOC650724	650724	-12.85	ND	ND
NM_002923	RGS2	5997	-12.61	0.99	FP
NM_021009	UBC	7316	-12.46	ND	ND
NM_006267	RANBP2	5903	-12.33	ND	ND
NM_001005526	SF3B1	23451	-12.22	ND	ND
XM_932809	LOC645321	645321	-12.10	ND	ND
XM_938635	LOC649563	649563	-12.01	ND	ND
NM_006503	PSMC4	5704	-11.88	-5.07	TP
NM_002809	PSMD3	5709	-11.84	-4.83	TP
NM_017790	RGS3	5998	-11.66	ND	ND
NM_002805	PSMC5	5705	-11.64	-5.49	TP
NM_002370	MAGOH	4116	-11.62	ND	ND
XM_001128039	hCG_1790474	643896	-11.61	ND	ND
NM_000982	RPL21	6144	-11.61	ND	ND
XM_931601	LOC643517	643517	-11.35	ND	ND
NM_002753	MAPK10	5602	-11.32	0.85	FP
NM_003716	CADPS	8618	-11.31	ND	ND
NM_053282	SH2D1B	117157	-11.29	ND	ND
NM_182947	GEFT	115557	-11.27	ND	ND
NM_014949	KIAA0907	22889	-11.25	ND	ND
NM_000779	CYP4B1	1580	-11.21	ND	ND
XM_001128792	LOC728748	728748	-11.19	ND	ND
NM_002804	PSMC3	5702	-11.11	ND	ND
NM_001079538	LOC728242	728242	-11.10	ND	ND
NM_002791	PSMA6	5687	-11.10	ND	ND
NM_002718	PPP2R3A	5523	-10.87	ND	ND
XM_926844	LOC643534	643534	-10.69	ND	ND
NM_006083	IK	3550	-10.66	ND	ND
XM_001131822	LOC729933	729933	-10.57	ND	ND

XM_942370	LOC652741	652741	-10.54	ND	ND
NM_001633	AMBP	259	-10.54	ND	ND
NM_002815	PSMD11	5717	-10.53	ND	ND
NM_001567	INPPL1	3636	-10.38	0.26	FP
NM_152375	KLHDC7A	127707	-10.32	ND	ND
NM_003401	XRCC4	7518	-10.31	ND	ND
XM_001126502	LOC728086	728086	-10.28	ND	ND
NM_020943	KIAA1604	57703	-10.25	ND	ND
NM_018950	HLA-F	3134	-10.16	ND	ND
NM_153221	CILP2	148113	-10.14	ND	ND
XM_945745	LOC644828	644828	-10.13	ND	ND
NM_015076	CDC2L6	23097	-10.05	ND	ND
XM_001126082	LOC727890	727890	-10.03	ND	ND
XM_001133259	LOC729093	729093	-9.97	ND	ND
XM_001131468	LOC729833	729833	-9.96	ND	ND
NM_181842	ZBTB12	221527	-9.95	ND	ND
NM_012368	OR2C1	4993	-9.95	ND	ND
NM_000192	TBX5	6910	-9.91	ND	ND
NM_014591	KCNIP2	30819	-9.90	ND	ND
XM_001130850	LOC645822	645822	-9.84	ND	ND
NM_033141	MAP3K9	4293	-9.83	ND	ND
NM_004761	RGL2	5863	-9.74	5.30	FP
NM_002803	PSMC2	5701	-9.69	ND	ND
XM_942117	LOC652595	652595	-9.67	ND	ND
XM_932240	LOC644558	644558	-9.66	ND	ND
NM_001655	ARCN1	372	-9.64	ND	ND
NM_001012993	C9orf152	401546	-9.64	ND	ND
NM_002807	PSMD1	5707	-9.60	ND	ND
NM_003390	WEE1	7465	-9.58	-5.09	TP
NM_001040179	MCHR2	84539	-9.56	ND	ND
NM_002712	PPP1R7	5510	-9.56	ND	ND
NM_002713	PPP1R8	5511	-9.54	ND	ND
XM_001132853	C3orf49	132200	-9.51	ND	ND
XM_001130568	LOC728392	728392	-9.40	ND	ND
NM_000947	PRIM2	5558	-9.36	ND	TP*
NM_001007255	KLHDC9	126823	-9.25	ND	ND
NM_153271	SNX33	257364	-9.21	ND	ND
NM_006389	HYOU1	10525	-9.21	ND	ND
XM_942254	LOC652673	652673	-9.16	ND	ND
NM_182506	MAGEB10	139422	-9.11	ND	ND
NM_003205	TCF12	6938	-9.07	ND	ND
NM_004884	IGDCC3	9543	-9.07	ND	ND
NM_002519	NPAT	4863	-9.06	ND	ND

NM_002802	PSMC1	5700	-9.01	ND	ND
NM_002808	PSMD2	5708	-9.00	ND	ND
NM_021221	LY6G5B	58496	-8.99	ND	ND
NM_015332	NUDCD3	23386	-8.99	ND	ND
XM_942445	LOC652788	652788	-8.94	ND	ND
NM_001039788	C3orf65	646600	-8.93	ND	ND
NM_001033930	UBA52	7311	-8.92	ND	ND
NM_001042749	STAG2	10735	-8.90	-2.38	B
NM_002481	PPP1R12B	4660	-8.89	ND	ND
XM_001129924	LOC729316	729316	-8.83	ND	ND
XM_937424	LOC653978	653978	-8.82	ND	ND
NM_001080848	CSAG2	728461	-8.81	ND	ND
NM_005301	GPR35	2859	-8.68	ND	ND
NM_176812	CHMP4B	128866	-8.68	ND	ND
XM_001133203	LOC729229	729229	-8.67	ND	ND
NM_001006656	ZNF473	25888	-8.65	ND	ND
XM_059074	LRRC38	126755	-8.63	ND	ND
NM_000022	ADA	100	-8.61	ND	ND
NM_000961	PTGIS	5740	-8.58	ND	ND
NM_001396	DYRK1A	1859	-8.58	ND	ND
NM_003416	ZNF7	7553	-8.55	ND	ND
NM_000102	CYP17A1	1586	-8.52	ND	ND
XM_942107	LOC652586	652586	-8.51	ND	ND
NM_020672	S100A14	57402	-8.40	ND	ND
XM_938562	LOC649486	649486	-8.39	ND	ND
NM_001080543	C19orf29	58509	-8.39	ND	ND
NM_021733	TSKS	60385	-8.37	ND	ND
NM_012451	SYNGR4	23546	-8.33	ND	ND
NM_001013839	EXOC7	23265	-8.27	ND	ND
NM_001274	CHEK1	1111	-8.21	0.41	FP
NM_182495	FAM55B	120406	-8.13	ND	ND
NM_152397	IQCF1	132141	-8.10	ND	ND
NM_000167	GK	2710	-8.08	ND	ND
NM_021047	ZNF253	56242	-8.08	ND	ND
NM_001001961	OR13C3	138803	-8.07	ND	ND
NM_001004316	LEKR1	389170	-8.02	ND	ND
XM_934473	LOC647188	647188	-8.02	ND	ND
NM_144693	ZNF558	148156	-8.01	ND	ND
NM_014347	ZNF324	25799	-7.99	ND	ND
NM_001001329	PRKCSH	5589	-7.97	ND	ND
NM_003010	MAP2K4	6416	-7.96	3.53	FP
XM_001126216	LOC727948	727948	-7.91	ND	ND
NM_002386	MC1R	4157	-7.90	ND	ND

NM_003318	TTK	7272	-7.88	-2.72	B
NM_031464	RPS6KL1	83694	-7.86	ND	ND
NM_002609	PDGFRB	5159	-7.81	ND	ND
NM_013233	STK39	27347	-7.79	ND	ND
XM_001130141	LOC729395	729395	-7.71	ND	ND
NM_032966	CXCR5	643	-7.66	-0.67	FP
NM_000741	CHRM4	1132	-7.61	3.49	FP
NM_002480	PPP1R12A	4659	-7.51	ND	ND
NM_006379	SEMA3C	10512	-7.50	ND	ND
NM_014594	ZNF354C	30832	-7.48	ND	ND
XM_942408	LOC652767	652767	-7.48	ND	ND
NM_144622	DCST2	127579	-7.48	ND	ND
XM_371164	WDR87	83889	-7.44	ND	ND
XM_499019	LOC441119	441119	-7.42	ND	ND
XM_034623	SNRPEL1	414153	-7.41	ND	ND
NM_001040056	MAPK3	5595	-7.39	-0.15	FP
NM_014365	HSPB8	26353	-7.31	ND	ND
NM_015028	TNIK	23043	-7.29	ND	ND
NM_001002759	C10orf78	119392	-7.28	ND	ND
NM_207448	FLJ45256	400511	-7.27	ND	ND
NM_053055	THEM4	117145	-7.24	ND	ND
XM_001129068	LOC731276	731276	-7.24	ND	ND
NM_003422	MZF1	7593	-7.23	ND	ND
NM_052950	WDFY2	115825	-7.17	ND	ND
XM_939332	TRIM75	391714	-7.15	ND	ND
XM_373688	LOC388279	388279	-7.14	ND	ND
NM_001012415	SOHLH1	402381	-7.11	ND	ND
NM_182499	TDRD10	126668	-7.08	ND	ND
NM_004154	P2RY6	5031	-7.04	ND	ND
NM_014874	MFN2	9927	-7.04	ND	ND
NM_133466	ZFP82	284406	-7.03	ND	ND
NM_001004354	NRARP	441478	-6.98	ND	ND
NM_033194	HSPB9	94086	-6.95	ND	ND
NM_006244	PPP2R5B	5526	-6.93	ND	ND
NM_002576	PAK1	5058	-6.92	1.28	FP
NM_001004330	PLEKHG7	440107	-6.89	0.71	FP
NM_001008739	LOC441150	441150	-6.83	ND	ND
NM_003425	ZNF45	7596	-6.82	ND	ND
NM_015354	NUP188	23511	-6.73	ND	ND
NM_182496	CCDC38	120935	-6.73	ND	ND
NM_006385	ZNF211	10520	-6.73	ND	ND
NM_005340	HINT1	3094	-6.72	ND	ND
NM_003331	TYK2	7297	-6.67	-2.87	B

NM_001037984	SLC38A10	124565	-6.66	ND	ND
NM_000032	ALAS2	212	-6.66	ND	ND
NM_002354	TACSTD1	4072	-6.59	ND	ND
XM_372447	LOC390282	390282	-6.51	ND	ND
XM_374461	LOC392713	392713	-6.49	ND	ND
NM_144681	CCDC42	146849	-6.45	ND	ND
NM_005585	SMAD6	4091	-6.45	-2.55	B
NM_005030	PLK1	5347	-6.45	-4.47	TP
NM_001004703	OR4C46	119749	-6.44	ND	ND
XM_061427	LOC119358	119358	-6.39	ND	ND
NM_004107	FCGRT	2217	-6.37	ND	ND
NM_004586	RPS6KA3	6197	-6.31	-1.27	FP
NM_173493	PASD1	139135	-6.31	ND	ND
NM_005400	PRKCE	5581	-6.30	-2.27	B
NM_002749	MAPK7	5598	-6.29	1.40	FP
NM_015896	ZMYND10	51364	-6.26	ND	ND
XM_942460	LOC652799	652799	-6.25	ND	ND
NM_004124	GMFB	2764	-6.21	ND	ND
XM_001131742	LOC731066	731066	-6.20	ND	ND
NM_001012507	C6orf173	387103	-6.19	ND	ND
NM_032134	QRICH2	84074	-6.18	ND	ND
NM_001316	CSE1L	1434	-6.08	ND	ND
XM_925903	FAM22E	283008	-6.06	ND	ND
NM_015343	DULLARD	23399	-6.03	ND	ND
XM_927529	GCNT6	644378	-5.99	ND	ND
NM_001954	DDR1	780	-5.97	ND	ND
XM_943137	LOC642587	642587	-5.93	ND	ND
NM_001040110	NRF1	4899	-5.93	ND	ND
NM_002622	PFDN1	5201	-5.88	ND	ND
NM_033256	PPP1R14A	94274	-5.87	ND	ND
NM_001004715	OR4K17	390436	-5.86	ND	ND
NM_002867	RAB3B	5865	-5.85	ND	ND
NM_015012	TMEM41B	440026	-5.85	ND	ND
NM_003827	NAPA	8775	-5.79	ND	ND
NM_014413	EIF2AK1	27102	-5.79	ND	ND
NM_005204	MAP3K8	1326	-5.77	ND	ND
XM_001128905	hCG_1988300	728638	-5.73	ND	ND
NM_173513	C2orf52	151477	-5.70	ND	ND
NM_003575	ZNF282	8427	-5.69	ND	ND
NM_001004694	OR2T29	343563	-5.68	ND	ND
NM_002816	PSMD12	5718	-5.65	ND	ND
NM_198568	GJB7	375519	-5.64	ND	ND
XM_001127326	LOC728366	728366	-5.58	ND	ND

NM_031965	GSG2	83903	-5.55	ND	ND
NM_182828	GDF7	151449	-5.54	4.11	FP
NM_000017	ACADS	35	-5.53	ND	ND
NM_003420	ZNF35	7584	-5.52	ND	ND
NM_001029976	ZNF16	7564	-5.52	ND	ND
NM_022356	LEPRE1	64175	-5.51	ND	ND
NM_005827	SLC35B1	10237	-5.51	ND	ND
NM_001085430	C17orf67	339210	-5.50	ND	ND
XM_936049	LOC642009	642009	-5.49	ND	ND
XM_001131041	LOC731851	731851	-5.47	ND	ND
NM_153225	RPESP	157869	-5.46	ND	ND
NM_024066	ERI3	79033	-5.36	ND	ND
NM_145268	C7orf45	136263	-5.35	ND	ND
NM_152888	COL22A1	169044	-5.33	ND	ND
NM_030920	ANP32E	81611	-5.29	ND	ND
NM_003756	EIF3H	8667	-5.28	ND	ND
NM_004358	CDC25B	994	-5.26	-1.27	FP
NM_003412	ZIC1	7545	-5.25	ND	ND
NM_002812	PSMD8	5714	-5.24	ND	ND
NM_001222	CAMK2G	818	-5.24	ND	ND
NM_001024680	FBXO48	554251	-5.24	ND	ND
NM_144615	TMIGD2	126259	-5.20	ND	ND
NM_006781	C6orf10	10665	-5.18	ND	ND
NM_138811	C7orf31	136895	-5.14	ND	ND
NM_006419	CXCL13	10563	-5.08	ND	ND
NM_031417	MARK4	57787	-5.03	ND	ND
NM_178470	WDR40B	139170	-5.01	ND	ND
XM_001127448	LOC728432	728432	-4.98	ND	ND
NM_001001410	C16orf42	115939	-4.97	ND	ND
XM_001132682	LOC402635	402635	-4.95	ND	ND
NM_145266	NUDCD2	134492	-4.89	ND	ND
XM_038150	MAST3	23031	-4.87	ND	ND
NM_006366	CAP2	10486	-4.86	ND	ND
NM_001081640	PRKDC	5591	-4.86	ND	ND
XM_001128633	LOC731158	731158	-4.82	ND	ND
NM_001080393	GLT8D4	727936	-4.82	ND	ND
NM_144994	ANKRD23	200539	-4.82	ND	ND
NM_020397	CAMK1D	57118	-4.81	ND	ND
XM_001132625	LOC149157	149157	-4.80	ND	ND
NM_001080511	CLEC2L	154790	-4.77	ND	ND
NM_001727	BRS3	680	-4.77	ND	ND
XM_168053	C6orf184	221261	-4.76	ND	ND
NM_203436	ASCL4	121549	-4.75	ND	ND

NM_001080447	TTLL8	164714	-4.74	ND	ND
NM_022460	HS1BP3	64342	-4.70	ND	ND
NM_145294	WDR90	197335	-4.63	ND	ND
NM_006437	PARP4	143	-4.62	0.36	FP
XM_001130706	C6orf100	729583	-4.61	ND	ND
XM_496597	FLJ30428	150519	-4.56	ND	ND
NM_001033	RRM1	6240	-4.51	ND	ND
NM_001080489	GLOD5	392465	-4.47	ND	ND
NM_005990	STK10	6793	-4.47	ND	ND
NM_001080462	TMEM202	338949	-4.46	ND	ND
NM_001211	BUB1B	701	-4.42	ND	ND
NM_153700	STRC	161497	-4.40	ND	ND
NM_153444	OR5P2	120065	-4.37	ND	ND
XM_001129200	LOC729065	729065	-4.34	ND	ND
NM_000867	HTR2B	3357	-4.34	ND	ND
NM_006101	NDC80	10403	-4.26	ND	ND
NM_173799	TIGIT	201633	-4.24	ND	ND
NM_000247	MICA	4276	-4.17	ND	ND
NM_001029869	PLAC8L1	153770	-4.16	ND	ND
XM_001130007	CCDC79	283847	-4.16	ND	ND
NM_080610	CST9L	128821	-4.16	ND	ND
NM_153038	CCDC140	151278	-4.15	ND	ND
NM_003410	ZFX	7543	-4.15	ND	ND
XM_001125909	LOC653103	653103	-4.13	ND	ND
NM_001013672	C17orf97	400566	-4.06	ND	ND
NM_181600	KRTAP13-4	284827	-4.05	ND	ND
XM_373926	LOC388814	388814	-4.05	ND	ND
NM_000478	ALPL	249	-4.04	ND	ND
NM_018401	STK32B	55351	-4.03	ND	ND
NM_173546	KLHDC8B	200942	-4.00	ND	ND
NM_014694	ADAMTSL2	9719	-3.99	ND	ND
NM_012125	CHRM5	1133	-3.99	1.17	FP
NM_001001923	OR5C1	392391	-3.98	ND	ND
XM_001133615	ZYG11A	440590	-3.97	ND	ND
XM_001130404	LOC645027	645027	-3.96	ND	ND
NM_152523	CCNYL1	151195	-3.94	ND	ND
NM_015981	CAMK2A	815	-3.90	-3.74	TP
NM_005028	PIP4K2A	5305	-3.83	ND	ND
NM_001015887	IGSF11	152404	-3.83	ND	ND
NM_001018059	LOC440348	440348	-3.83	ND	ND
XM_001128937	FLJ31485	440119	-3.82	ND	ND
NM_178126	FAM134C	162427	-3.81	ND	ND
XM_292963	LOC643997	643997	-3.81	ND	ND

RefSeq Accession Number	Gene Symbol	Gene ID	SSMD of the whole-genome validation screen	SSMD of custom library screen	Remark
NM_006430	CCT4	10575	-3.78	ND	ND
NM_001024594	C1orf53	388722	-3.78	ND	ND
NM_001017396	ZNF2	7549	-3.76	ND	ND
XM_001131633	LOC732024	732024	-3.76	ND	ND
NM_173855	MORN3	283385	-3.75	ND	ND
NM_001037728	DEFB110	245913	-3.75	ND	ND
XM_001134466	FAM92A3	403315	-3.75	ND	ND
NM_032037	TSSK6	83983	-3.74	ND	ND
NM_006997	TACC2	10579	-3.74	ND	ND
NM_018136	ASPM	259266	-3.73	ND	ND
XM_001129073	LOC731277	731277	-3.71	ND	ND
NM_001083330	ZNF133	7692	-3.64	ND	ND
NM_014262	LEPREL2	10536	-3.62	ND	ND
NM_145065	PELI3	246330	-3.58	ND	ND
XM_374880	FAM180B	399888	-3.55	ND	ND
XM_001130325	LOC728469	728469	-3.54	ND	ND
NM_153264	COL29A1	256076	-3.52	ND	ND
NM_152531	C3orf21	152002	-3.51	ND	ND
NM_015496	KIAA1429	25962	-3.50	ND	ND
XM_927854	EIF4E1B	253314	-3.45	ND	ND
NM_018650	MARK1	4139	-3.43	ND	ND
NM_014496	RPS6KA6	27330	-3.41	0.02	FP
NM_015483	KBTBD2	25948	-3.39	ND	ND
NM_018425	PI4K2A	55361	-3.38	ND	ND
NM_006293	TYRO3	7301	-3.38	ND	ND
XM_378454	LOC283547	283547	-3.36	ND	ND
NM_173622	CDRT4	284040	-3.35	ND	ND
NM_181724	TMEM119	338773	-3.33	ND	ND
NM_199047	TBPL2	387332	-3.29	ND	ND
NM_013941	OR10C1	442194	-3.29	ND	ND
NM_000026	ADSL	158	-3.24	ND	ND
NM_001001963	OR2L8	391190	-3.16	ND	ND
NM_001381	DOK1	1796	-3.10	ND	ND
XM_935188	LOC440456	440456	-3.08	ND	ND
NM_001039130	ALOX15B	247	-3.07	ND	ND
XM_001129114	LOC728437	728437	-3.06	ND	ND
XM_001129780	LOC729257	729257	-3.06	ND	ND
NM_001492	GDF1	2657	-3.02	-3.49	TP
Genes which increased vMYX-LacZ replication when silenced with siRNAs					
RefSeq Accession Number	**Gene Symbol**	**Gene ID**	**SSMD of the whole-genome validation screen**	**SSMD of custom library screen**	**Remark**
XM_001127406	LOC730835	730835	9.48	ND	ND
XM_001130166	LOC731592	731592	9.47	ND	ND

XM_001132878	LOC730195	730195	9.29	ND	ND
XM_001134296	LOC730118	730118	9.25	ND	ND
XM_001126473	LOC730596	730596	9.11	ND	ND
XM_001130328	LOC731646	731646	9.07	ND	ND
XM_001131736	LOC731062	731062	8.95	ND	ND
XM_001133225	LOC730243	730243	8.95	ND	ND
XM_001131164	FLJ36777	730971	8.90	ND	ND
XM_001132465	LOC730110	730110	8.88	ND	ND
XM_001131954	LOC732134	732134	8.85	ND	ND
XM_001129094	LOC731282	731282	8.79	ND	ND
XM_001132460	LOC731334	731334	8.63	ND	ND
XM_001132415	LOC730100	730100	8.56	ND	ND
XM_001134349	LOC730176	730176	8.39	ND	ND
XM_001133474	LOC731464	731464	8.01	ND	ND
XM_001128022	LOC730998	730998	7.79	ND	ND
XM_001126166	LOC730517	730517	7.65	ND	ND
XM_001133931	LOC732174	732174	7.59	ND	ND
XM_001133385	LOC730264	730264	7.55	ND	ND
NM_005108	XYLB	9942	7.48	1.89	FP
NM_031480	RIOK1	83732	7.40	ND	ND
NM_020639	RIPK4	54101	7.38	ND	ND
NM_032294	CAMKK1	84254	7.34	ND	ND
XM_001126762	LOC728176	728176	7.27	ND	ND
NM_003292	TPR	7175	7.20	ND	ND
XM_001132090	LOC730015	730015	7.17	ND	ND
XM_001134013	ULK3	25989	7.16	ND	ND
NM_017771	PXK	54899	7.13	ND	ND
NM_144682	SLFN13	146857	7.12	ND	ND
NM_014572	LATS2	26524	7.10	ND	ND
XM_001129999	LOC729345	729345	7.10	ND	ND
NM_001006665	RPS6KA1	6195	7.06	ND	ND
XM_001131052	LOC731860	731860	7.05	ND	ND
NM_001007156	NTRK3	4916	7.04	ND	ND
NM_006256	PKN2	5586	7.04	ND	ND
XM_001130144	LOC729397	729397	7.02	ND	ND
NM_001080849	DNLZ	728489	6.98	ND	ND
NM_001004731	OR5AU1	390445	6.96	ND	ND
XM_001126477	LOC728074	728074	6.95	ND	ND
NM_004672	MAP3K6	9064	6.89	ND	ND
XM_001127324	LOC728365	728365	6.89	ND	ND
NM_001009555	SH3D19	152503	6.88	ND	ND
XM_001132657	LOC730150	730150	6.87	ND	ND
NM_002732	PRKACG	5568	6.86	-0.30	FP

NM_001080400	KIAA1881	729359	6.85	ND	ND
XM_001131974	LOC729989	729989	6.85	ND	ND
XM_373904	LOC388780	388780	6.85	ND	ND
NM_015093	MAP3K7IP2	23118	6.83	ND	ND
XM_372423	LOC390231	390231	6.83	ND	ND
NM_182691	SRPK2	6733	6.82	ND	ND
NM_014429	MORC1	27136	6.82	ND	ND
NM_001004741	OR5M10	390167	6.77	ND	ND
NM_005372	MOS	4342	6.76	ND	ND
XM_001130170	LOC729275	729275	6.76	ND	ND
XM_001132121	LOC730022	730022	6.75	ND	ND
XM_096885	LOC145853	145853	6.72	ND	ND
NM_018584	CAMK2N1	55450	6.70	ND	ND
NM_152450	FAM81A	145773	6.68	ND	ND
XM_001128550	LOC728815	728815	6.68	ND	ND
NM_001083588	E2F5	1875	6.68	5.86	TP
XM_001131586	LOC729871	729871	6.66	ND	ND
NM_020633	VN1R1	57191	6.65	ND	ND
XM_001126715	LOC728155	728155	6.64	ND	ND
XM_001126849	LOC727900	727900	6.63	ND	ND
NM_001006115	IP6K1	9807	6.62	ND	ND
NM_024944	CHODL	140578	6.62	ND	ND
XM_001133051	LOC728844	728844	6.61	ND	ND
NM_001037380	DEFB109	641517	6.59	ND	ND
XM_001127527	LOC728475	728475	6.58	ND	ND
XM_001129809	LOC728308	728308	6.57	ND	ND
NM_001005732	C21orf34	388815	6.56	ND	ND
NM_207328	LOC150763	150763	6.56	ND	ND
XM_371655	LOC389137	389137	6.55	ND	ND
NM_001025778	VRK3	51231	6.54	ND	ND
NM_005279	GPR1	2825	6.53	ND	ND
XM_929316	LOC391771	391771	6.53	ND	ND
NM_001258	CDK3	1018	6.53	ND	ND
NM_001005167	OR52E6	390078	6.52	ND	ND
XM_001131495	LOC729847	729847	6.52	ND	ND
NM_006583	RRH	10692	6.50	ND	ND
NM_014602	PIK3R4	30849	6.49	ND	ND
NM_152416	C8orf38	137682	6.49	ND	ND
XM_001126445	LOC728058	728058	6.48	ND	ND
XM_943013	FAM92A1	137392	6.47	ND	ND
NM_002603	PDE7A	5150	6.46	ND	ND
NM_001006681	SPIN2B	474343	6.45	ND	ND
NM_145277	HFE2	148738	6.45	ND	ND

XM_001132136	ZNF860	344787	6.43	ND	ND
NM_006549	CAMKK2	10645	6.41	ND	ND
XM_001129177	LOC729056	729056	6.41	ND	ND
NM_006206	PDGFRA	5156	6.41	-0.86	FP
NM_003993	CLK2	1196	6.40	ND	ND
NM_080829	FAM65C	140876	6.37	ND	ND
NM_178829	C7orf34	135927	6.36	ND	ND
NM_006742	PSKH1	5681	6.35	ND	ND
XM_001134191	LOC729977	729977	6.35	ND	ND
NM_015419	MXRA5	25878	6.34	ND	ND
XM_001134358	LOC732273	732273	6.34	ND	ND
NM_007312	HYAL1	3373	6.33	ND	ND
NM_207372	SH2D4B	387694	6.33	ND	ND
NM_144708	ANKAR	150709	6.32	ND	ND
NM_020377	CYSLTR2	57105	6.32	ND	ND
NM_001005909	IP6K2	51447	6.31	ND	ND
XM_001133151	LOC729199	729199	6.27	ND	ND
NM_207414	FLJ43860	389690	6.27	ND	ND
NM_005296	LPAR4	2846	6.27	ND	ND
NM_000316	PTH1R	5745	6.26	ND	ND
XM_001131284	LOC729777	729777	6.26	ND	ND
NM_001008693	CST9	128822	6.26	ND	ND
NM_002378	MATK	4145	6.26	ND	ND
NM_145206	VTI1A	143187	6.26	ND	ND
NM_004160	PYY	5697	6.25	ND	ND
XM_001130708	LOC729585	729585	6.24	ND	ND
NM_001004719	OR4M2	390538	6.24	ND	ND
XM_001132500	LOC730116	730116	6.23	ND	ND
NM_178456	C20orf85	128602	6.23	ND	ND
NM_130388	ASB12	142689	6.23	ND	ND
NM_002688	41522	5413	6.22	ND	ND
NM_022494	ZDHHC6	64429	6.22	ND	ND
NM_006207	PDGFRL	5157	6.22	ND	ND
NM_032387	WNK4	65266	6.21	ND	ND
NM_002767	PRPSAP2	5636	6.21	ND	ND
NM_014462	LSM1	27257	6.20	ND	ND
NM_173495	PTCHD1	139411	6.20	ND	ND
NM_152540	SCFD2	152579	6.19	ND	ND
XM_001130643	LOC729568	729568	6.18	ND	ND
XM_942417	LOC652774	652774	6.18	ND	ND
NM_016335	PRODH	5625	6.18	ND	ND
NM_000566	FCGR1A	2209	6.17	ND	ND
NM_001079812	DIAPH1	1729	6.17	ND	ND

XM_942053	LOC652554	652554	6.17	ND	ND
NM_001042507	GAL7	653499	6.15	ND	ND
NM_000507	FBP1	2203	6.15	0.53	FP
NM_198450	APOOL	139322	6.14	ND	ND
NM_145185	MAP2K7	5609	6.14	5.10	TP
NM_001015891	TAF9	6880	6.14	ND	ND
XM_001125926	LOC727841	727841	6.13	ND	ND
NM_001220	CAMK2B	816	6.12	-4.51	FP
NM_001042465	PSAP	5660	6.12	ND	ND
NM_005393	PLXNB3	5365	6.11	ND	ND
NM_001014796	DDR2	4921	6.10	ND	ND
NM_144716	CCDC12	151903	6.09	ND	ND
NM_020679	MIF4GD	57409	6.08	ND	ND
NM_001012337	ROPN1B	152015	6.08	ND	ND
NM_004990	MARS	4141	6.08	ND	ND
NM_001013635	LOC387856	387856	6.07	ND	ND
NM_001010903	C6orf222	389384	6.06	ND	ND
NM_031460	KCNK17	89822	6.04	ND	ND
NM_002875	RAD51	5888	6.03	ND	ND
XM_001133790	LOC729441	729441	6.03	ND	ND
NM_001003686	PMS2L3	5387	6.02	ND	ND
NM_022139	GFRA4	64096	6.02	ND	ND
XM_940091	LOC442077	442077	6.01	ND	ND
NM_002874	RAD23B	5887	6.01	ND	ND
XM_926429	BTF3L4P	653189	6.01	ND	ND
NM_020699	GATAD2B	57459	6.00	ND	ND
XM_936778	LOC647718	647718	5.99	ND	ND
XM_001129762	LOC729254	729254	5.99	ND	ND
NM_000559	HBG1	3047	5.98	ND	ND
NM_001024677	LOC401296	401296	5.97	ND	ND
NM_005917	MDH1	4190	5.97	ND	ND
XM_001131433	LOC729821	729821	5.97	ND	ND
NM_000962	PTGS1	5742	5.97	ND	ND
NM_178497	C4orf26	152816	5.96	ND	ND
NM_004526	MCM2	4171	5.95	ND	ND
NM_080739	C20orf141	128653	5.95	ND	ND
NM_001616	ACVR2A	92	5.93	ND	ND
NM_080628	C20orf118	140711	5.93	ND	ND
NM_030756	TCF7L2	6934	5.93	-0.38	FP
NM_002734	PRKAR1A	5573	5.92	-2.26	FP
XM_001127041	LOC728270	728270	5.92	ND	ND
NM_002836	PTPRA	5786	5.92	ND	ND
NM_022772	EPS8L2	64787	5.90	ND	ND

NM_015878	AZIN1	51582	5.90	ND	ND
NM_015360	SKIV2L2	23517	5.90	ND	ND
NM_001259	CDK6	1021	5.90	ND	TP*
NM_153442	GPR26	2849	5.89	ND	ND
XM_374161	LOC389369	389369	5.88	ND	ND
XM_940875	LOC651672	651672	5.87	ND	ND
NM_006230	POLD2	5425	5.87	ND	ND
NM_001003937	TSPYL6	388951	5.87	ND	ND
XM_001134350	LOC730181	730181	5.86	ND	ND
NM_001452	FOXF2	2295	5.86	ND	ND
NM_001040710	FLJ30851	653140	5.85	ND	ND
XM_935586	LOC641845	641845	5.85	ND	ND
NM_006682	FGL2	10875	5.85	ND	ND
XM_940518	LOC651373	651373	5.85	ND	ND
NM_007047	BTN3A2	11118	5.84	ND	ND
XM_001130734	LOC729595	729595	5.84	ND	ND
XM_001130515	LOC650483	650483	5.84	ND	ND
XM_374137	LOC389328	389328	5.84	ND	ND
XM_001129779	LOC650218	650218	5.84	ND	ND
NM_001001557	GDF6	392255	5.84	ND	ND
NM_000300	PLA2G2A	5320	5.83	ND	ND
XM_942461	LOC652800	652800	5.83	ND	ND
XM_097977	FAM59B	150946	5.83	ND	ND
XM_001129903	LOC729308	729308	5.83	ND	ND
NM_002557	OVGP1	5016	5.82	ND	ND
NM_144564	SLC39A3	29985	5.82	ND	ND
NM_014243	ADAMTS3	9508	5.81	ND	ND
NM_000439	PCSK1	5122	5.81	0.96	FP
NM_139170	C16orf71	146562	5.81	ND	ND
NM_001033575	DUSP28	285193	5.80	1.09	FP
NM_031915	SETDB2	83852	5.80	ND	ND
NM_003558	PIP5K1B	8395	5.80	ND	ND
NM_003565	ULK1	8408	5.79	ND	ND
XM_945506	LOC652444	652444	5.78	ND	ND
NM_001356	DDX3X	1654	5.78	ND	ND
NM_020646	ASCL3	56676	5.78	ND	ND
NM_001031695	RBM9	23543	5.77	ND	ND
NM_022467	CHST8	64377	5.77	ND	ND
NM_002759	EIF2AK2	5610	5.77	ND	ND
NM_001918	DBT	1629	5.77	ND	ND
NM_000351	STS	412	5.77	ND	ND
XM_001133381	LOC730259	730259	5.76	ND	ND
NM_003190	TAPBP	6892	5.76	ND	ND

XM_001133963	LOC652516	652516	5.76	ND	ND
XM_932995	LOC645602	645602	5.76	ND	ND
XM_938321	LOC649259	649259	5.75	ND	ND
NM_001008388	CISD2	493856	5.73	ND	ND
XM_931994	LOC644090	644090	5.72	ND	ND
NM_003730	RNASET2	8635	5.72	ND	ND
NM_138701	C7orf11	136647	5.72	ND	ND
NM_018122	DARS2	55157	5.72	ND	ND
XM_001132868	LOC730194	730194	5.71	ND	ND
XM_929060	LOC646096	646096	5.70	ND	ND
XM_497357	LOC390364	390364	5.69	ND	ND
NM_002866	RAB3A	5864	5.68	ND	ND
NM_033224	PURB	5814	5.67	ND	ND
NM_004194	ADAM22	53616	5.65	ND	ND
NM_024295	DERL1	79139	5.65	ND	ND
NM_004759	MAPKAPK2	9261	5.65	-3.54	FP
XM_926017	LOC642521	642521	5.64	ND	ND
XM_932564	LOC644990	644990	5.63	ND	ND
NM_005605	PPP3CC	5533	5.62	ND	ND
XM_065445	LOC129870	129870	5.62	ND	ND
XM_929953	LOC646982	646982	5.62	ND	ND
NM_145262	GLYCTK	132158	5.61	ND	ND
NM_012267	HSPBP1	23640	5.61	ND	ND
XM_001127935	LOC728619	728619	5.60	ND	ND
NM_001870	CPA3	1359	5.59	ND	ND
NM_004430	EGR3	1960	5.59	ND	ND
NM_020315	PDXP	57026	5.59	ND	ND
NM_001042437	ST3GAL5	8869	5.58	ND	ND
XM_935598	LOC641857	641857	5.57	ND	ND
NM_145912	NFAM1	150372	5.56	ND	ND
NM_001946	DUSP6	1848	5.56	-0.96	FP
NM_182509	THSD3	145501	5.55	ND	ND
NM_153028	ZNF75A	7627	5.54	ND	ND
NM_023947	CHID1	66005	5.54	ND	ND
NM_000295	SERPINA1	5265	5.53	ND	ND
XM_001130778	LOC729608	729608	5.53	ND	ND
NM_001008925	RCHY1	25898	5.53	ND	ND
NM_003859	DPM1	8813	5.53	ND	ND
NM_003841	TNFRSF10C	8794	5.53	ND	ND
XM_936950	LOC647890	647890	5.52	ND	ND
NM_006166	NFYB	4801	5.52	ND	ND
NM_005515	MNX1	3110	5.52	ND	ND
NM_003142	SSB	6741	5.51	ND	ND

NM_001077619	UBXN2B	137886	5.50	ND	ND
NM_000400	ERCC2	2068	5.49	ND	ND
XM_001131502	LOC729849	729849	5.49	ND	ND
NM_014442	SIGLEC8	27181	5.49	ND	ND
XM_927936	LOC644841	644841	5.49	ND	ND
NM_000044	AR	367	5.48	ND	ND
XM_931228	LOC642998	642998	5.47	ND	ND
XM_001130743	LOC729599	729599	5.46	ND	ND
NM_001031801	LIMK2	3985	5.46	ND	ND
XM_498537	LOC440084	440084	5.46	ND	ND
XM_927505	C8orf68	619343	5.46	ND	ND
XM_942069	LOC652564	652564	5.46	ND	ND
NM_000106	CYP2D6	1565	5.46	ND	ND
NM_002067	GNA11	2767	5.45	-1.65	FP
NM_006587	CORIN	10699	5.44	ND	ND
NM_030791	SGPP1	81537	5.44	ND	ND
NM_019098	CNGB3	54714	5.43	ND	ND
XM_001133969	BCMS	647154	5.42	ND	ND
XM_001127355	LOC728377	728377	5.42	ND	ND
NM_016086	STYXL1	51657	5.42	1.04	FP
NM_004897	MINPP1	9562	5.42	ND	ND
XM_001132481	LOC730113	730113	5.41	ND	ND
NM_003253	TIAM1	7074	5.40	8.45	TP
XM_371820	FLJ90086	389389	5.40	ND	ND
NM_001239	CCNH	902	5.40	ND	ND
NM_207383	FLJ42289	388182	5.38	ND	ND
NM_020858	SEMA6D	80031	5.38	ND	ND
NM_013435	RAX	30062	5.38	ND	ND
XM_928198	RPL12P8	645161	5.37	ND	ND
NM_001042600	MAP4K1	11184	5.36	ND	ND
XM_942048	ELTD1	64123	5.36	ND	ND
XM_937698	LOC648629	648629	5.35	ND	ND
NM_000732	CD3D	915	5.35	ND	ND
NM_021203	SRPRB	58477	5.35	ND	ND
NM_000341	SLC3A1	6519	5.34	ND	ND
NM_017413	APLN	8862	5.34	ND	ND
NM_000030	AGXT	189	5.34	ND	ND
XM_001133420	LOC728991	728991	5.33	ND	ND
XM_931978	LOC644026	644026	5.33	ND	ND
NM_000582	SPP1	6696	5.33	ND	ND
NM_000314	PTEN	5728	5.32	4.86	TP
NM_020549	CHAT	1103	5.30	ND	ND
XM_932054	LOC644224	644224	5.30	ND	ND

XM_927653	LOC644524	644524	5.30	ND	ND
XM_931396	LOC643194	643194	5.30	ND	ND
NM_001354	AKR1C2	1646	5.29	ND	ND
XM_001133525	LOC731501	731501	5.29	ND	ND
NM_053041	COMMD7	149951	5.28	ND	ND
XM_936910	LOC647850	647850	5.28	ND	ND
XM_496360	hCG_23177	440585	5.27	ND	ND
NM_001709	BDNF	627	5.26	ND	ND
NM_001079527	FAM153C	653316	5.25	ND	ND
XM_001133842	LOC729446	729446	5.25	ND	ND
NM_001038705	GPR149	344758	5.24	ND	ND
NM_001004332	FLJ41170	440200	5.24	ND	ND
NM_000139	MS4A2	2206	5.24	ND	ND
XM_933693	LOC440731	440731	5.23	ND	ND
XM_496379	LOC401957	401957	5.21	ND	ND
NM_001002837	INPP5J	27124	5.21	ND	ND
NM_198542	ZNF773	374928	5.21	ND	ND
NM_052931	SLAMF6	114836	5.19	ND	ND
NM_001011538	LOC402176	402176	5.18	ND	ND
NM_033389	SSH2	85464	5.18	ND	ND
NM_004452	ESRRB	2103	5.16	ND	ND
XM_936088	LOC642018	642018	5.15	ND	ND
NM_001092	ABR	29	5.15	ND	ND
NM_021907	DTNB	1838	5.15	ND	ND
NM_001024847	TGFBR2	7048	5.15	ND	ND
XM_001128367	LOC439949	439949	5.14	ND	ND
NM_001904	CTNNB1	1499	5.14	5.96	TP
XM_498648	LOC440389	440389	5.13	ND	ND
NM_144635	FAM131A	131408	5.13	ND	ND
NM_033105	DNAJC5B	85479	5.13	ND	ND
NM_006539	CACNG3	10368	5.12	ND	ND
NM_004398	DDX10	1662	5.11	ND	ND
NM_001010909	C6orf205	394263	5.11	ND	ND
NM_020485	RHCE	6006	5.11	ND	ND
NM_002661	PLCG2	5336	5.10	-1.53	FP
NM_000128	F11	2160	5.09	ND	ND
NM_198484	ZNF621	285268	5.09	ND	ND
XM_001125855	MBOAT4	619373	5.08	ND	ND
NM_138473	SP1	6667	5.07	ND	ND
XM_001129640	LOC729197	729197	5.07	ND	ND
NM_001080487	LOC390748	390748	5.07	ND	ND
NM_000284	PDHA1	5160	5.07	ND	ND
NM_024670	SUV39H2	79723	5.06	ND	ND

XM_001131123	LOC729720	729720	5.06	ND	ND
NM_018208	ETNK2	55224	5.05	ND	ND
XM_944444	LOC643749	643749	5.04	ND	ND
NM_006133	DAGLA	747	5.04	ND	ND
NM_181715	CRTC2	200186	5.03	ND	ND
NM_000928	PLA2G1B	5319	5.03	ND	ND
NM_001938	DR1	1810	5.03	ND	ND
NM_003082	SNAPC1	6617	5.03	ND	ND
NM_000932	PLCB3	5331	5.01	5.64	TP
XM_373042	LOC391722	391722	5.01	ND	ND
NM_000208	INSR	3643	4.99	ND	ND
NM_002401	MAP3K3	4215	4.99	-1.82	FP
NM_198253	TERT	7015	4.98	ND	ND
NM_001008540	CXCR4	7852	4.98	-3.05	FP
NM_001017964	YDJC	150223	4.97	ND	ND
NM_014596	ZNRD1	30834	4.97	ND	ND
NM_024833	ZNF671	79891	4.97	ND	ND
NM_007168	ABCA8	10351	4.96	ND	ND
NM_001029997	ZNF181	339318	4.96	ND	ND
NM_002106	H2AFZ	3015	4.95	ND	ND
NM_000588	IL3	3562	4.95	ND	ND
XM_001125692	LOC642098	642098	4.94	ND	ND
NM_001042388	PPP4R1	9989	4.93	ND	ND
NM_033453	ITPA	3704	4.93	ND	ND
NM_001080446	LOC143678	143678	4.93	ND	ND
NM_007272	CTRC	11330	4.92	ND	ND
XM_941353	LOC402145	402145	4.92	ND	ND
NM_020126	SPHK2	56848	4.92	1.33	FP
NM_014214	IMPA2	3613	4.91	ND	ND
NM_001013710	LOC440742	440742	4.91	ND	ND
XM_371797	LOC389365	389365	4.91	ND	ND
NM_003506	FZD6	8323	4.90	ND	ND
NM_000960	PTGIR	5739	4.89	ND	ND
NM_005338	HIP1	3092	4.89	ND	ND
NM_203371	FIBIN	387758	4.89	ND	ND
NM_022474	MPP5	64398	4.89	ND	ND
NM_004581	RABGGTA	5875	4.87	ND	ND
NM_018941	CLN8	2055	4.86	ND	ND
NM_006916	RPE	6120	4.85	2.35	B
XM_939612	MT1CP	441771	4.85	ND	ND
NM_001010879	ZIK1	284307	4.85	ND	ND
NM_004065	CDR1	1038	4.85	ND	ND
XM_929136	LOC646177	646177	4.85	ND	ND

XM_936878	DKFZP781G0119	644041	4.85	ND	ND
NM_005142	GIF	2694	4.84	ND	ND
NM_001039770	FLJ45032	643853	4.84	ND	ND
NM_152445	FAM161B	145483	4.83	ND	ND
XM_931304	LOC643085	643085	4.82	ND	ND
XM_933781	LOC646626	646626	4.82	ND	ND
NM_003005	SELP	6403	4.82	ND	ND
XM_001130825	LOC728357	728357	4.82	ND	ND
NM_000318	PXMP3	5828	4.80	ND	ND
NM_003258	TK1	7083	4.78	ND	ND
NM_005050	ABCD4	5826	4.78	ND	ND
XM_001131864	LOC729950	729950	4.77	ND	ND
XM_925948	LOC642433	642433	4.77	ND	ND
XM_944526	hCG_1820801	441167	4.76	ND	ND
XM_001132315	LOC732226	732226	4.75	ND	ND
XM_496319	LOC648217	648217	4.75	ND	ND
NM_001087	AAMP	14	4.75	ND	ND
XM_496483	LOC440776	440776	4.75	ND	ND
NM_000641	IL11	3589	4.73	ND	ND
NM_001003799	TARP	445347	4.72	ND	ND
NM_207318	CXorf39	139231	4.72	ND	ND
NM_023002	HAPLN4	404037	4.71	ND	ND
XM_001132700	LOC730160	730160	4.70	ND	ND
NM_182700	SP8	221833	4.70	ND	ND
NM_032836	FIZ1	84922	4.69	ND	ND
NM_001759	CCND2	894	4.68	-2.21	FP
NM_017908	ZNF446	55663	4.67	ND	ND
NM_006268	DPF2	5977	4.66	ND	ND
NM_182594	ZNF454	285676	4.66	ND	ND
NM_021131	PPP2R4	5524	4.66	ND	ND
NM_001766	CD1D	912	4.65	ND	ND
NM_004966	HNRNPF	3185	4.65	ND	ND
NM_002513	NME3	4832	4.65	ND	ND
XM_379543	LOC401442	401442	4.64	ND	ND
NM_001012715	C9orf106	414318	4.64	ND	ND
NM_018077	RBM28	55131	4.63	ND	ND
XM_926936	LOC643631	643631	4.63	ND	ND
NM_001004461	OR10A6	390093	4.61	ND	ND
XM_001129688	LOC731447	731447	4.61	ND	ND
XM_496428	LOC440706	440706	4.60	ND	ND
XM_497098	hCG_1982709	441488	4.60	ND	ND
NM_014802	KIAA0528	9847	4.60	ND	ND
XM_926802	LOC643479	643479	4.59	ND	ND

NM_001040020	FAM3C	10447	4.59	ND	ND
XM_938374	LOC644010	644010	4.59	ND	ND
XM_001133397	LOC729335	729335	4.59	ND	ND
XM_001130492	LOC442175	442175	4.59	ND	ND
NM_006335	TIMM17A	10440	4.58	ND	ND
XM_497712	LOC441907	441907	4.58	ND	ND
XM_068229	LOC133185	133185	4.56	ND	ND
NM_018260	ZNF701	55762	4.55	ND	ND
NM_003622	PPFIBP1	8496	4.55	ND	ND
NM_005435	ARHGEF5	7984	4.55	ND	ND
NM_002762	PRM2	5620	4.55	ND	ND
NM_004299	ABCB7	22	4.55	ND	ND
NM_015933	CCDC72	51372	4.53	ND	ND
NM_173690	C9orf126	286205	4.50	ND	ND
NM_002781	PSG5	5673	4.50	ND	ND
NM_020832	ZNF687	57592	4.50	ND	ND
NM_021229	NTN4	59277	4.50	ND	ND
NM_032752	ZNF496	84838	4.50	ND	ND
XM_931025	LOC642995	642995	4.49	ND	ND
NM_002029	FPR1	2357	4.49	ND	ND
NM_005848	DENND4A	10260	4.48	ND	ND
NM_007156	ZXDA	7789	4.48	ND	ND
NM_016281	TAOK3	51347	4.48	ND	ND
NM_006905	PSG1	5669	4.47	ND	ND
XM_932941	LOC643275	643275	4.47	ND	ND
NM_006343	MERTK	10461	4.47	ND	ND
NM_000631	NCF4	4689	4.47	ND	ND
XM_927062	PNPLA10P	643773	4.47	ND	ND
XM_001131825	LOC729934	729934	4.47	ND	ND
NM_002830	PTPN4	5775	4.46	ND	ND
XM_936247	LOC642108	642108	4.46	ND	ND
NM_001039083	ARL17	641522	4.46	ND	ND
NM_001085479	IQCF3	401067	4.43	ND	ND
NM_001001794	FAM116B	414918	4.43	ND	ND
NM_001034852	SMOC1	64093	4.42	ND	ND
NM_033215	PPP1R3F	89801	4.41	ND	ND
NM_007282	RNF13	11342	4.41	ND	ND
NM_013363	PCOLCE2	26577	4.41	ND	ND
NM_005460	SNCAIP	9627	4.40	ND	ND
XM_373572	LOC387941	387941	4.40	ND	ND
NM_001039481	ETNK1	55500	4.40	ND	ND
XM_371825	C6orf140	389396	4.40	ND	ND
NM_005633	SOS1	6654	4.37	4.91	TP

XM_928291	LOC645249	645249	4.37	ND	ND
NM_002720	PPP4C	5531	4.36	ND	ND
XM_926796	CLDN22	53842	4.34	ND	ND
NM_020438	DOLPP1	57171	4.34	ND	ND
NM_172002	HSCB	150274	4.34	ND	ND
NM_153218	C13orf31	144811	4.33	ND	ND
NM_006851	GLIPR1	11010	4.33	ND	ND
NM_031432	UCK1	83549	4.33	ND	ND
NM_017432	PTOV1	53635	4.32	ND	ND
NM_001004341	ETV3L	440695	4.31	ND	ND
XM_001131048	LOC729691	729691	4.31	ND	ND
NM_022152	TMBIM1	64114	4.30	ND	ND
NM_153695	ZNF367	195828	4.30	ND	ND
NM_000304	PMP22	5376	4.30	ND	ND
NM_007045	FGFR1OP	11116	4.29	ND	ND
NM_014845	FIG4	9896	4.28	ND	ND
XM_001129578	LOC729180	729180	4.28	ND	ND
NM_031488	L3MBTL2	83746	4.27	ND	ND
NM_173531	ZNF100	163227	4.27	ND	ND
NM_001080509	TSPAN11	441631	4.27	ND	ND
XM_001130342	LY6H	4062	4.26	ND	ND
NM_207469	DEFB32	400830	4.25	ND	ND
XM_943378	LOC642335	642335	4.25	ND	ND
XM_941354	LOC401097	401097	4.24	ND	ND
XM_496194	TRE17	440414	4.24	ND	ND
XM_001126243	LOC727958	727958	4.24	ND	ND
NM_004419	DUSP5	1847	4.23	ND	ND
NM_001005519	OR6C68	403284	4.22	ND	ND
NM_130760	MADCAM1	8174	4.22	ND	ND
NM_003174	SVIL	6840	4.21	ND	ND
NM_012191	NAT6	24142	4.20	ND	ND
XM_001129741	LOC729244	729244	4.20	ND	ND
NM_001008778	SPDYC	387778	4.20	ND	ND
NM_002110	HCK	3055	4.19	ND	ND
NM_004294	MTRF1	9617	4.19	ND	ND
NM_178523	ZNF616	90317	4.18	ND	ND
NM_006586	CNPY3	10695	4.18	ND	ND
NM_007349	PAXIP1	22976	4.18	ND	ND
NM_002491	NDUFB3	4709	4.18	ND	ND
XM_001130684	DENND4B	9909	4.16	ND	ND
NM_006907	PYCR1	5831	4.15	ND	ND
XM_940242	LOC651112	651112	4.14	ND	ND
NM_001001732	CC2D2B	387707	4.13	ND	ND

NM_017544	NKRF	55922	4.13	ND	ND
NM_018433	JMJD1A	55818	4.12	ND	ND
NM_016050	MRPL11	65003	4.12	ND	ND
NM_022450	RHBDF1	64285	4.11	ND	ND
XM_001133712	LOC729651	729651	4.11	ND	ND
NM_014780	CUL7	9820	4.10	ND	ND
NM_020844	C8orf79	57604	4.09	ND	ND
NM_003985	TNK1	8711	4.09	ND	ND
NM_000723	CACNB1	782	4.08	ND	ND
NM_020197	SMYD2	56950	4.08	ND	ND
NM_002596	PCTK3	5129	4.08	ND	ND
NM_021967	SERF1A	8293	4.07	ND	ND
NM_000542	SFTPB	6439	4.07	ND	ND
NM_003839	TNFRSF11A	8792	4.05	ND	ND
NM_013399	C16orf5	29965	4.05	ND	ND
NM_206967	C16orf74	404550	4.05	ND	ND
XM_001132303	ZNF724P	440519	4.05	ND	ND
NM_003185	TAF4	6874	4.05	1.20	FP
NM_021149	COTL1	23406	4.05	ND	ND
NM_001014440	ODF3B	440836	4.04	ND	ND
NM_012375	OR52A1	23538	4.04	ND	ND
NM_144714	C3orf48	151649	4.03	ND	ND
NM_004608	TBX6	6911	4.03	ND	ND
NM_080928	ASB15	142685	4.02	ND	ND
NM_016940	RWDD2B	10069	4.01	ND	ND
NM_001008239	C18orf25	147339	4.01	ND	ND
NM_001003704	MTP18	51537	4.00	ND	ND
NM_003930	SKAP2	8935	3.99	ND	ND
NM_021637	TMEM35	59353	3.99	ND	ND
XM_379378	LOC401220	401220	3.98	ND	ND
NM_004069	AP2S1	1175	3.98	ND	ND
NM_194326	RPS19BP1	91582	3.97	ND	ND
NM_000151	G6PC	2538	3.97	ND	ND
NM_001926	DEFA6	1671	3.96	ND	ND
NM_021200	PLEKHB1	58473	3.95	ND	ND
NM_014171	CRIPT	9419	3.95	ND	ND
NM_016271	RNF138	51444	3.95	ND	ND
NM_053276	VIT	5212	3.94	ND	ND
NM_020761	KIAA1303	57521	3.93	ND	ND
NM_001031693	HHLA3	11147	3.92	ND	ND
NM_198541	IGFL1	374918	3.92	ND	ND
NM_024760	TLE6	79816	3.90	ND	ND
NM_016118	NUB1	51667	3.90	ND	ND

NM_199136	C7orf46	340277	3.89	ND	ND
NM_001005340	GPNMB	10457	3.89	ND	ND
NM_138689	PPP1R14B	26472	3.88	ND	ND
NM_022742	CCDC136	64753	3.88	ND	ND
NM_013351	TBX21	30009	3.87	ND	ND
NM_024877	CNTD2	79935	3.87	ND	ND
NM_018958	C15orf2	23742	3.87	ND	ND
NM_017575	SMG6	23293	3.87	ND	ND
NM_014721	PHACTR2	9749	3.86	ND	ND
NM_015391	ANAPC13	25847	3.86	1.26	FP
XM_379270	CSN1S2A	286828	3.86	ND	ND
NM_015570	AUTS2	26053	3.84	ND	ND
NM_021160	BAT5	7920	3.84	ND	ND
NM_001039457	ATP6V0B	533	3.84	ND	ND
NM_014015	DEXI	28955	3.84	ND	ND
XM_930189	LOC647163	647163	3.83	ND	ND
NM_031275	TEX12	56158	3.82	ND	ND
XM_001127655	LOC730891	730891	3.81	ND	ND
NM_006221	PIN1	5300	3.80	ND	ND
NM_024654	NOL9	79707	3.80	ND	ND
NM_003496	TRRAP	8295	3.80	ND	ND
NM_015938	NMD3	51068	3.79	ND	ND
NM_004189	SOX14	8403	3.78	ND	ND
NM_001039127	ZNF718	255403	3.77	ND	ND
NM_001042610	DBNDD1	79007	3.77	ND	ND
XM_211339	LOC284120	284120	3.76	ND	ND
XM_001133281	LOC283663	283663	3.75	ND	ND
NM_152462	AMAC1	146861	3.75	ND	ND
NM_018676	THSD1	55901	3.75	ND	ND
NM_000369	TSHR	7253	3.74	ND	ND
NM_014420	DKK4	27121	3.74	ND	ND
NM_004270	MED7	9443	3.74	ND	ND
NM_015229	KIAA0664	23277	3.74	ND	ND
NM_005672	PSCA	8000	3.72	ND	ND
NM_001023565	LOC401286	401286	3.72	ND	ND
NM_014791	MELK	9833	3.71	ND	ND
NM_012365	OR2A5	393046	3.71	ND	ND
NM_001085386	NF-E4	58160	3.70	ND	ND
NM_000953	PTGDR	5729	3.69	ND	ND
NM_024672	THAP9	79725	3.69	ND	ND
NM_003045	SLC7A1	6541	3.66	ND	ND
NM_015630	EPC2	26122	3.66	ND	ND
NM_001007246	BRWD1	54014	3.65	ND	ND

NM_198271	LMOD3	56203	3.65	ND	ND
XM_498945	FLJ30375	440982	3.63	ND	ND
NM_024523	GCC1	79571	3.62	ND	ND
XM_001127236	LOC730795	730795	3.62	ND	ND
NM_001030311	CERKL	375298	3.61	ND	ND
NM_001005468	OR8B2	26595	3.61	ND	ND
NM_022100	MRPS14	63931	3.60	ND	ND
NM_015525	IBTK	25998	3.59	ND	ND
NM_021222	PRUNE	58497	3.59	ND	ND
XM_001126438	LOC727845	727845	3.58	ND	ND
NM_005316	GTF2H1	2965	3.57	4.22	TP
NM_015392	NPDC1	56654	3.57	ND	ND
NM_019002	ETAA1	54465	3.57	ND	ND
NM_004655	AXIN2	8313	3.56	ND	ND
NM_000539	RHO	6010	3.56	ND	ND
NM_152437	ZNF664	144348	3.56	ND	ND
XM_001134448	BMS1P5	399761	3.56	ND	ND
XM_498955	LOC440995	440995	3.55	ND	ND
XM_933646	LOC646484	646484	3.55	ND	ND
NM_001013664	HMCN2	256158	3.55	ND	ND
XM_927777	hCG_1646420	644672	3.55	ND	ND
NM_015289	VPS39	23339	3.54	ND	ND
NM_021808	GALNT9	50614	3.54	ND	ND
NM_016055	MRPL48	51642	3.54	ND	ND
NM_001717	BNC1	646	3.54	ND	ND
NM_024727	LRRC31	79782	3.54	ND	ND
NM_016186	SERPINA10	51156	3.54	ND	ND
NM_000061	BTK	695	3.53	ND	ND
NM_001040662	C14orf138	79609	3.53	ND	ND
NM_017806	LIME1	54923	3.53	ND	ND
NM_001001998	EXOSC10	5394	3.51	ND	ND
NM_001025593	ARFIP1	27236	3.51	ND	ND
NM_003384	VRK1	7443	3.51	ND	ND
NM_001009959	ERMN	57471	3.50	ND	ND
XM_001133217	LOC732392	732392	3.50	ND	ND
XM_498696	LOC440491	440491	3.48	ND	ND
NM_152694	ZCCHC5	203430	3.45	ND	ND
XM_293354	WDR42C	347442	3.44	ND	ND
NM_015568	PPP1R16B	26051	3.44	ND	ND
NM_003475	RASSF7	8045	3.43	ND	ND
NM_015349	KIAA0240	23506	3.43	ND	ND
NM_017869	BANP	54971	3.43	ND	ND
NM_001204	BMPR2	659	3.42	ND	ND

NM_001029955	WDR21B	285429	3.42	ND	ND
NM_015299	KIAA0323	23351	3.41	ND	ND
NM_004226	STK17B	9262	3.41	ND	ND
NM_014612	FAM120A	23196	3.35	ND	ND
NM_014901	RNF44	22838	3.34	ND	ND
NM_003234	TFRC	7037	3.34	ND	ND
NM_001081675	C8ORFK36	340359	3.33	ND	ND
XM_941785	LOC652355	652355	3.33	ND	ND
NM_182562	FAM169B	283777	3.33	ND	ND
NM_002707	PPM1G	5496	3.32	ND	ND
NM_001024916	CBWD5	220869	3.32	ND	ND
NM_014155	ZBTB44	29068	3.32	ND	ND
NM_152379	C1orf131	128061	3.32	ND	ND
NM_001007525	NWD1	284434	3.31	ND	ND
XM_001126745	hCG_2003663	728061	3.31	ND	ND
XM_373453	LOC387654	387654	3.30	ND	ND
XM_495918	FLJ13224	79857	3.30	ND	ND
NM_181807	DCDC1	341019	3.30	ND	ND
XM_001133683	LOC732440	732440	3.30	ND	ND
XM_001133887	LOC729620	729620	3.29	ND	ND
NM_016038	SBDS	51119	3.29	ND	ND
NM_000222	KIT	3815	3.28	ND	ND
XM_001131372	LOC729804	729804	3.28	ND	ND
XM_001129009	LOC728222	728222	3.27	ND	ND
NM_001083910	SIRPB1	10326	3.26	ND	ND
NM_134424	RAD52	5893	3.26	ND	ND
NM_003731	SSNA1	8636	3.26	ND	ND
NM_024310	PLEKHF1	79156	3.24	ND	ND
XM_941053	hCG_1643176	122038	3.24	ND	ND
NM_001005404	YPEL2	388403	3.24	ND	ND
NM_015383	NBPF14	25832	3.23	ND	ND
XM_001130872	LOC731804	731804	3.22	ND	ND
NM_001005739	VPS54	51542	3.21	ND	ND
NM_198536	TMEM205	374882	3.21	ND	ND
NM_006010	ARMET	7873	3.20	ND	ND
XM_498354	LOC139604	139604	3.20	ND	ND
NM_139173	NHEDC1	150159	3.19	ND	ND
XM_944233	LOC400099	400099	3.19	ND	ND
NM_198555	ANKRD36	375248	3.18	ND	ND
NM_001080469	FBXO46	23403	3.18	ND	ND
NM_052898	XKR4	114786	3.14	ND	ND
NM_198521	C12orf42	374470	3.13	ND	ND
XM_001130923	LOC729653	729653	3.13	ND	ND

NM_005031	FXYD1	5348	3.13	ND	ND
NM_138296	PTCRA	171558	3.12	ND	ND
XM_001131438	LOC729823	729823	3.12	ND	ND
NM_018649	H2AFY2	55506	3.11	ND	ND
XM_927535	C11orf34	349633	3.11	ND	ND
NM_016067	MRPS18C	51023	3.11	ND	ND
XM_293416	LOC347549	347549	3.09	ND	ND
XM_001131221	LOC729763	729763	3.08	ND	ND
NM_003682	MADD	8567	3.08	ND	ND
NM_001002905	OR8G1	26494	3.07	ND	ND
NM_032027	TM2D1	83941	3.07	ND	ND
NM_006495	EVI2B	2124	3.06	ND	ND
NM_020056	HLA-DQA2	3118	3.06	ND	ND
NM_153445	OR5P3	120066	3.05	ND	ND
XM_001133224	LOC730242	730242	3.04	ND	ND
XM_292820	LOC342979	342979	3.04	ND	ND
NM_032870	SFRS18	25957	3.03	ND	ND
NM_015511	C20orf4	25980	3.02	ND	ND
NM_173472	C3orf24	115795	3.02	ND	ND
NM_024589	ROGDI	79641	3.00	ND	ND
NM_198441	FLJ40296	122183	3.00	ND	ND

ND = Not determined [Gene not included in the custom library screen]
TP = True positive [Hit both in validation screen and custom library screen (including borderline values)]
FP = False positive [Hit in the validation screen but non-hit in the custom library screen]
TP* = Hit confirmed by independent experiments